The subduction of continental crust - insights from eclogite geochronology and petrology

Dissertation

zur

Erlangung des Doktorgrades (Dr. rer. nat.)

der

Mathematisch-Naturwissenschaftlichen Fakultät

der

Rheinischen Friedrich-Wilhelms-Universität Bonn

vorgelegt von

Irena Miladinova

aus

Razlog, Bulgarien

Bonn, Januar 2019

Angefertigt mit Genehmigung der Mathematisch-Naturwissenschaftlichen Fakultät der
Rheinischen Friedrich-Wilhelms-Universität Bonn

1. Gutachter: Prof. Dr. Nikolaus Froitzheim
2. Gutachter: Prof. Dr. Thorsten Nagel
   Tag der Promotion: 07.06.2019
   Erscheinungsjahr: 2019

Teile dieser Arbeit wurden bereits an den nachstehenden aufgeführten Stellen auszugsweise veröffentlicht:

Froitzheim, N., Miladinova, I., Janák, M., Kullerud, K., Krogh Ravna, E., Majka, J., Fonseca, R.O.C., Münker, C., Nagel, T.J. (2016): Devonian subduction and syncollisional exhumation of continental crust in Lofoten, Norway. Geology, 44, 223-226.

Miladinova, I., Froitzheim, N., Nagel, T.J., Janák, M., Georgiev, N., Fonseca, R.O.C., Sandmann, S., Münker, C. (2018): Late Cretaceous eclogite in the Eastern Rhodopes (Bulgaria): evidence for subduction under the Sredna Gora magmatic arc. International Journal of Earth Sciences, 107, 2083-2099.

На майка ми...

Abstract

When continents collide slices of continental crust may be dragged down into the subduction zone to depths of up to 200 km. The most straightforward evidence for continental subduction refers to the presence of high-pressure (HP) and ultrahigh-pressure (UHP) eclogite terranes in many collisional mountain systems. In addition, as inferred from numerical modelling continental subduction provides a physically most consistent explanation for the formation and exhumation of these terranes. Reconstruction of the P-T-t paths of HP and UHP rocks can provide direct constraints on the thermo-mechanical processes in subduction zones. For that, a multidisciplinary approach is the most promising one for understanding the subduction dynamics as well as the mechanisms of continental convergence.

Three case studies were performed on HP and UHP eclogite terranes following similar procedures: the Eoalpine high-pressure belt in the Eastern Alps (Austria and Italy), the Byala Reka Dome in the Eastern Rhodopes (Bulgaria) and the Lofoten basement in the Scandinavian Caledonides (Norway). High precision Lu-Hf geochronology was applied on eclogites and combined with characterization of the chemical zoning in garnet. Additionally, thermodynamic modelling was performed on each of the dated samples for constraining the metamorphic conditions.

The Eoalpine belt includes (ultra)high-pressure rocks that crop out along a northwest-southeast trending line extending from the Texel Complex in Italy to the Pohorje Mountains in Slovenia. Dating of garnet growth during pressure increase was achieved by using Lu-Hf chronometry that yielded results between c. 100 and c. 90 Ma. This time span of c. 10 Ma suggests short-lived period of subduction. Combined with the already published data the estimated metamorphic conditions indicate a field gradient with increasing P and T from northwest to southeast where the rocks experienced UHP Eoalpine metamorphism. The oldest Cretaceous eclogites are found in the Saualpe-Koralpe area that comprises widespread Permian gabbros formed along rift zones within a thinned continental margin during Permian-Triassic time. This supports the hypothesis that subduction initiation was intracontinental and localized by e Permian rift. In Texel Complex Lu-Hf dating of two-phased garnets yielded a Variscan-Eoalpine mixed age

indicating re-subduction and eclogitization of Variscan eclogites during the Eoalpine orogeny.

In eclogite from the Byala Reka Dome in the Eastern Rhodopes, garnet growth was dated at 81.6 ± 3.5 Ma by Lu–Hf chronometry. Petrological data and modelling suggest peak-pressure conditions of 1.2–1.6 GPa and 570–620 °C. The eclogite-facies metamorphism coincides with the main phase of granitoid intrusions in the Sredna Gora Zone and, thus, suggests that metamorphism took place in a subduction zone dipping towards north under this section of the Apuseni–Banat–Timok–Sredna Gora continental magmatic arc. During the Late Cretaceous, the site of magmatic activity shifted southward and arrived in the Eastern Rhodopes at ~69 Ma, as evident by granite intrusions of that age near the locality of the dated eclogite sample. This proximity may be explained by south-directed rollback of the subduction zone, although also post-69 Ma tectonic displacement has to be considered. Together with published age data from other parts of the Rhodopes, the new data confirm that multiple subduction/exhumation cycles took place between ~200 and ~40 Ma along this section of the southern European plate boundary.

The Proterozoic basement of the Lofoten Islands contains Caledonian eclogite, although Caledonian deformation is only minor. Previous dating suggested that HP metamorphism in Lofoten occurred ca. 480 Ma, i.e., ~50 Ma before the collision between the major continents Baltica and Laurentia. Therefore, the Lofoten basement was considered not to originate from Baltica but rather to represent a stranded microcontinent. Newly discovered kyanite-bearing eclogites from the Lofoten Islands record deep subduction of continental crust during the main (Scandian) stage of Baltica-Laurentia collision ca. 400 Ma. Conventional geothermobarometry and thermodynamic modelling yield metamorphic conditions of 2.5-2.8 GPa and ~650 °C. Lu-Hf dating results in prograde garnet growth age of 399 ± 10 Ma. These results demonstrate that the Lofoten basement belonged to Baltica, was subducted to ~90 km depth during the collision with Laurentia, and was exhumed at an intermediate to high rate (>6 mm/yr) while thrusting of a Caledonian allochthon (Leknes Group) was still ongoing. This supports the challenging conclusions that (1) subducted continental crust may stay rigid down to a depth of ~90 km, and (2) it may be exhumed during ongoing collision and crustal shortening.

Table of Contents

Mineral abbreviations

Am	**Amphibole**
Ap	**Apatite**
Chl	**Chlorite**
Coe	**Coesite**
Cpx	**Clinopyroxene**
Czo	**Clinozoisite**
Ep	**Epidote**
Fsp	**Feldspar**
Grt	**Garnet**
Hem	**Hematite**
Ilm	**Ilmenite**
Kfs	**K-Feldspar**
Ky	**Kyanite**
Law	**Lawsonite**
Mag	**Magnetite**
Omp	**Omphacite**
Pl	**Plagioclase**
Qtz	**Quartz**
Rt	**Rutile**
Tlc	**Talc**
Ttn	**Titanite**
Wm	**White mica**

Chapter 1

Introduction

1.1. Subduction-exhumation processes

Studying the processes acting along subduction zones is crucial to the understanding of the dynamics of the Earth as they represent the essential driving force behind the movement of tectonic plates. On the other hand, understanding subduction margins is particularly important for the assessing of associated hazards like earthquakes, tsunamis and volcanic eruptions.

The prevalent view is that only oceanic lithosphere is able to sink deeply into the mantle along the subduction channel, because the continental crustal material is too light (Fig. 1.1). Thus, when a large piece of continent enters the subduction zone it may be dragged down along the subduction channel but only for a short period of time as its buoyancy would eventually lead to standstill (e.g., Stern 2004). However, the continent-continent collision causes intense deformation of both upper and lower plate resulting in the formation of mountain ranges like the Himalayas and the Alps.

The discovery of coesite and diamond inclusions in rocks of the continental crust has revealed that subduction of continental lithosphere to more than 100 km depth is possible (e.g., Chopin 1984, Smith 1984). However, the mechanisms of continental subduction and exhumation of high-pressure (HP) and ultrahigh-pressure (UHP) material are still very much in debate and require further investigation. Previous models suggested that the UHP units can be exhumed by the remaining positive buoyancy of the SiO2-rich continental rocks (e.g., Chemenda et al. 1995). Yet, during high-pressure modification coesite- and diamond-bearing rocks increase their density and, thus, decrease their buoyancy indicating that a purely buoyancy driven exhumation mechanism of UHP terranes is highly unlikely. In any case, it has been suggested that thin, distal continental margins are generally subducted and exhumed faster than thick, proximal continental portions (Kylander-Clark et al. 2012).

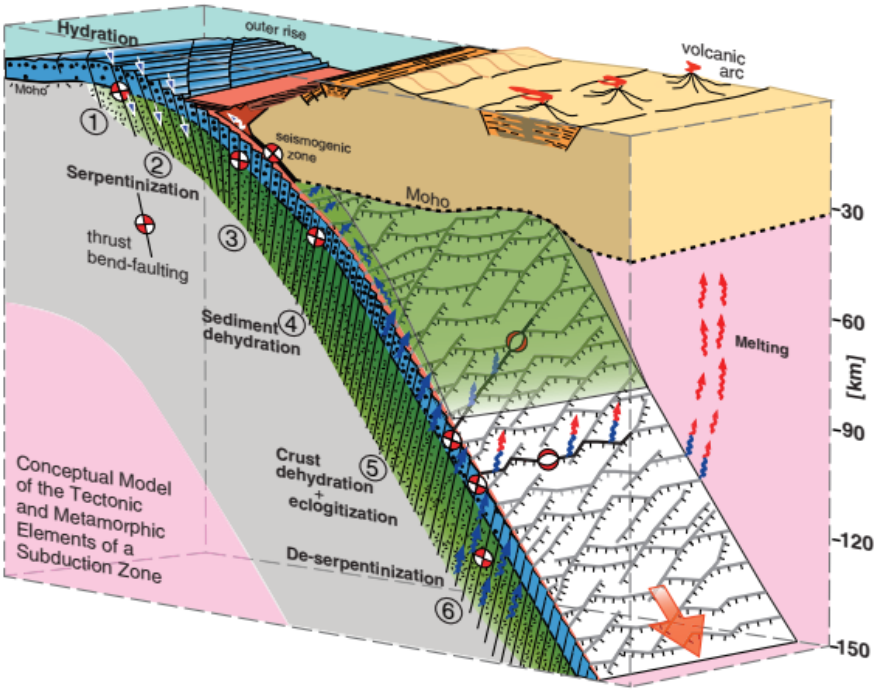

Fig. 1.1. Conceptual model of the structure and metamorphic evolution of subducting lithosphere (from Ranero et al. 2005).

Numerical modelling combined with the existing pressure-temperature-time-deformation data resulted in a wide range of tectonic settings and mechanisms by which continental rocks can reach mantle depth, including subduction of continental margin (e.g., Chopin 2003), intracontinental subduction (e.g., Faure et al. 2009), subduction erosion (e.g., Gerya & Stöckhert 2006), subduction of microcontinent (e.g., Kylander-Clark et al. 2012) and sediment subduction (e.g., Cloos & Shreve 1988).

Several models have been proposed to explain the exhumation mechanisms of continental HP and UHP rocks (e.g., Hacker & Gerya 2013). Numerical and conceptual models include eduction (e.g., Anderson et al. 1991, Duretz et al. 2012), microplate rotation (e.g., Hacker et al. 2000), slab rollback (e.g., Brun & Faccena 2008), crustal stacking (e.g., Duertz & Gerya 2013), slab extraction (e.g., Froitzheim et al. 2003), extensional collapse (e.g., Platt 1993) and subduction channel flow (e.g., Li & Gerya 2009).

The proposed models for exhumation are mechanically and geologically plausible. Also, the different formation and exhumation mechanisms of HP and UHP rocks are not necessarily independent. For example, crustal stacking can occur after subduction of

continental margin, intracontinental subduction or microcontinent subduction. Still, there is not one example for an UHP terrane worldwide that matches the predicted geological characteristics of the different models. In any case, multidisciplinary approach would best resolve the driving mechanisms of subduction-exhumation processes. Combining the many advances made in the past decades in the fields of geophysics, petrology, geochemistry and geodynamics can contribute greatly to the understanding of subduction dynamics.

1.2. Aim of the study

The work presented in this thesis aims to combine detailed petrographic observations with thermodynamic modelling and precise radiometric dating of high-pressure rocks to better understand the deep subduction-exhumation processes in continental collision zones as well as the link between magmatic and metamorphic processes at convergent plate boundaries. For that, eclogites from three collisional orogens have been investigated: the Eoalpine high-pressure belt of the Eastern Alps, the Byala Reka Dome of the Eastern Rhodopes and the Lofoten basement of the Scandinavian Caledonidnes. Based on the obtained and previously published data tectonic model for each case study was developed.

Estimating the time and duration of high-pressure metamorphism can greatly contribute to the understanding the process of subduction initiation and continental collision. Moreover, it can decipher the geodynamic evolution of single orogen as well as the driving processes behind orogenesis.

1.3. Principles of radiometric dating: the Lu-Hf system

Radiometric dating is fundamental to understanding geologic processes and geologic time. It uses naturally occurring, long-lived radioactive isotopes and depending on the rate of decay different isotope systems can be used for dating different geologic periods. The underlying principal of radiometric dating is that a particular parent radioisotope decays to a stable daughter product at rate (λ) that has remained invariant over geologic time. The decay constant λ is unique to every radioactive system and does not show changes due to variations of pressure, temperature or chemical environment. In this case, using the abundances of the radioisotopes and their daughter products in rocks and/or particular minerals we can determine the age of their formation.

The isochron dating method is the most used geochronological tool for calculating the radiometric ages (Fig. 1.2; Nicolaysen 1961). In practice the determination of ages uses ratios between different isotopes, measured with great precision in mass spectrometers. The results can be interpreted graphically on an isochron plot. In this case, the parent concentrations are plotted against these of the daughter. A t=0 there are no daughter atoms present in the original rock but a certain amount of parent atoms, so the composition plots on the parent axis. After time a number of parent atoms have decayed and the number of daughters increase. Eventually there will be no parents and only daughters - the composition will plot on the daughter axis. Therefore, the gradient of the line is a function of time. However, there are commonly daughter atoms already present in a material. In these cases a correction must be made, estimating the original daughter concentration. This is done by normalising against a stable isotope of the daughter atom (^{177}Hf for the Lu-Hf system).

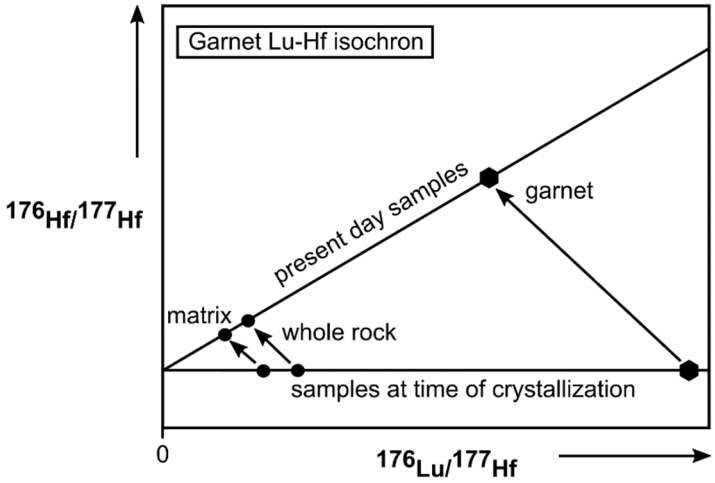

Fig. 1.2. The isochron method applied to garnet Lu-Hf geochronology. The isochron is a straight line defined by the measured present-day compositions and its slope determines the age of garnet growth.

The rapid progress of the multicollector inductively coupled plasma mass spectrometry technique (MC-ICP-MS) during the last two decades made the Lu-Hf isotopic system one of the most innovative and powerful tools for geochronological and isotopic studies (e.g., Blichert-Toft et al. 1997). Above all, this technical advance allowed the analysis of Hf-poor rocks such as chondritic meteorites and mineral phases like garnet. Furthermore, the new

instrumentation has made possible the more precise and accurate determination of the ^{176}Lu decay constant (Scherer et al. 2001, Söderlund et al. 2004).

For the successful applying of the Lu-Hf geochronometer there are three key assumptions that has to be met: (1) the sample being dated has been a closed system for Lu and Hf since the time of mineral growth, (2) all minerals have the same isotopic composition at the time of formation, and (3) all the minerals formed at the same time (i.e., have the same age; Scherer et al. 2000). Both Lu and Hf are immobile and insoluble elements, which makes them highly resistant to significant degrees of alteration and metamorphism. In particular, metamorphic garnets have high affinity for Lu and the highest known ^{176}Lu/^{177}Hf ratios of the rock-forming mineral phases, which makes them the most suitable for accurate and precise Lu-Hf dating of high-grade rocks (e.g., Baxter & Scherer 2013, Blichert-Toft et al. 1999, Duchêne et al. 1997, Scherer et al. 2000, Smit et al. 2013). In addition, slow REE diffusion rates allow garnets to preserve their isotopic compositions at high temperatures (Bloch et al. 2015, Burton et al. 1995, Ganguly et al. 1998, Tirone et al. 2005, van Orman et al. 2002). Still, the Lu-Hf closure temperature (Tc) depends on several other factors besides temperature, such as grain size, mineral composition, oxygen fugacity and cooling rate (e.g., Smit et al. 2011). However, numerous studies predict that the Tc the Lu-Hf system in garnet is at least 540 °C (e.g., Scherer et al. 2000, Skora et al. 2006) and, thus, will generally date garnet growth rather than cooling in subduction-related high-pressure rocks.

The presence of accessory phases, especially as inclusions in garnets, could have a precision-reducing effect on the Lu-Hf ages (e.g., Scherer et al. 2000). In particular, zircons are extraordinarily enriched in Hf (~10,000 ppm Hf in zircon) relative to garnet (<1 ppm) and, therefore, can easily lower the Lu/Hf ratios of the garnet dissolutions. Furthermore, pre-existing zircons, which are not likely to be re-equilibrated prior to metamorphic growth, will have a less radiogenic Hf isotopic composition than the bulk rock. This would significantly affect the measured ^{176}Hf/^{177}Hf of the garnet sample by lowering it and, thus, result in erroneous ages (e.g., Scherer et al. 2000). However, applying of selective digestion methods (e.g., Lagos et al. 2007) effectively excludes those phases from the garnet analyses.

In sum, the determination of absolute ages is a key to revealing the evolution of magmatic processes as well as different metamorphic stages of subduction-exhumation cycles. In this study Lu-Hf geochronology was performed on eclogite rocks from the Eastern Alps, Eastern Rhodopes and Norwegian Caledonides.

1.4. Analytical methods

1.4.1. Electron Microprobe Analyses

For all samples the major element compositions of minerals as well as the element zoning in garnets were determined by using a JEOL Superprobe JXA 8200 electron microprobe at Steinmann Institute in Bonn. Quantitative analyses were performed by using wavelength-dispersive spectrometers (WDS) with a focused beam with an acceleration voltage of 15 kV and a beam current of 15nA. Element concentration maps of the garnets were obtained for Al, Mg, Ca, Fe and Mn also by WDS using a focused beam with an accelerated voltage of 15 kV and 50 nA beam current.

Mineral compositions in the eclogite sample RV-6 from Lofoten were determined by WDS analysis using a CAMECA SX-100 electron microprobe at the Dionýz Štúr Institute of Geology in Bratislava. The analytical conditions were as follows: 15 kV accelerating voltage and 20 nA beam current, peak counting time 20 s and beam diameter of 2-10 μm. Raw counts were corrected using on-line PAP routine. Mineral standards (Si, Ca: wollastonite, Na: albite, K: orthoclase, Fe: fayalite, Mn: rhodonite), pure element oxides (TiO_2, Al_2O_3, Cr_2O_3, MgO) and metals (Ni) were used for calibration.

1.4.2. Whole-rock compositions

All samples were crushed in a steel mortar. For the whole rock bulk composition analysis representative aliquot of every sample was powdered in an agate mill. Major oxides and trace elements were determined by X-ray fluorescence analysis, carried out using a PANalytical ProTrace X-ray fluorescence spectrometer. Loss of ignition (L.O.I.) was determined by weight loss before and after heating every sample up to 1,000 °C. All the Fe is reported as ferric (Fe^{3+}: Fe_2O_3) in the XRF analysis.

1.4.3. LA-ICPMS analyses

Trace element distributions in garnets were measured in situ by laser ablation mass spectrometry along line profiles. The analyses were carried out using a Resonetics M50-E ATL Excimer 193 nm laser system coupled to a Thermo X-series 2 quadrupole ICP-MS at the Steinmann Institute in Bonn. The laser was operated using fluency of 7.4 J/cm^2 at the sample surface and repetition rate of 15 Hz. Different spot sizes were used depending on the grain size of the garnets: 33 µm, 44 µm, 55 µm, 58 µm and 73 µm. Count rates were normalized using ^{29}Si as an internal standard and NIST-SRM-612 glass as an external standard (Jochum et al. 2011). Reproducibility was checked by measuring the NIST-SRM-610 reference glass, and treating it as an unknown. Concentration values were always within 10 % or lower of the preferred concentrations reported for that reference material (see Jochum et al. 2011). The isotopes ^{43}Ca, ^{47}Ti, ^{55}Mn, ^{89}Y, ^{175}Lu and ^{177}Hf were monitored. Data reduction and evaluation were carried out following standard procedures (Longerich et al. 1996).

1.4.4. Lu-Hf dating

The samples selected for Lu-Hf dating were crushed in a steel mortar. One portion of every sample was powdered in an agate mill for bulk rock analysis. For mineral separation, second portion of every sample was sieved and the target fractions were then purified using a Franz magnet separator. Subsequently, garnet and omphacite were hand-picked under a binocular microscope from 180-255µm, 250-355 µm and 355-500 µm size fractions.

1.4.4.1. Sample digestion and element separation

The mineral separates were cleaned in an ultrasonic bath in 2.5 M HCl and rinsed repeatedly with deionized water. A mixed ^{176}Lu-^{180}Hf tracer was added to the whole rock powders as well as to the mineral separates prior to acid digestion. For a complete sample digestion one whole rock powder split of each sample was digested with HF-HNO_3 (4:2) inside steel-jacketed PARR bombs for four days at 180 °C. $HClO_4$ was added to the samples. They were then dried down and re-dissolved in 6 N HCl. The mineral separates and a second whole rock fraction from each sample were dissolved following the selective tabletop procedure described by Lagos et al. (2007). This method avoids digestion of refractory Hf-rich phases like zircon and rutile. The samples were digested in a 4:2:1 acid

mixture of HF-HNO_3-$HClO_4$ in Savillex® PFA beakers on a 120 °C hotplate. Subsequently the samples were dried down and re-dissolved in 6 N HCl. The digestion procedure was repeated at least one more time for all samples to achieve complete sample digestion.

The single-column element separation procedure (Münker et al. 2001) was used to separate Lu and Hf from the rock matrix. In addition, the Hf cuts were processed a second time in order to remove remaining matrix elements Lu and Yb.

1.4.4.2. MC-ICP-MS

The isotopic analyses of Lu and Hf were carried out in static mode using a Thermo-Finnigan Neptune MC-ICP-MS. Measured Hf isotope ratios were corrected for mass fractionation using the exponential law and a $^{179}Hf/^{177}Hf$ of 0.7325. All measured $^{176}Hf/^{177}Hf$ ratios are reported relative to $^{176}Hf/^{177}Hf$ = 0.282160 for the Münster Ames Hf standard, which is isotopically identical to the JMC-475 standard. Interferences on ^{176}Hf and ^{180}Hf were corrected by monitoring ^{173}Yb, ^{175}Lu, ^{181}Ta and ^{182}W signals. The external reproducibilities were estimated using the empirical relationship 2σ external reproducibility ≈ 4σm (σm = standard error of a single analysis; Bizzaro et al. 2003). Isochron regressions and ages were obtained using the Isoplot v. 2.49 program of Ludwig (2001) and the ^{176}Lu decay constant $\lambda = 1.867 \times 10^{-11}$ yr^{-1} (Scherer et al. 2001, Söderlund et al. 2004). Total procedural blanks were typically <58 pg for Lu and <64 pg for Hf (Table 1.1). The depleted-mantle Hf model age (TDM Hf) for sample LOF 3/12 was calculated using $^{176}Lu/^{177}Hf$ = 0.0384 and $^{176}Hf/^{177}Hf$ = 0.28325 as the present-day parameters of the depleted mantle (Chauvel & Blichert-Toft 2001).

1.5. Study areas

1.5.1. Eoalpine high-pressure belt, Eastern Alps

The Eastern Alps in Austria, Slovenia and Italy originate from the closure of ocean basins and collision between European and Adriatic continents during the Late Cretaceous-Tertiary. The Austroalpine superunit, which is derived from the former Adria continent, is widely exposed in this part of the orogen. The Austroalpine nappe stack is subdivided from bottom to top into Lower, Lower Central and Upper Central Austroalpine (Fig. 1.3a; Janák et al. 2004). It represents a fold-and-thrust belt established during the Cretaceous Eoalpine orogeny (e.g., Schmid et al. 2004, Handy et al. 2010).

The Eoalpine high-pressure belt belongs to the basement of the Lower Central Austroalpine and exposes high-pressure rocks along a distance of c. 350 km from Pohorje in the southeast to Texel in the west (Fig. 1.3b). Previously published P-T estimates constrain a field gradient with increasing pressure and temperature from west to southeast (e.g., Habler et al. 2006, Hauke et al. 2019, Konzett et al. 2012, Neubauer et al. 1999b, Thöni et al. 2008) by reaching ultrahigh-pressure conditions in Pohorje (≥3.5 GPa and 800-850 °C; Janák et al. 2015). Based on several isotopic systems (U-Pb zircon, Sm-Nd garnet and Lu-Hf garnet) the timing of high-pressure metamorphism was confirmed to be exclusively Cretaceous (Konzett et al. 2012, Sandmann et al. 2016, Thöni 2006 and references therein, Thöni et al. 2008). Recently, Hauke et al. (2019) showed that both Variscan and Eoalpine eclogites are present within the basement of Schobergruppe. This indicates involvement of Variscan crust within the Eoalpine subduction cycle.

For this work eclogite samples were collected from Koralpe, Saualpe, Texel complex and Sieggraben for bulk rock compositions, mineral chemistry, P-T modelling and garnet geochronology.

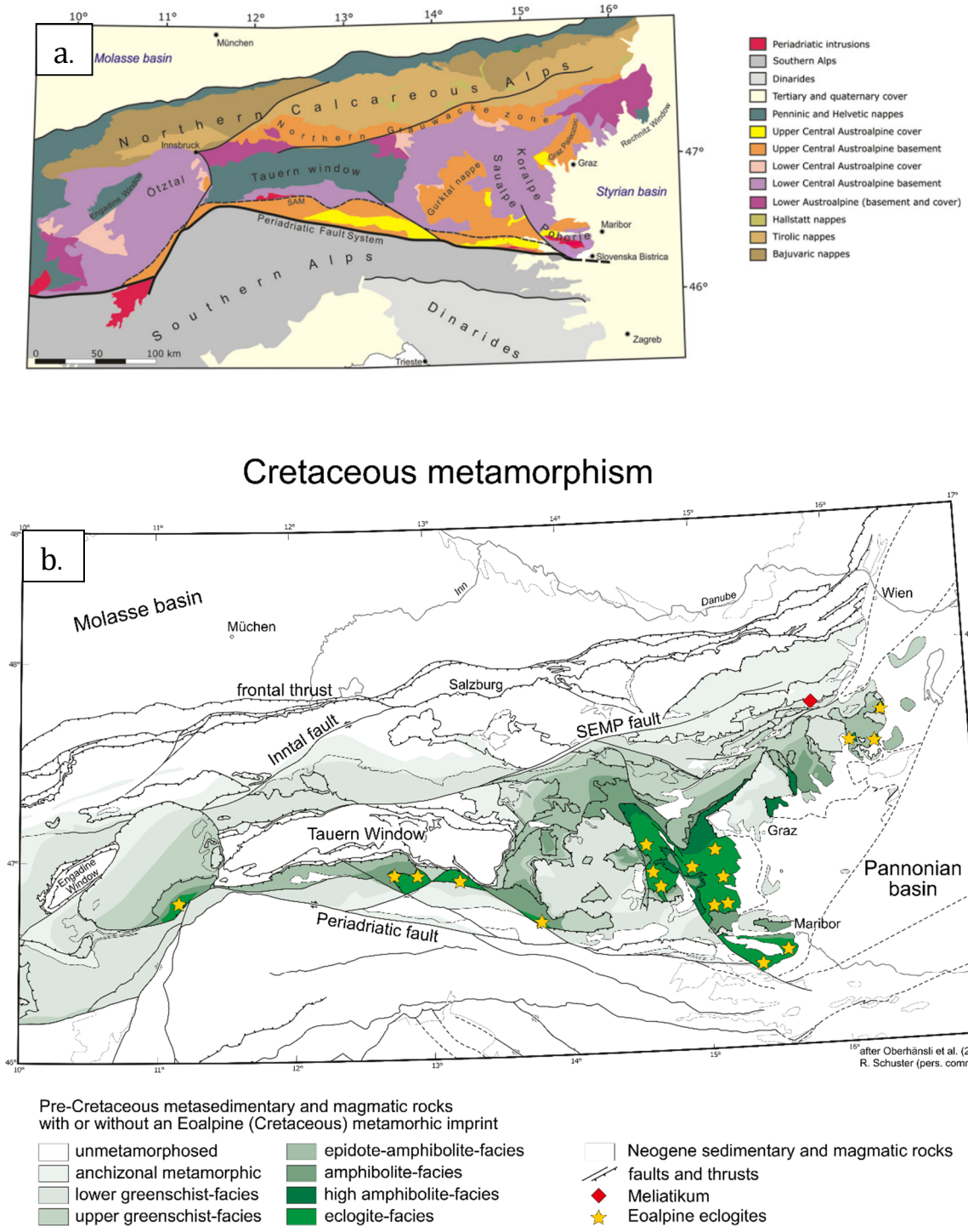

Fig. 1.3. (a) Tectonic map of the Eastern Alps modified after Janák et al. (2006), Neubauer & Höck (2000b) and Schmid et al. (2004). SAM – Southern border of Alpine metamorphism after Hoinkes et al. (1999). (b) Metamorphic map of the Eastern Alps (after Oberhänsli et al. 2004, R. Schuster pers. comm.).

1.5.2. Byala Reka Dome, Eastern Rhodopes

The Rhodope Metamorphic Complex (RMC) in southern Bulgaria and north-eastern Greece is located between the north verging Balkanides to the north and the south-west verging Hellenides to the southwest (Fig. 1.4). It represents a nappe stack that developed during a protracted history of obduction, subduction and collisional processes from Jurassic to Paleogene. Based on the age of deformation, metamorphism as well as the oldest overlying sediments, Janák et al. (2011) subdivided the RMC into four allochthons: Lower, Middle, Upper and Uppermost Allochthon.

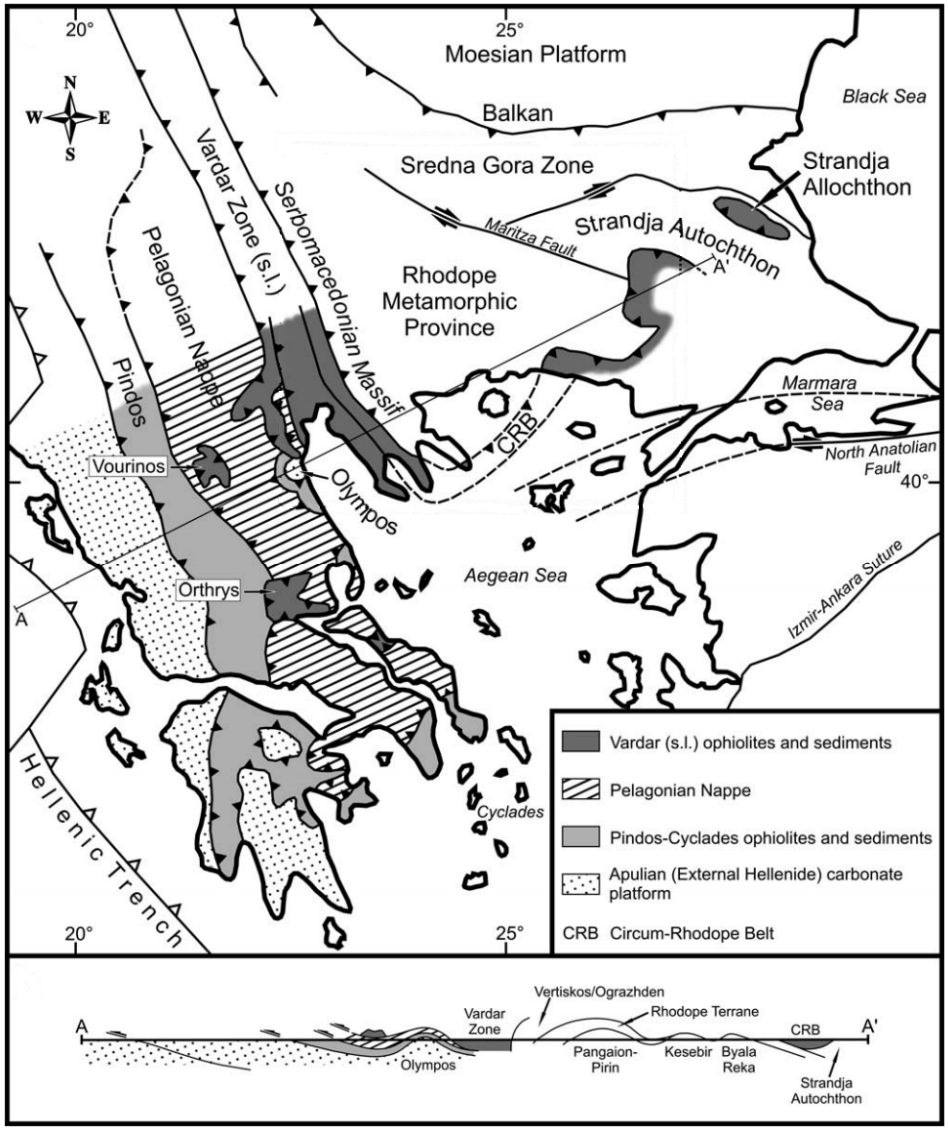

Fig. 1.4. Tectonic units and SW-NE cross-section of the Balkan Peninsula (after Jahn-Awe et al. 2010, Papanikolaou 2009).

The Byala Reka Dome of the Eastern Rhodopes (Fig. 1.5) comprises mainly orthogneisses of the Lower Allochthon derived from Carboniferous to Permian granitoids (e.g., Liati & Fanning 2005, Peytcheva & von Quadt 1995). These are surrounded and overlain by the rocks of the Upper Allochthon, whereas remnants of the Uppermost Allochthon occur only locally on top (Bonev 2006). Eclogites crop out as part of a metaophiolitic suit comprising also serpentinites, amphibolites, metagabbros and mica schists (e.g., Sarov et al. 2007a). In a recent study Peytcheva et al. (2018) obtained a Devonian protolith age for the eclogite that experienced high-pressure metamorphism in the Late Cretaceous.

An eclogite sample from the metaophiolite sequence of the Byala Reka Dome was collected for detailed petrological investigations, thermodynamic modelling as well as garnet geochronology.

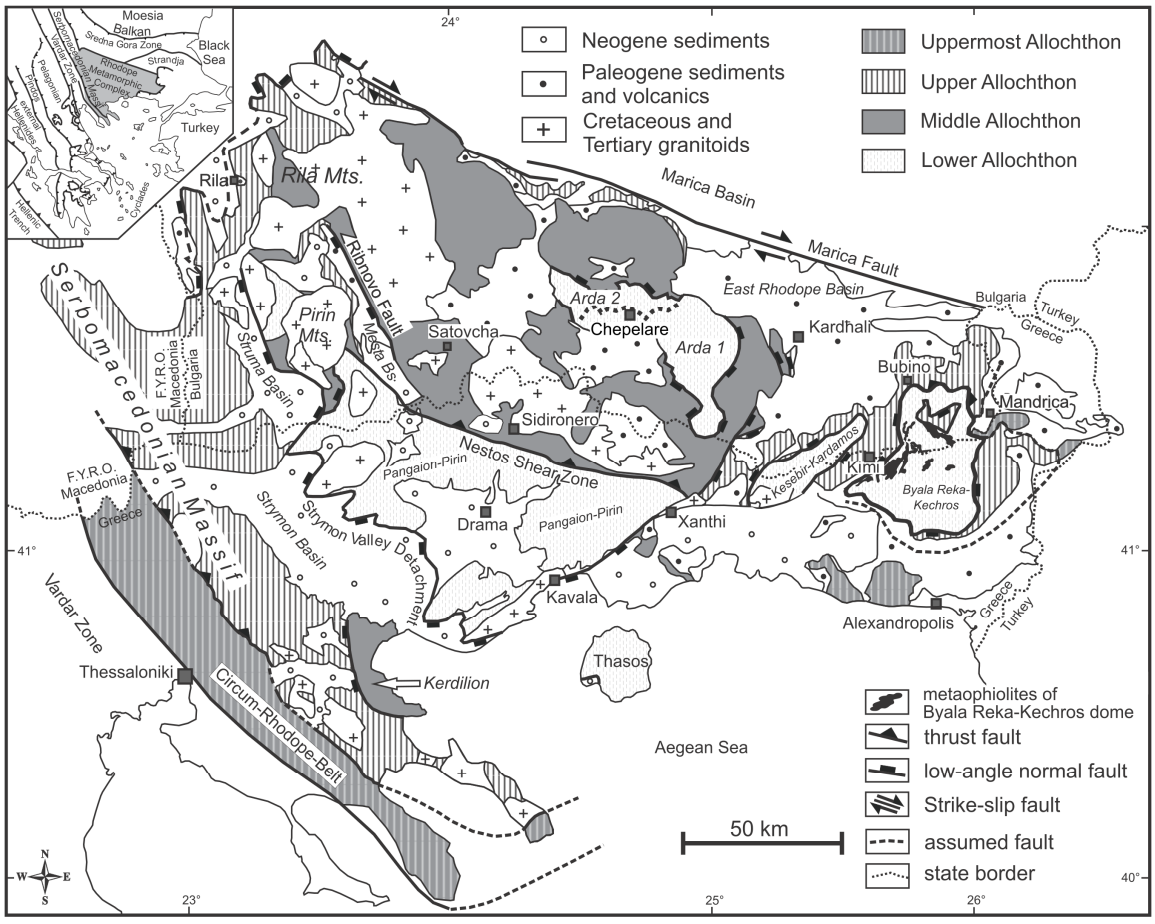

Fig. 1.5. Tectonic map of the RMC (after Bonev et al. 2006, Burg et al. 1996, Ricou et al. 1998).

1.5.3. Lofoten basement, Scandinavian Caledonides

The Scandinavian Caledonides represent a large NNE- to SSW-trending stack of nappes (Fig. 1.6) emplaced eastward onto the western margin of Baltica during continental collision with Laurentia, which occurred during the Scandian orogeny (430-400 Ma; Fossen 2010, Gee et al. 2008). The basement of Baltica is exposed in tectonic windows along the axis of the orogen with the Western Gneiss Region (WGR) being the largest and most intensely metamorphosed of them. It is also one of the best studied terranes as it comprises high-pressure und ultrahigh-pressure rocks that recorded very deep levels of the Baltic subduction (e.g., Dobrzhinetskaya et al. 1995, Hacker et al. 2010, Van Roermund & Drury 1998). Dating of the high-grade metamorphism yield ages between 430 and 400 Ma (e.g., DesOrmeau et al. 2015, Krogh et al. 2011, Kylander-Clark et al. 2007, 2009).

The Lofoten Islands in north Norway occupy a position similar to that of the WGR to the south (Fig. 1.6). The basement comprises Neoarchean migmatite complex overlain by Paleoproterozoic supracrustal sequence (Griffin et al. 1978). These were intruded by plutons of anorthosite-mangerite–charnockite–granite suit in two pulses at 1870-1860 Ma and 1800-1790 Ma (Corfu 2004b). By using U-Pb data for titanite and zircon, Corfu (2004a) constrained that the amphibolite-facies metasedimentary assemblage of the Leknes Group (Fig. 1.6) was emplaced on the Lofoten basement contemporaneous with metamorphism dated between 469 ± 3 Ma and 461 ± 1 Ma. In addition, Steltenpohl et al. (2011) dated zircons from a prekinematic granitoid dike in a retrogressed eclogite lens and estimated an age of 478 ± 41 Ma. They interpreted this data to represent the age of the eclogite-facies metamorphism that precedes the regional amphibolite-facies overprint. However, the constrained ages for the Caledonian metamorphism in WGR are younger, which led to the assumption that the Lofoten basement does not originate from Baltica (Corfu 2004a).

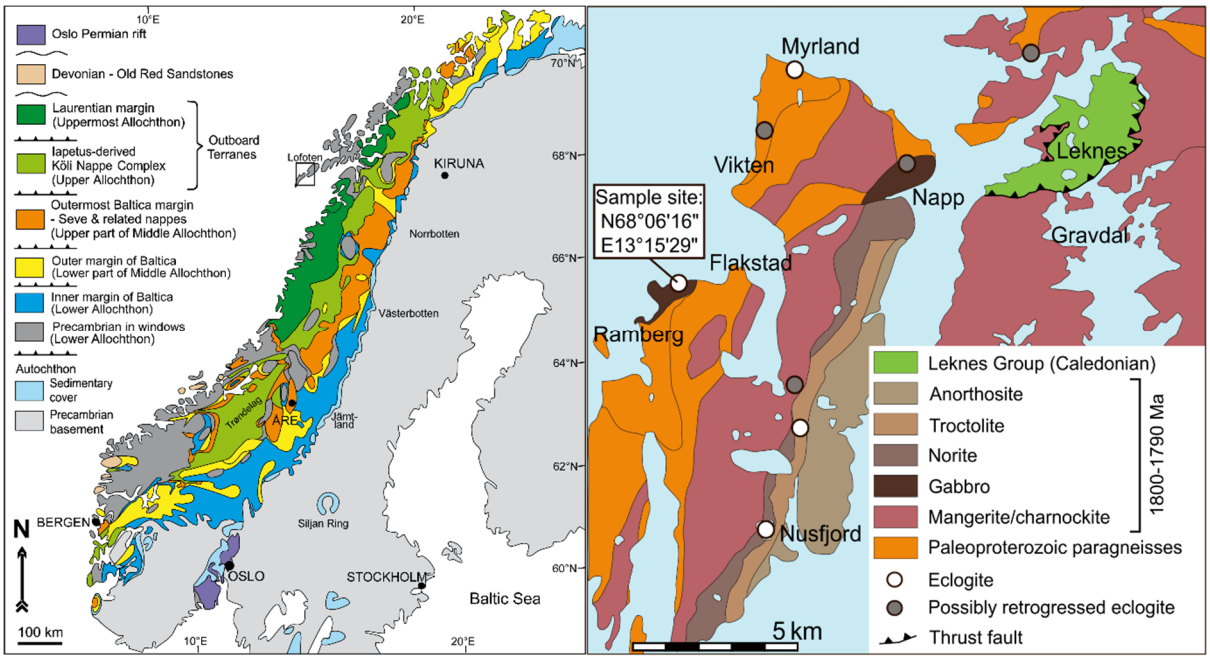

Fig. 1.6. Tectonic map of the Scandinavian Caledonides after Gee et al. (2013). Rectangle outlines the detailed geological map on the right.

Major attention in this work was dedicated to the sampled kyanite-bearing eclogites from Flakstad, which were collected for petrological observations, thermodynamic modelling and geochronology.

Chapter 2

Constraining the process of intracontinental subduction in the Austroalpine domain: implications from petrology and Lu-Hf geochronology of eclogites

2.1. Introduction

How a new subduction zone forms remains an unresolved question of the global tectonics, despite the many studies on subduction initiation from the last four decades (e.g., Casey & Dewey 1984, Cloetingh et al. 1982, 1989, Faccenna et al. 1999, Kemp & Stevenson 1996, McKenzie 1977, Nikolaeva et al. 2010, Stern 2004, Stern & Gerya 2017). Two general scenarios have been proposed for the physical mechanism of nucleation of subduction zones: spontaneous, which is caused by gravitational instability of oceanic lithosphere, and induced, which is a result of compressive stress acting on a plate (Stern 2004). In all discussed cases the subduction starts within an oceanic plate. However, there are strong evidences that in the presently active intracontinental belts of Central Asia, i.e. Pamir and Tien Shan mountain ranges, subduction was initiated within a pre-existing zone of weakness in the continental lithosphere as a response to the compressive stress caused by the India-Asia collision to the south (e.g., Burtman & Molnar 1993, Hamburger et al. 1992, Poupinet et al. 2002, Sobel et al. 2013). Furthermore, according to the same authors evidence of preceding, long-lasting subduction of oceanic lithosphere is lacking.

The model of intracontinental subduction has also been suggested for the Austroalpine high-pressure belt of the Eastern Alps (Janák et al. 2004, 2006, Kurz & Fritz 2003, Stüwe & Schuster 2010), where basement rock complexes were subducted to eclogite-facies and partly ultrahigh-pressure (UHP) conditions in the Cretaceous (e.g., Hoinkes et al. 1991,

Janák et al. 2015, Miller 1990, Miller & Thöni 1997, Thöni & Jagoutz 1992, Thöni & Miller 1996, Tenszer & Stüwe 2003). The zone covers a distance of at least 350 km from the Pohorje Mountains in the east to the Texel complex in the west. Originally, the Austroalpine units were interpreted to have resulted from a long-lived subduction of the Penninic ocean underneath the Adriatic plate, which should explain the Cretaceous (Eoalpine) and Cenozoic age data obtained throughout the Alps (Frank et al. 1987, Tollmann 1977). However, the precise dating of the high-pressure (HP) rocks indicated a rather short-lived high-pressure event that lasted c. 5-7 Ma with peak P-T conditions at c. 91 Ma, followed by rapid exhumation (Miller et al. 2005a, b, Thöni et al. 2008, Wiesinger et al. 2006). Therefore, a model with two separate subduction zones was suggested (Froitzheim et al. 1996, Neubauer et al. 1999b, 2000a, Thöni & Jagoutz 1993). The model includes an older south- or southeast-dipping subduction zone, which consumed the Meliata-Hallstatt ocean. Subduction initiated around 170 Ma and resulted in stacking of the Austroalpine nappes as well as the eclogite formation since 135 Ma. A second, younger southeast-directed subduction of the Penninic domain caused the emplacement of the Austroalpine nappe stack on the Penninic rocks. Although this model seems to be reasonable, it remains problematic to locate the position of the Meliata-Hallstatt subduction zone, because a clear ophiolitic suture is lacking (e.g., Schmid et al. 2004). The only relicts of the Meliata-Hallstatt ocean consist of pelagic sediments as well as small serpentinite slivers and Jurassic flysch (Mandl & Ondrejickova 1993).

The mechanism of ablative subduction has been proposed to explain the geodynamic evolution of the Austroalpine domain in the Eastern Alps (Polino et al. 1990, Roda et al. 2012). The numerical model of Roda et al. (2012) involves hydrated mantle wedge in an ocean-continent system. For the Austroalpine eclogites in the Eastern Alps it showed low correspondence between the natural data and the simulated thermobarometric conditions. Particularly the high T/P ratio observed in the Austroalpine could not be reproduced by numerical simulations. Roda et al. (2012) suggested modification of several factors to improve the model fitting: variation of the oceanic and/or upper plate thickness, variation of the subduction rate and/or the slab dip, the initial thermal state of the passive margin, the occurrence of continental collision or an oblique subduction.

Janák et al. (2004) suggested intracontinental subduction as an alternative interpretation of the tectonic and metamorphic evolution of the Austroalpine. According to this model

the north-western parts of the Austroalpine domain (Lower Central Austroalpine) represented the footwall that was subducted under the south-eastern parts (Upper Central Austroalpine), forming the hangingwall. The site of the subduction zone can be traced along the east-west trending zone of Eoalpine high-pressure metamorphic rocks. The subduction was initiated in the NW foreland of the Meliata suture, most probably within a pre-existing Permian-age rift that was reactivated when convergence across the suture continued after the closing of the Meliata ocean (Janäk et al. 2004, Kurz & Fritz 2003, Stüwe & Schuster 2010). This model is very appealing as it explains many features of the tectonic evolution of the Eastern Alps, like the lack of unambiguous remnants of former oceanic material, the high T/P ratio of the rocks as well as the short time span of subduction (5-7 Ma; Thöni et al. 2008).

To contribute to the better understanding of the mechanisms of subduction initiation as well as the reconstruction of the paleogeographical environment of the Cretaceous (Eoalpine) orogeny in the Eastern Alps, detailed petrological and geochronological investigations were performed on eclogites from different localities throughout the Austroalpine high-pressure belt. The P-T evolution of the eclogites was constrained by pseudosection modelling. The dating of the high-pressure metamorphism was accomplished by using high-precision Lu-Hf geochronology.

2.2. Regional geology: the Eastern Alps

The Eastern Alps show a complex architecture built up mainly during the Cretaceous and Tertiary orogenies. The structurally lowest units in the nappe stack are the Penninic nappes. They crop out along the northern margin of the Eastern Alps as well as in the Engadine Window, Tauern Window and Rechnitz Window (Fig. 2.1). These comprise slices of the Piemont-Ligurian Ocean, the Valais Ocean and the Briançonnais terrane. The Lower Penninic Nappes are made up of Cretaceous to Tertiary flysch sediments of the Valais Ocean (Rhenodanubian flysch) along the northern margin of the Alps as well as ophiolitic fragments and Cretaceous to Tertiary calcareous schists in the windows. The Middle Penninic Nappes are only present in the Western and Central Alps as well as in the Engadine Window and are attributed to the Briançonnais microcontinent. The Upper Penninic Nappes are derived from the Piemont-Ligurian Ocean and the accretionary

wedge at the southern margin of the Alpine Tethys (Schmid et al. 2004). They occur as a thin layer immediately below the Austroalpine nappes.

The Austroalpine nappes are the structurally highest units in the nappe stack (Fig. 2.1). They are derived from the north-western continental margin of Apulia and are subdivided into Lower and Upper Austroalpine units (Schmid et al. 2004). The Lower Austroalpine units occur only locally along the base of the Austroalpine, i.e., in the Err-Bernina nappe system, the Innsbruck Quartz Phyllite, Radstatt nappes and in the Wechsel nappes at the eastern margin of the Alps (Froitzheim et al. 1994, Schmid et al. 2004).

The Upper Austroalpine comprises the Permo-Mesozoic sediments of the Northern Calcareous Alps to the north and the Central Austroalpine to the south. The latter consists of Variscan basement with minor Permo-Mesozoic sedimentary cover. The Northern Calcareous Alps have almost no Alpine metamorphism, whereas the Central Austroalpine has been metamorphosed up to eclogite-facies conditions (e.g., Frank 1987, Thöni 1999).

The Central Austroalpine is subdivided into (1) Lower Central Austroalpine, which consists of basement largely affected by Cretaceous metamorphism up to eclogite facies and scarce or only locally present Mesozoic sediment cover, and (2) Upper Central Austroalpine comprising low-grade Variscan basement and unmetamorphosed Mesozoic cover remnants (Janák et al. 2004). The latter includes the Northern Grauwacke zone, the Graz Paleozoic and the Gurktal nappe (Fig. 2.1). The Lower Central Austroalpine comprises the Ötztal-Bundschuh, the Koralpe-Wölz and the Silvretta-Seckau nappe systems of Schmid et al. (2004).

The Silvretta-Seckau nappe system is the westernmost exposure of the Austroalpine basement (Fig. 2.1). The Variscan high-grade metamorphism reached up to eclogite-facies conditions at c. 350 Ma (Ladenhauf et al. 2001).

The Ötztal-Bundschuh nappe system is represented by the Ötztal-Stubai nappe to the west and the Bundschuh nappe east of the Tauern Window. These nappes were connected as one crystalline unit prior to the unroofing and exhumation of the Tauern Window in Late Oligocene-Early Miocene (Kurz et al. 2008, Nagel et al. 2013). Both nappes show a polymetamorphic character, similar lithologies and ages, as well as an increasing metamorphic field gradient towards their footwall units (Schmid et al. 2004).

The Koralpe-Wölz high-pressure nappe system comprises mainly high-grade metamorphic series that were subducted towards the SE beneath the units of the Upper Central Austroalpine in the Late Cretaceous (e.g., Janák et al. 2004, Tenczer & Stüwe 2003, Thöni & Jagoutz 1992). These eclogite-bearing units belong to a west-east trending zone, the Eoalpine high-pressure belt, extending from the Texel Complex towards east to the Saualpe, Koralpe and Pohorje Mountains. In contrast to the overlying Ötztal-Bundschuh nappe system, the nappes of the Eoalpine high-pressure belt were not all affected by Variscan metamorphism. They show a polymetamorphic character, generated by Permian and Eoalpine metamorphic events (e.g., Miller & Thöni 1997, Thöni 1999).

Evidence for ultra-high-pressure metamorphism is documented in the Pohorje Mountains in Slovenia (Janàk et al. 2015). There, kyanite-bearing eclogites and garnet peridotites, together with microdiamond-bearing gneisses were buried to depths exceeding 100 km and thus represent the most deeply subducted units. For the Texel complex, the western-most eclogites of the Eoalpine high-pressure belt, minimum P-T conditions of 1.3 GPa and 600 °C were estimated (Habler et al. 2006), which correspond to ~40 km burial depth for this part of the subduction zone. In contrast, Zanchetta et al. (2013) suggested UHP metamorphic conditions of at least 2.65 GPa and 630-690 °C for the Texel complex.

Location	Sample	Coordinates
Koralpe		
Hohl	Ho1 & Ho2	N46°43'49.4" E15°08'48.9"
Saualpe		
Grünburgerbach	Grü1 & Grü2	N46°51'21" E14°34'29.5"
Wolfsberger Hütte	Wol1	N46°49'60" E14°39'33.5"
Sieggraben		
	Sig3	N47°39'31" E16°21'25"
Texel		
Saltaus Valley	Sal1 & Sal2a	N46°44'07.5" E11°10'32.8"

Table 2.1. Sample locations and GPS coordinates.

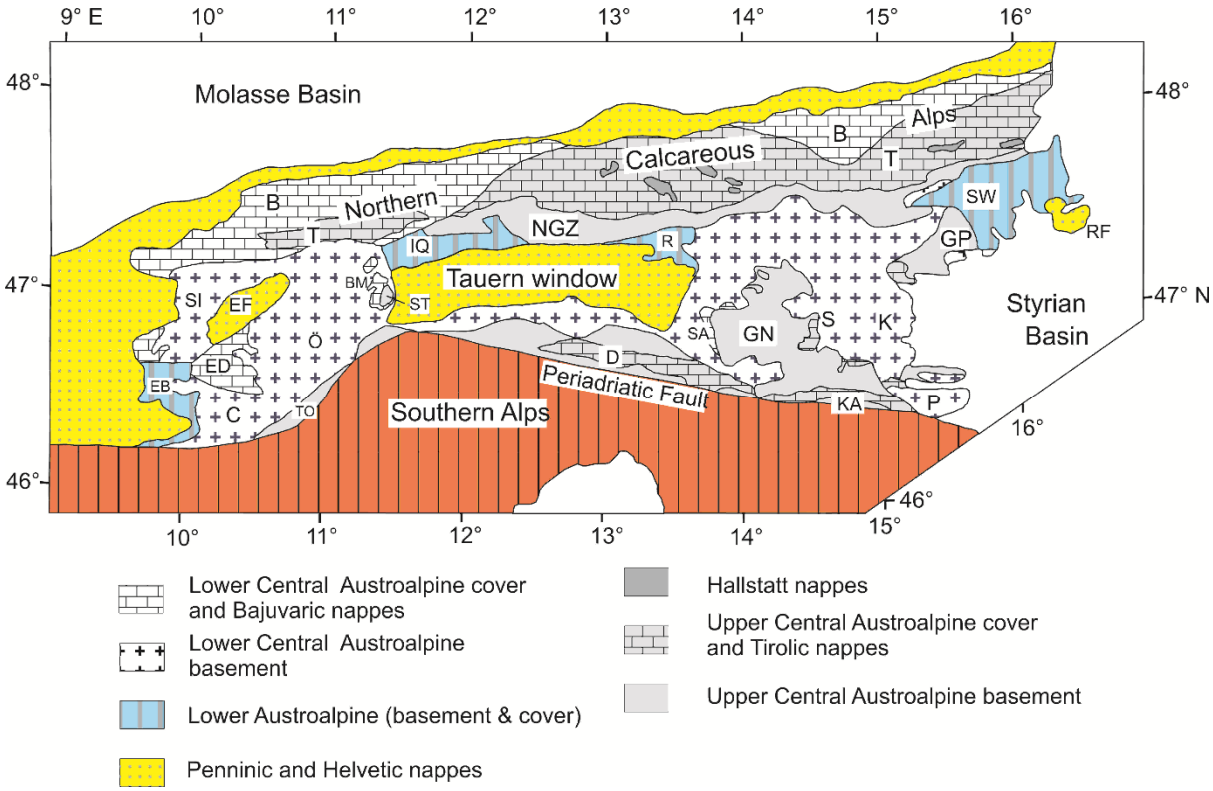

Fig. 2.1. Subdivision of the Austroalpine nappes after Janák et al. (2004). B: Bajuvaric; BM: Brenner Mesozoic; C: Campo Nappe; D: Drauzug; EB: Err and Bernina Nappes; ED: Engadine Dolomites, EF: Engadine Window; GN: Gurktal Nappe; GP: Graz Paleozoic; IQ: Innsbruck Quartz Phyllite; K: Koralpe; KA: Karawanken; NGZ: Northern Grauwackenzone; Ö: Ötztal Nappe; P: Pohorje Massif; R: Radstadt Nappes; S: Saualpe; SA: Stangalm Mesozoic; SI: Silvretta Nappe; ST: Steinach Nappe; SW: Semmering and Wechsel nappes; T: Tirolic; TO: Tonale Nappe.

2.3. High-pressure metamorphism in the Austroalpine domain

Eclogite-facies, partly UHP metamorphic rocks crop out in the western and northern parts of the Austroalpine basement as well as along the west-east trending Eoalpine high-pressure belt to the south. Here are described the main localities from west to east.

2.3.1. Silvretta basement

U–Pb SHRIMP data for zircons from phengite- and kyanite-bearing eclogites of the Silvretta nappe yielded an age of 351 ± 22 Ma (Ladenhauf et al. 2001), similar to the Sm-Nd ages determined by Miller & Thöni (1995) for eclogites from the Ötztal basement. Ladenhauf et al. (2001) interpreted this age as reflecting zircon growth during the Variscan high-pressure metamorphic overprint of the Cambrian protolith.

2.3.2. Ötztal basement

A pre-alpine metamorphic evolution has been recorded in the high-grade rocks of the Ötztal Complex (ÖC) (e.g., Miller & Thöni 1995, Thöny et al. 2008). The oldest metamorphic event within the ÖC has been recognized in migmatites of the Winnebach area, for which Klötzli-Chowanetz et al. (1997) and Thöny et al. (2008) estimated Ordovician/Silurian ages ranging between 490 ± 9 Ma (U-Pb zircon age) and 441 ± 18 Ma (U-Th-Pb monazite age). Sm-Nd garnet geochronology combined with Rb-Sr dating of mica constrained the age of the high-pressure imprint in ÖC during the Variscan orogeny at c. 350 Ma and Variscan cooling ages at c. 310 Ma (Miller & Thöni 1995, Neubauer et al. 1999a, Thöni 1999). Hoinkes et al. (1982) determined maximum Variscan temperatures of 670 °C in the northern part of the ÖC. Sm-Nd dating of eclogites from the central Ötztal yielded Variscan ages of ~370-340 Ma under P-T conditions of 2.7 GPa and 730 °C (Miller & Thöni 1995).

2.3.3. Texel complex

The Texel complex is the westernmost exposure of high-pressure rocks of the Eoalpine high-pressure belt. HP conditions of 1.2-1.4 GPa and 560-620 °C were estimated for the eclogite-facies overprint (Hoinkes et al. 1991, Habler et al. 2006). Zanchetta et al. (2013) proposed UHP metamorphic conditions of 2.65-2.90 GPa and 630-690 °C, based on high Si-content in the matrix phengites as well as K-feldspar and phengite lamellae within omphacite. Dating of the eclogites is rather difficult, because the garnets are inclusion-rich and display two growth stages. Whether or not these growth stages are part of the same metamorphic cycle is still controversial. However, U-Pb zircon dating as well as Sm-Nd garnet data constrain eclogite-facies metamorphism at 85 ± 4 and 85.2 ± 4.6 Ma, respectively (Habler et al. 2006, Zanchetta 2007). These results are in line with the Rb-Sr and Ar-Ar mica ages from eclogite host rocks (e.g., Sölva et al. 2001, Thöni 1983). The consistent mica cooling ages indicate that temperatures of ≤300 °C were reached close to 70 Ma (Thöni 1999).

To the north and north-west the Texel complex is bounded by the Schneeberg Complex, which comprises mainly metapelites, marbles and quartzites. It is interpreted as Palaeozoic sedimentary sequence that experienced only Eoalpine metamorphism up to amphibolite-facies conditions (Hoinkes et al. 1987, Konzett & Hoinkes 1996). The

transition between Texel and Schneeberg complexes is marked by the Schneeberg Normal Fault Zone, along which the Texel HP unit in the footwall has been interpreted to be exhumed by tectonic extrusion (Sölva et al. 2005). Sm-Nd geochronology on garnet micaschists from Texel and Schneeberg complexes, performed by the same authors, indicates that exhumation started around 95 Ma, which is not in agreement with the high-pressure ages of c. 85 Ma, obtained by Habler et al. (2006).

2.3.4. Ulten zone

The Ulten zone in the Tonale nappe comprises migmatitic gneisses associated with lenses of eclogite and garnet peridotite (Godard et al. 1996, Hauzenberger et al. 1996, Obata & Morten 1987, Tumiati et al. 2003). P-T conditions for the high-pressure metamorphism were estimated at 1.5 GPa and 600-850 °C (Godard et al. 1996). Sm-Nd geochronology, applied to the above mentioned rock types, yielded ages of c. 330 Ma for the Variscan high-pressure and high-temperature event (Tumiati et al. 2003). The similar ages for the high-grade metamorphism and the partial melting were interpreted to represent an episode of crustal subduction at the end of the Variscan orogenic cycle.

2.3.5. Schobergruppe

Linner (1999) determined HP metamorphic conditions of 1.6-1.8 GPa and 630-690 °C in the eclogites from the Prijakt-Barrenle See area. Sm-Nd and Rb-Sr data of eclogites indicate that the Eoalpine pressure peak occurred at c. 115 Ma, followed by amphibolite facies recrystallization before 86 Ma. In contrast, Schulz (1993) interpreted the eclogites to be Variscan. Recently, Hauke et al. (2019) applied Lu-Hf geochronometry on two eclogite samples from the same area. They obtained a minimum age of 313.3 ± 1.8 Ma for one of the samples and a maximum age of 96.92 ± 0.82 Ma for the other sample, showing that the rocks in this area experienced eclogite-facies metamorphism twice, during the Variscan and the Eoalpine cycle. Thermodynamic modelling, performed by the same authors, resulted in Alpine peak pressure conditions of c. 1.9 GPa and 650 °C.

2.3.6. Kreuzeckgruppe

In the northern part of Kreuzeckgruppe, Eoalpine eclogites crop out in the cores of big garnet amphibolite bodies (Polinik unit, Hoke 1990). In a tourmaline-bearing eclogite Konzett et al. (2012) determined P-T conditions of 2.1 GPa and 650-680 °C, together with U-Pb zircon ages of 86 ± 1 and 109 ± 2 Ma, which are in line with the Eoalpine HP ages

from Saualpe, Koralpe and Pohorje to the east (Sandmann et al. 2016, Thöni 2006 and references therein, Thöni et al. 2008).

2.3.7. Millstatt Complex

Only relics of eclogites are preserved within the Millstatt Complex (Schuster & Frank 1999, Teiml 1996). Thermobarometric data indicate HP conditions of at least 1.2-1.3 GPa and 580–600 °C for the Millstatt Complex (Teiml 1996). Schuster & Frank (1999) obtained a Sm-Nd garnet age of 100.6 ± 6.3 Ma from paragonite-bearing amphibolites and interpreted it to be related to the high-pressure imprint of the rocks. In addition, garnet from quartz- and feldspar-rich metapelite shows a Sm-Nd age of 84 ± 6 Ma, reflecting the crystallisation of the late-kinematic garnet (Schuster & Frank 1999).

2.3.8. Saualpe

The polymetamorphic Saualpe complex comprises eclogites embedded in high-grade paragneisses (e.g., Tenczer & Stüwe 2003). The gabbroic protoliths have N-MORB affinity and are of Permian age (Thöni & Jagoutz 1992, Miller & Thöni 1997, Miller et al. 2007). The Eclogite unit of Saualpe includes the localities Kupplerbrunn, Prickler Halt, Gertrusk, Kirchberg, Wolfsberg, Grünburg etc. It is characterized by well proven Eoalpine eclogite-facies metamorphic imprint. The peak conditions reached up to 2.2 GPa and 630-740 °C (Thöni et al. 2008 and references therein). Similar P-T conditions of 1.8 GPa and 690 °C have been reported from high-grade micaschists (Thoni & Miller 2010). Sm-Nd and Lu-Hf ages obtained from kyanite-bearing and kyanite-free eclogites range between c. 94 and 89-87 Ma (e.g., Miller 1990, Miller et al. 2005a, Thöni & Jagoutz 1992, Thöni & Miller 1996, Thöni et al. 2008).

2.3.9. Koralpe

Similar to the adjacent Saualpe, the Koralpe complex is dominated by eclogite-facies rocks with Alpine metamorphic overprint. Investigation of the almost unaltered gabbroic protoliths from the localities Bärofen and Gressenberg resulted in Sm-Nd age of 255 ± 22 Ma (Miller & Thöni 1997, Miller et al. 2005a, Thöni & Jagoutz 1992).

Sm-Nd dating of eclogites from the localities Hohl, Bärofen, Mauthnereck and Krumbachgraben yielded ages between 108.7 ± 8.8 and 91.4 ± 6.7 Ma (Lichem et al. 1997, Miller & Thöni 1997, Miller et al. 2005a, Thöni & Jagoutz 1992). Dating of the HP

metapelites resulted in slightly younger ages between 89.5 ± 2.7 and 85.9 ± 1.2 Ma (Miller & Thöni 1997, Miller et al. 2005a).

Based on geochemical and petrological data Miller (1990) distinguished two different types of eclogites in the Koralpe-Saualpe region: (1) quartz-rich eclogites and (2) kyanite-rich eclogites. Both types are derived from N-MORB-type gabbroic protolith, but represent different fractionation stages of the igneous source. The quartz-rich eclogites are enriched in FeO and TiO_2 and usually are kyanite-free. They indicate formation from basaltic liquids with normal MORB-affinities. The kyanite-rich eclogites, on the other hand, are characterized by high MgO and Al_2O_3 and low TiO_2 contents. They are derived from plagioclase-rich cumulates of the same gabbroic rock-suite.

2.3.10. Pohorje Mountains

The Pohorje Mountains comprise the south-easternmost high-grade rocks of the Eoalpine high pressure belt. The HP and UHP rocks include eclogites and garnet peridotites (3-4 GPa and 710-940 °C; Janák et al. 2004, 2006, Vrabec et al. 2012) as well as microdiamond-bearing gneisses (≥3.5 GPa and 800-850 °C; Janák et al. 2015). Late Cretaceous age for the HP metamorphism has been documented by various geochronological studies. U–Pb zircon dating of eclogites and metapelites yielded ages between c. 93 and c. 90 Ma (Janák et al. 2009, Miller et al. 2005b). These ages are identical to the Sm–Nd garnet ages and one Lu–Hf garnet age of eclogites, determined by Miller et al. (2005b) and Thöni et al. (2008). Sandmann et al. (2016) obtained ages of 96.6 ± 1.2 and 94.8 ± 5.1 Ma for the eclogites and 91.6 ± 4.1 Ma for the garnet peridotite and interpreted the age results to be related to the burial of the rocks. Taken together, the UHP stage in Pohorje took place between 97 and 90 Ma.

2.3.11. Speik Complex

Metamorphosed ultramafic and mafic rocks with rare lenses of retrogressed eclogite occur in the Speik Complex, east of Tauern Window (e.g., Faryad et al. 2002, Melcher & Meisel 2004, Neubauer & Frisch 1993). In the Hochgrössen Massif, early or pre-Variscan eclogite-facies conditions were determined in metabasites (1.8-2.2 GPa and 700 °C). $^{40}Ar/^{39}Ar$ dating of edenitic hornblende in textural equilibrium with omphacite in the eclogites yielded an age of 397.3 ± 7.8 Ma (Faryad et al. 2002), which is interpreted to be a minimum age for metamorphism in the area. This would suggest that the Speik Complex

in the Austroalpine basement east of the Tauern Window represents remnants of the oldest eclogite-facies units preserved in the Eastern Alps.

2.3.12. Sieggraben

Sieggraben is an eclogite-bearing tectonic melange within the Austroalpine basement on the border of the Eastern Alps, south of Vienna. The eclogites are the north-easternmost exposure of high-grade rocks in the Eastern Alps. Neubauer et al. (1999b) estimated peak conditions of 1.4-1.5 GPa and 670-750 °C. $^{40}Ar/^{39}Ar$ dating of hornblende was conducted by the same authors and yielded ages between c. 136 and 108 Ma. These were interpreted to represent different stages of decompressional retrogression following the HP event (Neubauer et al. 1999b). Additionally, Kromel et al. (2011) defined a new P-T path for the eclogites, in which peak pressure conditions were reached at 1.6-1.7 GPa and 610-650 °C.

For the purposes of this study eclogite samples were collected from Texel unit, Saualpe, Koralpe and Sieggraben. The exact coordinates of the sample localities are presented in Table 2.1.

2.4. Analytical methods

Some of the isotope dilution measurements were performed on the ThermoFisher Neptune MC-ICPMS at University of Cologne. All other measurements and analyses were concluded at Steinmann Institute, Bonn. A detailed description of all methods can be found in Chapter 1.4.

2.5. Results

2.5.1. Petrography and mineral chemistry

Representative microprobe analyses of minerals from the investigated samples are listed in Table 2.2. Additional garnet X-ray maps as well as compositional profiles of every sample are presented in the Appendix.

2.5.1.1. Koralpe

Sample Ho1: quartz-rich eclogite, Hohl

Sample Ho1 is a medium- to coarse-grained eclogite composed of garnet, clinopyroxene, clinozoisite, amphibole and quartz. Accessory rutile, ilmenite and apatite are also present. Retrogression is locally restricted and documented by symplectites of Na-poor clinopyroxene, calcic amphibole and sodic plagioclase around omphacite (Fig. 2.2).

Garnet crystals are anhedral and reach up to 1.5 mm in size. Usually the garnet cores contain inclusions of quartz, rutile and apatite, but may also be inclusion-free. The overall composition of garnet is $Alm_{44-51}Prp_{22-30}Grs_{22-29}Sps_{0.5-2.1}$. High-resolution X-ray maps reveal a patchy chemical zonation with respect to the major element composition (Fig. 2.3). However, the garnet cores display slightly elevated Mn- and Ca-components, which can be interpreted as prograde growth type of zonation. Lu concentration profiles display bell-shaped distribution through the garnet (Fig. 2.3), suggesting that Lu diffusion after the garnet growth was only limited or absent.

Omphacite occurs as large anhedral crystals in the matrix and is unzoned. The jadeite component in omphacite varies between 39 and 41 wt%. Locally, diopside-rich clinopyroxene (Jd_{12}) together with Na-rich plagioclase (An_{14-17}) and calcic amphibole form symplectitic rims around omphacite.

Amphibole is a minor phase and occurs as poikiloblasts or intergrowths in symplectites replacing omphacite. Both varieties have pargasitic composition with Al_2O_3 contents varying between 13.17 and 14.08 wt% and Na_2O of 3.47-3.89 wt%.

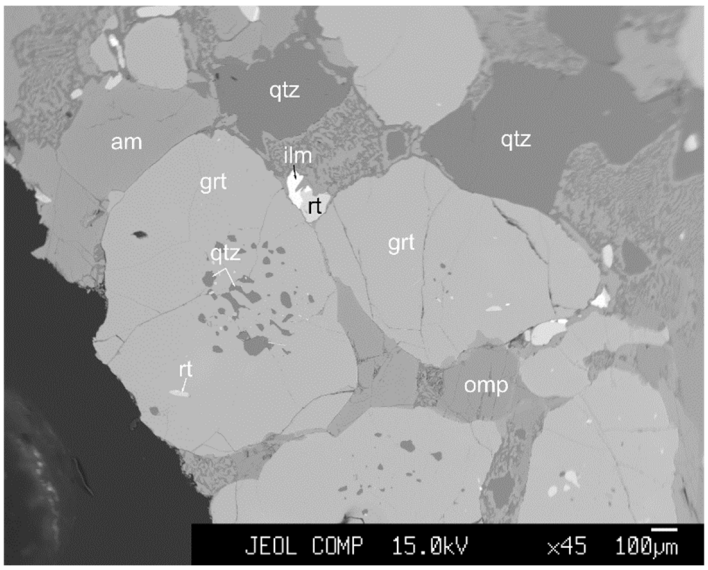

Fig. 2.2. Back-scattered electron (BSE) image of the eclogite sample Ho1. The matrix consists mainly of omphacite and quartz with minor amphibole, rutile and ilmenite. Inclusions in garnet are mostly quartz, rutile and apatite.

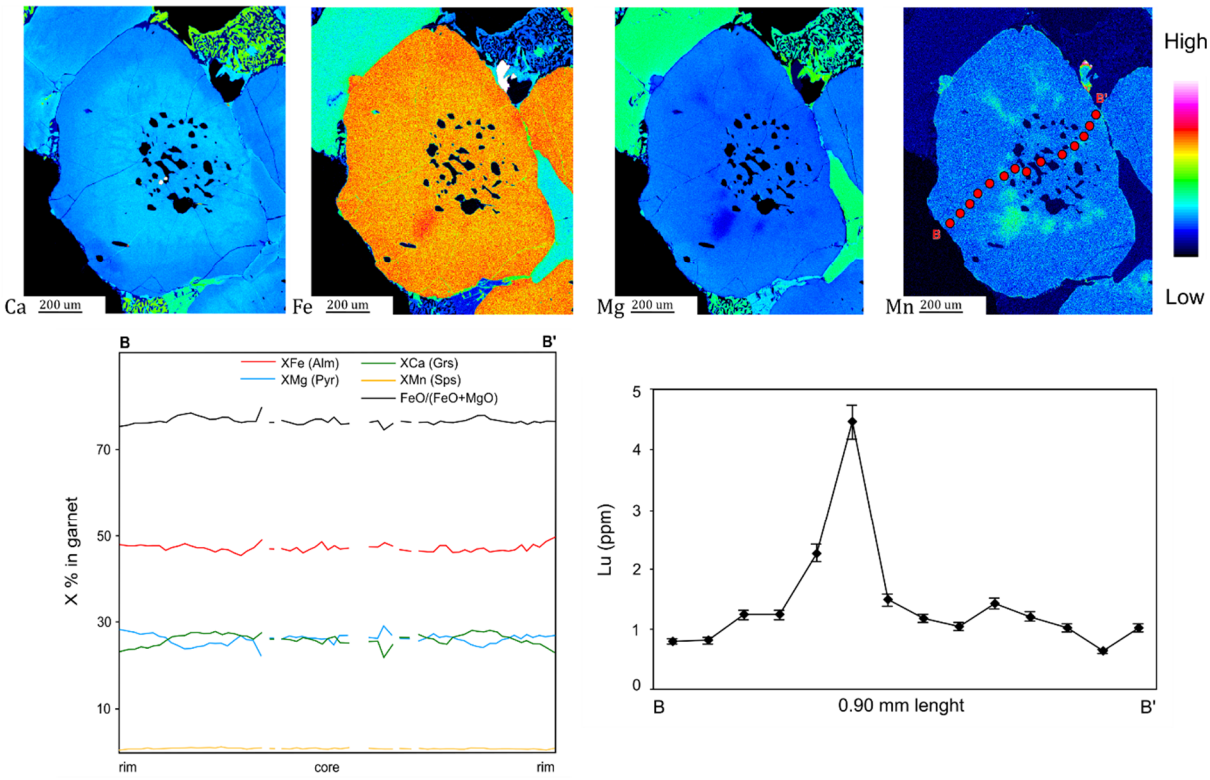

Fig. 2.3. Major element distribution maps of a representative garnet of sample Ho1. Compositional and Lu concentration profiles follow the trace B-B' indicated on the map. The bell-shaped pattern of Lu shows preserved prograde growth zonation.

Sample Ho2: kyanite-rich eclogite, Hohl

Sample Ho2 contains garnet, omphacite, clinozoisite, kyanite, quartz, amphibole and rutile (Fig. 2.4). Retrogressive alteration is very limited and locally restricted to narrow symplectite rims around omphacite consisting of Na-poor clinopyroxene + sodic plagioclase ± calcic amphibole.

The garnets are poikiloblastic with inclusions of omphacite, kyanite, amphibole, clinozoisite, quartz and minor rutile in the cores, whereas the rims are inclusion-free. The chemical composition of the garnets is near homogenous with little variation in content of the major elements ($Prp_{39-42}Alm_{34-37}Grs_{22-25}Sps_{0.4-0.8}$), which is also displayed by the compositional maps (Fig. 2.5). A slight increase of Fe at the garnet rims could reflect partial reequilibration during decompression.

Unzoned omphacite with jadeite content between 25 and 30 wt% occurs as single crystals in the matrix. Omphacite inclusions in garnet and quartz have the same composition as the matrix omphacite. Clinopyroxene in symplectites after omphacite is Na-poor and has diopside composition with up to 18 wt% jadeite component.

Amphibole occurs in the matrix and as inclusions in garnet. According to the classification of Hawthorne et al. (2012) the matrix amphibole is magnesio-hornblende with Al_2O_3 content ranging between 12.92 and 15.29 wt%. Pargasite is characterized by Al_2O_3 content of 13.08-13.92 wt%. It occurs as inclusions in garnet and commonly replaces omphacite in symplectites together with diopside and plagioclase. Kelyphitic amphibole replacing garnet at the rims displays very Al-rich composition with Al_2O_3 up to 21 wt%.

Clinozoisite with Fe_2O_3 content varying from 1.14 to 1.95 wt% occurs in textural equilibrium with omphacite and amphibole in the matrix. Clinozoisite enclosed by garnet has the same composition.

Kyanite is unaltered and occurs as prismatic, subhedral crystals in the matrix. Its composition is homogenous and contains 0.02-0.12 wt% Cr_2O_3 and 0.18-0.34 wt% Fe_2O_3 as main impurities. Numerous small needles of kyanite enclosed by garnet can contain up to 1.02 wt% Fe_2O_3.

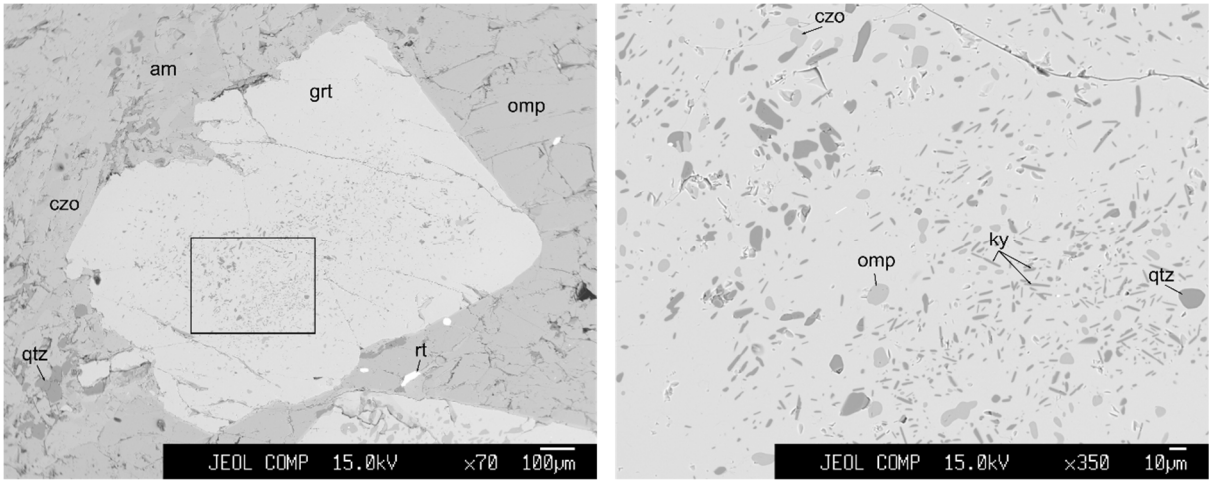

Fig. 2.4. BSE images of garnet and the surrounding matrix (left) from eclogite sample Ho2. The rectangle outlines close up of the inclusions in garnet (right). The matrix consists mainly of omphacite and clinozoisite as well as minor amphibole, quartz and rutile. Garnet encloses mostly kyanite, omphacite, clinozoisite and quartz.

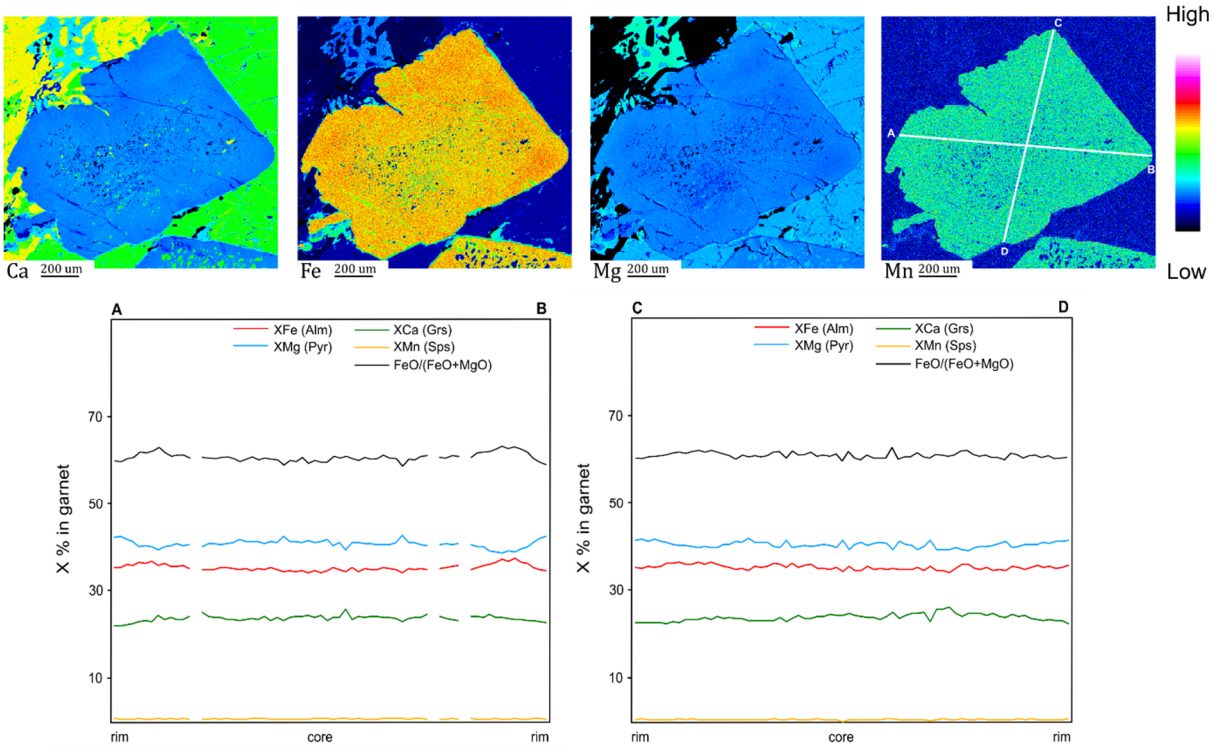

Fig. 2.5. Major element distribution maps of a representative garnet of sample Ho2. Compositional profiles follow the lines A-B and C-D indicated on the map. Maps and profiles show homogenized element distribution related to equilibrium during the thermal stage of metamorphism.

2.5.1.2. Saualpe

Samples Grü1 & Grü2: quartz-rich eclogite, Grünburger Bach

The eclogite from Grünburger Bach is coarse-grained and made up of garnet, omphacite, clinozoisite, quartz, rutile and apatite (Fig. 2.6). Weak retrogression is indicated by the breakdown of omphacite to symplectites composed of Na-poor clinopyroxene, sodic plagioclase and calcic amphibole.

Garnet crystals are anhedral to subhedral and reach up to 2.5 mm in size. The garnet is almandine-rich and may contain inclusions of quartz and rutile. X-ray maps of major elements as well as compositional profiles show typical prograde zoning with high spessartine- and grossular-components in the core, whereas the pyrope-component is increasing toward the rims (Fig. 2.7a and b). Bell-shaped distribution of Lu through the garnets confirms that the major element zoning pattern reflects garnet growth during peak conditions.

Omphacite is present as relative large anhedral crystals in the matrix. It contains 36 to 41 wt% jadeite in addition to 1-6 wt% acmite. These may contain inclusions of rutile, apatite and quartz. Omphacite is variably replaced by diopside-rich clinopyroxene (Jd_8) together with albite-rich plagioclase (An_{20}) and pargasitic amphibole.

Clinozoisite is abundant in the matrix and forms medium to small grains. Its composition varies between 2.02 and 2.63 wt% Fe_2O_3.

Amphibole forms poikiloblasts with pargasitic composition. It also occurs in narrow symplectite rims replacing omphacite. Pargasite shows Al_2O_3 content from 13.96 to 16.67 wt% and Na_2O of 3.48-4.17 wt%. In contact with garnet extremely Al-rich amphibole occurs with Al_2O_3 reaching up to 21 wt%.

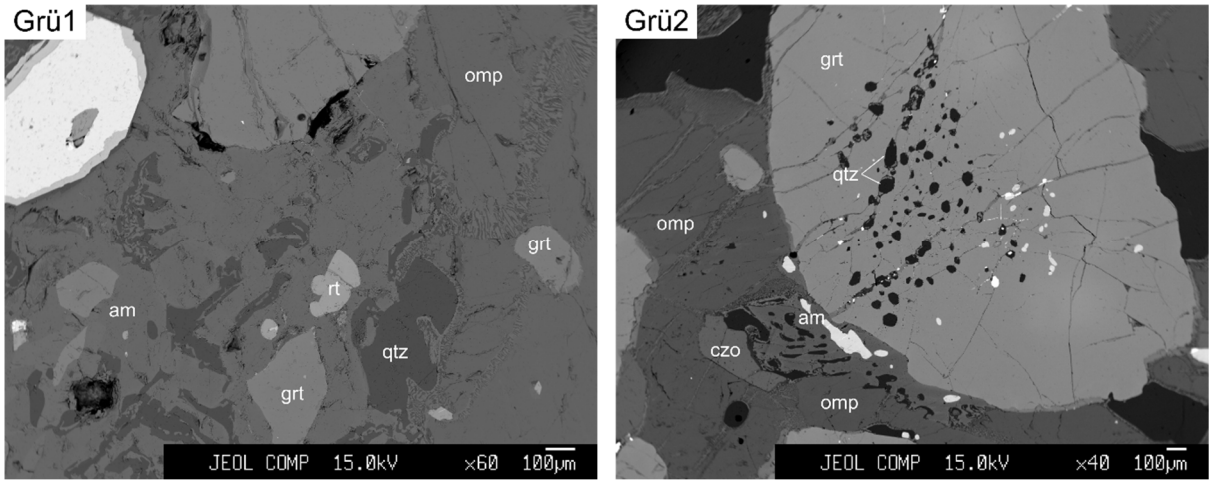

Fig. 2.6. BSE images of the dated eclogite samples Grü1 (left) and Grü2 (right). The matrix in both samples is made up of omphacite, clinozoisite, amphibole and quartz with minor rutile and ilmenite. Inclusions in garnet are mainly quartz and rutile.

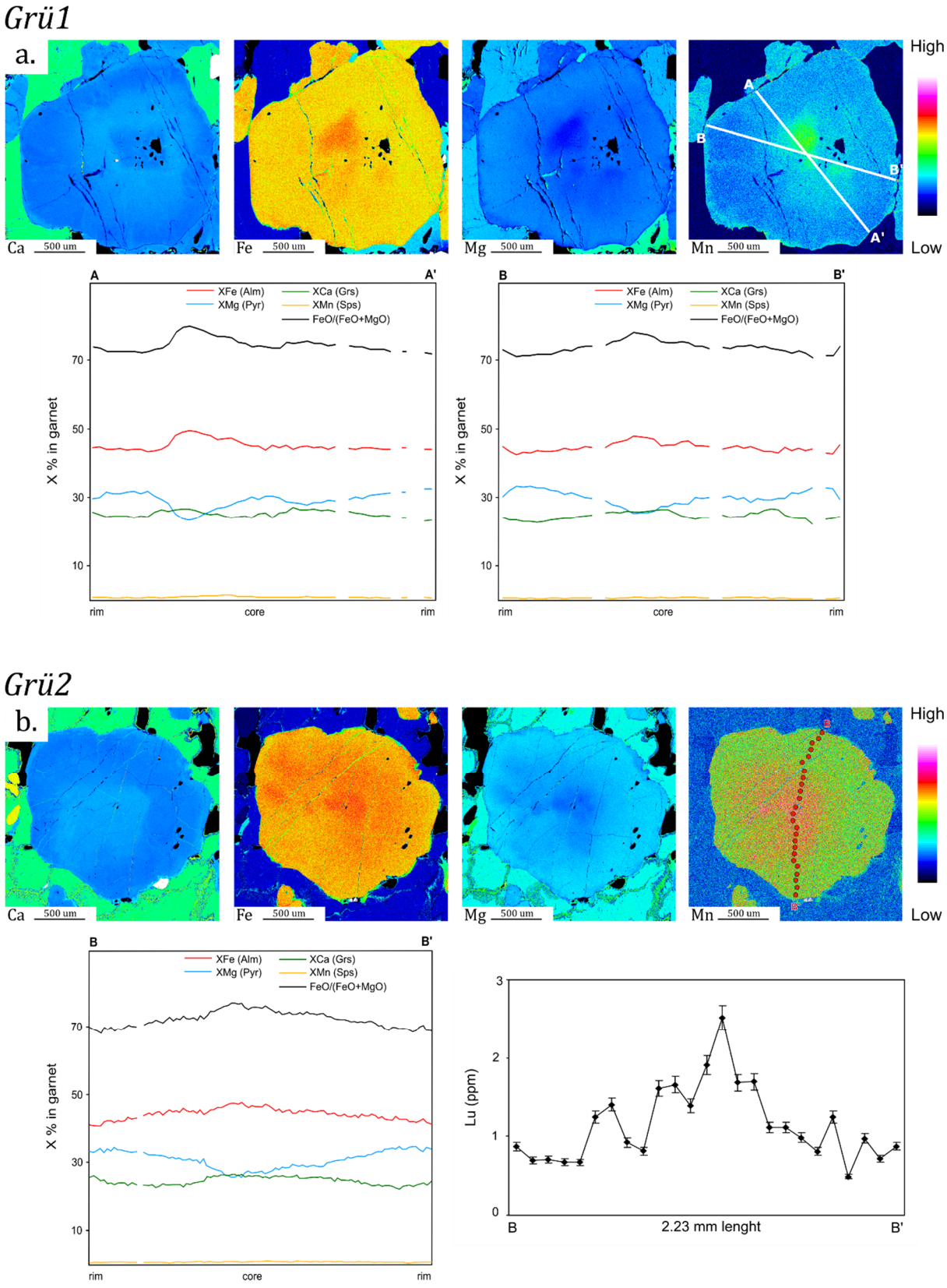

Fig. 2.7. Major element distribution maps of a representative garnets of samples (a) Grü1 and (b) Grü2. Compositional profiles in both samples as well as Lu concentration profile in garnet of sample Grü2 show bell-shaped distribution indicating prograde garnet growth.

Sample Wol1: quartz-rich eclogite, Wolfsberger Hütte

Sample Wol1 is a coarse-grained eclogite and consists of garnet, clinopyroxene, clinozoisite, amphibole, quartz, rutile, titanite and minor ilmenite (Fig. 2.8). Zircon and apatite are accessory phases.

Garnet crystals are anhedral to subhedral and can vary in size. Two types of grains can be identified within this sample: (1) smaller garnet crystals (< 1.5 mm) that reveal relatively weak and patchy compositional zoning, and (2) larger garnet crystals (< 3.5 mm) with more distinct compositional zoning (Fig. 2.9a and b, respectively). Altogether, garnet is almandine-rich and frequently contains inclusions of omphacite, quartz, rutile, titanite, clinozoisite and apatite. High-precision X-ray maps displaying the concentration of the major elements in garnet indicate typical prograde zoning with high X_{Mn} and Fe/(Fe+Mg) in the core and X_{Mg} increasing from core to rim. The overall composition of garnet is $Am_{45-52}Grs_{26-34}Prp_{14-26}Sps_{0.2-2.0}$. The Lu distribution in the smaller garnets shows a small central peak and enrichment in the rim domains, whereas the larger crystals display Lu peaks only close to the rims (Fig. 2.9a and b).

Omphacite is the second most abundant mineral phase after garnet. It is unzoned and occurs as large anhedral grains in the matrix as well as small inclusions in garnet. The composition of the omphacite displays 23 to 39 wt% jadeite in addition to 1-4 wt% acmite component. Occasionally, omphacite has been replaced by Na-poor clinopyroxene (Jd_{15}) + sodic plagioclase (An_{6-16}) + calcic amphibole.

Amphibole is present as poikiloblasts in the matrix or as intergrowths in symplectitic aggregates replacing omphacite. The composition of this amphibole is pargasite. It displays Al_2O_3 content between 12.97 and 16.22 wt% and less variable Na_2O between 2.97 and 3.88 wt%. Keliphitic amphibole containing up to 20 wt% Al_2O_3 occurs at the contact with garnet.

Clinozoisite appears in textural equilibrium with omphacite and garnet. Matrix clinozoisite as well as inclusions in garnet display similar compositions with Fe_2O_3 ranging between 1.25 and 2.52 wt%.

Ilmenite is the least abundant Ti-phase in this eclogite and occurs only in association with rutile. Pure rutile is present as inclusions in garnet, but also commonly occurs as irregular grains in the matrix. Locally, it is rimmed by titanite. The latter is frequent also as inclusion in garnet porphyroblasts. Thus, observations suggest a sequence ilmenite – rutile - titanite in line with a clockwise pressure-temperature evolution.

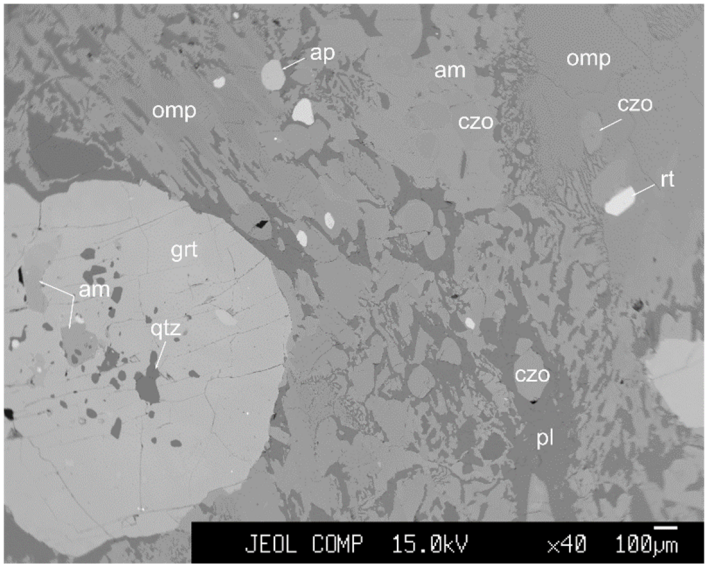

Fig. 2.8. BSE image of the eclogite sample Wol1 shows matrix consisting mainly of omphacite and clinozoisite as well as minor amphibole, quartz, rutile and apatite. Garnet encloses mainly quartz and rutile, but inclusions of apatite and amphibole are also present.

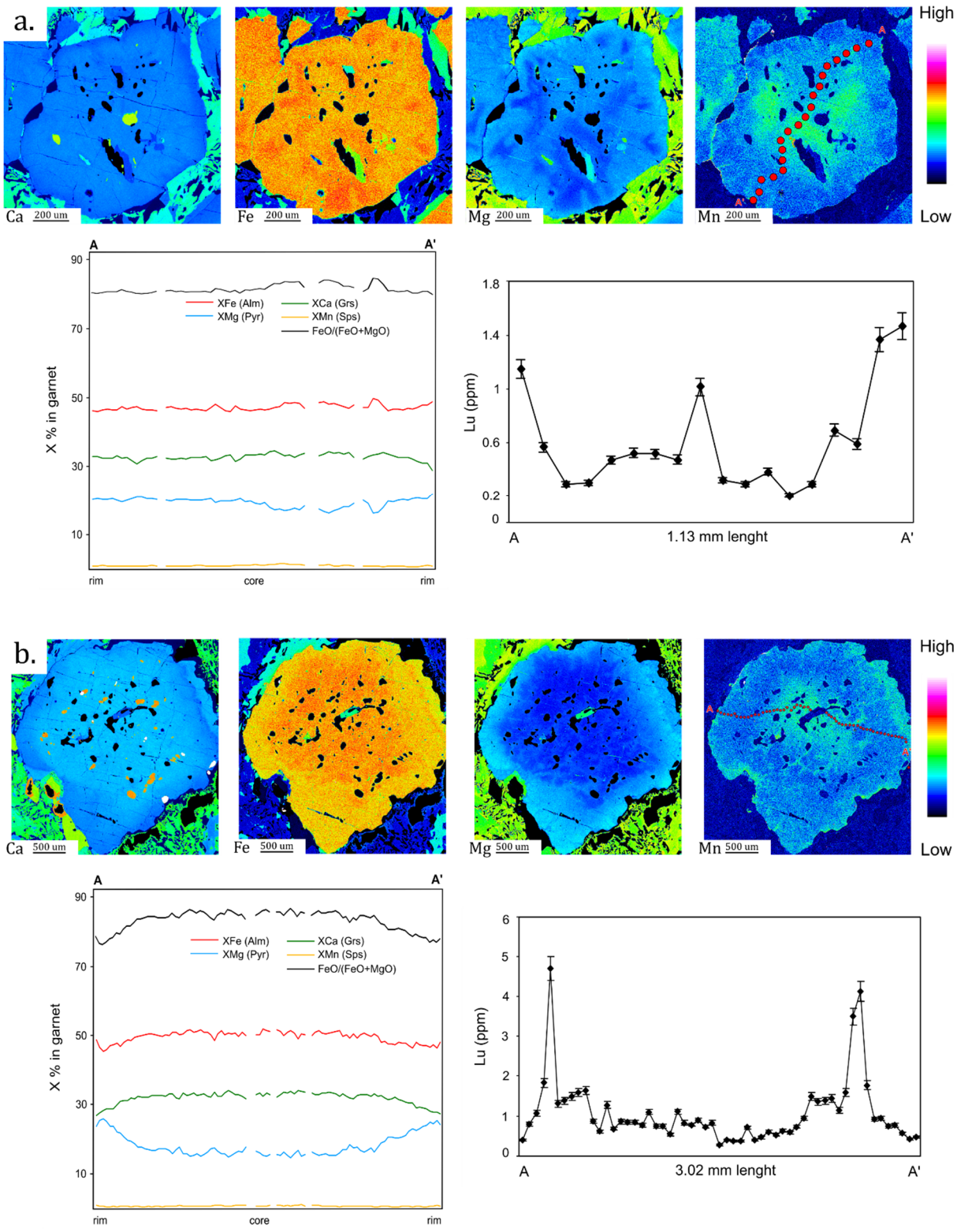

Fig. 2.9. Major element distribution maps of representative garnet crystals from sample Wol1. (a) Small garnet with patchy major element compositional zoning shows a bell-shaped distribution of Lu indicating prograde garnet growth. (b) Larger garnet crystals show prograde major element zoning, whereas Lu is concentrated near the rims. See text for details.

2.5.1.3. Sieggraben

Sample Sig3

The eclogite from Sieggraben is coarse-grained and contains garnet, clinopyroxene, amphibole, epidote, rutile, titanite, plagioclase, K-feldspar, quartz and calcite.

Garnet crystals are anhedral to subhedral and reach up to 2.5 mm in size. Garnet is almandine-rich and encloses amphibole, plagioclase, epidote, K-feldspar, quartz, rutile, titanite and ilmenite. The chemical zoning is distinct and is characterized from core to rim by increasing pyrope- and almandine components, whereas the grossular- and spessartine-components are decreasing (Fig. 2.10). The overall composition of garnet is $Am_{49-55}Grs_{26-34}Prp_{11-21}Sps_{0.3-5.0}$. The Lu distribution in garnet as well as that of the other heavy REEs shows high concentrations near the garnet rims and missing central peak (Fig. 2.10). In contrast, the distributions of Hf and the light REEs display bell-shaped profiles, suggesting limited diffusion after garnet growth (Fig. 2.10).

Small omphacite crystals with jadeite component of c. 24 wt% occur in the matrix (Fig. 2.11). Most of the omphacite was replaced by symplectites of diopside-rich clinopyroxene (Jd_{9-16}) and albite-rich plagioclase (An_{10-20}) during a stage of retrograde overprint.

Calcic amphibole occurs as poikiloblasts, but also as narrow symplectitic intergrowths replacing omphacite. Amphibole displays Al_2O_3 content varying between 10.44 and 17.97 wt%. The Na_2O content ranges from 2.31 to 3.16 wt%. Keliphitic amphibole replacing garnet shows Al_2O_3 of at least 19 wt%.

Epidote occurs as single grains in textural equilibrium with garnet and amphibole (Fig. 2.11). The Fe_2O_3 content ranges from 7.64 to 8.46 wt%. Epidote inclusions in garnet contain up to 15.31 wt% Fe_2O_3.

Plagioclase and K-feldspar occur as inclusions in garnet as well as in clinopyroxene + amphibole + plagioclase symplectites formed by replacement of omphacite and garnet.

Rutile and ilmenite are abundant in the matrix and occur as irregular grains. Rutile inclusions in garnet are present as single grains or partly replaced by titanite. Titanite is mainly present as single inclusion in garnet. Associations of titanite, rutile and ilmenite also occur.

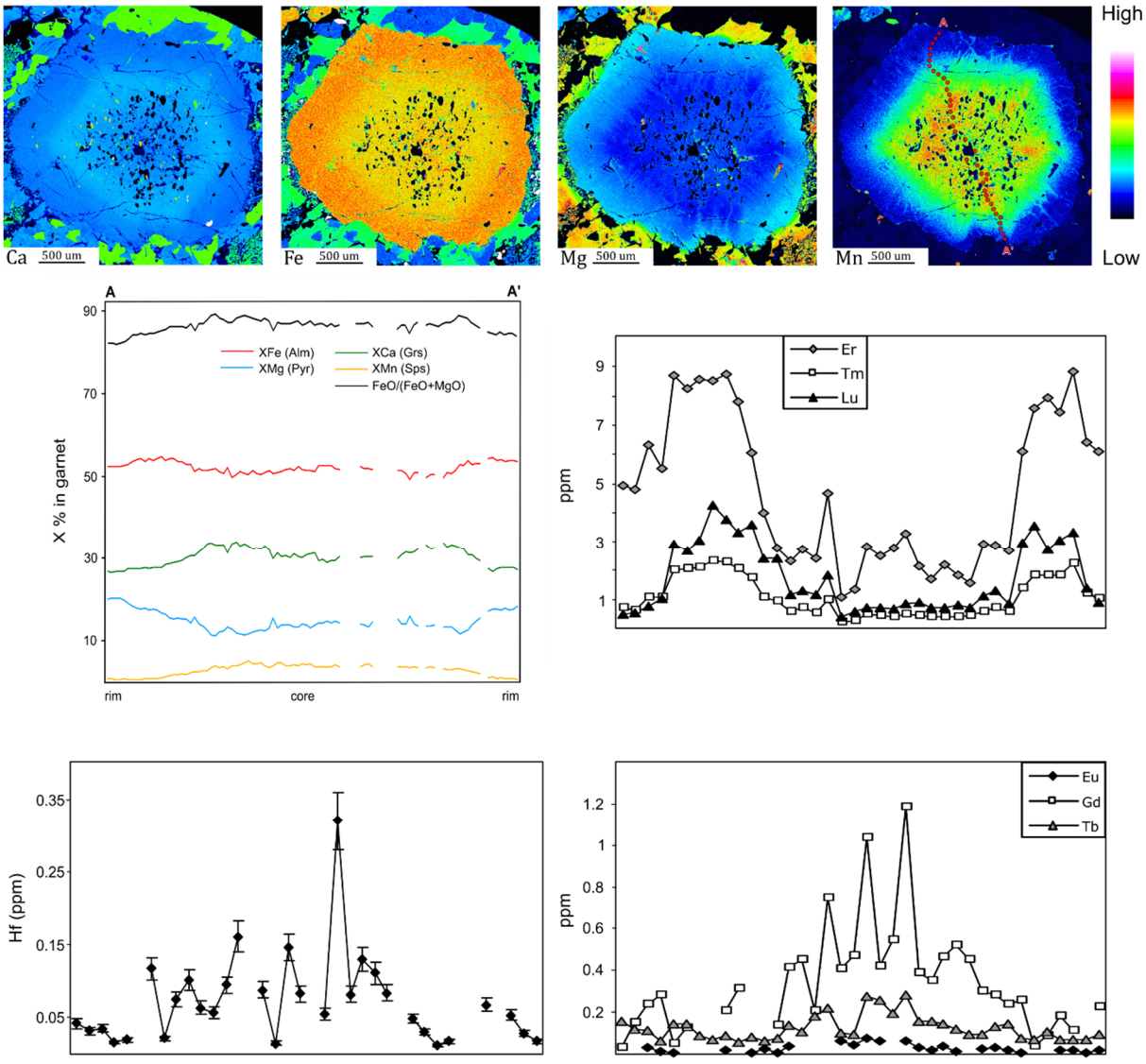

Fig. 2.10. Major element distribution maps of a representative garnet from sample Sig3. Compositional profiles as well as Hf and some LREE (Eu, Gd, Tb) concentration profiles show bell-shaped distribution indicating prograde garnet growth. The distribution of HREE (Er, Tm, Lu) shows elevated concentrations near the garnet rims, whereas a central peak is missing. See text for details.

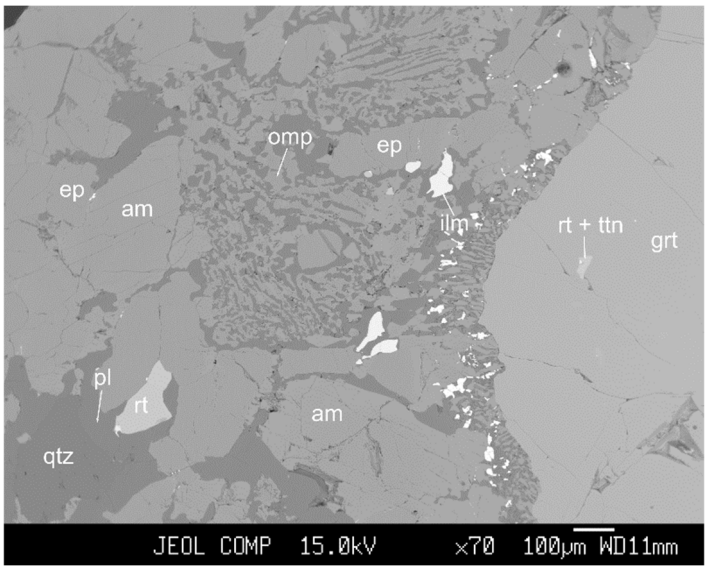

Fig. 2.11. BSE image of the dated eclogite sample Sig3. The matrix consists of omphacite, amphibole, epidote and quartz. Rutile, titanite and ilmenite as well as symplectites composed of Na-poor clinopyroxene + amphibole + plagioclase are also present.

2.5.1.4. Texel complex

Sample Sal1, Saltaus valley

Sample Sal1 is fine- to medium-grained eclogite composed of garnet, omphacite, amphibole, rutile, ilmenite, quartz and minor titanite and epidote. Fine-grained symplectites locally replace omphacite in the matrix (Fig. 2.12). They are made up of diopside-rich clinopyroxene, plagioclase and calcic amphibole. Accessory zircon can be found as single grains in the matrix and as inclusions in garnet. The eclogite displays weak foliation defined by elongated omphacite and aligned amphibole.

The garnets are subhedral to anhedral and reach up to 1 mm in size. They are almandine-rich and show clearly two growth stages (Fig. 2.13). Idiomorphic Grt 1 displays compositional zoning with high spessartine (Sps) and grossular (Grs) components in the core and increasing Mg-content (Prp) toward the rims. The overall composition of Grt 1 is $Alm_{53\text{-}65}Grs_{15\text{-}35}Prp_{8\text{-}20}Sps_{0.5\text{-}2.4}$. An abrupt change in chemical composition marks the second garnet growth stage (Grt 2). It is characterized by sharp increase in Ca-content, as well as decrease in Mg- and Fe-contents relative to the rims of Grt 1 (Table 2.2). Inclusions of omphacite, quartz, amphibole, rutile, titanite, epidote, plagioclase, zircon, and apatite are abundant in Grt 1 and along the boundary between Grt 1 and Grt 2. Grt 2 is inclusion-free. The distribution of Lu mimics well the zoning of the Ca and Mn in garnet (Fig. 2.13).

The core of Grt 1 is characterized by the highest Lu concentrations, which decrease toward Grt 2, where it is increasing again.

Omphacite comprises large, anhedral crystals in the matrix with 37-48 wt% Jd component. They are unzoned and may contain inclusions of quartz and amphibole. Smaller aggregates among the symplectitic matrix have lower Jd component that ranges between 25-34 wt% (Fig. 2.12; Table 2.2). Larger and smaller omphacite crystals with the same compositions are also included in garnet. Locally, symplectites of diopside-rich clinopyroxene and albite-rich plagioclase (An_{2-8} and rarely An_{13-18}) replace omphacite in the matrix. The symplectitic diopside contains 19-21 wt% of jadeite.

Amphibole with katophorite composition (Hawthorne et al. 2012) occurs in textural equilibrium with omphacite and garnet in the matrix, indicating crystallization during high-pressure conditions. Its Al_2O_3 content ranges between 10.35 and 13.32 wt% and Na_2O reaches up to 4.74 wt% (Table 2.2). The retrogressive amphiboles have pargasitic composition. They form intergrowths in symplectites together with plagioclase and clinopyroxene, or replace coarse-grained primary amphiboles. Extremely Al-rich amphiboles (up to 20 wt% Al_2O_3) are developing in rims at the contact with garnet and can be interpreted as reaction products from garnet during decompression. Most of the amphibole inclusions in garnet are pargasite and rarely kataphorite with compositions similar to the matrix amphiboles, suggesting that pargasite inclusions actually reflect reequilibrated inclusions.

Rutile is abundant as inclusions in garnet. In the matrix rutile occurs as single grains or is replacing ilmenite. Sometimes both phases are rimmed by titanite. Inclusions of pure titanite are observed mainly in the garnet core, while matrix titanite is always associated with ilmenite and rutile. Hence, observations suggest a growth sequence of the Ti-phases such as ilmenite => rutile => titanite, which is in line with a clockwise pressure-temperature evolution.

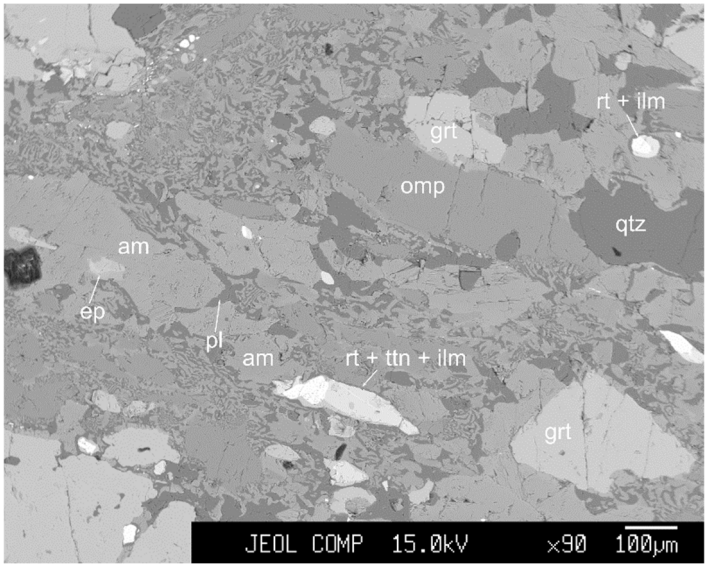

Fig. 2.12. BSE image of the eclogite sample Sal1. The matrix is mainly composed of omphacite and amphibole, but also quartz, epidote, rutile, titanite and ilmenite are abundant.

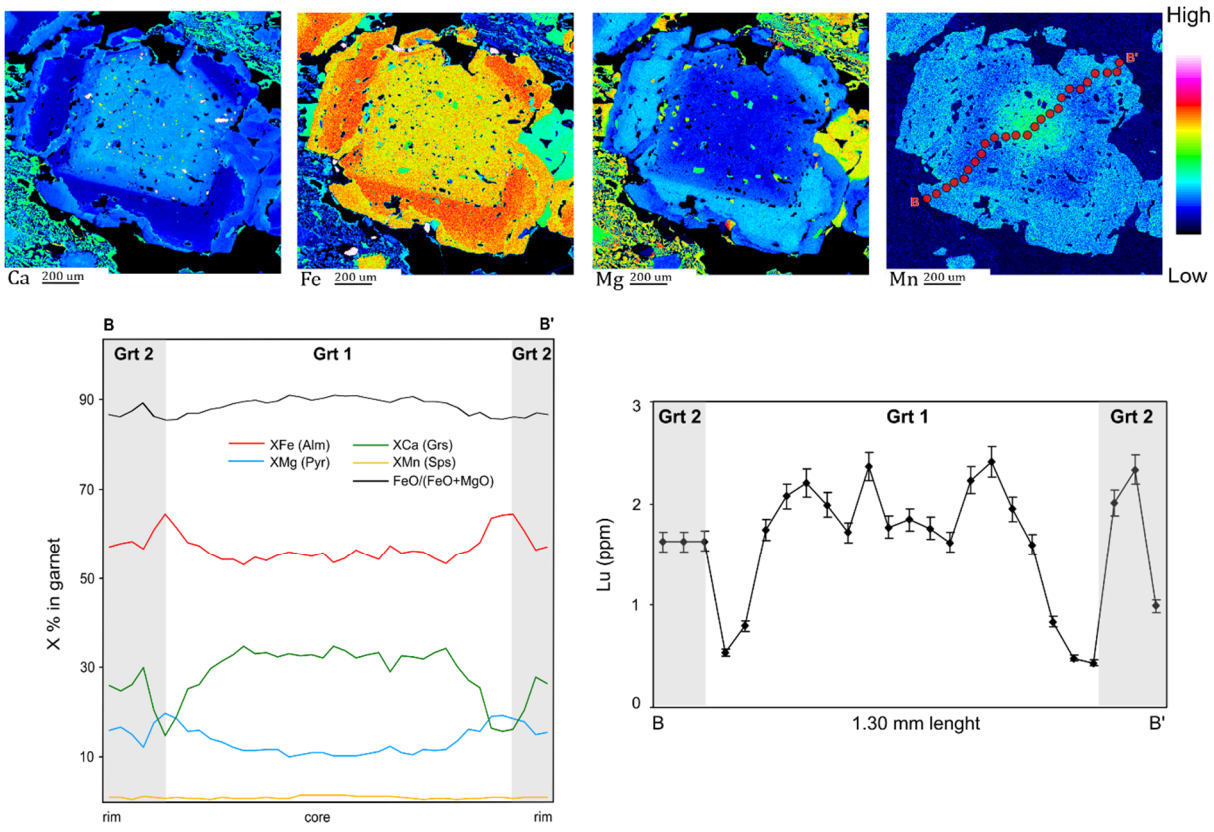

Fig. 2.13. Major element distribution maps of a representative garnet from sample Sal1. Compositional and Lu concentration profiles follow the trace B-B' indicated on the map. They clearly show the presence of two growth phases (Grt 1 and Grt 2). The bell-shaped pattern of Lu indicates preserved prograde growth zonation.

Sample	**Ho1**	**Ho1**	**Ho1**	**Ho1**	**Ho1**	**Ho1**	**Ho2**	**Ho2**	**Ho2**	**Ho2**	**Ho2**	**Ho2**	**Ho2**	**Grü1**	**Grü1**	**Grü1**	**Grü1**	**Grü1**	**Grü1**
Mineral	Grt rim	Grt core	Omp/ mtx	Cps/ sympl	Am	Pl	Grt rim	Grt core	Omp/ mtx	Cps/ sympl	Am	Ep/Czo	Pl	Grt rim	Grt core	Omp/ mtx	Cps/ sympl	Am	Pl
SiO_2	39.25	39.07	55.06	53.46	43.58	65.26	40.16	39.86	54.84	52.92	46.37	39.09	63.40	40.94	38.50	54.12	52.25	43.38	63.80
TiO_2	0.05	0.06	0.09	0.04	0.73	0.00	0.05	0.05	0.15	0.10	0.62	0.05	0.06	0.07	0.07	0.18	0.22	0.57	0.00
Al_2O_3	21.46	21.43	10.56	2.19	13.17	22.19	22.94	22.94	8.63	5.79	15.29	32.32	23.08	19.35	21.95	11.10	7.84	16.67	23.51
FeO/Fe_2O_3	22.70	21.97	5.21	9.01	13.19	0.18	16.94	16.13	2.54	3.72	6.42	1.29	0.06	21.25	21.55	4.48	5.55	0.02	0.20
MnO	0.25	0.46	0.04	0.09	0.06	0.01	0.22	0.21	0.01	0.01	0.06	0.01	0.00	0.26	0.32	0.00	0.01	0.01	0.03
MgO	7.37	6.41	8.92	12.15	12.67	0.00	11.37	11.01	11.98	13.63	15.36	0.07	0.01	9.10	7.40	9.05	11.34	10.79	0.01
CaO	8.51	10.05	14.38	20.88	10.42	2.64	8.22	8.98	18.57	21.97	10.99	23.82	4.24	8.29	9.60	14.91	19.71	12.34	3.75
Na_2O	0.06	0.07	6.08	1.97	3.47	10.19	0.01	0.05	3.94	1.82	2.63	0.00	9.34	0.02	0.06	5.73	3.05	9.64	9.81
K_2O	0.01	0.01	0.01	0.00	0.41	0.03	0.01	0.00	0.01	0.00	0.20	0.00	0.08	0.01	0.03	0.01	0.00	4.17	0.03
Cr_2O_3	0.06	0.03	0.00	0.04	0.01	0.04	0.08	0.01	0.11	0.06	0.07	0.04	0.00	0.01	0.00	0.06	0.03	0.14	0.01
Sum	99.70	99.55	100.34	99.84	97.71	100.54	100.00	99.23	100.77	100.02	98.00	96.68	100.26	99.29	99.48	99.63	100.00	97.74	101.15
Si	6.04	6.04	1.97	1.99	6.38	2.86	5.98	5.98	1.95	1.92	6.50	3.01	2.80	6.27	5.94	1.94	1.91	6.25	2.79
Ti	0.01	0.01	0.00	0.00	0.08	0.00	0.01	0.01	0.00	0.00	0.07	0.00	0.00	0.01	0.01	0.00	0.01	0.06	0.00
Al	3.89	3.90	0.44	0.10	2.27	1.15	4.03	4.05	0.36	0.25	2.53	2.93	1.20	3.49	3.99	0.47	0.34	2.83	1.21
Fe	2.92	2.84	0.16	0.28	1.62	0.01	2.11	2.02	0.08	0.11	0.75	0.07	0.00	2.72	2.78	0.13	0.17	1.20	0.01
Mn	0.03	0.06	0.00	0.00	0.01	0.00	0.03	0.03	0.00	0.00	0.01	0.00	0.00	0.03	0.04	0.00	0.00	0.00	0.00
Mg	1.69	1.48	0.47	0.68	2.77	0.00	2.52	2.46	0.63	0.74	3.21	0.01	0.00	2.08	1.70	0.48	0.62	2.65	0.00
Ca	1.40	1.66	0.55	0.83	1.64	0.12	1.31	1.44	0.71	0.86	1.65	1.96	0.20	1.36	1.59	0.57	0.77	1.49	0.18
Na	0.02	0.02	0.42	0.14	0.99	0.87	0.00	0.01	0.27	0.13	0.71	0.00	0.80	0.01	0.02	0.40	0.22	1.20	0.83
K	0.00	0.00	0.00	0.00	0.08	0.00	0.00	0.00	0.00	0.00	0.04	0.00	0.00	0.00	0.01	0.00	0.00	0.03	0.00
Cr	0.01	0.00	0.00	0.00	0.00	0.00	0.01	0.00	0.00	0.00	0.01	-	0.00	0.00	0.00	0.00	0.00	0.00	0.00
Sum	16.01	16.01	4.02	4.03	15.82	5.00	16.00	16.00	4.00	4.01	15.47	7.99	5.00	15.98	16.07	4.01	4.03	15.72	5.02
O	24.00	24.00	6.00	6.00	22.00	8.00	24.00	24.00	6.00	6.00	22.00	12.50	8.00	24.00	24.00	6.00	6.00	22.00	8.00
Xalm	0.48	0.47	-	-	-	-	0.35	0.34	-	-	-	-	-	0.44	0.46	-	-	-	-
Xgrs	0.23	0.28	-	-	-	-	0.22	0.24	-	-	-	-	-	0.22	0.26	-	-	-	-
Xprp	0.28	0.24	-	-	-	-	0.42	0.41	-	-	-	-	-	0.34	0.28	-	-	-	-
Xjd	-	-	0.41	0.11	-	-	-	-	0.29	0.15	-	-	-	-	-	0.41	0.22	-	-

Table 2.2. Representative microprobe analyses of eclogite minerals in wt% and p.f.u. Fe is calculated as Fe^{2+}, except for epidote/clinozoisite where Fe is Fe^{3+}.

Sample	**Grü2**	**Grü2**	**Grü2**	**Grü2**	**Grü2**	**Grü2**	**Wol1**	**Wol1**	**Wol1**	**Wol1**	**Wol1**	**Wol1**	**Wol1**	**Sig3**	**Sig3**	**Sig3**	**Sig3**	**Sig3**	**Sig3**	**Sig3**	**Sig3**
Mineral	Grt rim	Grt core	Omp/ mtx	Am	Pl	Ep/Czo	Grt rim	Grt core	Omp/ mtx	Cpx/ sympl	Am	Pl	Ep/Czo	Grt rim	Grt core	Omp/ mtx	Cpx/ sympl	Am	Pl	Kfs	Ep/Czo
SiO_2	39.53	39.45	54.97	46.16	63.38	39.65	39.03	38.36	55.65	54.16	43.63	64.72	40.06	38.13	38.35	51.68	51.66	42.29	65.48	62.84	38.53
TiO_2	0.01	0.10	0.13	0.86	0.00	0.04	0.02	0.12	0.13	0.19	0.80	0.04	0.08	0.08	0.25	0.19	0.11	0.84	0.02	0.04	0.16
Al_2O_3	22.64	22.31	10.05	13.96	23.04	31.09	21.96	21.81	10.31	4.58	14.15	21.77	32.19	22.01	21.64	6.61	3.43	13.09	22.07	18.34	27.69
FeO/Fe_2O_3	20.42	20.64	3.88	8.68	0.07	2.17	22.66	23.02	3.76	4.96	11.63	0.11	1.25	24.43	22.70	9.78	10.14	16.55	0.09	0.65	8.46
MnO	0.19	0.37	0.00	0.11	0.00	0.00	0.22	0.40	0.00	0.04	0.09	0.03	0.01	0.22	1.65	0.09	0.07	0.06	0.00	0.05	0.03
MgO	9.41	8.22	9.67	13.92	0.01	0.05	6.51	4.05	9.75	13.16	12.55	0.01	0.04	5.00	3.09	8.84	11.10	10.19	0.01	0.00	0.12
CaO	8.34	9.56	15.53	10.00	3.59	24.15	9.64	11.98	15.77	21.29	11.11	3.22	24.09	9.74	11.75	18.22	20.82	11.90	2.64	0.06	23.60
Na_2O	0.03	0.01	5.25	3.48	9.98	0.05	0.03	0.00	5.34	2.08	3.32	10.32	0.01	0.01	0.03	3.37	1.83	2.59	9.39	0.43	0.00
K_2O	0.00	0.01	0.00	0.13	0.00	0.01	0.00	0.01	0.00	0.00	0.23	0.02	0.01	0.02	0.01	0.00	0.01	0.36	0.08	16.17	0.00
Cr_2O_3	0.00	0.06	0.03	0.04	0.02	0.05	0.05	0.07	0.08	0.04	0.06	0.04	0.02	0.11	0.00	0.00	0.00	0.08	0.03	0.00	0.04
Sum	100.58	100.73	99.50	97.33	100.10	97.26	100.11	99.80	100.79	100.49	97.55	100.28	97.77	99.74	99.47	98.77	99.16	97.93	99.80	98.59	98.63
Si	5.95	5.97	1.97	6.60	2.80	3.05	6.00	5.98	1.97	1.97	6.37	2.85	3.04	5.95	6.02	1.94	1.95	6.32	2.88	2.97	2.99
Ti	0.00	0.01	0.00	0.09	0.00	0.00	0.00	0.01	0.00	0.01	0.09	0.00	0.00	0.01	0.03	0.01	0.00	0.09	0.00	0.00	0.01
Al	4.02	3.98	0.42	2.35	1.20	2.81	3.98	4.01	0.43	0.20	2.43	1.13	2.88	4.04	4.00	0.29	0.15	2.30	1.14	1.02	2.53
Fe	2.57	2.61	0.12	1.04	0.00	0.13	2.91	3.00	0.11	0.15	1.42	0.00	0.07	3.18	2.98	0.31	0.32	2.07	0.00	0.03	0.49
Mn	0.02	0.05	0.00	0.01	0.00	0.00	0.03	0.05	0.00	0.00	0.01	0.00	0.00	0.03	0.22	0.00	0.00	0.01	0.00	0.00	0.00
Mg	2.11	1.85	0.52	2.96	0.00	0.01	1.49	0.94	0.51	0.71	2.73	0.00	0.00	1.16	0.72	0.50	0.63	2.27	0.00	0.00	0.01
Ca	1.35	1.55	0.60	1.53	0.17	1.99	1.59	2.00	0.60	0.83	1.74	0.15	1.96	1.63	1.98	0.73	0.84	1.90	0.12	0.00	1.96
Na	0.01	0.00	0.37	0.96	0.85	0.01	0.01	0.00	0.37	0.15	0.94	0.88	0.00	0.00	0.01	0.25	0.13	0.75	0.80	0.04	0.00
K	0.00	0.00	0.00	0.02	0.00	0.00	0.00	0.00	0.00	0.00	0.04	0.00	0.00	0.00	0.00	0.00	0.00	0.07	0.00	0.97	0.00
Cr	0.00	0.01	0.00	0.00	0.00	-	0.01	0.01	0.00	0.00	0.01	0.00	-	0.01	0.00	0.00	0.00	0.01	0.00	0.00	-
Sum	16.04	16.03	4.00	15.58	5.03	7.99	16.01	16.00	3.99	4.00	15.77	5.02	7.97	16.02	15.96	4.03	4.03	15.78	4.95	5.03	7.99
O	24.00	24.00	6.00	22.00	8.00	12.50	24.00	24.00	6.00	6.00	22.00	8.00	12.50	24.00	24.00	6.00	6.00	22.00	8.00	8.00	12.50
Xalm	0.43	0.43	-	-	-	-	0.48	0.50	-	-	-	-	-	0.53	0.51	-	-	-	-	-	-
Xgrs	0.22	0.26	-	-	-	-	0.26	0.33	-	-	-	-	-	0.27	0.34	-	-	-	-	-	-
Xprp	0.35	-	-	-	-	-	0.25	0.16	-	-	-	-	-	0.19	0.12	-	-	-	-	-	-
Xjd	-	-	0.38	-	-	-	-	-	0.39	0.15	-	-	-	-	-	0.24	0.12	-	-	-	-

Table 2.2. Representative microprobe analyses of eclogite minerals in wt% and p.f.u. Fe is calculated as Fe^{2+}, except for epidote/clinozoisite where Fe is Fe^{3+}.

Sample	**Sal1**	**Sal1**	**Sal1**	**Sal1**	**Sal1**	**Sal1**	**Sal1**	**Sal1**
Mineral	Grt1 rim	Grt1 core	Grt2	Omp/ mtx	Cpx/ sympl	Am	Pl	Ep/Czo
SiO_2	36.87	39.23	37.44	55.48	52.30	44.72	67.25	38.16
TiO_2	0.08	0.05	0.03	0.14	0.08	0.63	0.00	0.14
Al_2O_3	21.90	21.19	21.61	10.36	4.24	12.42	20.40	26.66
FeO/Fe_2O_3	28.97	25.76	25.31	6.73	8.68	15.45	0.36	9.59
MnO	0.41	0.42	0.37	0.01	0.00	0.04	0.02	0.03
MgO	4.85	2.73	3.75	7.31	11.12	11.00	0.02	0.08
CaO	5.48	11.28	9.79	12.09	18.89	7.91	1.13	22.09
Na_2O	0.05	0.07	0.05	7.58	3.15	4.52	11.00	0.01
K_2O	0.00	0.03	0.02	0.02	0.01	0.55	0.03	0.00
Cr_2O_3	0.01	0.00	0.01	0.02	0.07	0.00	0.00	0.00
Sum	98.61	100.75	98.37	99.74	98.53	97.23	100.21	96.75
Si	5.89	6.11	5.96	2.00	1.97	6.60	2.94	3.01
Ti	0.01	0.01	0.00	0.00	0.00	0.07	0.00	0.01
Al	4.12	3.89	4.06	0.44	0.19	2.16	1.05	2.48
Fe	3.87	3.35	3.37	0.20	0.27	1.91	0.01	0.57
Mn	0.06	0.05	0.05	0.00	0.00	0.01	0.00	0.00
Mg	1.15	0.63	0.89	0.39	0.62	2.42	0.00	0.01
Ca	0.94	1.88	1.67	0.47	0.76	1.25	0.05	1.87
Na	0.02	0.02	0.01	0.53	0.23	1.29	0.93	0.00
K	0.00	0.00	0.00	0.00	0.00	0.10	0.00	0.00
Cr	0.00	0.00	0.00	0.00	0.00	0.00	0.00	0.00
Sum	16.05	15.95	16.02	4.04	4.05	15.81	5.00	7.95
O	24.00	24.00	24.00	6.00	6.00	22.00	8.00	12.50
Xalm	0.64	0.57	0.56	-	-	-	-	-
Xgrs	0.16	0.32	0.28	-	-	-	-	-
Xprp	0.19	0.11	0.15	-	-	-	-	-
Xjd	-	-	-	0.48	0.19	-	-	-

Table 2.2. Representative microprobe analyses of eclogite minerals in wt% and p.f.u.
Fe is calculated as Fe^{2+}, except for epidote/clinozoisite where Fe is Fe^{3+}.

Sample	Grü1	Grü2	Ho1	Ho2	Sal1	Sig3	Wol1
Major oxides (wt %)							
SiO_2	49.10	49.74	51.47	49.24	49.85	48.39	47.59
Al_2O_3	14.47	14.74	14.76	20.87	13.39	14.18	15.15
Fe_2O_3	11.86	11.15	11.67	4.85	16.50	13.95	12.51
MnO	0.20	0.16	0.18	0.08	0.22	0.30	0.22
MgO	7.99	7.94	7.82	7.39	5.46	6.72	7.18
CaO	10.70	11.22	10.30	13.78	8.49	11.60	12.05
Na_2O	3.25	2.60	2.98	1.68	3.17	2.95	2.67
K_2O	0.00	0.00	0.09	0.01	0.09	0.17	0.09
TiO_2	1.62	1.55	1.59	0.32	2.50	1.18	1.70
P_2O_5	0.12	0.11	0.12	b.d.	0.25	0.09	0.11
SO_3	0.01	0.10	0.11	0.09	0.26	0.14	0.06
l.O.I.	-0.04	-0.01	0.08	1.87	-0.6	1.07	-0.03
Total sum	99.28	99.30	101.17	100.18	99.58	100.74	99.30
Trace elements (ppm)							
Sc	37.50	31.00	34.20	23.70	37.70	38.10	30.40
V	327.60	301.70	320.90	133.20	451.10	331.60	331.50
Cr	255.60	256.20	165.60	577.40	248.70	423.70	225.10
Co	40.60	66.00	41.60	25.00	43.40	46.00	75.40
Ni	69.30	121.80	57.40	77.70	38.70	75.80	175.60
Cu	38.70	84.30	35.40	75.90	26.00	150.30	32.10
Zn	92.50	58.70	55.00	31.00	77.70	154.40	158.30
Ga	16.40	16.00	15.60	13.60	19.80	15.20	16.50
As	5.10	1.70	1.40	1.90	3.00	b.d.	2.40
Rb	1.00	1.50	3.10	1.80	b.d.	3.30	3.50
Sr	42.50	128.50	100.40	156.40	72.90	223.70	144.50
Y	33.70	30.90	34.10	7.90	58.60	27.40	36.50
Zr	89.10	81.20	102.20	6.40	181.10	66.10	99.80
Nb	2.20	2.40	2.10	b.d.	11.00	2.60	3.90
Mo	3.20	2.40	b.d.	3.90	8.30	1.20	1.50
Cs	4.40	b.d.	b.d.	4.20	b.d.	2.10	b.d.
Ba	b.d.	2.80	11.80	49.40	11.10	18.60	5.80
La	48.50	37.80	49.50	b.d.	82.90	32.00	58.70
Ce	16.20	5.10	16.40	10.70	35.10	14.60	9.90
Nd	4.00	1.70	6.30	6.40	24.20	6.30	5.00
Sm	b.d.	b.d.	b.d.	b.d.	10.50	1.30	3.90
Hf	2.10	3.50	3.20	b.d.	3.60	b.d.	3.20
W	32.90	68.10	36.30	14.50	54.10	45.50	58.70
Pb	11.50	15.20	11.70	16.00	11.40	8.80	18.60
Th	b.d.	b.d.	b.d.	b.d.	2.80	1.20	2.10
U	1.70	b.d.	b.d.	2.80	1.90	2.20	1.90

Table 2.3. XRF analyses of the dated eclogite samples, used as input data for thermodynamic modelling.

Samples	ppm Lu	ppm Hf	$^{176}Lu/^{177}Hf$	2 s.d.	$^{176}Hf/^{177}Hf$	2 s.d.	Age (Ma)
Grü1							
WR tt	0.544	0.596	0.1296	0.0003	0.283321	0.000018	100.3 ± 1.0
WR b	0.544	2.00	0.03871	0.00008	0.283165	0.000020	99.8 ± 1.2
Omp	0.0180	0.595	0.004292	0.000009	0.283093	0.000024	
Grt 1	1.16	0.133	1.232	0.002	0.285402	0.000024	
Grt 2	1.14	0.134	1.203	0.002	0.285312	0.000034	
Grt 3	1.18	0.129	1.294	0.003	0.285508	0.000035	
Grü2							
WR tt	0.482	0.600	0.1141	0.0002	0.283300	0.000017	101.79 ± 0.92
WR b	0.498	2.18	0.03244	0.00006	0.283127	0.000030	102.2 ± 1.5
Omp	0.0170	0.623	0.003886	0.000008	0.283072	0.000024	
Grt 1	1.12	0.134	1.185	0.002	0.285326	0.000018	
Grt 2	1.12	0.119	1.340	0.003	0.285626	0.000027	
Grt 3	1.11	0.130	1.211	0.002	0.285416	0.000062	
Ho1							
WR tt	0.536	0.605	0.1256	0.0003	0.283248	0.000015	98.80 ± 0.65
WR b	0.544	2.22	0.03480	0.00007	0.283118	0.000021	97.97 ± 0.71
Omp	0.0238	0.625	0.005419	0.000011	0.283003	0.000037	
Grt 1	1.72	0.0925	2.647	0.005	0.287921	0.000048	
Grt 2	1.66	0.0861	2.735	0.005	0.288030	0.000048	
Grt 3	1.72	0.0888	2.744	0.005	0.288093	0.000054	
Ho2							
WR 1 tt	0.119	0.248	0.06813	0.00014	0.283329	0.000039	92.6 ± 2.0
WR 2 tt	0.118	0.248	0.06778	0.00014	0.283330	0.000024	
Grt 1	0.561	0.0734	1.086	0.002	0.285096	0.000035	
Grt 2	0.501	0.0779	0.9137	0.0018	0.284742	0.000195	
Grt 3	0.448	0.0787	0.8089	0.0016	0.284578	0.000081	
Sal1							
WR 1 tt	0.944	0.471	0.2848	0.0006	0.284134	0.000034	232.0 ± 6.4
WR 2 tt	0.959	0.424	0.3207	0.0006	0.284256	0.000029	
WR b	0.983	4.87	0.02863	0.00006	0.283081	0.000022	231 ± 10
Grt 1	2.56	0.0567	6.448	0.013	0.310865	0.000062	
Grt 2	2.54	0.0554	6.539	0.013	0.311817	0.000078	
Grt 3	2.53	0.0495	7.286	0.015	0.314069	0.000067	
Sig3							
WR 1 tt	0.434	0.656	0.09375	0.00019	0.283330	0.000019	89.89 ± 0.37
WR 2 tt	0.424	0.670	0.08972	0.00018	0.283325	0.000025	
WR 3 tt	0.428	0.662	0.09177	0.00018	0.283317	0.000022	
WR b	0.438	1.69	0.03676	0.00007	0.283208	0.000026	90.12 ± 0.43
Grt 1	3.11	0.0830	5.319	0.011	0.292100	0.000056	
Grt 2	3.16	0.0861	5.216	0.010	0.291933	0.000064	
Grt 3	3.17	0.0776	5.805	0.012	0.292921	0.000060	
Wol1							
WR tt	0.584	0.650	0.1277	0.0003	0.283279	0.000017	101.0 ± 1.2
WR b	0.590	2.30	0.03643	0.00007	0.283079	0.000020	101.9 ± 1.2
Grt 1	1.47	0.119	1.754	0.004	0.286370	0.000059	
Grt 2	1.51	0.125	1.717	0.003	0.286246	0.000062	
Grt 3	1.49	0.119	1.782	0.004	0.286407	0.000051	

Table 2.4. Lu-Hf isotope compositions of eclogites from the Eastern Alps.

2.5.2. P-T estimations

In order to better understand the metamorphic evolution of the eclogites from the Austroalpine high-pressure belt, equilibrium phase diagram modelling was used to estimate the peak metamorphic conditions of the studied samples. Equilibrium phase diagrams, based on the XRF-determined whole rock compositions and the mineral compositions of garnet, omphacite, amphibole and plagioclase obtained by electron microprobe analyses (Tables 2.2 and 2.3), were constructed using the software package Theriak/Domino (de Capitani & Petrakakis 2010) together with a modified thermodynamic dataset of Holland & Powell (1998). Non-ideal solution models for garnet (White et al. 2007), clinopyroxene (Green et al. 2007) and amphibole (Diener et al. 2007) were used for the calculations. Fluid phase was considered to be pure water and in excess. The Si-Al-Fe-Mg-Ca-Na-O input compositions were calculated assuming bivalent iron and normalized to 100 cations. In order to account for the observed minor trivalent iron in clinozoisite/epidote, omphacite and amphibole, a small amount of oxygen (up to 1.0 mol) was added.

Sample Ho1: quartz-rich eclogite, Hohl

The stable equilibrium assemblage in sample Ho1 is garnet-omphacite-amphibole-clinozoisite-quartz-rutile. It is predicted to be stable over a relatively large pressure-temperature range between 1.45 and 2.25 GPa and 580-770 °C (Fig. 2.14a). However, the observed mineral chemistry corresponds to the upper part of this stability field. To verify this the garnet growth was modelled. The calculated isopleths for grossular and almandine content in garnet constrain the peak conditions to ~2.2 GPa and 670 °C. The intersection between modelled garnet volume isopleths and the corresponding grossular and almandine contents confirm the estimated conditions. This interpretation is much in agreement with the published eclogite peak conditions from this region (1.65-2.05 GPa / 620-720 °C, Bruand et al. 2010; 2.2-2.8 GPa / 635-720 °C, Miller et al. 2007 and references therein).

Sample Ho2: kyanite, rich eclogite, Hohl

The observed mineral assemblage of sample Ho2 contains garnet, omphacite, kyanite, amphibole, clinozoisite, quartz and rutile, corresponding to 1.8-2.3 GPa and 700-800 °C in the equilibrium phase diagram (Fig. 2.14b). These constraints are in line the published P-T data, which ranges from 2.2-2.4 GPa and 630-785 °C (Miller et al. 2005a, Miller et al.

2007). For more precise estimation of P and T grossular and pyrope isopleths were calculated. They intersect at ~2.2 GPa and 730°C. This temperature is higher than the one constrained for the quartz-rich eclogite from the same locality. Based on the homogenized major element distribution in garnet as well as the younger age of this sample (see "Geochronology" below), we propose that the estimated P-T conditions for the kyanite-rich eclogite reflect the thermal peak of metamorphism.

Sample Grü2: quartz-rich eclogite, Grünburger Bach

The peak mineral assemblage of the quartz-rich eclogite from Grünburger Bach is garnet-omphacite-clinozoisite-quartz-rutile. The predicted stability field for this assemblage extends over a wide pressure-temperature range between 1.7-2.8 GPa and 680-850 °C. However, the observed and modelled grossular and almandine contents in garnet intersect at ~2.4 GPa and 700 °C in the peak assemblage stability field (Fig. 2.14c). This result is well in agreement with the published peak conditions of 2.2-2.4 GPa and 629-727 °C (Miller et al. 2005a, Miller et al. 2007). In addition, garnet volume isopleths reveal that garnet grew with increasing pressure and temperature, similar to sample Ho1.

Sample Wol1: quartz-rich eclogite, Wolfsberger Hütte

Sample Wol1 contains the high-pressure assemblage garnet-omphacite-clinozoisite-quartz-rutile, which is found on the equilibrium phase diagram in a very large field between 1.6-2.8 GPa and 650-870 °C. However, the metamorphic peak can be constrained to ~2.4 GPa and 680°C by calculating isopleths for the composition of almandine and grossular components in garnet (Fig. 2.14d). These conditions overlap with the estimations for the quartz-rich eclogites from Grünburger Bach as well as the published data for Saualpe (Miller et al. 2005a, Miller et al. 2007). Similar to the samples described above, modelling the volume percentage of garnet shows that garnet grew along a prograde path by increasing temperature and pressure.

Sample Sig3

The peak pressure assemblage of the Sieggraben eclogite contains garnet, omphacite, amphibole, epidote, rutile and quartz. The phase equilibrium modelling predicts relatively large stability field for this assemblage. Nevertheless, the peak P-T conditions can be specified by calculating isopleths for the composition of garnet. The grossular and almandine components that reflect garnet rim composition culminate at peak pressure

conditions ranging between 1.7 and 1.9 GPa and temperature of 600-650 °C (Fig. 2.14e). The temperature estimations are in good agreement with the published P-T data for the eclogites from Sieggraben (Kromel et al. 2011, Neubauer et al. 1999b). However, the estimated peak pressure is higher than previously suggested, but is still in line with the high T/P ratios of the eclogites from the Austroalpine high-pressure belt.

Sample Sal1

As explained above, the garnets in sample Sal1 display a two-stage growth history. The obtained Triassic Lu-Hf-garnet age is a mixing age and thus insignificant (see Geochronology below), but it clearly shows that the two garnet generations did not grow during a single high-pressure event. In this case, Grt 1, which is also the main garnet generation, is a pre-Alpine relic that was overgrown by Grt 2 during the regional eclogite-facies event in the Cretaceous. This would also suggest that the relic matrix was reequilibrated and thus is the observed assemblage in equilibrium with Grt 2. Therefore, it is not possible to reconstruct the P-T conditions of the pre-Alpine metamorphic event.

In contrast, the Alpine peak pressure assemblage contains garnet, omphacite, amphibole, clinozoisite, quartz and rutile. The compositional isopleths as well as the amount of garnet indicate that the assemblage is stable within the upper part of relatively large stability field, i.e. 1.9-2.1 GPa and 570-600 °C (Fig. 2.14f). The temperature estimations fit well with the published data for eclogites from Saltaus valley. Yet, the peak pressure estimations obtained in this study differ strongly from these published in Habler et al. (2006). The same authors applied albite-jadeite-quartz barometry and estimated notably lower pressure probably due to its limited application based upon the breakdown of albite (e.g., Page et al. 2003, Tropper et al. 1999). Zanchetta et al. (2013) proposed UHP metamorphic conditions for the formation of the eclogite, but evidence for that is lacking in samples from Saltaus valley.

▼Fig. 2.14. Equilibrium phase diagrams calculated for SiAlFeMgCaNaOH bulk compositions of the dated eclogite samples Ho1, Ho2, Grü2, Wol1, Sig3 and Sal1. Additionally, compositional isopleths for almandine (red lines), grossular (green lines) and pyrope (blue lines; only for sample Ho2) components in garnet were calculated. Grey isopleths show volume percentage of garnet. The yellow stars correspond to the estimated peak conditions.

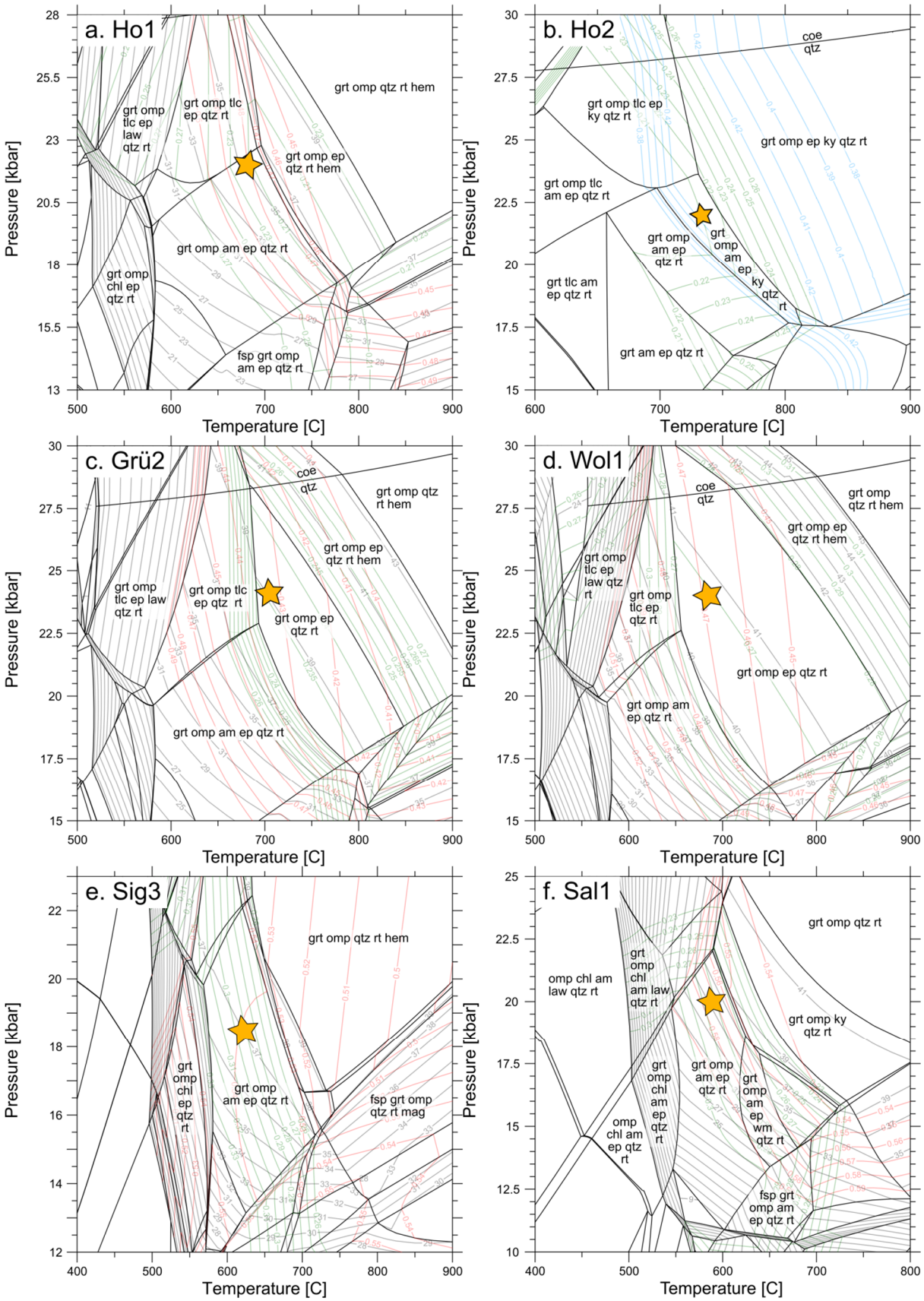
a. Ho1
grt omp tlc ep law qtz rt
grt omp tlc ep qtz rt
grt omp qtz rt hem
grt omp ep qtz rt hem
grt omp am ep qtz rt
grt omp chl ep qtz rt
fsp grt omp am ep qtz rt
b. Ho2
coe
qtz
grt omp tlc ep ky qtz rt
grt omp ep ky qtz rt
grt omp tlc am ep qtz rt
grt omp am ep qtz rt
grt omp am ep ky qtz rt
grt tlc am ep qtz rt
grt am ep qtz rt
c. Grü2
coe
qtz
grt omp qtz rt hem
grt omp ep qtz rt hem
grt omp tlc ep law qtz rt
grt omp tlc ep qtz rt
grt omp ep qtz rt
grt omp am ep qtz rt
d. Wol1
coe
qtz
grt omp qtz rt hem
grt omp ep qtz rt hem
grt omp tlc ep law qtz rt
grt omp tlc ep qtz rt
grt omp ep qtz rt
grt omp am ep qtz rt
e. Sig3
grt omp qtz rt hem
grt omp chl ep qtz rt
grt omp am ep qtz rt
fsp grt omp qtz rt mag
f. Sal1
grt omp qtz rt
omp chl am law qtz rt
grt omp chl am law qtz rt
grt omp ky qtz rt
grt omp chl am ep qtz rt
grt omp am ep qtz rt
grt omp am ep wm qtz rt
omp chl am ep qtz rt
fsp grt omp am ep qtz rt
Pressure [kbar]
Temperature [C]

2.5.3. Geochronology

New Lu-Hf isotope data are presented here for seven eclogite samples from the Austroalpine basement of the Eastern Alps. The results are given in Table 2.4.

Sample Ho1 (quartz-rich eclogite) and sample Ho2 (kyanite-rich eclogite) from Hohl, Koralpe

Three garnet separates of each sample as well as selectively digested whole rocks were used to calculate the Lu-Hf isochrons. Additionally, an omphacite fraction from sample Ho1 was handpicked and analysed. The garnet fractions of both samples show distinctly different $^{176}Lu/^{177}Hf$ ratios of 2.65-2.74 for Ho1 and 0.81-1.09 for Ho2. The Hf content in the garnets of Ho1 range from 86 to 93 ppb, and this in the garnets of Ho2 is between 73 and 79 ppb. The resulting Lu-Hf ages are 98.80 ± 0.65 Ma (MSWD 1.3; n=5) for Ho1 and 92.6 ± 2.0 Ma (MSWD 0.35; n=4) for Ho2. The results are plotted on Fig. 2.15.

Samples Grü1 and Grü2 (quartz-rich eclogite) from Grünburger Bach, Saualpe

Garnet and omphacite separates as well as table top digested whole rocks were used for the calculations of the isochrons for samples Grü1 and Grü2. Both samples show very similar isotopic compositions with Hf content in the garnets ranging from 119 to 134 ppb and $^{176}Lu/^{177}Hf$ ratio between 1.19 and 1.34. Omphacites display Hf content of 595 and 623 ppb and $^{176}Lu/^{177}Hf$ of 0.00429 and 0.00329, respectively. The resulting ages are 100.3 ± 1.0 Ma (MSWD 1.03; n=5) for Grü1 and 101.79 ± 0.92 (MSWD 1.01; n=5) for Grü2, both identical within error. Fig. 2.15 illustrates the calculated isochrons for the two samples.

Sample Wol1 (quartz-rich eclogite) from Wolfsberger Hütte, Saualpe

Three handpicked garnet separates and one table top digested whole rock were used to determine the age of sample Wol1. The $^{176}Lu/^{177}Hf$ ratio of the garnets ranges from 1.72 to 1.78 and their Hf content is between 119 and 125 ppb. The obtained age is 101.0 ± 1.2 Ma (MSWD 0.87; n=4; Fig. 2.15). An isochron calculated with the completely digested whole rock yields an identical age. The age is also identical with both ages from Grünburger Bach.

Sample Sig3 from Sieggraben

From sample Sig3, three garnet separates and one selectively digested whole rock were used to determine its age. The garnets display Hf concentrations between 78 and 86 ppb and $^{176}Lu/^{177}Hf$ ratio from 5.22 to 5.81. The determined age is 89.89 ± 0.37 Ma (MSWD

0.15; n=4; Fig. 2.15). A second isochron, calculated using the completely digested whole rock gives the same age within the error limits.

Sample Sal1 from Saltaus valley, Texel complex

For sample Sal1, three garnet separates and whole rock aliquot define a statistically insignificant isochron with mean square weighted deviates (MSWD) >74 (Fig. 2.15). The resulting Lu-Hf age of 232.0 ± 6.4 Ma (n=5) indicates a variable mixing of Alpine (Grt 2) and relic pre-Alpine garnets (Grt 1).

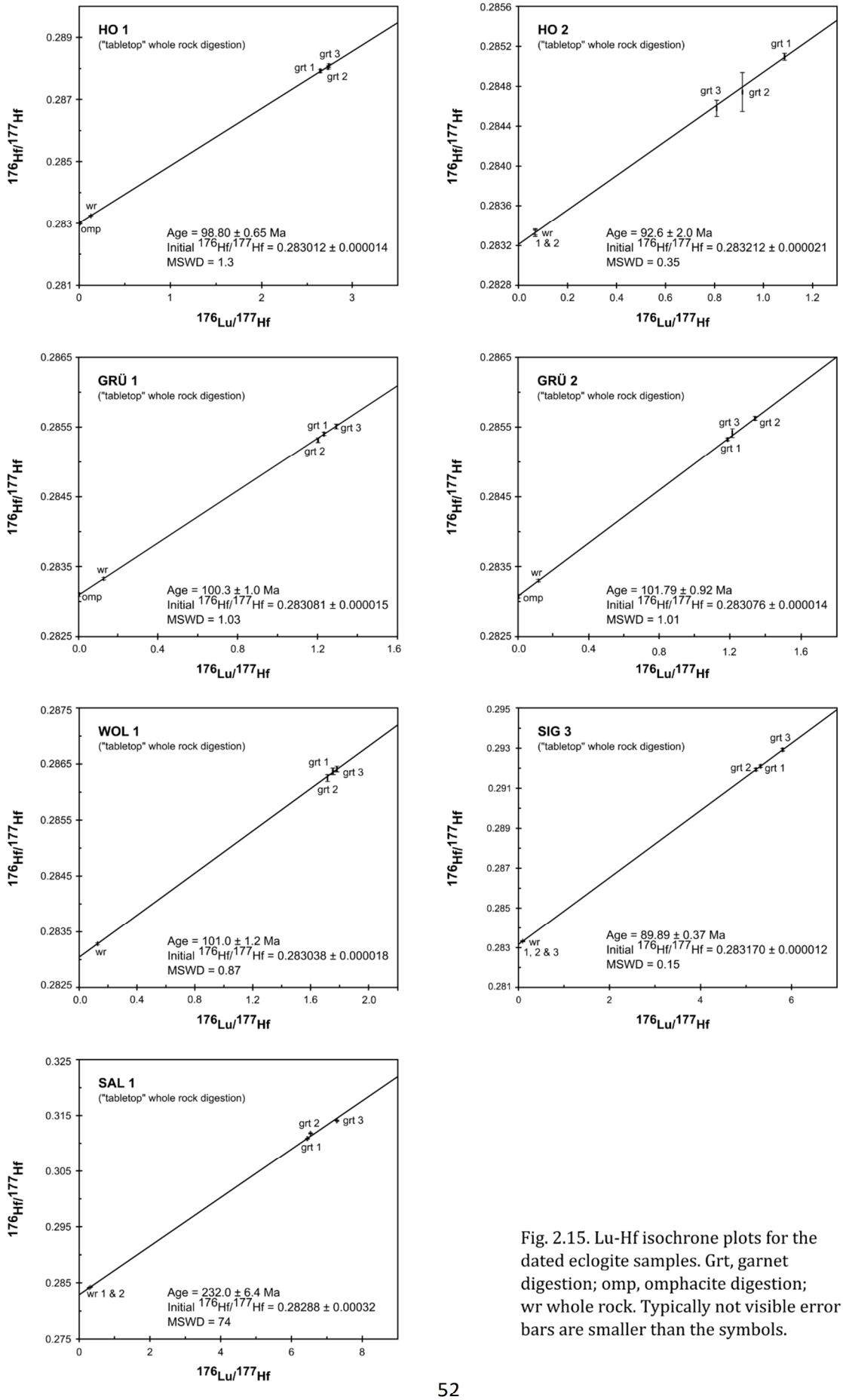

Fig. 2.15. Lu-Hf isochrone plots for the dated eclogite samples. Grt, garnet digestion; omp, omphacite digestion; wr whole rock. Typically not visible error bars are smaller than the symbols.

2.6. Discussion

2.6.1. The problem with inclusions in garnet

Inclusions in garnet may compromise the accuracy of the Lu-Hf ages. The effects of zircon and rutile inclusions on the garnet dates are well documented (e.g., Baxter & Scherer 2013, Scherer et al. 2000) and depend on the age of the inclusions and their hafnium concentration relative to those of garnet. Inclusions with very low hafnium concentrations as well as Hf-rich zircon and/or rutile with the same age as the garnet would barely affect the garnet ages. Inclusions with rather different age than the garnet would displace the garnet analyses away from the true garnet–matrix isochron, leading to loss of accuracy. In this study the selective digestion method described by Lagos et al. (2007) was applied to all garnet separates in order to exclude the effects of garnet inclusions on the estimated ages. This technique dissolves garnet and leaves the Hf-bearing refractory phases (e.g., zircon and rutile) intact.

According to Baxter & Scherer (2013) cleansed garnet analyses yield $^{176}Lu/^{177}Hf$ ratios > 1 and exhibit Hf concentrations generally < 0.5 ppm. All of the investigated samples but one (Ho2) in this study fulfil these conditions (Table 2.4). The lower $^{176}Lu/^{177}Hf$ ratios of the garnets from sample Ho2 can be explained with the generally lower Lu and Hf concentrations.

2.6.2. Interpretation of the Lu-Hf ages: prograde garnet growth vs. cooling

Crucial for the interpretation of Lu-Hf ages are the growth mechanisms of garnet as well as the major and trace elements zoning. Particularly, the distribution patterns of REEs can provide valuable information about the processes that operated during garnet growth (e.g., Hickmott et al. 1987). Two rate-limiting end-member processes for porphyroblast growth have been discussed in numerous studies, i.e. interface- and diffusion-controlled growth (e.g., Carlson 1989, Daniel & Spear 1999, Fisher 1978, Kretz 1974, Skora et al. 2005, 2006, Spear & Daniel 1998, 2001). Interface-controlled garnet growth implies that the attachment or incorporation of material at the garnet surface is relatively slow compared to diffusion to the growing garnet. Thus, pre-existing garnet crystals do not influence the nucleation of new ones. Moreover, garnet will be randomly distributed in a homogeneous matrix and will grow with equal radial increments

regardless of size. When the diffusion of material to the growing garnet is slower compared to the growth rate, then growth is diffusion-controlled. This results in developing of a reaction rim around growing porphyroblasts, which suppresses nucleation adjacent to the growing garnet. Therefore, garnet crystals will have a non-random distribution in a homogenous matrix, where smaller garnet appears at greater distances to large garnet.

Regarding the Lu-Hf system, a key assumption is that garnet behaves as closed system upon crystallization. Hence, Lu and Hf are effectively retained in the garnet and do not undergo substantial diffusional reequilibration during the thermal peak of metamorphism and/or consequent cooling of the system. However, element diffusivity in garnet depends on several other factors in addition to temperature: grain size, oxygen fugacity, cooling rate, ionic charge, presence or absence of fluid (e.g., Bloch et al. 2015, Caddick et al. 2010, Skora et al. 2006, Smit et al. 2011). Experimental studies showed that the ionic charge of an element is a major control factor on its diffusivity, i.e. 2+ ions (e.g., Mn^{2+}) diffuse by orders of magnitude faster than 3+ (e.g., Lu^{3+}), whereas the diffusion of 4+ (e.g., Hf^{4+}) is substantially slow (e.g., Bloch et al. 2015, Carlson 2006, 2012, Ganguly et al. 1998, van Orman et al. 2002). Furthermore, the published estimates of the closing temperature of the Lu-Hf system appear to be in the range of ~800-850 °C for garnets with 1mm diameter (Smit et al. 2013, Van Orman et al. 2002), thus, well above the peak temperatures for the eclogites from the Austroalpine high-pressure belt.

As described above, the garnets from samples Ho1, Grü1 and Grü2 exhibit compositional zoning with high Ca and Mn distributions as well as bell-shaped Lu concentrations in the cores (Figs. 2.3, 2.7a and b). This means that the garnets have preserved their prograde growth zonation pattern for Lu-Hf. Therefore, the obtained Lu-Hf ages of 98.80 ± 0.65 Ma, 100.3 ± 1.0 Ma and 101.79 ± 0.92 Ma (Fig. 2.15), respectively, clearly reflect the time of garnet growth during increasing P and T.

The garnets in the kyanite-rich eclogite Ho2 show a complete homogenization in the distribution of major elements. Unfortunately, due to the very abundant inclusions in the garnet cores as well as the very low concentrations of REE it was not possible to obtain Lu concentration profiles within the framework of this study. Samples Ho1 and Ho2 belong to the same eclogite body, but the obtained Lu-Hf age of 92.6 ± 2.0 Ma from Ho2 is

younger than the prograde age of Ho1 (Fig. 2.15). Nevertheless, the P-T equilibrium modelling of sample Ho2 constraints higher temperature (~730 °C, Fig. 2.14b) than for Ho1 (~670 °C). All this suggests that the kyanite-rich eclogite recorded the thermal peak of metamorphism and the younger age reflects equilibrium during the thermal peak. Possible explanation for this situation is that Ho1 belongs to the outer part of the eclogite body and cooled off quickly, so that it experienced the peak temperature not long enough to equilibrate by diffusion. Therefore, the age reflects prograde garnet growth. In contrast, Ho2 probably belongs to the internal part of the eclogite body and, thus, cooled off slower, allowing diffusive mobilization of major and trace elements in garnet near the temperature peak. Hence, the younger age dates the onset of cooling after temperature peak.

The garnets from sample Wol1 display Ca-, Fe- and Mn-poor and Mg-rich rims. As described above, the distribution of Lu differs in the smaller and larger garnet crystals (Fig. 2.9a and b). According to Sckora et al. (2006) most of the heavy REE (Lu + Yb + Tm + Er) and Y behave similar to the major elements, but Lu concentrations in the cores of smaller garnets are enriched relative to the Lu concentrations at the corresponding distance from the rim of larger garnets, resulting from a depletion halo surrounding them. The measured Lu profiles in the garnets from sample Wol1 may be well explained by a model where incorporation of Lu is controlled by diffusion, whereas the overall garnet growth is dominated by interface-controlled mechanism.

Considering the nearly identical Lu–Hf age of Wol1 (101.0 ± 1.2 Ma) with that of Grü1 and Grü2 (100.3 ± 1.0 Ma and 101.79 ± 0.92 Ma, respectively), it is evident that the diffusion-limited uptake of Lu barely limits the precision of the Lu-Hf isochron. In fact, the obtained ages represent prograde garnet growth at peak pressure conditions.

The garnets in sample Sig3 display similar zoning patterns to those in sample Wol1. The major elements show distinct zoning with high Mn- and Ca-contents in the garnet core, whereas Mg and Fe are enriched at the rims (Fig. 2.10). In contrast, Lu is concentrated near the rims and a shows no apparent central peak. Similar to Wol1, diffusion-controlled garnet growth may be responsible for that pattern. However, Hf as well as the light REEs (Eu + Gd + Tb) show bell-shaped distributions (Fig. 2.10), which suggests that a very narrow central peak of Lu may have been missed if garnet was not sectioned precisely

through its centre. If so, the near rim peaks would represent a secondary maximum of Lu that was released from the decomposition of pre-existing REE-bearing minerals within the adjacent matrix (e.g., Fassmer et al. 2016, Konrad-Schmolke et al. 2008). In any case, partial resetting (resorption) has not been identified in the garnets of that sample. Otherwise, the fit of the Lu-Hf isochron would have been compromised resulting in an apparently younger age (Kelly et al. 2011). Therefore, the obtained age of 89.89 ± 0.37 Ma is interpreted to be related to burial during subduction.

Both growth stages in the garnets from sample Sal1 (Grt 1 and Grt 2) indicate prograde growth zonation with high contents of spessartine and grossular components in the inner parts (Fig. 2.13, see also appendix). The Lu concentration through garnet also shows a bell-shaped distribution in Grt 1 and a second enrichment towards the rims (Grt 2). Hence, the estimated P-T conditions reflect prograde growth of Grt 2 during subduction. However, an age cannot be assigned to any of the growth stages. The obtained Triassic age (232.0 ± 6.4 Ma, Fig. 2.15) suggests a variable mixing of pre-Alpine (Grt 1) and Alpine (Grt 2) garnet, with most of the garnet being to be pre-Alpine, most probably Variscan, and significant "contamination" by Alpine garnets that grew during the Eoalpine high-pressure event. This interpretation is very appealing as it is in agreement with the latest Lu-Hf garnet dating of eclogites from Schobergruppe, where both Variscan and Alpine ages were obtained (Hauke et al. 2019).

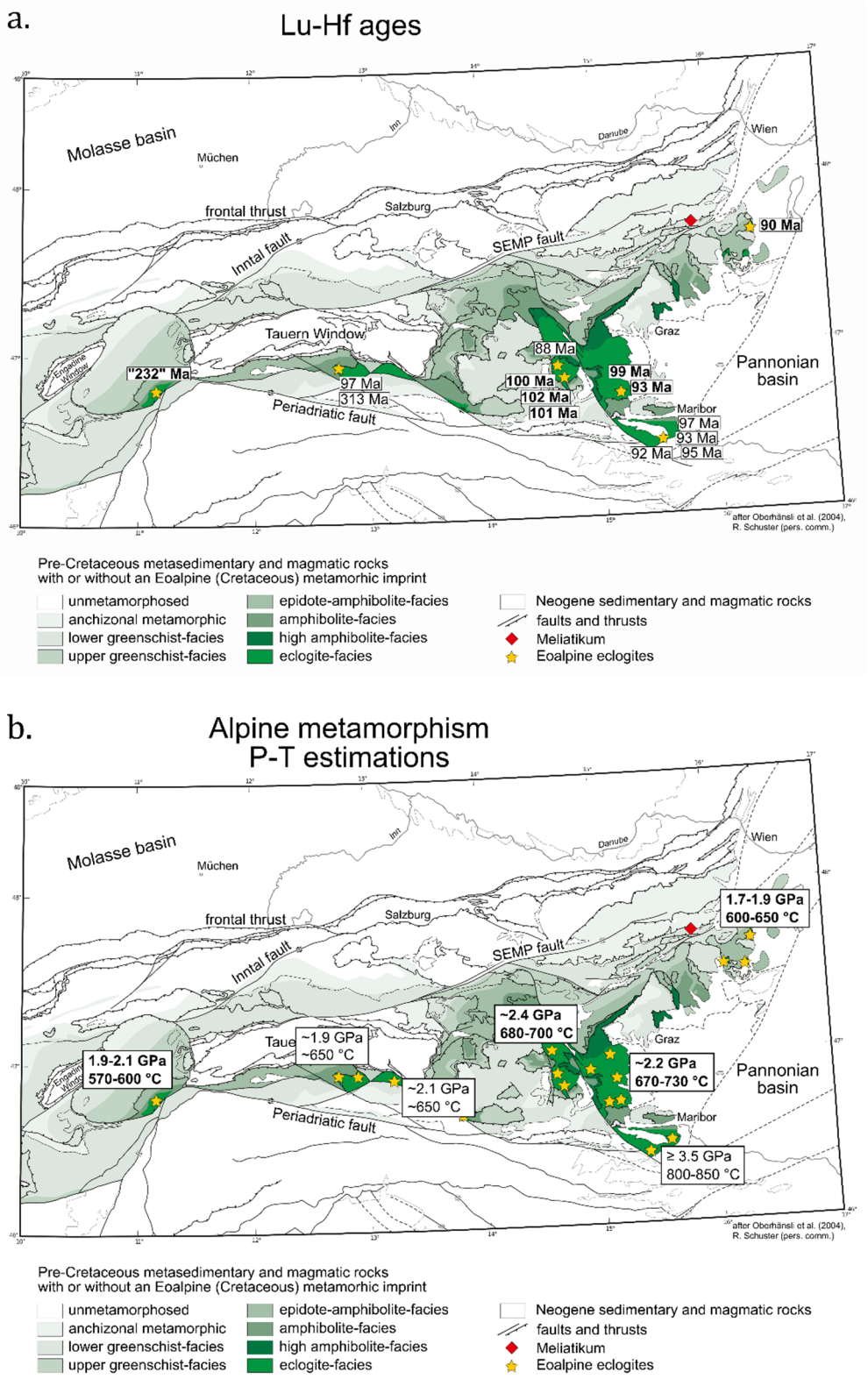

Fig. 2.16. Metamorphic map of the Eastern Alps (after Oberhänsli et al. 2004, R. Schuster pers. comm.). Bold numbers represent the data obtained in this study. a. Compilation of Lu-Hf garnet ages established in the Austroalpine HP belt (data from Hauke et al. 2019, Sandmann et al. 2016, Thöni et al. 2008 and this study). b. Compilation of the estimated P-T conditions (data from Hauke et al. 2019, Janák et al. 2015, Konzett et al. and this study).

2.6.3. Tectonic implications

Fig. 2.16a shows a compilation of geochronological data from different eclogite localities throughout the Eastern Alps, related to the Eoalpine subduction. All of the data is based on Lu-Hf dating of garnet (garnet-whole rock regression) from this and other studies (Hauke et al. 2019, Sandmann et al. 2016, Thöni et al. 2008). The oldest rocks yield an age of ca. 100 Ma and are located in the Koralpe and Saualpe. As previously described, this age is interpreted to be related to burial. This area is also characterized by intense igneous and metamorphic activity of regional importance during the Permian–Triassic period (e.g., Schuster et al. 2001). The gabbroic protoliths of the Koralpe-Saualpe eclogites were derived from a depleted mantle source (Miller et al. 1988, 2007, Miller & Thöni 1997, Thöni & Jagoutz 1992) and embedded within the thinned crust of a rift zone that was probably located northwest of the Meliata-Hallstatt ocean (Fig. 2.17a; Janák et al. 2004, Schuster et al. 2001, Schuster & Stüwe 2008). This indicates that the onset of subduction was intracontinental and localized by the reactivated Permian rift.

Further south, the eclogites from Pohorje Mountains are also derived from the Permian MORB-type gabbroic protoliths generated in a rift zone, just as these in Saualpe and Koralpe (Fig. 2.17a; Miller et al. 2005b, 2007, Thöni & Jagoutz 1992). However, Lu-Hf dating of these eclogites as well as garnet peridotites yields ages of ~95 Ma (Sandmann et al. 2016, Thöni et al. 2008). These ages were interpreted to reflect garnet growth during progressive subduction. Also, the finding of metamorphic diamond in paragneisses from the Pohorje Mountains confirmed that this rock complex experienced ultrahigh-pressure metamorphism with P-T conditions of ≥ 3.5 GPa and 800-850 °C during the Eoalpine subduction event (Janák et al. 2015), whereas the phase equilibria constraints on eclogites from Saualpe-Koralpe indicate peak pressure conditions of 2.2-2.4 GPa and 670-700 °C. Altogether, this may be explained in two ways. Either, Pohorje and Saualpe-Koralpe are two distinct coherent terranes and while the first one was still progressively subducting, the latter was already accreted to the upper plate (Fig. 2.17b). Alternatively, they may represent one single terrane and the c. 100 Ma ages from Koralpe and Saualpe reflect an earlier stage of the subduction, while the c. 95 Ma ages from Pohorje reflect a later stage of the P-T path. The occurrence of a ~99 Ma quartz-rich eclogite and a ~93 Ma kyanite-rich eclogite together in one locality in the southern part of the Koralpe, i.e. rather close to Pohorje, speaks for this second explanation. The two

eclogites from Hohl definitely belong to the same terrane because they were sampled in the same eclogite lens, only about few meters apart.

In the same time subduction continued including the polymetamorphic basement of Schobergruppe and Texel complex (Fig. 2.17b), which comprises rocks with pre-Alpine and Alpine overprint. Up to recently, the timing of the high-pressure metamorphism within these complexes has been based mainly on U-Pb zircon and Sm-Nd garnet dating, which constrained only Cretaceous ages (Habler et al. 2006, Linner 1999, Zanchetta et al. 2013). Schulz (1993) estimated eclogite-facies conditions of 1.4-1.6 GPa and 550-650 °C in Schobergruppe. He correlated this result with the estimated P-T conditions from adjacent parts of the Austroalpine nappes south of the Tauern Window and considering also the published Late Variscan cooling ages, he argued that the high-pressure metamorphism in Schobergruppe is Early Variscan. A recent detailed petrological and geochronological study by Hauke et al. (2019) showed that the eclogites from Schobergruppe recorded two high-pressure metamorphic events, Variscan with a minimum age of ~314 Ma and Alpine with a maximum age of ~97 Ma. They estimated pressure peak conditions during the Late Cretaceous subduction of c. 1.9 GPa and 650 °C, whereas the Variscan eclogite experienced conditions of at least 1.6 GPa, as inferred from the amount of garnet.

There are several zircon ages that constrain the timing of formation of the magmatic protoliths of the rocks from both Schobergruppe and Texel complex. Schulz & Bombach (2003) investigated the eclogites and their adjacent rock suits from the Austroalpine basement of Schobergruppe. They obtained a protolith age of 587.5 ± 5.2 Ma for an eclogitic amphibolite with typical N-MORB element abundances, an age of 531 ± 12 Ma for hornblende-plagioclase gneisses with compositions typical for calc-alkaline volcanic arc magmatites as well as an age of 471 ± 7 Ma for a biotite orthogneiss with composition matching continental arc granites. This data correlates well with the zircon protolith ages from the Texel complex obtained by Klug et al. (in prep.). An amphibole-bearing orthogneiss from Saltaus valley shows a geochemical signature of an I-type volcanic-arc granitoid and yields a protolith age of 470 ± 11 Ma, whereas a leucocratic orthogneiss from an adjacent rock suit has S-type continent-collision-granitoid characteristics and yields an age of 449 ± 7 Ma. According to Schulz et al. (2008) the Austroalpine basement was part of the northern continental margin of Gondwana that was active from

Neoproterozoic to Ordovician and the rocks bear the characteristics typical for evolution from continental arc to collisional setting.

Similar to Schobergruppe, previous dating of the eclogites from the Texel complex yields Late Cretaceous ages. Using Sm-Nd garnet geochronology, Habler et al. (2006) dated eclogites from Saltaus valley as well as their host-rock. The study derived an eclogite age of 85.2 ± 4.6 Ma, which was interpreted to reflect maximum burial stage during subduction. The authors assumed that polyphase garnet growth in the eclogites occurred during a single eclogite-facies metamorphic event. However, the Sm-Nd garnet dating of orthogneisses and metapelites resulted is ages of 205.7 ± 5.3 Ma and 208.5 ± 8.4 Ma, respectively, which indicates the presence of pre-Cretaceous mineral relics. Zanchetta et al. (2013) confirmed the Late Cretaceous metamorphic age of the eclogites from Texel by using U-Pb zircon geochronology. They derived an age of 85 ± 4 Ma and considered it to represent a stage near to the high-pressure metamorphism. However, the Lu-Hf garnet dating in this study resulted in a Triassic age of ~232 Ma. As discussed above, this age is interpreted as a Variscan-Eoalpine mixed age. Considering the distribution of Lu-Hf garnet ages throughout the Austroalpine high-pressure belt as well as the estimated P-T conditions that show a clear temperature and pressure decrease from southeast to northwest (Fig. 2.16b), the age of the Alpine metamorphism in the Texel complex should be ≤97 Ma.

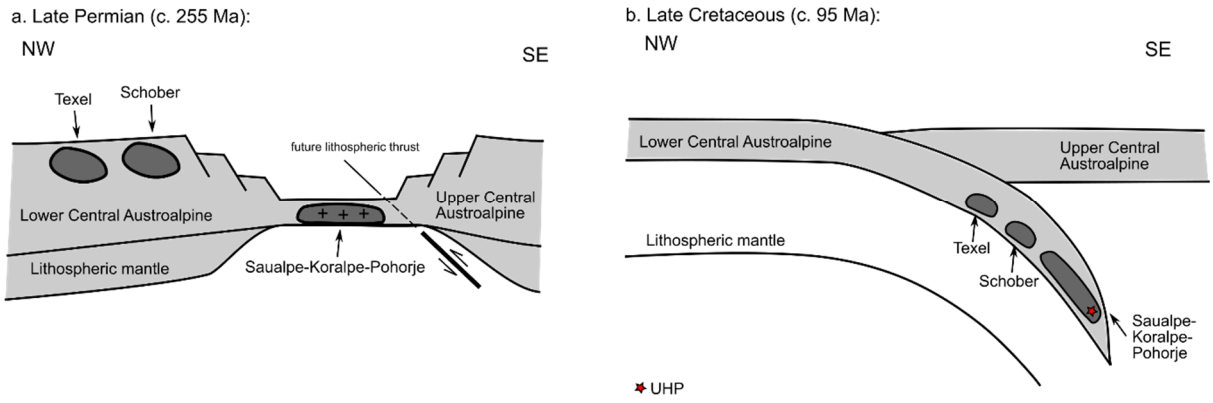

Fig. 2.17. Tectonic model illustrating the proposed evolution of the Austroalpine domain. a. Gabbroic intrusions embedded within the thinned crust of a rift zone during extension in the Late Permian.
b. progressive subduction of the Saualpe-Koralpe-Pohorje terrane and the Variscan eclogites from Schobergruppe and Texel complex during the Late Cretaceous.

Accordingly, from ~97 Ma continental crust comprising Variscan eclogites was subducted. These rocks were exhumed after the Variscan orogeny and subducted to high-pressure conditions again in the Late Cretaceous. In this scenario the Texel complex represents the deeper subducted southeastern part of the Ötztal nappe.

The observed discrepancy between Lu-Hf and Sm-Nd data is common for the eclogites from the Eoalpine high-pressure belt. One reason for that might be the presence of unequilibrated inclusions within garnet that are capable to bias the estimated ages (e.g., Scherer et al. 2000). On the other hand, the different diffusion kinetic properties of Nd^{3+} and Hf^{4+} cause the $^{147}Sm–^{143}Nd$ decay system to be easier affected by diffusive resetting, which leads to a lower closure temperature than that of the $^{176}Lu–^{176}Hf$ system in garnet (e.g., Scherer et al. 2000). Thus, the younger Sm-Nd ages can be attributed to the early stages of cooling from high-grade conditions (e.g., Smit et al. 2013).

All this data suggests that the Eoalpine subduction began ~100 Ma within the Permian rift and lasted until ~90 Ma, as inferred from the high-pressure ages from Pohorje and Sieggraben. The observed field gradient of the depth and the timing of the subduction indicates that the Eoalpine high-pressure belt does not represent a subduction-channel mélange, mixing rocks with different P-T history, as suggested by Roda et al. (2012). It rather represents one coherent terrane or parts of one terrane that were progressively subducted and accreted in a short phase (~10 Ma) of intracontinental subduction. Ages outside that time window previously interpreted to be prograde, are probably result of isotopic reequilibration or excess Ar, as in the case of the 136 Ma age from Sieggraben (Neubauer et al. 1999b).

2.7. Conclusions

1. Lu-Hf dating of eclogites from the Austroalpine high-pressure belt yielded prograde garnet growth ages between 101.79 ± 0.92 Ma and 89.89 ± 0.37 Ma, suggesting a short period of (ultra)high-pressure metamorphism.

2. The oldest eclogites are localized in the Saualpe-Koralpe area, where also Permian gabbros are wide-spread. This supports the hypothesis that subduction was intracontinental and was initiated within a pre-existing weakness zone in the lithosphere, a Permian-age rift.

3. The scattered age data from the eclogite from Saltaus valley is explained by the variable mixing between pre-Alpine and Alpine garnets. Therefore, Texel complex is interpreted to represent continental crust that contained Variscan high-grade rocks and was re-subducted during the Eoalpine orogeny.

4. Thermodynamic modelling indicates overall high T/P ratio and gradient with increasing temperatures and pressures from northwest to southeast.

Chapter 3

Late Cretaceous eclogite in the Eastern Rhodopes (Bulgaria): evidence for subduction under the Sredna Gora magmatic arc

3.1. Introduction

Magmatic arcs form when oceanic lithosphere is subducted beneath oceanic (island arcs) or continental (continental arcs) lithosphere. The magmatism is generally interpreted to result from dehydration of the descending slab causing partial melting in the overlying mantle wedge (Davies & Stephenson 1992, Schmidt & Poli 1998). Particular insights into the fluxes and dynamics of convergent plate boundaries are provided, where rocks from the subducting slab are exhumed back to the surface and can be studied together with the arc magmatic rocks. Such a situation potentially occurs in southeast Europe where the Apuseni-Banat-Timok-Sredna Gora Belt is a Late Cretaceous magmatic arc (Jankovic 1977, Mitchell 1996, Neubauer 2002, Stampfli & Mosar 1999) and the adjacent Rhodope Metamorphic Complex contains exhumed high-pressure (HP) and ultrahigh-pressure (UHP) metamorphic rocks (Collings et al. 2016, Janák et al. 2011, Kirchenbaur et al. 2012, Kolčeva et al. 1986, Kozhukharova 1980, Liati & Mposkos 1990, Liati & Seidel 1996, Liati 2005, Mposkos & Kostopoulos 2001, Nagel et al. 2011, Perraki et al. 2006, Petrík et al. 2016, Schmidt et al. 2010).

The ca. 1000 km long Apuseni-Banat-Timok-Sredna Gora belt is the westernmost part of an extensive system of magmatic arcs in the Alpine-Himalayan collision zone (Gallhofer et al. 2015). It is a continental arc formed along the southern margin of Eurasia during the Late Cretaceous subduction of Neotethys and hosts important porphyry-type and epithermal Cu-Au deposits, e.g. in the Sredna Gora Zone of Bulgaria (Moritz et al. 2003, Peytcheva et al. 2003, von Quadt et al. 2003, 2005; Fig. 3.1). Arc magmatism lasted from ca. 95 to 67 Ma (Marchev et al. 2015, von Quadt and Peytcheva 2005, von Quadt et al.

2005). The associated subduction zone dipped northward under the arc and its activity started ca. 110 Ma (Gallhofer et al. 2015). There is an age gradient across the belt with ages becoming younger towards south, i.e. towards the paleotrench, from ~95 Ma in the Eastern Balkan, to ~75 Ma in the southern part of the Sredna Gora Zone, to ~69-67 Ma in the Rhodopes immediately to the South (Georgiev et al. 2009, 2014, Marchev et al. 2006, 2015, von Quadt & Peytcheva 2005, von Quadt et al. 2005). The shift may be explained by slab retreat, i.e. roll-back (von Quadt et al. 2005), or, alternatively, by slab steepening (Gallhofer et al. 2015). The emplacement of the Upper Cretaceous plutons in the Sredna Gora Zone was controlled by dextral shear zones (Georgiev et al. 2009, Naydenov et al. 2013) as plutons intruded at middle to shallow crustal levels in local extensional environments (Georgiev et al. 2009, 2014).

It is still controversial if and to what extent the HP/UHP rocks of the Rhodope Metamorphic Complex record Late Cretaceous subduction under the Sredna Gora Zone. Attempts to date HP and UHP metamorphism resulted in ages between ca. 200 Ma (Nagel et al. 2011, Petrík et al. 2016) and ca. 42 Ma (Kirchenbaur et al. 2012, Liati & Gebauer 1999). These were interpreted in contrasting ways. Burg (2012) interpreted ages between >170 Ma and ca. 117 Ma to be related to HP/UHP metamorphism, and ca. 73 Ma and younger ages to amphibolite-facies and lower-grade overprint under decreasing pressure. In contrast, Liati et al. (2011) assumed four events of at least HP metamorphism, at ca. 150, 73, 51, and 42 Ma. The second event at ca. 73 Ma falls into the life span of the Sredna Gora magmatic arc. So far, Late Cretaceous ages were determined by U-Pb dating of zircons from various gneisses and schists (Georgiev et al. 2016, Liati et al. 2011, 2016), and by Sm-Nd dating of garnets from diamond-bearing garnet-kyanite gneisses (Collings et al. 2016). The attribution of the Late Cretaceous zircon ages to HP or UHP metamorphism is contested by some authors (Bauer et al. 2007, Burg 2012, Moulas et al. 2017). The Late Cretaceous Sm-Nd garnet ages are also difficult to interpret since Petrík et al. (2016) studied another sample of similar rock from the same area and determined ca. 200 Ma for the UHP metamorphism by U-Th-Pb monazite dating. Therefore, there still remains doubt if Late Cretaceous, prograde HP or UHP rocks exist in the Rhodopes at all. In the present article, we report the first dating of Late Cretaceous eclogites from the Eastern Rhodopes, ~82 Ma old. These rocks are crucial for linking the

tectonic evolution of the Rhodope nappe stack with the Late Cretaceous magmatic evolution of the Sredna Gora Zone.

3.2. Regional setting: Rhodope Metamorphic Complex

The Rhodope Metamorphic Complex in Bulgaria and Greece is a stack of nappes emplaced during a protracted Alpine tectonic history. Contacts between units are only partly original thrusts but often represent Late Eocene to Oligocene extensional detachments (e.g., Bonev et al. 2006, Burchfiel et al. 2003, Burg et al. 1996, Georgiev et al. 2010, Jahn-Awe et al. 2010, Krohe & Mposkos 2002, Nagel et al. 2011, Pleuger et al. 2011). The Rhodope Metamorphic Complex was intruded by granitoid plutons ranging from Late Cretaceous to Miocene (Dinter et al. 1995, Eleftheriadis et al. 2001, Jahn-Awe et al. 2010, Marchev et al. 2006, Meyer 1968, Ovtcharova et al. 2004, von Quadt & Peytcheva 2005) and is partly covered by Paleogene and Neogene sedimentary and Paleogene volcanic rocks (Kilias et al. 2013 and references therein). Several tectonic subdivision schemes have been proposed for the metamorphic units (e.g., Burg et al. 1996, Krohe & Mposkos 2002). We follow the subdivision of Janák et al. (2011) into Lower, Middle, Upper and Uppermost Allochthon (Fig. 3.1).

The Lower Allochthon is represented by the Pangaion-Pirin Unit in the Western Rhodopes, by the Arda-1 and Arda-2 orthogneiss units of the Arda Dome in the Central Rhodopes (Burg 1990), and by the orthogneiss cores of the Kesebir-Kardamos and Byala Reka-Kechros domes in the Eastern Rhodopes. It comprises Variscan basement and metasedimentary rocks, regionally metamorphosed under upper greenschist to amphibolite facies conditions with migmatite formation in the Arda and Kesebir-Kardamos domes. The Lower Allochthon has been interpreted to represent continental crust derived from Adria (Dinter 1998, Jahn-Awe et al. 2012, Krohe & Mposkos 2002, Nagel et al. 2011), the Pelagonia continental block (Kydonakis et al. 2015a), or an independent microcontinent (Ricou et al. 1998, Turpaud & Reischmann 2010).

The Middle Allochthon includes the Kerdilion Unit in the Serbo-Macedonian Massif and the Sideronero-Mesta and Asenica units in the Western and Central Rhodopes, respectively. The Middle Allochthon is a mixed unit including metaophiolites, paragneisses and orthogneisses. The orthogneisses are partly derived from Jurassic to Early Cretaceous granitoids (Himmerkus et al. 2012, Ovtcharova et al. 2004, Turpaud &

Reischmann 2010), partly from Variscan granitoids (Himmerkus et al. 2012, Peytcheva & von Quadt 1995, Peytcheva et al. 1998). One of the metaophiolites at Satovcha in the Western Rhodopes yielded ~160 Ma protolith ages (Froitzheim et al. 2014). According to our interpretation, the Middle Allochthon includes the suture of Neotethys (Vardar Ocean) in the form of Mesozoic ophiolites and arc granitoids, and Variscan basement rocks from the margins of this ocean. So far, units of the Middle Allochthon have not yet been recognized in the Eastern Rhodopes.

The Upper Allochthon is mainly exposed in the Eastern Rhodopes and in the Serbo-Macedonian Massif where it is represented by the Vertiskos-Ograzhden Unit. It comprises various metamorphic rocks, including metaophiolites. Orthogneisses from the Upper Allochthon mostly yielded Early Paleozoic protolith ages (Ordovician and Silurian; Himmerkus et al. 2009, Macheva et al. 2006, Peytcheva et al. 2009, Peytcheva et al. 2015). Ophiolites and ophiolite-like mafic-ultramafic successions from the Upper Allochthon have yielded Neoproterozoic (Carrigan et al. 2003), Ordovician, and Triassic ages (Bonev et al. 2013, Bonev et al. 2016, Liati et al. 2011, Peytcheva et al. 2009). The Upper Allochthon is interpreted to represent the Mesozoic continental margin of Europe (e.g., Bonev et al. 2015, Froitzheim et al. 2014).

The Uppermost Allochthon, also known as the Circum-Rhodope Belt, comprises units along the southwestern margin of the Rhodope Metamorphic Complex as well as the Mandrica and Alexandropolis greenschists in the Eastern Rhodopes (Meinhold & Kostopoulos 2013 and references therein). The rocks are of lower metamorphic grade compared to the underlying allochthons, i.e. of blueschist facies (Michard et al. 1994), greenschist facies, and anchizonal grade (e.g., Bonev & Stampfli 2003). Protoliths are sedimentary and volcanic rocks, partly of oceanic affinity. The Uppermost Allochthon is interpreted to represent a Mesozoic arc together with back-arc ophiolites from the Neotethys realm as well as sediments from the European margin, emplaced towards north onto the more proximal European margin already in the Jurassic (Bonev & Stampfli 2003, Bonev et al. 2015).

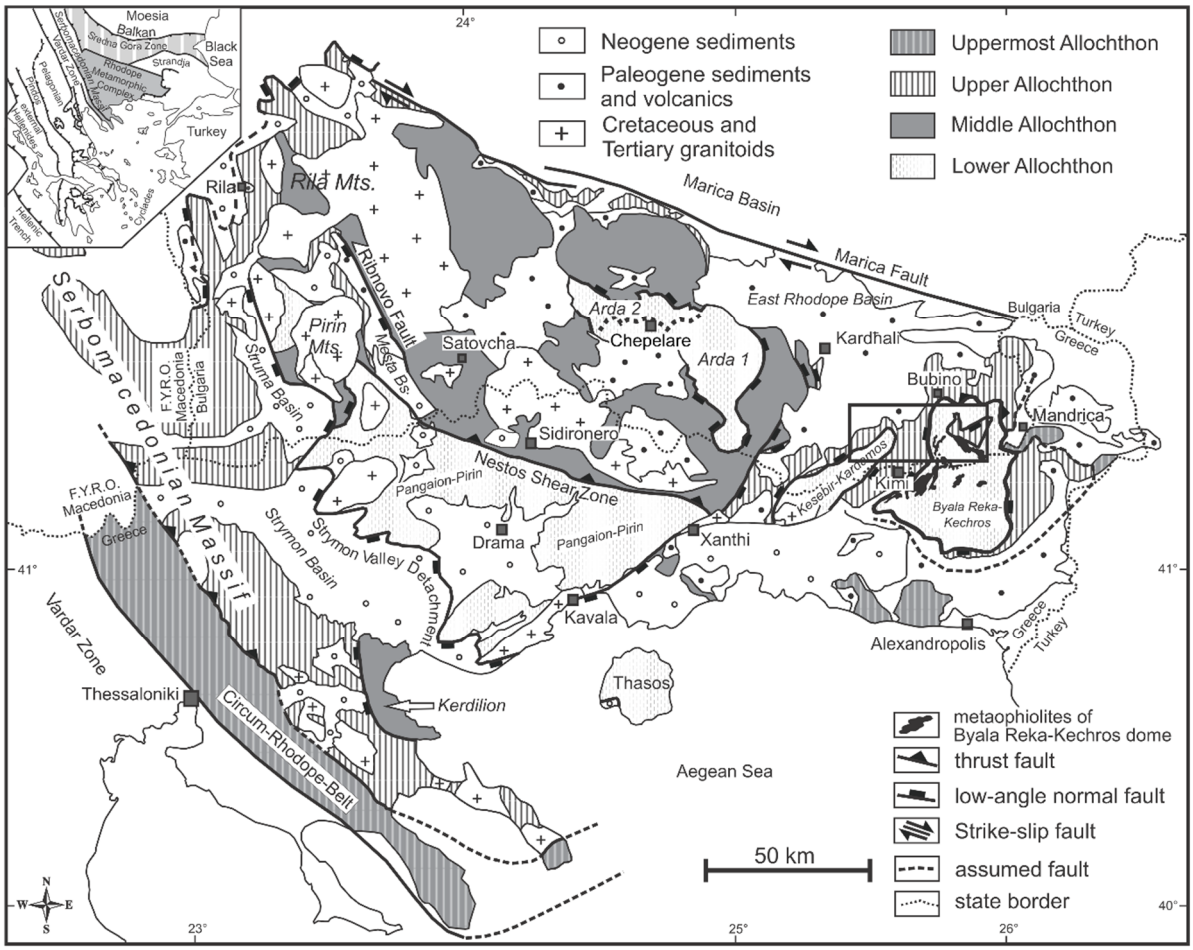

Fig. 3.1. Tectonic overview of the Rhodope Metamorphic Complex and its surroundings (modified after Bonev et al. 2006, Burg et al. 1996, Ricou et al. 1998). Inset (upper left): tectonic sketch map of the Balkan Peninsula. Rectangle: outline of Fig. 3.2.

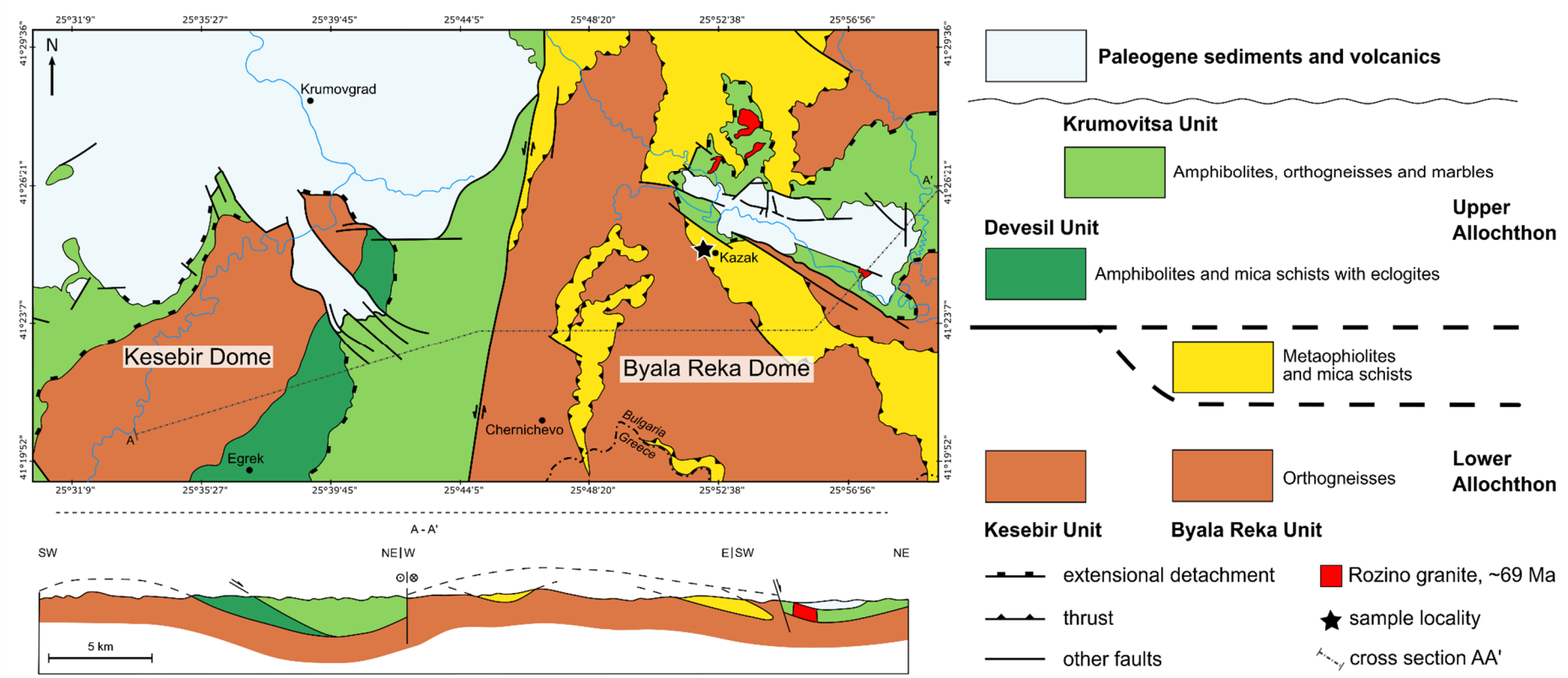

Fig. 3.2. Simplified tectonic map and cross-section of the study area based on Sarov et al. (2007a, b).

3.3. Occurrence and age of HP/UHP rocks in the Rhodope Metamorphic Complex

Eclogite-facies, partly UHP metamorphic rocks occur at different structural levels of the nappe stack, from base to top:

3.3.1. Lower Allochthon

In the Central Rhodopes, an eclogite boudin included in orthogneiss yielded a Lu-Hf age of 43.5 ± 0.4 Ma (Kirchenbaur et al. 2012). Originally it was interpreted to belong to the Middle Allochthon (Kirchenbaur et al. 2012) but according to the Geological map sheet Devin (Sarov et al. 2009) the sample locality is in the Arda-1 Unit, i.e. Lower Allochthon. High-pressure micaschists from the Lower Allochthon in the Pirin Mountains reached ~16 kbar/500 °C at 45.8 ± 5.8 Ma (Massonne 2016), dated by U-Th-Pb on monazite.

3.3.2. Middle Allochthon

A strongly sheared zone along the base of the Middle Allochthon (Nestos Shear Zone, Chepelare Mélange) comprises various HP and UHP rocks, including eclogites (Kolčeva et al. 1986, Liati & Seidel 1996) and microdiamond-bearing gneisses (Collings et al. 2016, Mposkos & Kostopoulos 2001, Petrik et al. 2016, Schmidt el al. 2010). The HP and UHP rocks have yielded various age clusters which are partly controversially interpreted: ~200 Ma (U-Th-Pb monazite; Nagel et al. 2011, Petrík et al. 2016); ~150-140 Ma (U-Pb zircon, Liati 2005; U-Th-Pb monazite, Gautier et al. 2017); 92.7-70.5 Ma (Sm-Nd garnet, Collings et al. 2016); 51-42 Ma (Lu-Hf garnet, Kirchenbaur et al. 2012; U-Pb zircon, Liati 2005). The Eocene eclogites dated by Liati (2005) and Kirchenbaur et al. (2012) have been interpreted as parts of the Lower Allochthon incorporated in the shear zone (Petrík et al. 2016). The other age groups are also known from the Upper Allochthon (see below) and, therefore, these rocks have been interpreted as parts of the Upper Allochthon that were captured in the Lower/Middle Allochthon boundary by out-of-sequence thrusting (e.g., Petrík et al. 2016).

3.3.3. Upper Allochthon

The Upper Allochthon in the Eastern Rhodopes comprises eclogites and diamond-bearing gneisses. Geochronological work yielded the following ages for HP/UHP metamorphism, again partly controversial: >170 Ma (U-Pb zircon, Bauer et al. 2007); ~158 Ma (U-Pb zircon, Liati et al. 2016); 126-117 Ma (U-Pb zircon, Liati et al. 2002; Sm-Nd garnet,

Wawrzenitz & Mposkos 1997; Lu-Hf garnet, Kirchenbaur et al. 2012); ~74 Ma (U-Pb zircon; Liati et al. 2002, 2011, 2016). In the western part of the Rhodope Metamorphic Complex, the Upper Allochthon comprises eclogite and eclogite-facies metasediments in the Rila Mountains (Kabul Unit; Sarov et al. 2011), Pirin Mountains (Obidim Unit; Janák et al. 2011), and Serbo-Macedonian Massif (Ograzhden Unit: Zidarov et al. 1995; Vertiskos Unit: Kydonakis et al. 2015b). The age of HP/UHP metamorphism in these units is still unknown; Kydonakis et al. (2015b) suggested a Mesozoic age.

3.4. Eastern Rhodopes: geology and sample location

The Eastern Rhodopes are characterized by two antiformal domes, the Kesebir-Kardamos Dome in the west and the Byala Reka-Kechros Dome in the east (Fig. 3.1). These expose orthogneiss of the Lower Allochthon ("Lower high-grade unit" of Bonev 2006) in the cores, overlain and surrounded by rocks of the Upper Allochthon ("Upper high-grade unit"). Remnants of the Uppermost Allochthon locally occur at the top of the nappe stack ("Greenschist rocks" of Bonev 2006).

Sample KAS2 comes from the Byala Reka-Kechros Dome (Fig. 3.2). The core of the dome, called Byala Reka Lithotectonic Unit in Bulgaria (Sarov et al. 2007a), is formed by (1) orthogneisses with protolith ages from 326.3 ± 4.4 to 254.3 ± 2.2 Ma (U-Pb on zircon, Cornelius 2008, Liati & Fanning 2005, Peytcheva & von Quadt 1995), in one place intruded by a dyke of ~256 Ma old gabbro (Liati & Fanning 2005) later metamorphosed to kyanite eclogite (2.2 GPa/615 °C; Mposkos et al. 2012); (2) metaophiolites comprising serpentinite, metagabbro, common, i.e. kyanite-free eclogite, amphibolite, garnet-bearing two-mica schist, and other mica schists (Mposkos et al. 2012, Sarov et al. 2007a). Our sample KAS2 is a common eclogite from the largest metaophiolite body in the Bulgarian part of the dome. The sampling locality (coordinates: 41°24'45.9", 25°52'30.6") is in the valley floor west of the village Kazak. Variably retrogressed eclogites are exposed along the stream. Towards southwest, they rest with a northeast-dipping contact on orthogneisses. Towards northeast, the metaophiolite body is overlain by similar orthogneisses along another northeast-dipping contact. This situation probably represents a syncline with a northeast-dipping axial plane, with the metaophiolites in the core (Zhalti Chal Syncline; Kozhoukharova 2010). Whereas Sarov et al. (2007a) treated the metaophiolites as part of the Byala Reka Lithotectonic Unit, Bonev (2006) interpreted

them as part of the Upper high-grade unit (Upper Allochthon) folded into the orthogneisses. Protolith ages of the metaophiolites are not known. Kozhoukharova (2010) suggested that they are Meso- to Neoproterozoic. Von Quadt et al. (2010) published undocumented zircon dating results from an eclogite in the "Bjala Reka mélange" which yielded an age of 566.4 ± 6.3 Ma for the magmatic protolith and 72.7 ± 3.6 Ma for the high-pressure metamorphism. This sample comes from the metaophiolites near Chernichevo (Fig. 3.2; pers. comm. Irena Peytcheva).

Further south in Greece, common (kyanite-free) eclogite in similar metaophiolites within the Byala Reka-Kechros Dome records conditions of 1.7 GPa/620 °C (Mposkos et al. 2012). Rb-Sr mineral ages from amphibolite-facies orthogneisses from the same area range between ~35 and ~42 Ma (Peytcheva 1997, Wawrzenitz & Mposkos 1997). Therefore ~42 Ma is a minimum age for the high-pressure metamorphism.

Northeast of Kazak, a klippe of various metamorphic rocks (gneiss, amphibolite, and marble) intruded by the ~69 Ma Rozino granite (Marchev et al. 2006) rests upon the Byala Reka Unit along an extensional detachment fault (Sarov et al. 2007a). This klippe is correlated with the Krumovitsa Unit (Upper Allochthon; Marchev et al. 2006).

3.5. Analytical methods

All measurements and analyses were made at Steinmann Institute, Bonn. A detailed description can be found in Chapter 1.4.

3.6. Results

3.6.1. Petrology and mineral chemistry

Sample KAS2 is a medium- to fine-grained eclogite with a rather iron-rich basaltic composition. Garnet, omphacite, amphibole and epidote together with quartz and rutile are inferred to represent the high-pressure, eclogite facies assemblage (Fig. 3.3a). Minor retrogressive overprint is manifested by formation of a second generation of Al-rich amphibole locally replacing garnet rims, plagioclase and diopside symplectites after omphacite, as well as ilmenite and titanite in the matrix. Representative microprobe analyses of minerals are listed in Table 3.1. Amphibole nomenclature follows Hawthorne et al. (2012) and Oberti et al. (2012).

Garnets are euhedral to subhedral and contain abundant inclusions of titanite and amphibole, but also epidote, rutile, quartz, apatite and omphacite (Fig. 3.3b). Epidote, omphacite and rutile inclusions occur typically close to the garnet rims. Garnet shows a spread in composition ($Alm_{58-61}Grs_{28-35}Prp_{4-11}Sps_{0.1-6}$). Individual garnet grains display a pronounced zoning with bell-shaped concentrations of Mn and Lu in the core and increase in Mg from core to rim (Fig. 3.4a, b; Fig. 3.5), typical for a prograde growth. Relatively sharp variations in composition imaging euhedral garnet shapes demonstrate that garnets well preserve their growth zoning being not much affected by diffusion (Fig. 3.4a).

Matrix omphacite as well as inclusions in garnet show 5-10% of acmite component reflecting the overall oxidized chemistry. Jadeite/acmite components range from Jd/Acm_{37} to Jd/Acm_{44} with no systematic difference between matrix grains and inclusions. Locally, symplectites of albite or plagioclase together with diopside-rich clinopyroxene (Jd/Acm_{16}) or amphibole replace the rims of large omphacite grains.

Amphibole occurs in a very different textural and compositional variety. Matrix amphiboles show high winchite components with Al_2O_3 content ranging from 5.52 to 9.60 wt% and Na_2O from 2.69 to 3.89 wt% (Table 3.1). This amphibole partly shows rims with more pargasitic composition. Symplectitic amphibole, replacing omphacite, is magnesiohornblende. Kelyphitic amphibole around garnet and winchite near the garnet rim shows the highest Al_2O_3 contents (up to ~21 wt%). Amphibole inclusions in garnet are winchite, pargasite and magnesiohornblende with compositions similar to the matrix amphiboles and we propose that at least pargasite and hornblende inclusions actually reflect re-equilibrated inclusions.

Epidote occurs as single grains in the matrix and as inclusions in garnet and omphacite. It displays somewhat different Fe_2O_3 contents with inclusions showing Fe_2O_3 contents between 9.90 and 13.29 wt% and in matrix epidote varying between 7.89 to 9.25 wt%.

Titanite is abundant as inclusions in garnet and omphacite. A second generation of titanite occurs in the matrix where it replaces ilmenite and rutile. Ilmenite is also preserved as single grains in the matrix, but never as inclusions in garnet or omphacite. Small inclusions of pure rutile in garnet occur mainly in the outer rim while matrix rutile

is often associated with ilmenite without a clear age relation between the two. The composite grains show rims of a second generation of titanite.

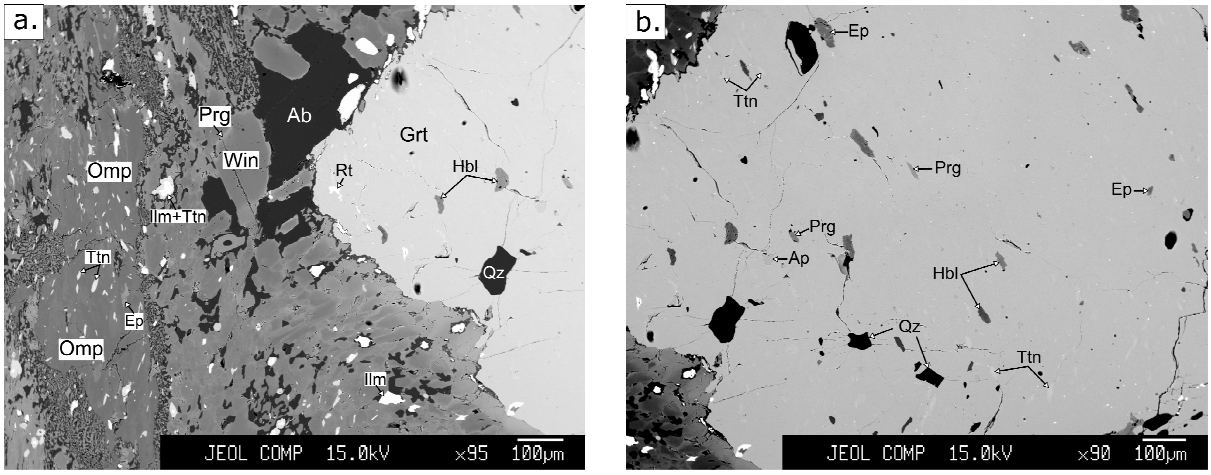

Fig. 3.3. Back-scattered electron images of the eclogite sample KAS2. (a) Matrix consisting mainly of omphacite and amphibole with minor plagioclase, epidote, ilmenite and titanite. The amphiboles have a winchite-rich core and a more pargasitic rim. (b) Garnet with inclusions of amphibole, titanite, quartz, epidote, omphacite and rutile. Ab, albite; Ap, apatite; Ep, epidote; Grt, garnet; Ilm, ilmenite; Omp, omphacite; Prg, pargasite; Qz, quartz; Rt, rutile; Ttn, titanite; Win, winchite.

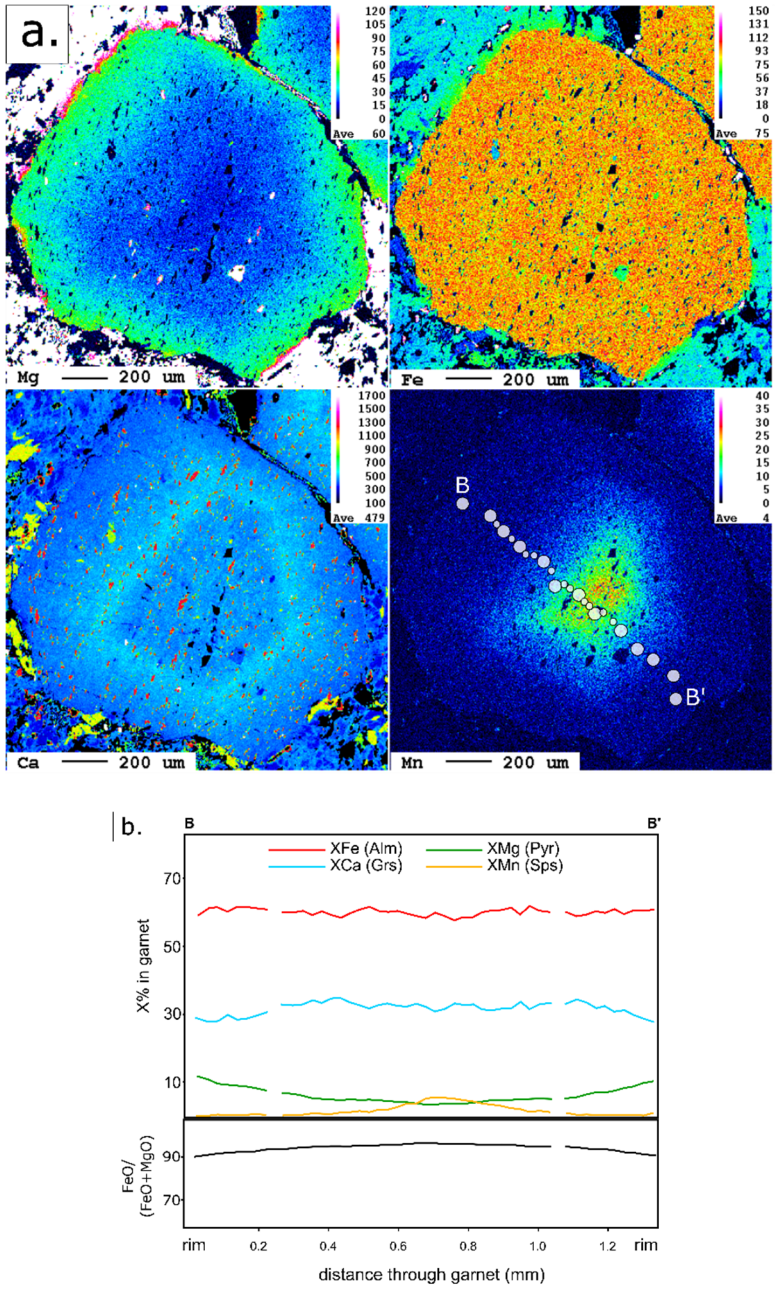

Fig. 3.4. (a) Major element distribution maps of a representative garnet grain of the eclogite sample KAS2 from the Byala Reka-Kechros Dome. Numbers on color scales are count rates. (b) Compositional profiles through the same grain. The profile follows the line B-B' indicated on Fig. 3.4a. Maps and profile show typical growth zoning pattern.

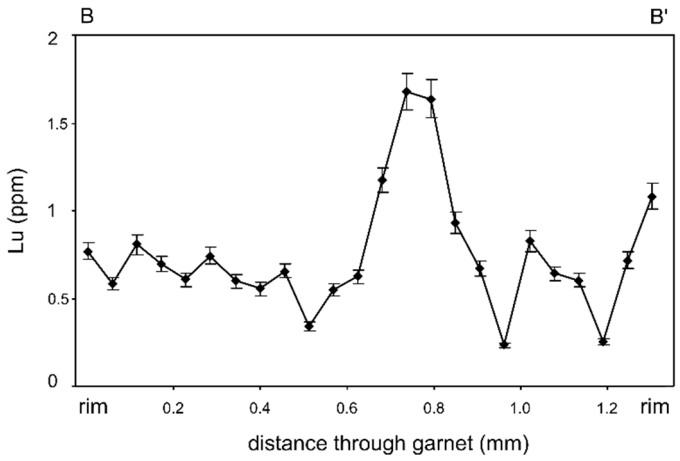

Fig. 3.5. Lu concentration profile obtained by LA-ICPMS through the same garnet of Fig. 3.4a. The indicated errors are 10 % of the value.

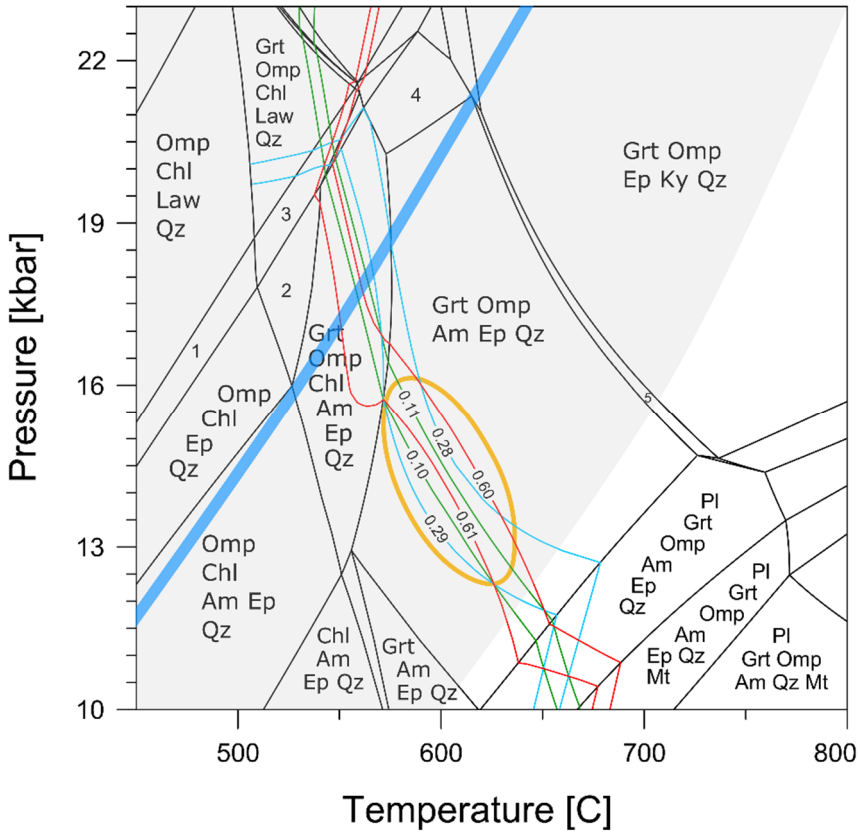

Fig. 3.6. Equilibrium phase diagram for the SiAlFeMgCaNaHO bulk composition of the eclogite (sample KAS2) with compositional isopleths of almandine (red lines), pyrope (green lines) and grossular (blue lines) components in garnet. Orange oval encloses the estimated peak conditions. (1) Omp + Chl + Ep + Law + Qz; (2) Grt + Omp + Chl + Ep + Qz; (3) Grt + Omp + Chl + Ep + Law + Qz; (4) Grt + Omp + Tlc + Am + Ep + Qz; (5) Grt + Omp + Am + Ep + Ky + Qz. The thick blue line represents the global mean distribution of rock-based P-T estimates for subduction zones with 2σ confidence envelopes (grey area) after Penniston-Dorland et al. (2015).

3.6.2. P-T conditions

Fig. 3.6 is an equilibrium phase diagram calculated for the XRF-determined bulk composition of sample KAS2 (Table 3.2) assuming water-saturation. Theriak/Domino software package (de Capitani & Petrakakis 2010) and the database of Holland & Powell (1998) updated for complex solution models of relevant minerals (Diener et al. 2007, Green et al. 2007, White et al. 2007) were used for calculation. The SiAlFeMgCaNaO input composition was normalized to 100 cations and the oxygen amount was initially calculated assuming bivalent iron. To account for trivalent iron in epidote, omphacite, and amphibole, 1.5 mol of oxygen were added resulting in about 25% of Fe^{3+} in the system. Displayed isopleths for almandine, grossular and pyrope component in garnet correspond to the composition of the mineral rim.

The observed high-pressure assemblage garnet-omphacite-amphibole-epidote-quartz is predicted to be stable over a large pressure-temperature range between 550 and 700 °C and 10 and 20 kbar. The best correspondence between observed and modelled mineral chemistries is found at conditions around 570-620 °C and 12 to 16 kbar (see garnet isopleths in Fig. 3.6). Several general aspects also point to conditions at the low end of the predicted stability range and rather low eclogite-facies conditions with respect to P and T. The overall very high Fe/(Fe+Mg) ratio with particular low Mg concentrations in garnets suggest an early stage of garnet stability. The observation that titanite is the dominant Ti-inclusion in garnet and also the well-preserved growth zoning in garnet are in line with this conclusion.

In summary, petrological observations and modelling show that the investigated eclogite experienced a metamorphic evolution culminating at lower eclogite-facies conditions. Typical zonings in garnet with respect to bivalent elements and Lu point to a single metamorphic cycle and indicate that garnet was not subject to any significant amount of subsequent diffusive re-equilibration.

3.6.3. Geochronology

To determine the age of the Kazak eclogite we calculated an isochron defined by three garnet separates and two omphacite separates. The results are given in Table 3.3. The Hf content in the omphacite separates is 342 and 416 ppb. The garnets display Hf concentrations from 267 to 300 ppb and $^{176}Lu/^{177}Hf$ in the range from 0.608 to 0.686. The resulting Lu-Hf age is 81.6 ± 3.5 Ma with a mean square of weighted deviates (MSWD) of 1.7 (n=5; Fig. 3.7). The completely digested and the table top digested whole rocks plot below the isochron, which is probably due to the presence of mineral phases with unequilibrated Hf component in the matrix of the rock.

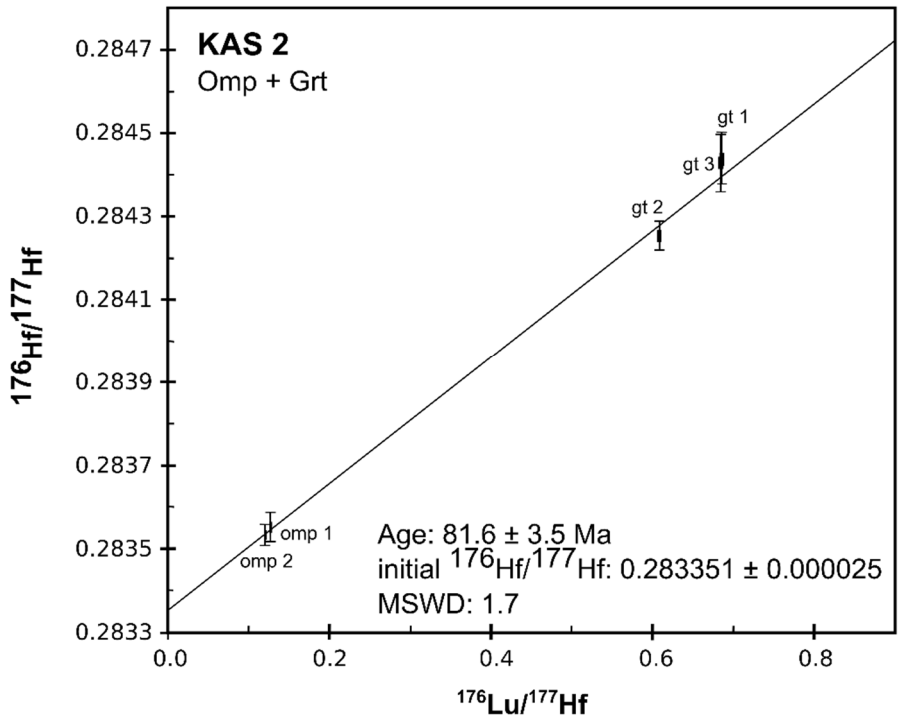

Fig. 3.7. Lu-Hf isochron plot of the eclogite sample KAS2 from the Byala Reka-Kechros Dome.

3.7. Discussion

3.7.1. Significance of the Lu-Hf ages

The calculation of prograde growth ages using the Lu-Hf geochronometer requires that garnet remained a closed system for Lu-Hf since the formation of the high-pressure mineral assemblage (Hickmott et al. 1987, Hollister 1966, Otamendi et al. 2002, Skora et al. 2006). Published estimates for the closure temperature (T_C) of the Lu-Hf system in garnet range from 630 °C (Skora et al. 2008) to around 1000 °C (Shu et al. 2014). Although the small grain size pushes these estimations of Tc to lower values (Scherer et al. 2000, Skora et al. 2008), the obtained maximum temperature of 620 °C for KAS2 suggests that garnet and omphacite crystallized below their T_C. In addition, the zoning in the content of major elements and Lu indicates that the growth zoning in garnet was not subject to later diffusion. Hence, in this case Lu-Hf age records garnet growth and since garnet clearly belongs to the peak-pressure assemblage, we interpret this age as reflecting prograde metamorphism up to eclogite-facies conditions.

Garnets have been proven to be the most suitable rock-forming minerals for Lu-Hf geochronometry because of their high $^{176}Lu/^{177}Hf$ ratios. However, the accuracy of that geochronometer could be limited by the presence of trace mineral inclusions. Zircon in particular can have very high Hf content (as much as 10 wt%), which has the potential to strongly affect the isotopic systematics of the whole rock and garnets (e.g. Scherer et al. 2000). Klemme et al. (2005, 2006) identified that Hf is compatible also in ilmenite and rutile. If these minerals would be preserved from a premetamorphic stage they would contain inherited Hf leading to artificially steep isochrones, thus driving ages to higher values. This appears to be the case for all of our whole-rock measurements regardless of digestion method. In fact, Mposkos et al. (2012) proposed relic magmatic ilmenite from their common eclogites and based on textural relations this cannot be excluded for ilmenite in our sample. For this reason, we discarded whole rock data and used only omphacite and garnet to calculate the isochron. Omphacite is part of the high-pressure assemblage and is co-genetic with garnet. Therefore, it can be assumed that omphacite and garnet were initially in isotopic equilibrium with each other.

3.7.2. Tectonic implications

The age result from the Kazak eclogite underlines that prograde high-pressure metamorphism occurred in the Rhodope Metamorphic Complex during the Late Cretaceous. Together with the existing age determinations, as shown in Fig. 3.9, our results support previous ideas about multiple events of subduction-related high-pressure metamorphism in the Rhodopes (e.g., Liati et al. 2011). It is important to note that our results do not contradict the evidence for older (i.e. Jurassic) and younger (Eocene) HP-UHP metamorphism in other tectonic units of the Rhodopes. Instead, we propose that different tectonic units of the Rhodopes were affected by HP metamorphism at different times.

The pressures of 1.2-1.6 GPa determined for sample KAS2 correspond to a depth of ~45–60 km, assuming lithostatic pressure and a density of the overlying rocks of 2700 kg/m^3. Since garnet grew on the prograde path, as detailed above, and Lu is concentrated in the garnet cores, we assume that the Lu-Hf age of ~82 Ma is related to the burial of the rocks. Because of the temporal coincidence with subduction-related magmatism in the Sredna Gora Zone to the north, and the structural evidence for south-vergent thrusting in the Eastern Rhodopes during the Cretaceous (e.g., Bonev 2006), we assume that the rocks were buried in the relatively shallow part of the subduction zone that consumed the Neotethys Ocean and dipped north under the Sredna Gora Zone. The depth range of 45–60 km and the temperature of 570–620 °C result in a thermal gradient of 9.5–13.8 °C/km. This is higher than subduction zone thermal gradients predicted by numerical modelling (e.g., Syracuse et al. 2010). Our P-T estimates are, however, within the range of typical subduction zone conditions as derived from a compilation of petrological P-T estimates from paleo-subduction zones worldwide (Penniston-Dorland et al. 2015; see Fig. 3.6). The systematic difference between modelled and petrologically determined thermal structures of subduction zones may be a result of heat sources not incorporated in modelling (Penniston-Dorland et al. 2015).

The age of the protolith of the Kazak eclogite is unknown and we did not succeed in separating zircon grains large enough for protolith dating. However, the zircon dating results of von Quadt et al. (2010) from the Chernichevo eclogite, although only published in an abstract, may be tentatively used as information about the protolith. The Chernichevo eclogite belongs to the same tectonic unit as the Kazak eclogite, is of a similar

composition, and yielded zircon ages of 566.4 ± 6.3 Ma for the magmatic protolith and 72.7 ± 3.6 Ma for the high-pressure metamorphism. The latter age postdates our Lu-Hf age by a few Ma, which is typically observed in eclogites (e.g., Herwartz et al. 2008). The Neoproterozoic protolith age (566.4 ± 6.3 Ma) is identical to the age of the Bubino metagabbro (572 ± 5 Ma; published in an extended abstract by Carrigan et al. 2003), a component of the Krumovitsa Unit at the northwest border of the Byala Reka-Kechros Dome (see Fig. 3.1). If the same age is assumed for the protolith of the Kazak eclogite, it follows that this rock was not part of the Mesozoic oceanic crust of the Neotethys Ocean but rather an old ophiolite in the continental crust. If KAS2 contains inherited older zircon and/or rutile, as suggested by the isotope composition of the whole rock plotting below the garnet-omphacite isochron, this would also speak for an "old" ophiolite which already experienced Variscan metamorphism before it was eclogitized in the Late Cretaceous. However, the whole rock εHf values of ~11 clearly demonstrate a depleted mantle source for the protolith of the Kazak eclogites, with no continental influence.

Because of the correlation with the Bubino metagabbro in the Krumovitsa Unit (Upper Allochthon), we tentatively assume that the Kazak and other metaophiolite bodies in the Byala Reka-Kechros Dome were derived from the hanging wall of the subduction zone, i.e. the European continental margin (Upper Allochthon), by tectonic erosion, carried to depth in the Late Cretaceous, and exhumed back to the surface (Fig. 3.8). We therefore interpret that the Kazak eclogite and other metaophiolites of the Byala Reka-Kechros Dome are rather in an Upper Allochthon position (as in Bonev 2006) than in a Lower Allochton position (as in Sarov et al. 2007a) (Fig. 3.9).

According to the reconstruction of Gallhofer et al. (2015), the north-dipping Neotethys subduction zone was installed shortly before 110 Ma. At 90 Ma, ~300 km of oceanic lithosphere still remained to be subducted, and collision of the Pelagonian block and Europe after complete subduction of the ocean occurred at ~66 Ma (Gallhofer et al. 2015, Schenker et al. 2015 and references therein). Pre-110-Ma HP and UHP metamorphism in the Rhodopes is related to other tectonic processes, i.e. the continent-continent collision after the closure of Palaeotethys (~200 Ma, Petrík et al. 2016) and/or burial of the European margin in a south-dipping subduction zone during arc-continent-collision at 170 to 150 Ma (e.g., Bonev et al. 2015). The change from a south-dipping to a north-dipping subduction zone at the southern European margin is reflected by a Mid-

Cretaceous change in thrust vergence from northward in the Jurassic and Early Cretaceous to southward in the Late Cretaceous and Tertiary (e.g., Okay et al. 2001).

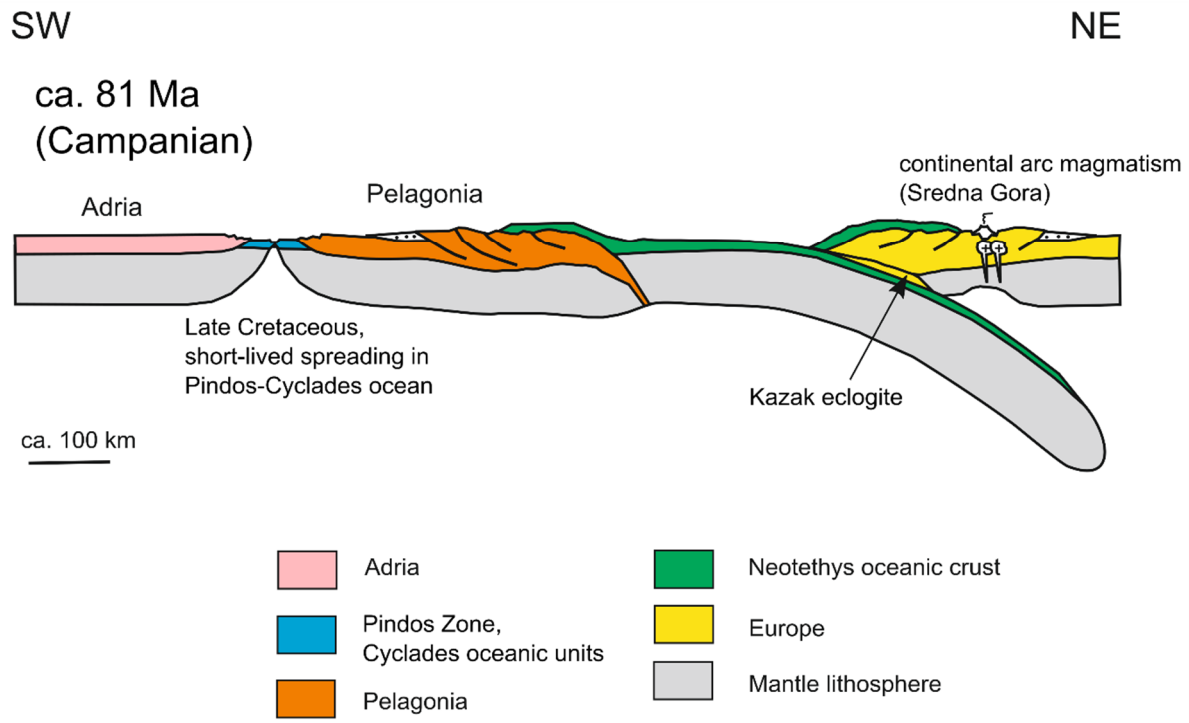

Fig. 3.8. Hypothetic cross section of the Rhodopes in the Late Cretaceous, following the interpretation that the Kazak eclogite represents a piece of upper-plate crust detached by tectonic erosion during subduction of Neotethys. Subduction is contemporaneous with continental arc magmatism in the Serdna Gora Zone and with separation of Pelagonia from Adria leading to short-lived spreading in the Pindos-Cyclades Ocean. The profile is a modification of earlier versions (Froitzheim et al. 2014, Petrík et al. 2016) and is partly based on data and references discussed in these papers.

Another line of evidence supporting Late Cretaceous subduction of the Kazak eclogite is the tectonic history of the hinterland of the Rhodopes, i.e. the Balkan fold-and-thrust belt (Fig. 3.9). It is widely accepted that collision leads to higher intraplate compressive stresses in the upper plate than oceanic subduction (Ziegler et al. 1995). Therefore, periods of compressional hinterland deformation may be related to collision events along the Rhodope margin, and tectonically quiet periods may be related to oceanic subduction. According to Burchfiel and Nakov (2015; see Fig. 3.9), the age of the Kazak eclogite falls into a quiet period followed by two periods of compressional deformation, the first beginning at ~65 Ma (Pelagonia-Europe collision?) and the second beginning at ~45 Ma (Adria-Europe collision?). Lu-Hf eclogite ages of ~50 Ma from the Cyclades island of Syros

(Lagos et al. 2007) reflect the subduction of the short-lived basin between Pelagonia and Adria and fall into the quiet period between the 65 and 45 Ma compressional periods.

During the activity of the Sredna Gora magmatic arc, from 95 to 67 Ma, the site of magmatic activity shifted southward, either due to slab rollback (von Quadt et al. 2005) or slab steepening (Gallhofer et al. 2015). At ~69 Ma, magmatism had arrived in the Eastern Rhodopes. The ~69 Ma Rozino granite is found as small intrusions in rocks of the Upper Allochthon (Fig. 3.2), only 4 km north of the Kazak eclogite. This may be explained by slab rollback. Alternatively, the close proximity could also result from post-69-Ma southward thrusting of the Upper Allochthon. However, the significant amount of post-69-Ma thrusting necessary to bridge the arc-trench gap (100 to 300 km in modern convergent margins) is not supported by geological evidence.

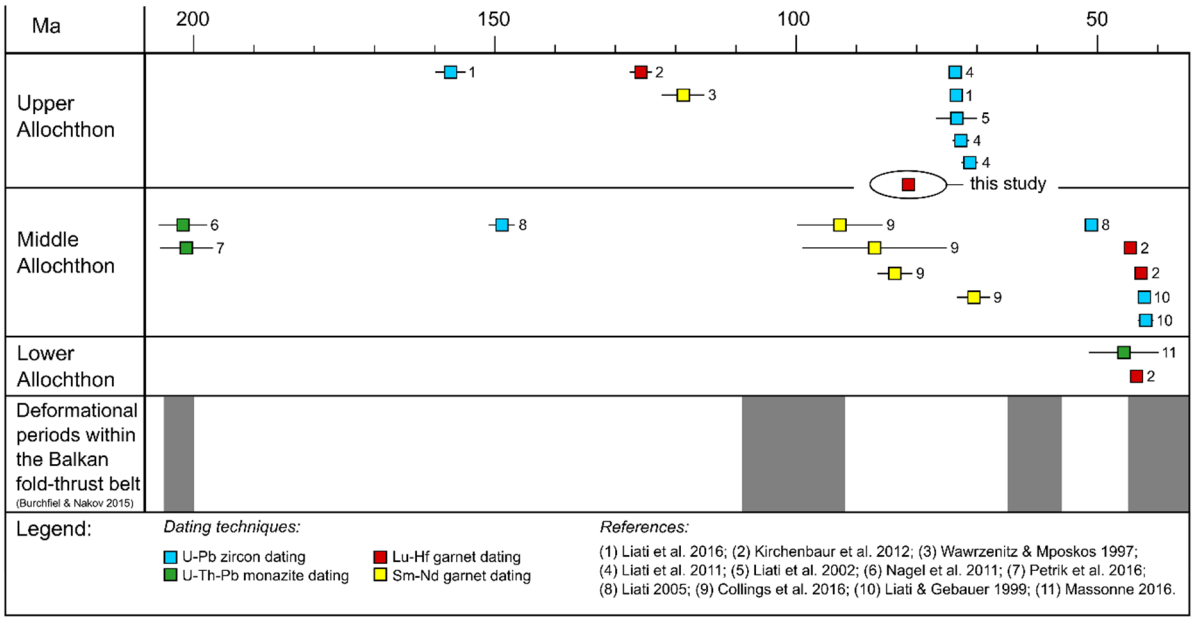

Fig. 3.9. Distribution of geochronological data in the Rhodopes, which were interpreted to reflect subduction-related HP and UHP metamorphism, as compared to deformational periods in the Balkan fold-and-thrust belt, i.e. the hinterland of the Rhodopes.

3.8. Conclusions

1. Eclogite KAS2 from the Byala Reka-Kechros Dome in the Eastern Rhodopes of Bulgaria underwent high-pressure metamorphic conditions of 1.2-1.6 GPa, 570-620 °C.

2. An isochron based on three garnet and two omphacite separates indicates an age of 81.6 ± 3.5 Ma for KAS2. The whole rock analyses plot below the isochron, probably due to the presence of considerably older zircon and/or rutile.

3. Garnet shows preserved prograde growth zoning. The Lu-Hf age can therefore be interpreted as dating the growth of garnet during prograde eclogite-facies metamorphism.

4. The eclogite-facies metamorphism coincides in time with supra-subduction magmatism in the Sredna Gora continental magmatic arc (~95 to ~67 Ma), suggesting a genetic link between the two processes.

5. The close proximity between ~69 Ma arc granitoids and the ~82 Ma eclogite may be explained by southward slab rollback.

Chapter 4

Devonian subduction and syn-collisional exhumation of continental crust in Lofoten, Norway

4.1. Introduction

The collision of continents is one of the most dramatic tectonic processes with large impact on mountain building, climate and earthquake hazard. Deep-seated processes in collision zones may be reconstructed by determining age and conditions of high-pressure metamorphic rocks, especially eclogite. In this respect, the eclogite-bearing but little-deformed basement of the Lofoten islands in Northern Norway (Fig. 4.1) plays a key role (Markl & Bucher 1997, Steltenpohl et al. 2003, 2006, 2011). It occupies a similar tectonic position as the Western Gneiss Complex (WGC; Fig. 4.1) exposed farther southwest, one of the best-exposed and -studied high-pressure/ultrahigh-pressure (HP/UHP) terranes worldwide (e.g., Andersen et al. 1991, Hacker et al. 2010). Peak-pressure metamorphism in the WGC occurred at c. 420-400 Ma (e.g., Kylander-Clark et al. 2009), during the Scandian phase of the Caledonian orogeny when the major continents Laurussia and Baltica collided after the closure of the Iapetus Ocean. Baltica, including the WGC, was subducted westward beneath Laurentia. Older, c. 500-450 Ma HP/UHP rocks are found in allochthonous nappes thrust southeastward over Baltica (e.g., Brueckner et al. 2004). These were formed during subduction and collision events preceding Laurentia-Baltica collision. Previous dating suggested that HP metamorphism in Lofoten took place c. 60 ma earlier than in the WGC (Steltenpohl et al. 2011), leading to suggestions that the Lofoten basement does not represent the margin of Baltica but a separate Lofoten terrane (Corfu 2004a). Here we present petrological and geochronological data from newly discovered kyanite eclogites. These record considerably higher P-T conditions than previously reported from Lofoten eclogites. Lu- Hf geochronology resulted in a typical

"Scandian" age of the eclogite-facies metamorphism. These results have important implications for the processes of subduction and exhumation of continental crust, in the case of the Caledonides and in general.

4.2. Regional Geology

The Precambrian rocks of the Lofoten–Vesterålen Complex (LVC) occur on the islands along the coast of northern Norway (Fig. 4.1). The LVC is composed of a late Archaean migmatite complex and an overlying series of early Proterozoic supracrustal rocks (Griffin et al. 1978). These were intruded by plutons of anorthosite, mangerite, charnockite, and granite during two short-lived events at c. 1870 and 1800-1790 Ma (Corfu 2004b). Exposed c. 400 km north of the Western Gneiss Complex, the LVC occupies a similar tectonic position in the hinterland below the allochthons. Caledonian deformation of the LVC is much weaker than in large parts of the WGC (Hacker et al. 2010), except for the Leknes Group, a Caledonian allochthon consisting of amphibolite-facies metasedimentary and metavolcanic rocks (Fig. 4.1), and for a subhorizontal shear zone along which the Leknes Group was emplaced on the basement (Tull 1977). The subvertical Gullesfjorden Shear Zone (Steltenpohl et al. 2006) separates the LVC from Baltican basement further east where Caledonian deformation is more conspicuous (Fig. 4.1). The few eclogites discovered so far on the Lofoten islands yielded considerably lower P-T conditions of 1.5 GPa, 680 °C (Markl & Bucher 1997) compared to the WGC where eclogites record up to ~3.6 GPa, 820 °C (Terry et al. 2000). The eclogite-forming event in the LVC appeared to be considerably older than in the WGC, based on a poorly constrained U-Pb zircon lower intercept age of 478 ± 41 Ma from a pre-kinematic granitoid dyke in a retrogressed eclogite lens at Myrland (Steltenpohl et al. 2011) (Fig. 4.1). With reference to the available $^{40}Ar/^{39}Ar$ data (Hames & Andresen 1996, Steltenpohl et al. 2003), in addition to U-Pb data for titanite and zircon from the Leknes group (Corfu 2004a), it was concluded that the eclogites underwent upper amphibolite facies metamorphism between 469 and 461 Ma ago and subsequently cooled below 500 °C ~433 Ma ago, and below 350 °C ~343 Ma ago (Steltenpohl et al. 2011). The relatively old ages for Caledonian metamorphism in Lofoten suggested that the Lofoten basement may originate from a terrane outboard of Baltica (Corfu, 2004a).

The base of the Leknes Group is a top-ESE directed thrust (Klein et al. 1999). Minor, kinematically similar faults also thrust basement slivers over rocks of the Leknes Group, underlining the contractional nature of this deformation phase. Thrusting took place between 420 and 390 Ma (^{40}Ar-^{39}Ar data; Hames & Andresen 1996). During this thrusting, both the Leknes Group and the underlying basement were under amphibolite-facies conditions of c. 0.6 GPa and 600 °C (Klein et al. 1999). The basal thrust was overprinted by extensional, top-W ductile shear zones and brittle normal faults (Klein et al. 1999).

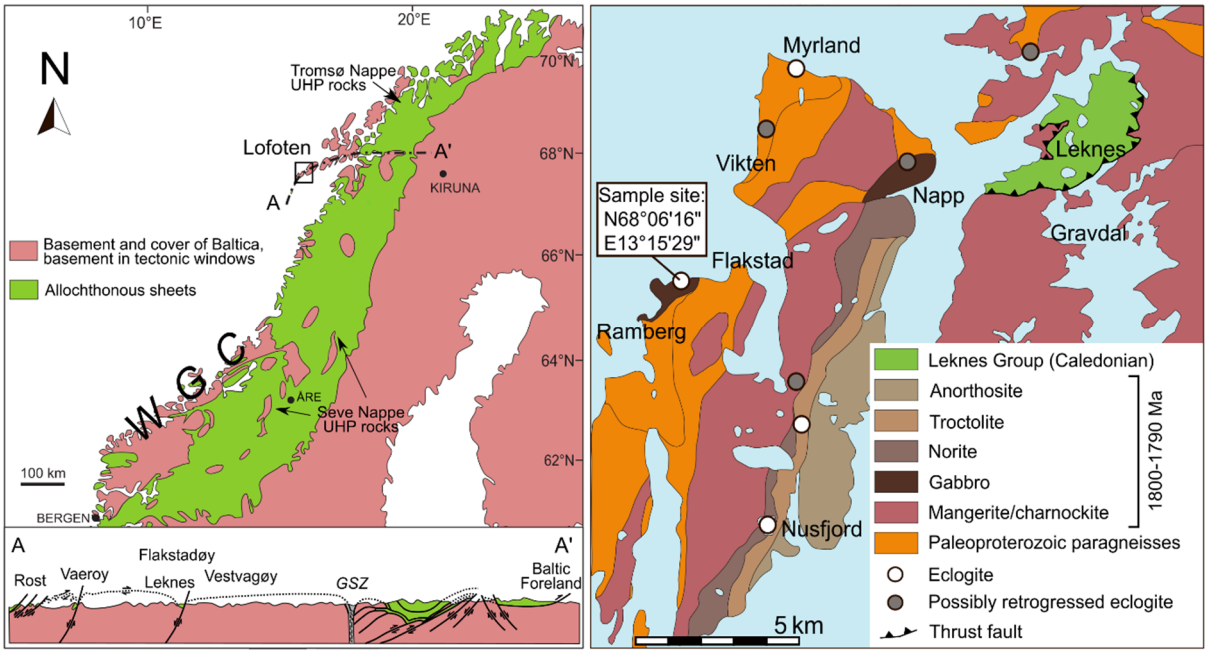

Fig. 4.1. Left: Simplified tectonic map (after Gee et al. 2013) and profile (after Steltenpohl et al. 2006) of the Scandinavian Caledonides. Black square indicates area of detailed map to the right. GSZ - Gullesfjorden shear zone (i.e., the boundary between the Lofoten-Vesterålen complex to the west and Baltica basement to the east); UHP - ultrahigh-pressure; WGC - Western Gneiss Complex. Right: Geological map of Flakstadøy and parts of Vestvågøy (Lofoten Islands).

4.3. Analytical methods

Part of the electron microprobe measurements was accomplished at the Dionýz Štúr Institute of Geology in Bratislava. All other measurements were performed at Steinmann Institute, Bonn. For a detailed description see Chapter 1.4.

4.4. Kyanite eclogite: P-T conditions and age

Previously reported eclogites from Lofoten are all bimineralic, garnet- and omphacite-bearing rocks without kyanite (Markl & Bucher 1997, Kullerud et al. 2001). The kyanite-bearing eclogite studied here occurs between Flakstad and Ramberg (Fig. 4.1) in a strongly deformed gabbronorite, often together with common eclogite of basaltic protolith which intruded the gabbronorite (Fig. 4.2). The kyanite eclogite is composed of garnet, omphacite, kyanite and phengite, considered to be the primary eclogite-facies minerals. These are variably overprinted by lower-pressure ones (Fig. 4.2). Garnet is poikiloblastic with inclusions of omphacite, amphibole, quartz, kyanite, phengite, zoisite, and rutile. Garnet shows compositional variations, with higher grossular (X_{Grs} = 0.23-0.24 mol%) and pyrope (X_{Prp} = 0.30–0.35 mol%) content in the core than in the rim (X_{Grs} = 0.18–0.20 mol%; X_{Prp} = 0.30–0.32 mol%). Omphacite with jadeite content of up to 45 mol% occurs as inclusions in the garnet and kyanite. Matrix omphacite is partly replaced by diopside + plagioclase symplectite. Kyanite is present as subhedral porphyroblasts in the matrix and tiny inclusions in garnet; matrix kyanite is mantled by sapphirine, spinel, corundum and plagioclase. Minor phengite with up to 3.5 Si a.p.f.u. occurs in the matrix and as inclusions in garnet, being partly replaced by biotite + plagioclase symplectite.

Peak metamorphic P-T conditions have been calculated from equilibria between garnet, omphacite, kyanite, phengite, and quartz in sample RV-6, using the garnet with the highest grossular, omphacite with the highest jadeite, and phengite with the highest Si content (Table 4.1). The following methods were used: a) "conventional" geothermobarometry (Ravna & Terry 2004), b) average PT method of THERMOCALC (Holland & Powell 1998), and c) thermodynamic modeling with Perple_X (Connolly 1990); the results are shown in Figure 4.3. The P-T results obtained from conventional geothermobarometry (2.6 GPa; 656 °C) and average PT method (2.2 GPa; 650 °C) plot within the stability field of the Grt + Omp + Ph + Ky + Qz assemblage. The compositional isopleths of garnet (X_{Ca}^{Grt} = 0.23), omphacite (X_{Na}^{Omp} = 0.46–0.47) and phengite (3.4-3.45

Si p.f.u.) constrain P-T conditions of 2.4-2.8 GPa and 630–680 °C. Therefore, we conclude that P-T conditions of Lofoten eclogites reached 2.5–2.8 GPa and ~650 °C.

Lu-Hf chronometry was applied to sample LOF 3/12 (Fig. 4.4, Table 4.2). For the whole rock, two different digestion methods were applied, selective digestion ("table top") and complete digestion ("bombed"). An isochron defined by a selectively digested whole rock, four hand-picked garnet separates, and one hand-picked omphacite separate yielded an age of 399 ± 10 Ma with a mean square weighted deviation (MSWD) of 0.45 (Fig. 4.4). The selective digestion method leaves back potential older grains of refractory Hf-bearing phases like zircon and rutile, which, if present, could affect the age. A completely digested whole rock together with the four garnet separates yielded an age of 416 ± 20 Ma with an MSWD of 0.55 (n = 5). This age is identical within error with the age obtained using the selectively digested whole rock. The low initial $^{176}Hf/^{177}Hf$ ratio of the whole rock suggests that the protolith of these eclogites is older than the magmatic suites emplaced at 1870-1790 Ma. Other gabbros in the Lofoten have been dated at ca. 1789-1796 Ma (Corfu 2004b) but the protolith of the sampled eclogite has not yet been dated and may be older. To account for the measured composition (εHf_t = -28.6 at 399 Ma) it would have to be Archean. We calculated a depleted-mantle Hf model age (TDM Hf) of ~2900 Ma. Alternatively, the metamorphic event at ~400 Ma could have reset almost entirely the Lu-Hf system and produced the observed Hf isotopic composition.

The bell-shaped concentration profiles of Lu and Y across a garnet grain (Fig. 4.5) show that garnet remained a closed system for these elements since the formation of the high-pressure mineral assemblage. This is in line with estimates of the closure temperature of the Lu-Hf system in garnet (Shu et al. 2014) ranging from 630 °C to ~1000 °C. This range is almost entirely above the peak temperature reached by the Lofoten eclogite (~650 °C). Therefore, 399 ± 10 Ma represents the age of garnet growth during pressure increase, i.e., subduction.

Mineral	**Grt**	**Omp**	**Ph**
SiO_2	39.84	56.26	53.00
TiO_2	0.12	0.04	0.02
Al_2O_3	21.86	11.13	27.41
Cr_2O_3	0.02	0.01	0.02
FeOt	21.67	3.35	4.50
MnO	0.42	0.02	0.02
MgO	7.87	8.95	3.03
CaO	8.69	13.76	0.35
Na_2O		6.73	0.05
K_2O			8.20
Total	100.49	100.25	96.60
Si	3.025	1.986	3.434
Ti	0.007	0.001	0.001
Al	1.956	0.463	2.093
Cr	0.001	0.000	0.001
Fe^{3+}		0.023	0.171
Fe^{2+}	1.376	0.076	0.073
Mn	0.027	0.001	0.001
Mg	0.891	0.471	0.293
Ca	0.707	0.518	0.024
Na		0.461	0.006
K			0.678
XAlm	0.46		
XSps	0.01		
XPrp	0.30		
XGrs	0.24		
XJd		0.45	

Table 4.1. Representative compositions of garnet, omphacite, and phengite from sample RV-6 used for P-T calculations.

Sample	Lu (ppm)	Hf (ppm)	$^{176}Lu/^{177}Hf$	2σ	$^{176}Hf/^{177}Hf$	2σ
LOF 3/12						
WR tt	0.0694	0.187	0.05269	0.00011	0.282238	0.000047
WR bmb	0.0731	0.799	0.01298	0.00003	0.281857	0.000104
Grt 1	0.195	0.0916	0.3025	0.0008	0.284110	0.000032
Grt 2	0.192	0.113	0.2425	0.0005	0.283732	0.000275
Grt 3	0.204	0.107	0.2714	0.0005	0.283931	0.000405
Grt 4	0.195	0.0824	0.3366	0.0007	0.284531	0.000286
Omp 1	0.0295	0.168	0.02490	0.00005	0.282047	0.000065

Table 4.2. Lu-Hf data Lofoten kyanite eclogite. Uncertainties on the $^{176}Lu/^{177}Hf$ and $^{176}Hf/^{177}Hf$ ratios are the estimated 2σ external reproducibilities, as described in text.
WR tt whole rock tabletop digestion, WR bmb whole rock PARR bomb digestion.

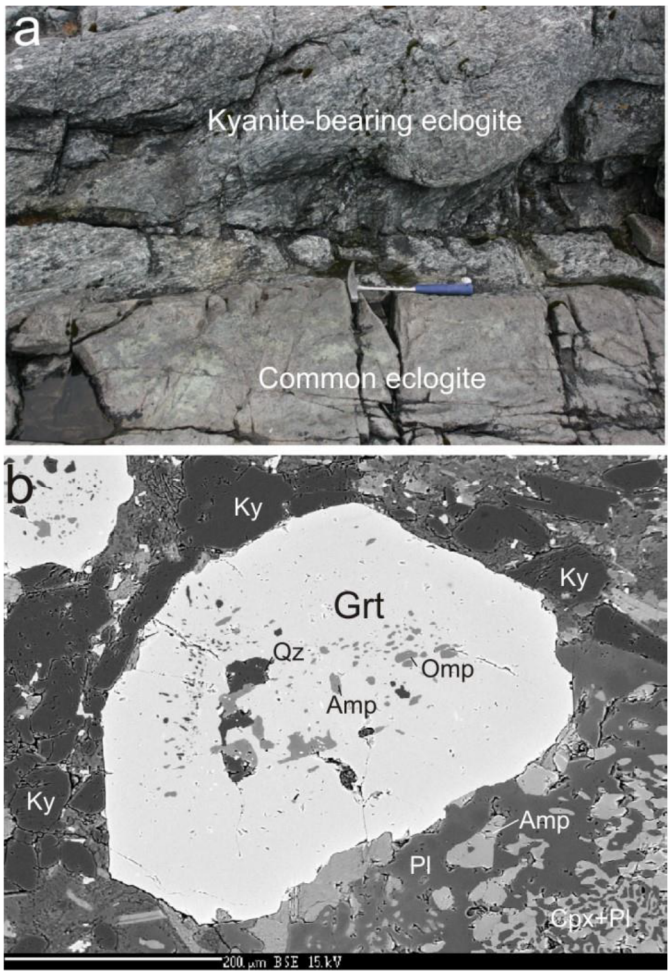

Fig. 4.2. Kyanite eclogite from Lofoten. a. Outcrop of kyanite-bearing and common eclogite in a strongly deformed gabbro-anorthosite at the sample locality near Flakstad. b. BSE image of kyanite eclogite RV-6 showing garnet porphyroblast with inclusions of omphacite (Omp), amphibole (Amp) and quartz (Qz), and kyanite (Ky) as dark grains next to garnet. Symplectite of clinopyroxene (Cpx) + plagioclase (Pl) and retrograde amphibole (Amp) in the matrix are also shown.

▼Fig. 4.3. Pressure-temperature (P-T) section for the kyanite eclogite sample RV-6, from the same locality as the dated sample, in the system NCKFMASH (Na_2O = 2.87, CaO = 10.71, K_2O = 0.65, FeO = 8.65, MgO = 12.61, Al_2O_3 = 12.88, SiO_2 = 51.63, H_2O = 1.4 mol%) with compositional isopleths of garnet [X_{Ca}^{Grt} = Ca/(Ca + Mg + Fe)], omphacite [X_{Na}^{Omp} = Na/(Na + Ca)], and phengite (Si^{Ph} apfu). Yellow oval encompasses estimated peak conditions. Amp - amphibole; coe - coesite; grt - garnet; ky - kyanite; lw - lawsonite; Omp - omphacite; Ph - phengite; phl - phlogopite; Pl - plagioclase; qz - quartz; San - sanidine; ta - talc. Results from conventional geothermobarometry (RT, yellow dot) of Krogh Ravna and Terry (2004) and average P-T method (TC, blue dot) of THERMOCALC are also shown.

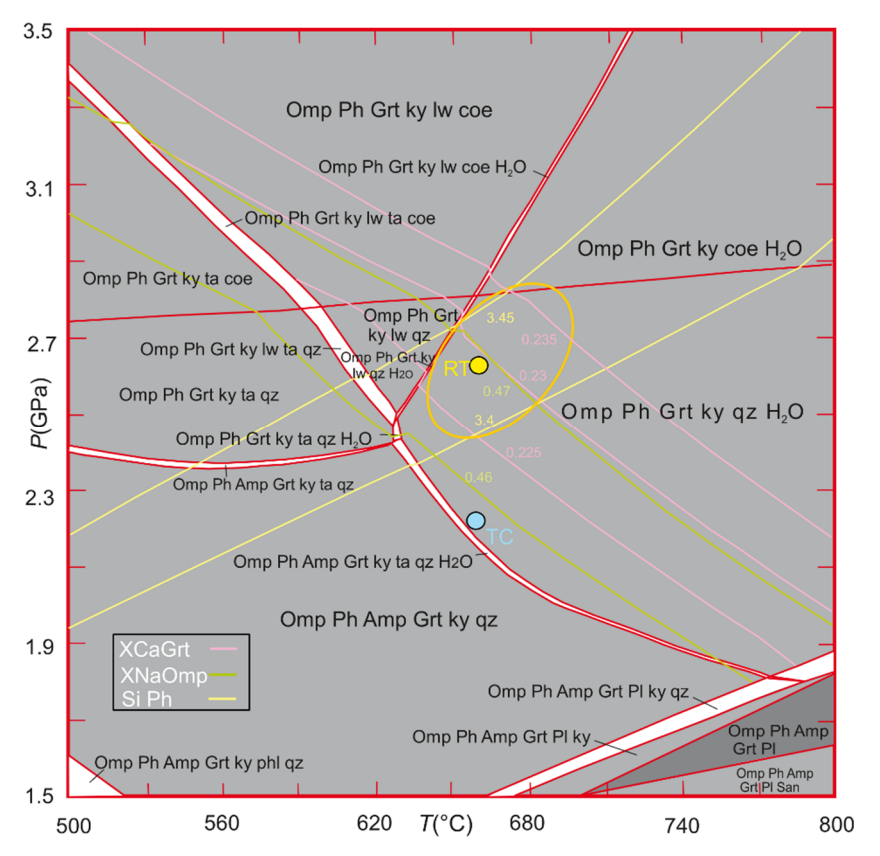

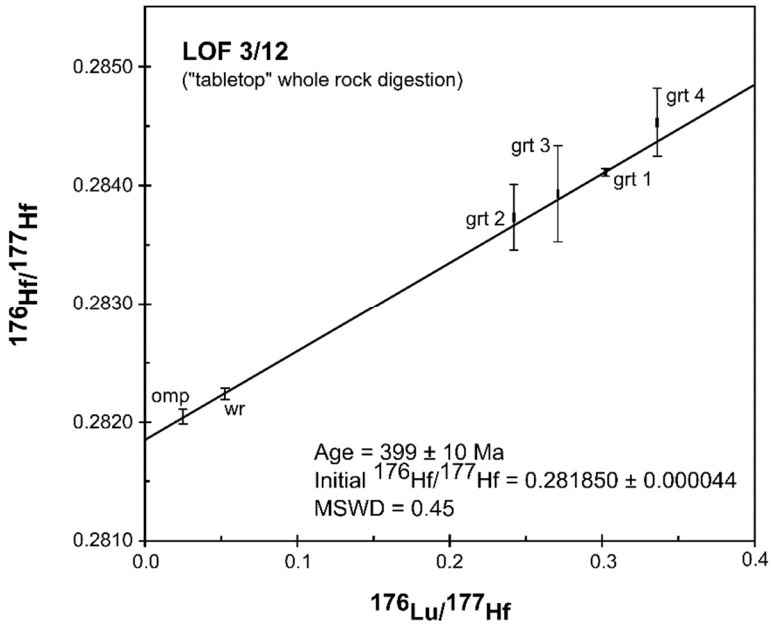

Fig. 4.4. Lu-Hf isochron for kyanite eclogite LOF 3/12. MSWD - mean square of weighted deviates; grt - garnet; omp - omphacite; wr - whole rock.

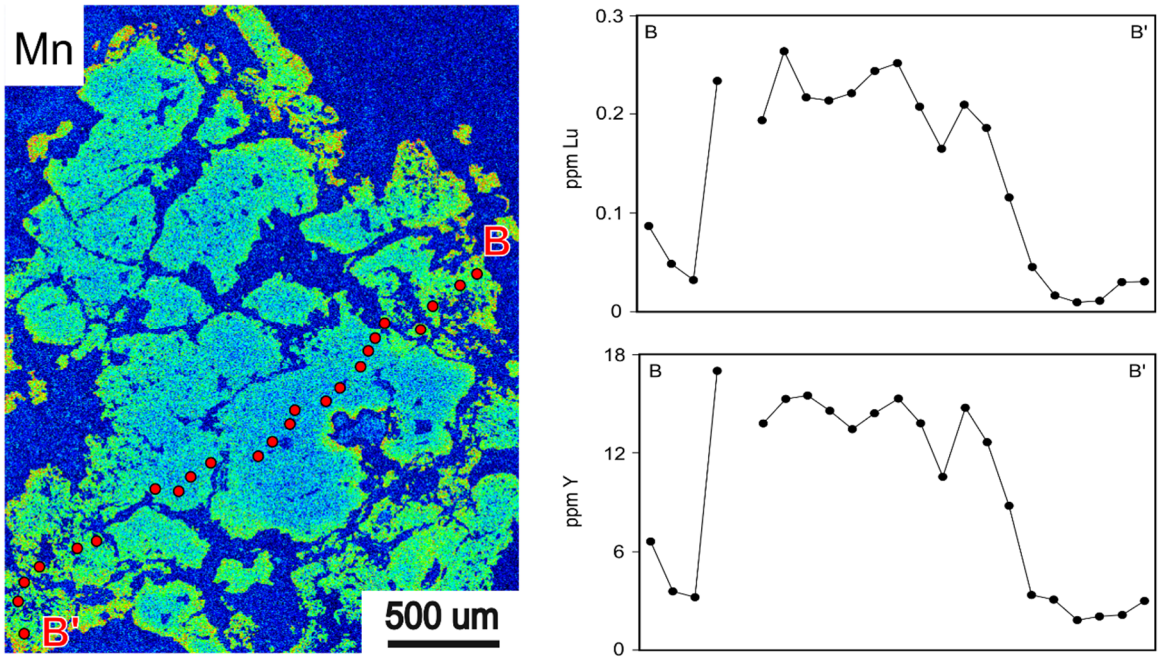

Fig. 4.5. Mn distribution map and Lu and Y concentration profiles of a large garnet grain in the dated sample LOF 3/12. The profile is interupted where a measurement hits an inclusion. Profile length is 2.74 mm.

4.5. Discussion

The new Lu-Hf isochron represents the first direct dating of eclogite in Lofoten. The age of 399 ± 10 Ma is also typical for eclogites in the WGC, confirming the correlation between these two areas. We interpret an $^{40}Ar/^{39}Ar$ hornblende age of ~433 Ma from the Lofoten eclogites (Steltenpohl et al. 2003) to be affected by excess Ar, a common phenomenon in high-pressure rocks (Kelley 2002).

The evidence presented here for contemporaneous deep subduction of continental crust in Lofoten and the WGC at ~400 Ma largely simplifies the tectonic reconstruction of the Scandinavian Caledonides. 500-450 Ma old HP/UHP rocks remain restricted to the allochthons, i.e., the Seve Nappe Complex (Middle Allochthon) and the Tromsø Nappe (Uppermost Allochthon; Fig. 4.1). Their formation preceded the continent collision between Laurentia and Baltica. Assuming near-lithostatic stress and that half of the thickness of the overburden was formed by crustal rocks (density of 2.7 g/cm^3) and half by mantle rocks (3.3 g/cm^3), the pressure derived from the Lofoten kyanite eclogite corresponds to a depth of ca. 90 km reached during Caledonian collision. Assuming a higher proportion of crustal rocks would lead to a greater depth. The limited Caledonian deformation of the LVC shows that a large volume of crust was subducted deeply, stayed rigid, and was exhumed in one piece. The absence of major ductile deformation and pervasive HP metamorphism probably resulted from the anhydrous nature of most of the basement rocks in the LVC (Bartley 1982) and is in line with the observation of earthquake-generated pseudotachylyte formed under eclogite-facies conditions (Steltenpohl et al. 2006). The almost complete erosion of the allochthons since the Devonian brought the surface of the subducted Baltican crust back into a subhorizontal position (Fig. 4.1), almost as it was before the Caledonian orogeny.

Our results have far-reaching implications for the unresolved issue of how deeply subducted rocks return to the surface. The emplacement of the Leknes Group on the eclogite-bearing basement plays a key role in this respect. This allochthon was thrusted eastward over the basement under amphibolite-facies conditions, i.e., after considerable decompression of the basement from c. 2.8 - 2.5 GPa (eclogite facies, our data) to 0.6 GPa (amphibolite facies, Klein et al. 1999). Assuming lithostatic pressures, such decompression corresponds to ~60 km of exhumation from mantle depth to the lower

crust. This occurred still in a framework of crustal shortening, as underlined by the thrust character of the contact and the imbrication of basement slivers on top of Leknes Group (Klein et al. 1999). Regionally, crustal shortening took place until ~400 Ma (e.g., Hacker et al. 2010). Therefore, the exhumation rate was intermediate to high (> 6.6 mm/a), even if the actual pressure peak occurred at 409 Ma, the upper end of the error bar (60 km in 9 Ma). Figure 4.6 depicts a possible scenario for exhumation in a convergent plate setting, assuming two subduction zones. Space for eduction of the subducted Baltican margin (Andersen et al. 1991, Tucker et al. 2004) was created at depth by the extraction of the Iapetus lithosphere (driven by slab pull) while shortening took place at the surface, governed by the convergence of Baltica and Laurentia. The Leknes Group was thrust over the exhumed Baltican basement. Extensional collapse of the Caledonides (e.g., Fossen 2000) commenced immediately after this and may have been caused by the increase in buoyancy resulting from the removal of the dense Iapetus lithospheric slab.

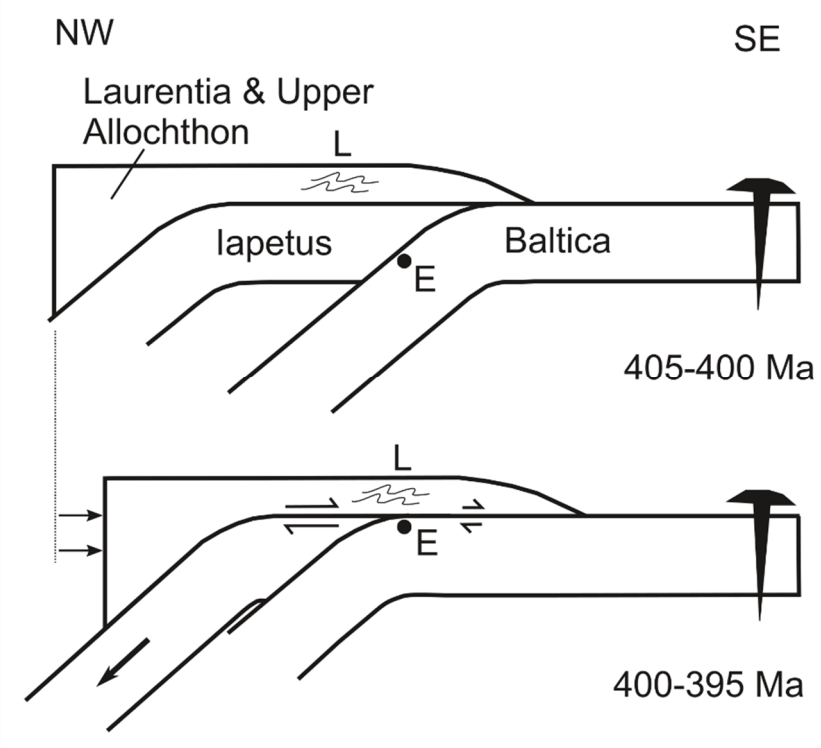

Fig. 4.6. Schematic cross sections showing subduction and exhumation of Lofoten eclogites (E). Upper panel shows subduction of Baltica, including the Lofoten basement, in a three-plate scenario. L denotes the Leknes Group, which was metamorphosed earlier (ca. 469-461; Corfu 2004a), probably in the framework of Iapetus subduction under Laurentia. Lower panel shows slab pull– driven descent and extraction of the Iapetus oceanic lithosphere. This leads to eduction of Baltica and unroofing of Lofoten eclogites, although the motion of major plates Laurentia and Baltica is convergent (small arrows on lower left "pushing" Laurentia).

4.6. Conclusions

The Lofoten basement belonged to the continental margin of Baltica and occupied a similar position as the WGC. It was subducted at c. 400 Ma when Baltica collided with Laurentia, and reached conditions of 2.5-2.8 GPa and ~650 °C. These were, however, only recorded by eclogite lenses whereas the bulk of the basement preserved its older granulite-facies parageneses and suffered only minor Caledonian deformation. This supports the conclusion that under favorable conditions, subducted continental crust may stay rigid down to a depth of c. 90 km. Thrust emplacement of the Leknes Group under amphibolite-facies conditions requires exhumation of the basement during crustal shortening. This may be explained by a three-plate scenario where slab-pull-driven descent of the Iapetus Plate caused eduction of Baltica.

References

Andersen, T.B., Jamtveit, B., Dewey, J.F., Swensson, E. (1991): Subduction and eduction of continental crust: Major mechanisms during continent-continent collision and orogenic extensional collapse, a model based on the southern Norwegian Caledonides. Terra Nova, 3, 303–310.

Bartley, J.M. (1982): Limited basement involvement in Caledonian deformation, Hinnøy, north Norway, and tectonic implications. Tectonophysics, 83, 185–203.

Bauer, C., Rubatto, D., Krenn, K., Proyer, A., Hoinkes, G. (2007): A zircon study from the Rhodope metamorphic complex, N-Greece: Time record of a multistage evolution. Lithos, 99, 207-228.

Baxter, E.F., Scherer, E.E. (2013): Garnet geochronology: Timekeeper of tectonometamorphic processes. Elements, 9, 433-438.

Bizzaro, M., Baker, J.A., Haack, H., Ulfbeck, D., Rosing, M. (2003): Early history of Earth's crust-mantle system inferred from hafnium isotopes in chondrites. Nature, 421, 931-933.

Blichert-Toft, J., Chauvel, C., Albarède, F. (1997): Separation of Hf and Lu for high-precision isotope analysis of rock samples by magnetic sector-multiple collector ICP-MS. Contribution to Mineralogy and Petrology, 127, 248-260.

Blichert-Toft, J., Albarède, F., Kornprobst, J. (1999): Lu-Hf isotope systematics of garnet pyroxenites from Beni Bousera, Morocco: Implications for basalt origin. Science, 283, 1303-1306.

Bloch, E., Ganguly, J., Hervig, R., Cheng, W. (2015): 176Lu–176Hf geochronology of garnet I: experimental determination of the diffusion kinetics of Lu3+ and Hf4+ in garnet, closure temperatures and geochronological implications. Contributions to Mineralogy and Petrology, 169:12.

Bonev, N., Stampfli, G. (2003): New structural and petrologic data on Mesozoic schists in the Rhodope (Bulgaria): geodynamic implications. Comptes Rendus Geoscience, 335, 691–699.

Bonev, N. (2006): Cenozoic tectonic evolution of the eastern Rhodope massif (Bulgaria): Basement structure and kinematics of syn- to postcollisional extensional deformation. Geological Society of America Special Papers, 409, 211-235.

Bonev, N., Burg, J.-P., Ivanov, Z. (2006): Mesozoic-Tertiary structural evolution of an extensional gneiss dome – the Kesebir-Kardamos dome, eastern Rhodope (Bulgaria-Greece). International Journal of Earth Sciences, 95, 318-340.

Bonev, N., Ovtcharova-Schaltegger, M., Moritz, R., Marchev, P., Ulianov, A. (2013): Peri-Gondwanan Ordovician crustal fragments in the high-grade basement of the Eastern Rhodope Massif, Bulgaria: evidence from U-Pb LA-ICP-MS zircon geochronology and geochemistry. Geodinamica Acta, 26, 207-229.

Bonev, N., Marchev, P., Moritz, R., Collings, D. (2015): Jurassic subduction zone tectonics of the Rhodope Massif in the Thrace region (NE Greece) as revealed by new U-Pb and 40Ar/39Ar geochronology of the Evros ophiolite and high-grade basement rocks. Gondwana Research, 27, 760-775.

Bonev, N., Borisova, M., Filipov, P. (2016): Middle Triassic magmatic crystallization of the Volvi metamafic body, Serbo-Macedonian Massif, Northern Greece: new evidence for Triassic rifting history. In: National Conference ‘‘Geosciences 2016’’, proceedings, Sofia 2016, pp. 51–52.

Braund, E., Stüwe, K., Proyer, A. (2010): Pseudosection modelling for a selected eclogite body from the Koralpe (Hohl), Eastern Alps. Mineralogy and Petrology, 99, 75-87.

Brueckner, H.K., van Roermund, H.L.M., Pearson, N. (2004): An Archean to Paleozoic evolution for a garnet peridotite lens with sub-Baltic Shield affinity within the Seve Nappe Complex of Jämtland, Sweden, Central Scandinavian Caledonides. Journal of Petrology, 45, 415–437.

Brun, J.-P., Faccenna, C. (2008): Exhumation of high-pressure rocks driven by slab roll-back. Earth and Planetary Science Letters, 272, 1–7.

Burchfiel, B.C., Nakov, R., Tzankov, T. (2003): Evidence from the Mesta half-graben, SW Bulgaria, for the Late Eocene beginning of Aegean extension in the Central Balkan Peninsula. Tectonophysics, 375, 61–76.

Burchfiel, B.C., Nakov, R. (2015): The multiply deformed foreland fold-thrust belt of the Balkan orogen, northern Bulgaria. Geosphere, 11, 463-490.

Burg, J.-P., Ivanov, Z., Ricou, L.E., Dimov, D., Klain, L. (1990): Implications of shear sense criteria for the tectonic evolution of the Central-Rhodopes Massif, southern Bulgaria. Geology, 18, 451-454.

Burg, J.-P., Ricou, L.E., Ivanov, Z., Godfriaux, I., Dimov, D., Klain, L. (1996): Syn-metamorphic nappe complex in the Rhodope massif: structure and kinematics. Terra Nova, 8, 6-15.

Burg, J.-P. (2012): Rhodope: From Mesozoic convergence to Cenozoic extension. Review of petro-structural data in the geochronological frame. Journal of virtual explorer, 42, 44pp.

Burtman, V., Molnar, P. (1993): Geological and geophysical evidence for deep subduction of continental crust beneath the Pamir. Geological Society of America, Special papers, 281, 1–70.

Burton, K.W., Kohn, M.J., Cohen A.S., O'Nions, R.K. (1995): The relative diffusion of Pb, Nd, Sr and O in garnet. Earth and Planetary Science Letters, 133, 199–211.

Caddick, M.J., Konopásek, J., Thompson, A.B. (2010): Preservation of garnet growth zoning and the duration of prograde metamorphism. Journal of Petrology, 51, 2327–2347.

Carlson, W.D. (1989): The significance of intergranular diffusion to the mechanism and kinetics of porphyroblast crystallization. Contributions to Mineralogy and Petrology, 103, 1–24.

Carlson, W.D. (2006): Rates of Fe, Mg, Mn and Ca diffusion in garnet. American Mineralogist, 91, 1–11.

Carlson, W.D. (2012): Rates and mechanism of Y, REE, and Cr diffusion in garnet. American Mineralogist, 97, 1598–1618.

Carrigan, C.W., Mukasa, S.B., Haydoutov, I., Kolcheva, K. (2003): Ion microprobe U-Pb zircon ages of pre-Alpine rocks in the Balkan, Sredna Gora and Rhodope terranes of Bulgaria: Constraints on Neoproterozoic and Variscan tectonic evolution. Journal of the Czech Geological Society, 48, 32-33.

Casey, J., Dewey, J. (1984): Initiation of subduction zones along transform and accreting plate boundaries, triple-junction evolution, and forearc spreading centres—implications for ophiolitic geology and obduction. Geological Society, London, Special Publications, v. 13, no. 1, 269-290.

Chauvel, C., Blichert-Toft, J.E. (2001): A hafnium isotope and trace element perspective on melting of the depleted mantle. Earth and Planetary Science Letters, 190, 137–151.

Chemenda, A.I., Mattauer, M., Malavieille, J., Bokun, A.N. (1995): A mechanism for syncollision rock exhumation and associated normal faulting: results from physical modelling. Earth and Planetary Science Letters, 132, 225–232.

Chopin, C. (1984): Coesite and pure pyrope in high-grade blueschists of the western Alps: a first record and some consequences. Contributions to Mineralogy and Petrology, 86, 107–118.

Chopin, C. (2003): Ultrahigh-pressure metamorphism: tracing continental crust into the mantle. Earth and Planet Science Letters, 212, 1–14.

Cloetingh, S., Wortel, M.J.R., Vlaar, N.J. (1982): Evolution of passive continental margins and initiation of subduction zones. Nature, 297, 139-142.

Cloetingh, S., Wortel, R., Vlaar, N.J. (1989): On the initiation of Subduction zones. Pure and Applied Geophysics, 129, 7–25.

Cloos, M., Shreve, R.L. (1988): Subduction-channel model of prism accretion, melange formation, sediment subduction, and subduction erosion at convergent plate margins: 2. Implications and discussion. Pure and Applied Geophysics, 128, 501–545.

Collings, D., Savov, I., Maneiro, K., Baxter, E., Harvey, J., Dimitrov, I. (2016): Late Cretaceous UHP metamorphism recorded in kyanite-garnet schists from the Central Rhodope Mountains, Bulgaria. Lithos, 246-247, 165-181.

Connolly, J.A.D. (1990): Multivariable phase diagrams: an algorithm based on generalized thermodynamics. American Journal of Science, 290, 666–718.

Corfu, F. (2004a): U-Pb geochronology of the Leknes Group: an exotic Early-Caledonian metasedimentary assemblage stranded on Lofoten basement, N-Norway. Journal of the Geological Society, 161, 619–627.

Corfu, F. (2004b): U-Pb age, setting and tectonic significance of the anorthosite-mangerite-charnockite-granite suite, Lofoten-Vesterålen, Norway. Journal of Petrology, 45, 1799-1819.

Cornelius, N.K. (2008): UHP metamorphic rocks of the Eastern Rhodope Massif, NE Greece: New constraints from petrology, geochemistry and zircon ages. PhD dissertation, Johannes Gutenberg University, Mainz.

Daniel, C.G., Spear, F.S. (1999): The clustered nucleation and growth processes of garnet in regional metamorphic rocks from North-west Connecticut, USA. Journal of Metamorphic Geology, 17, 503–520.

Davies, J.H., Stevenson, D.J. (1992): Physical model of source region of subduction zone volcanics. Journal of Geophysical Research, 97, 2037-2070.

De Capitani, C., Petrakakis, K. (2010): The computation of equilibrium assemblage diagrams with Theriak/Domino software. American Mineralogist, 95, 1006-1016.

DesOrmeau, J.W., Gordon, S.M., Kylander-Clark, A.R.C., Hacker, B.R., Bowring, S.A., Schoene, B., Samperton, K.M. (2015): Insights into (U)HP metamorphism of the Western Gneiss Region, Norway: a high-spatial resolution and high-precision zircon study. Chemical Geology, 414, 138–155.

Diener, J.F.A., Powell, R., White, R.W., Holland, T.J.B. (2007): A new thermodynamic model for clino- and orthoamphiboles in the system Na2O-CaO-FeO-MgO-Al2O3-SiO2-H2O-O. Journal of Metamorphic Geology, 25, 631-656.

Dinter, D.A., MacFarlane, A., Hames, W., Isachsen, C., Bowring, S., Royden, L. (1995): U-Pb and 40Ar/39Ar geochronology of the Symvolon granodiorite: Implications for the thermal and structural evolution of the Rhodope metamorphic core complex, northeastern Greece. Tectonics, 14, 886-908.

Dinter, D.A. (1998): Late Cenozoic extension of the Alpine collisional orogen, northeastern Greece: Origin of the north Aegean basin. Bulletin of the Geological Society of America, 110, 1208-1226.

Dobrzhinetskaya, L.F., Eide, E.A., Larsen, R.B., Sturt, B.A., Tronnes, R.G., Smith, D.C., Taylor, W.R., Posukhova, T.V. (1995): Microdiamonds in high-grade metamorphic rocks of the Western Gneiss Region, Norway. Geology, 23, 597–600.

Duretz, T., Gerya, T.V., Kaus, B.J.P., Andersen, T.B. (2012): Thermomechanical modelling of slab eduction. Journal of Geophysical Research 117.

Duretz, T., Gerya, T.V. (2013): Slab detachment during continental collision: influence of crustal rheology and interaction with lithospheric delamination. Tectonophysics, 602, 124-140.

Duchêne, S., Blichert-Toft, J., Luais, B., Téluk, P., Lardeaux, J.M., Albarède, F. (1997): The Lu-Hf dating of garnets and the ages of the Alpine high-pressure metamorphism. Nature, 387, 586–589.

Eleftheriadis, G., Frank, W., Petrakakis, K. (2001): 40Ar/39Ar dating and cooling history of the Pangeon granitoids, Rhodope massif (Eastern Macedonia, Greece). Bulletin of Geological Society of Greece, 34, 911-916.

Faccenna, C., Giardini, D., Devy, P., Argentiri, A. (1999): Initiation of subduction at Atlantic-type margins: Insights from laboratory experiments. Journal of Geophysical Research, 104, 2749-2766.

Faryad, S.W., Melcher, F., Hoinkes, G., Puhl, J., Meisel, T., Frank, W. (2002): Relics of eclogite-facies metamorphism in the Austroalpine basement, Hochgrössen (Speik Complex), Austria. Mineralogy and Petrology, 74, 49–73.

Fassmer, K., Obermüller, G., Nagel, T.J., Kirst, F., Froitzheim, N., Sandmann, S., Miladinova, I., Fonseca, R.O.C., Münker, C. (2016): High-pressure metamorphic age and significance of eclogite-facies continental fragments associated with oceanic lithosphere in the Western Alps (Etirol-Levaz Slice, Valtournenche, Italy). Lithos, 252-253, 145-159.

Faure, M., Shu, L., Wang, B., Charvet, J., Choulet, F., Monie, P. (2009): Intracontinental subduction: a possible mechanism for the Early Palaeozoic Orogen of SE China. Terra Nova, 21, 360-368.

Fischer, G.W. (1978): Rate laws in metamorphism. Geochimica et Cosmochimica Acta, 42, 1035–1050.

Fossen, H. (2000): Extensional tectonics in the Caledonides: Synorogenic or postorogenic? Tectonics, 19, 213–224.

Fossen, H. (2010): Extensional tectonics in the North Atlantic Caledonides: a regional view. In: Law, R., Butler, R., Holdsworth, B., Krabbendam, R.A., Strachan, M. (eds): Continental tectonics and mountain building: the legacy of Peach and Horn. Geological Society Special Publication, London, vol. 335, pp 767–793.

Frank, W. (1987): Evolution of the Austroalpine elements in the Cretaceous. In Flügel, H.W., Faupl, P. (eds) Geodynamics of the Eastern Alps. Deuticke, Vienna, 379–406.

Frank, W., Kralik, M., Scharbert, S., Thöni, M. (1987): Geochronological data from the Eastern Alps. In: Flügel, H.W., Faupl, P. (eds): Geodynamics of the Eastern Alps. Vienna, Deuticke, p. 272-281.

Froitzheim, N., Schmid, S.M., Conti, P. (1994): Repeated change from crustal shortening to orogen-parallel extension in the Austroalpine units of Graubünden. Eclogae Geologicae Helvetiae. 87, 559-612.

Froitzheim, N., Schmid, S.M., Frey, M. (1996): Mesozoic paleogeography and the timing of eclogite metamorphism in the Alps: A working hypothesis. Eclogae Geologicae Helvetiae, v. 89, p. 81–110.

Froitzheim, N., Pleuger, J., Roller, S., Nagel, T. (2003): Exhumation of high- and ultrahigh-pressure metamorphic rocks by slab extraction. Geology, 31, 925-928.

Froitzheim, N., Jahn-Awe, S., Frei, D., Wainwright, A.N., Maas, R., Georgiev, N., Nagel, T.J., Pleuger, J. (2014): Age and composition of meta-ophiolite from the Rhodope Middle Allochthon (Satovcha, Bulgaria): A test for the maximum-allochthony hypothesis of the Hellenides. Tectonics, 33, 1477-1500.

Gallhofer, D., von Quadt, A., Peytcheva, I., Schmid, S.M., Heinrich, C.A. (2015): Tectonic, magmatic, and metallogenic evolution of the Late Cretaceous arc in the Carpathian-Balkan orogen. Tectonics, 34, 1813-1836.

Ganguly, J., Cheng, W., Chakraborty, S. (1998): Cation diffusion in aluminosilicate garnets: experimental determination in pyrope-almandine diffusion couples. Contributions to Mineralogy and Petrology, 131, 171–180.

Gautier, P., Bosse, V., Cherneva, Z., Didier, A., Gerdjikov, I., Tiepolo, M. (2017): Polycyclic alpine orogeny in the Rhodope metamorphic complex: the record in migmatites form the Nestos shear zone (N. Greece). Bulletin de la Société géologique de France, 188, 36.

Gee, D.G., Fossen, H., Henriksen, N., Higgins, A.K. (2008): From the early Paleozoic platforms of Baltica and Laurentia to the Caledonide Orogen of Scandinavia and Greenland. Episodes, 31(1), 44–51.

Gee, D., Janák, M., Majka, J., Robinson, P., van Roermund, H. (2013): Subduction along and within the Baltoscandian margin during closing of the Iapetus Ocean and Baltica-Laurentia collision. Lithosphere, 5, 169–178.

Georgiev, N., Henry, B., Jordanova, N., Froitzheim, N., Jordanova, D., Ivanov, Z., Dimov, D. (2009): The emplacement mode of Upper Cretaceous plutons from the southwestern part of the Sredna Gora Zone (Bulgaria): structural and AMS study. Geologica Carpathica, 60, 15-33.

Georgiev, N., Pleuger, J., Froitzheim, N., Sarov, S., Jahn-Awe, S., Nagel, T.J. (2010): Separate Eocene-Oligocene and Miocene stages of extension and core complex formation in the Western Rhodopes, Mesta Basin, and Pirin Mountains (Bulgaria). Tectonophysics, 487, 59-84.

Georgiev, N., Henry, B., Jordanova, N., Jordanova, D., Naydenov, K. (2014): Emplacement and fabric-forming conditions of plutons from structural and magnetic fabric analysis: A case study of the Plana pluton (Central Bulgaria). Tectonophysics, 629, 138-154.

Georgiev, N., Froitzheim, N., Cherneva, Z., Frei, D., Grozdev, V., Jahn-Awe, S., Nagel, T.J. (2016): Structure and U-Pb zircon geochronology of an Alpine nappe stack telescoped by extensional detachment faulting (Kulidzhik area, Eastern Rhodopes, Bulgaria). International Journal of Earth Sciences, 105, 1985-2012.

Gerya, T.V., Stöckhert, B. (2006): Two-dimensional numerical modeling of tectonic and metamorphic histories at active continental margins. International Journal of Earth Sciences 95, 250–274.

Godard, G., Martin, S., Prosser, G., Kienast, J.R., Morten, L. (1996): Variscan migmatites, eclogites and garnet peridotites of the Ulten zone, Eastern Austroalpine system. Tectonophysics, 259, 313–341.

Green, E.C.R., Holland, T.J.B., Powell, R. (2007): An order-disorder model for omphacite pyroxenes in the system jadeite-diopside-hedenbergite-acmite with applications to eclogite rocks. American Mineralogist, 92, 1181-1189.

Griffin, W.L., Taylor, P.N., Hakkinen, J.W., Heier, K.S., Iden, I.K., Krogh, E.J., Malm, O., Olsen, K.I., Ormaasen, D.E., Tveten, E. (1978): Archaean and Proterozoic crustal evolution in Lofoten-Vesterålen, N. Norway. Journal of the Geological Society, 135, 629–647.

Habler, G., Thöni, M., Sölva, H. (2006): Tracing the high pressure stage in the polymetamorphic Texel Complex (Austroalpine basement unit, Eastern Alps): P-T-t-d constraints. Minerogy and Petrology, 88, 269–296.

Hacker, B.R., Ratschbacher, L., Webb, L., McWilliams, M.O., Ireland, T., Calvert, A., Dong, S., Wenk, H.-R., Chateigner, D. (2000): Exhumation of ultrahigh-pressure continental crust in east central China: Late Triassic-Early Jurassic tectonic unroofing, Journal of Geophysical Research, 105(B6), 13339–13364.

Hacker, B.R., Andersen, T.B., Johnston, S., Kylander-Clark, A.R.C., Peterman, E.M., Walsh, E.O., Young, D. (2010): High-temperature deformation during continental-margin subduction & exhumation: The ultrahigh-pressure Western Gneiss Region of Norway. Tectonophysics, 480, 149–171.

Hacker, B.R., Gerya, T.V. (2013): Paradigms, new and old, for ultrahigh-pressure tectonism. Tectonophysics, 603, 79-88.

Hamburger, M.W., Sarewitz, D.R., Pavlis, T.L., Popandopulo, G.A. (1992): Structural and seismic evidence for intracontinental subduction in the Peter the First Range, Central Asia. Geological Society of America Bulletin, 104, 397-408.

Hames, W.E., Andresen, A. (1996): Timing of orogeny and extension in the continental shelf of north-central Norway as indicated by laser 40Ar/39Ar muscovite dating. Geology, 24, 1005-1008.

Handy, M.R., Schmid, S.M., Bousquet, R., Kissling, E., Bernoulli, D. (2010): Reconciling plate-tectonic reconstructions of Alpine Tethys with the geological-geophysical record of spreading and subduction in the Alps. Earth-Science Reviews, 102, 121–158.

Hauke, M., Froitzheim, N., Nagel, T.J., Miladinova, I., Fassmer, K., Fonseca, R.O.C., Sprung, P., Münker, C. (2019): Two high-pressure metamorphic events, Variscan and Alpine, dated by Lu-Hf in an eclogite complex of the Austroalpine nappes (Schobergruppe, Austria). International Journal of Earth Sciences, 108, 1317-1331.

Hauzenberger, C.A., Höller, W., Hoinkes, G. (1996): Transition of eclogite to amphibolite-facies metamorphism in the Austroalpine Ulten Zone. Mineralogy and Petrology, 58, 111–130.

Hawthorne, F.C., Oberti, R., Harlow, G.E., Maresch, W.V., Martin, R.F., Schumacher, J.C., Welch, M.D. (2012): IMA report, nomenclature of the amphibole supergroup. American Mineralogist, 97, 2031-2048.

Herwartz, D., Münker, C., Scherer, E.E., Nagel, T.J., Pleuger, J., Froitzheim, N. (2008): Lu-Hf garnet geochronology of eclogites from the Balma Unit (Pennine Alps): implications for Alpine paleotectonic reconstructions. Swiss Journal of Geosciences, 101, 1, 173-189.

Hickmott, D.D., Shimizu, N., Spear, F.S., Selverstone, J. (1987): Trace-element zoning in a metamorphic garnet. Geology, 15, 573-576.

Himmerkus, F., Reischmann, T., Kostopoulos, D.K. (2009): Serbo-Macedonian revisited: a Silurian basement terrane from northern Gondwana in the internal Hellenides, Greece. Tectonophysics, 473, 20-35.

Himmerkus, F., Zachariadis, P., Reischmann, T., Kostopoulos, D. (2012): The basement of the Mount Athos peninsula, northern Greece: insights from geochemistry and zircon ages. International Journal of Earth Sciences, 101, 1467-1485.

Hoinkes, G., Purtscheller, F., Tessadri, R (1982): Polymetamorphose im Ostalpin westlich der Tauern (Ötztaler Masse, Schneeberger Zug, Brennermesozoikum). Geologisch-Paläontologische Mitteilungen Innsbruck, 12, 5, 95-113.

Hoinkes, G., Frank, W., Mauracher, J., Peschel, R., Purtscheller, F., Tessadri, R. (1987): Petrography of the Schneeberg Complex. In: Flügel H.W., Faupl P. (eds): Geodynamics of the Eastern Alps. Deuticke, Vienna, pp. 190-199.

Hoinkes, G., Kostner, A., Thöni, M. (1991): Petrologic constraints for Eo-Alpine eclogite facies metamorphism in the Austroalpine Ötztal basement. Mineralogy and Petrology, 43, 237–254.

Hoinkes, G., Koller, F., Rantitsch, G. et al. (1999): Alpine metamorphism of the Eastern Alps. Schweizerische Mineralogische und Petrographische Mitteilungen, 79, 155–181.

Hoke, L. (1990): The Altkristallin of the Kreuzeck Mountains, SE Tauern Window, Eastern Alps - basement crust in a convergent plate boundary. Jahrbuch der Geologischen Bundesanstalt Wien, 133, 5-87.

Holland, T.J.B., Powell, R. (1998): An internally consistent thermodynamic data set for phases of petrological interest. Journal of Metamorphic Geology, 16, 309-343.

Hollister, L.S. (1966): Garnet zoning: an interpretation based on the Rayleigh fractionation model. Science, 154, 1647-1651.

Jahn-Awe, S., Froitzheim, N., Nagel, T.J., Frei, D., Georgiev, N., Pleuger, J. (2010): Structural and geochronological evidence for Paleogene thrusting in the Western Rhodopes (SW Bulgaria) - elements for a new tectonic model of the Rhodope Metamorphic Province. Tectonics, 29, TC3008.

Jahn-Awe, S., Pleuger, J., Frei, D., Georgiev, N., Froitzheim, N., Nagel, T.J. (2012): Time constraints for low-angle shear zones in the Central Rhodopes (Bulgaria) and their significance for the exhumation of high-pressure rocks. International Journal of Earth Sciences, 101, 1971-2004.

Janák, M., Froitzheim, N., Lupták, B., Vrabec, M., Krogh Ravna, E.J. (2004): First evidence for ultrahigh-pressure metamorphism of eclogites in Pohorje, Slovenia: tracing deep continental subduction in the Eastern Alps. Tectonics, 23, TC5014.

Janák, M., Froitzheim, N., Vrabec, M., Krogh Ravna, E.J., De Hoog, J.C.M. (2006): Ultrahigh-pressure metamorphism and exhumation of garnet peridotite in Pohorje, Eastern Alps. Journal of Metamorphic Geology, 24, 19–31.

Janák, M., Cornell, D., Froitzheim, N., De Hoog, J.C.M., Broska, I., Vrabec, M., Hurai, V. (2009): Eclogite-hosting metapelites from the Pohorje Mountains (Eastern Alps): P–T evolution, zircon geochronology and tectonic implications. European Journal of Mineralogy, 21, 1191–1212.

Janák, M., Froitzheim, N., Georgiev, N., Nagel, T.J., Sarov, S. (2011): P-T evolution of kyanite eclogite from the Pirin Mountains (SW Bulgaria): implications for the Rhodope UHP Metamorphic Complex. Journal of Metamorphic Geology, 29, 317-332.

Janák, M., Froitzheim, N., Yoshida, K., Sasinková, V., Nosko, M., Kobayashi, T., Hirajima, T., Vrabec, M. (2015): Diamond in metasedimentary crustal rocks from Pohorje, Eastern Alps: a window to deep continental subduction. Journal of Metamorphic Geology, 33, 495–512.

Jankovic, S. (1977): Major Alpine ore deposits and metallogenic units in the northeastern Mediterranean and concepts of plate tectonics. In: Metallogeny and plate tectonics in the northeastern Mediterranean. Faculty of Mining Geology, Belgrad University, pp. 105-171.

Jochum, K.P., Weiss, U., Stoll, B., Kuzmin, D., Yang, Q., Raczek, I., Jacob, D.E., Stracke, A., Birbaum, K., Frick, D.A., Günther, D., Enzweiler, J. (2011): Determination of reference values for NIST SRM 610-617 glasses following ISO guidelines. Geostandards and Geoanalytical Research, 35, 397-429.

Kelley, S. (2002): Excess argon in K-Ar and Ar-Ar geochronology. Chemical Geology, 188, 1-22.

Kelly, E.D., Carlson, W.D., Connelly, J.N. (2011): Implications of garnet resorption for the Lu–Hf garnet geochronometer: an example from the contact aureole of the Makhavinekh Lake Pluton, Labrador. Journal of Metamorphic Geology, 29, 901–916.

Kemp, D.V., Stevenson, D.J. (1996): A tensile, flexural model for the initiation of subduction. Geophysical Journal International, 125, 73-93.

Kilias, A., Falalakis, G., Sfeikos, A., Papadimitriou, E., Vamvaka, A., Gkarlaouni, C. (2013): The Thrace basin in the Rhodope province of NE Greece – A tertiary supradetachment basin and its geodynamic implications. Tectonophysics, 595-596, 90-105.

Kirchenbaur, M., Pleuger, J., Jahn-Awe, S., Nagel, T.J., Froitzheim, N., Fonseca, R.O.C., Münker, C. (2012): Timing of high-pressure metamorphic events in the Bulgarian Rhodopes from Lu-Hf garnet geochronology. Contributions to Mineralogy and Petrology, 163, 897-921.

Klein, A.C., Steltenpohl, M.G., Hames, W.E., Andresen, A. (1999) Ductile and brittle extension in the southern Lofoten archipelago, North Norway: Implications for differences in tectonic style along an ancient collisional margin: American Journal of Science, 299, 69–89.

Klemme, S., Prowatke, S., Hametner, K., Günther, D. (2005): The partitioning of trace elements between rutile and silicate melts: Implications for subduction zones. Geochimica et Cosmochimica Acta, 69, 2361-2371.

Klemme, S., Günther, D., Hametner, K., Prowatke, S., Zack, T. (2006): The partitioning of trace elements between ilmenite, ulvospinel, armalcolite and silicate melts with implications for the early differentiation of the moon. Chemical Geology, 234, 251-263.

Klötzli-Chowanetz, E., Klötzli, U., Koller, F. (1997): Lower Ordovician migmatisation in the Ötztal crystalline basement (Eastern Alps, Austria): linking U-Pb and Pb-Pb dating with zircon morphology. Schweizerische Mineralogische und Petrologische Mitteilungen, 77, 315-324.

Klug, L., Schmidtke, M., Froitzheim, N., Tomachek, F., Miladinova, I. (in prep.): Deformation and metamorphism in Saltaus valley (Texel complex, South Tyrol).

Kolčeva, K., Željažkova-Panajotova, M., Dobrecov, N.L., Stojanova, V. (1986): Eclogites in Central Rhodope Metamorphic group and their retrograde metamorphism. Geochemistry, Mineralogy and Petrology, 20-21, 130-144.

Konrad-Schmolke, M., Zack, T., O'Brien, P.J., Jacob, D.E. (2008): Combined thermodynamic and rare earth element modelling of garnet growth during subduction: Examples from ultrahigh-pressure eclogite of the Western Gneiss Region, Norway. Earth and Planetary Science Letters, 272, 488–498.

Konzett, J., Hoinkes, G. (1996): Paragonite-hornblend assemblages and their petrological significance; an example from the Austroalpine Schneeberg Complex, souther Tyrol, Italy. Journal of Metamorphic Geology, 14 (1), 85-101.

Konzett, J., Krenn, K., Hauzenberger, Ch., Whitehouse, M., Hoinkes, G. (2012): High-pressure tourmaline formation and fluid activity in Fe-Ti-rich eclogites from the Kreuzeck Mountains, Eastern Alps, Austria. Journal of Petrology, 53, 99-125.

Kozhukharova, E. (1980): Eclogites in the Precambrian from the Eastern Rhodope block. Comptes Rendus de l'Academie Bulgare des Sciences, 33(3), 375-378.

Kozhoukharova, E. (2010): Metaophiolite association in the Rhodope Massif as a stratigraphical and structural marker. XIX CBGA Congress Thessaloniki, Proceedings, 165-171.

Kretz, R. (1974): Some models for the rate of crystallization of garnet in metamorphic rocks. Lithos, 7, 123–131.

Krogh, T.E., Kamo, S.L., Robinson, P., Terry, M.P., Kwok, K. (2011): U–Pb zircon geochronology of eclogites from the Scandian Orogen, northern Western Gneiss Region, Norway: 14–20 million years between eclogite crystallization and return to amphibolite facies conditions. Canadian Journal of Earth Sciences, 48, 441–472.

Krohe, A., Mposkos, E. (2002): Multiple generations of extensional detachments in the Rhodope Mountains (northern Greece): evidence of episodic exhumation of high-pressure rocks. In: Blundell, D.J., Neubauer, F., von Quadt, A. (eds): The Timing and Location of Major ore Deposit in an Evolving Orogen. Geological Society London Special Publications, 204, 151-178.

Kromel, J., Putis, M., Bacik, P. (2011): The Middle Austro-Alpine Sieggraben structural complex – new data on geothermobarometry. Acta Geologica Slovaca, 3, 1-12.

Kullerud, K., Flaat, K., Davidsen, B. (2001): High-pressure fluid–rock reactions involving Cl-bearing fluids in lower-crustal ductile shear zones of the Flakstadøy Basic Complex, Lofoten, Norway. Journal of Petrology, 42, 1349-1372.

Kurz, W., Fritz, H. (2003): Tectonometamorphic evolution of the Austroalpine Nappe Complex in the Central Eastern Alps—consequences for the Eo-Alpine evolution of the Eastern Alps. International Geology Review, 45, 1100-1127.

Kurz, W., Handler, R., Bertholdy, C. (2008): Tracing the exhumation of the Eclogite Zone (Tauern Window, Eastern Alps) by 40Ar/39Ar dating of white mica in eclogites. Swiss Journal of Geosciences, 101 Supplement 1, S191-S206.

Kydonakis, K., Brun, J.-P., Sokoutis, D. (2015a): North Aegean core complexes, the gravity spreading of a thrust wedge. Journal of Geophysical Research - Solid Earth, 120, 595-616.

Kydonakis, K., Moulas, E., Chatzitheodoridis, E., Brun, J.-P., Kostopoulos, D. (2015b): First-report on Mesozoic eclogite-facies metamorphism preceding Barrovian overprint from the western Rhodope (Chalkidiki, northern Greece). Lithos, 220, 147-163.

Kylander-Clark, A.R.C., Hacker, B.R., Johnson, C.M., Beard, B.L., Mahlen, N.J., Lapen, T.J. (2007): Coupled Lu–Hf and Sm–Nd geochronology constrains prograde and exhumation histories of high- and ultrahigh-pressure eclogites from western Norway. Chemical Geology, 242, 137–154.

Kylander-Clark, A.R.C., Hacker, B.R., Johnson, C.M., Beard, B.L., Mahlen, N.J. (2009): Slow subduction of a thick ultrahigh-pressure terrane. Tectonics, 28, TC2003.

Kylander-Clark, A.R.C., Hacker, B.R., Mattinson, C.G. (2012): Size and exhumation rate of ultrahigh-pressure terranes linked to orogenic stage. Earth and Planetary Science Letters, 321-322, 115-120.

Ladenhauf, C., Armstrong, R.A., Konzett, J., Miller, C. (2001): The timing of the pre-alpine HP-metamorphism in the Eastern Alps: constraints from U-Pb SHRIMP dating of eclogite zircons from the Austro-Alpine Silvretta nappe. Geologisch-Paläontologische Mitteilungen Innsbruck, 25, 131.

Lagos, M., Scherer, E.E., Tomaschek, F., Münker, C., Keiter, M., Berndt, J., Ballhaus, C. (2007): High precision Lu-Hf geochronology of Eocene eclogite-facies rocks from Syros, Cyclades, Greece. Chemical Geology, 243, 16-35.

Li, Z., Gerya, T.V. (2009): Polyphase formation and exhumation of high- to ultrahigh-pressure rocks in continental subduction zone; numerical modeling and application to

the Sulu ultrahigh-pressure terrane in eastern China. Journal of Geophysical Research, 114 (B9).

Liati, A., Mposkos, E. (1990): Evolution of the eclogites in the Rhodope Zone of northern Greece. Lithos, 25, 89-99.

Liati, A., Seidel, E. (1996): Metamorphic evolution and geochemistry of kyanite eclogites in central Rhodope, northern Greece. Contributions to Mineralogy and Petrology, 123, 293-307.

Liati, A., Gebauer, D. (1999): Constraining the prograde and retrograde P-T-t path of Eocene HP rocks by SHRIMP dating of different zircon domains: inferred rates of heating, burial, cooling and exhumation for central Rhodope, northern Greece. Contributions to Mineralogy and Petrology, 135, 340-354.

Liati, A., Gebauer, D., Wysoczanski, R. (2002): U–Pb SHRIMP-dating of zircon domains from UHP garnet-rich mafic rocks and late pegmatoids in the Rhodope zone (N Greece); evidence for Early Cretaceous crystallization and Late Cretaceous metamorphism. Chemical Geology, 184, 281-299.

Liati, A. (2005): Identification of repeated Alpine (ultra) high-pressure metamorphic events by U-Pb SHRIMP geochronology and REE geochemistry of zircon: the Rhodope zone of Northern Greece. Contributions to Mineralogy and Petrology, 150, 608-630.

Liati, A., Fanning, C.M. (2005): Eclogites and their country rock orthogneisses in East Rhodope representing upper permian gabbros and upper carboniferous granitoids: geochronological constraints. Mitteilungen der Oesterreichischen Mineralogischen Gesellschaft, 150, p. 88.

Liati, A., Gebauer, D., Fanning, C.M. (2011): Geochronology of the Alpine UHP Rhodope zone: A review of isotopic ages and constraints on the geodynamic evolution. In: Dobrzhinetskaya, L.F., Faryad, S.W., Wallis, S., Cuthbert, S. (eds): Ultrahigh-pressure metamorphism. Elsevier, Amsterdam, pp. 295-324.

Liati, A., Theye, T., Fanning, C.M., Gebauer, D., Rayner, N. (2016): Multiple subduction cycles in the Alpine orogeny, as recorded in single zircon crystals (Rhodope zone, Greece). Gondwana Research, 29, 199-207.

Lichem, Ch., Hoinkes, G., Gregurek, D. (1997): Polymetamorphism of the Austroalpine Koralm basement: new evidence for a Permian event. Terra Nova Abstract 9 (Supplement 1), 489.

Linner, M. (1999): Die P–T–t Entwicklung der Eklogite im Schoberkristallin als Beleg für frühalpidische kontinentale Subduktion im Ostalpinen Kristallin. PhD Thesis, Institute of Petrology, University of Vienna, 167 pp.

Longerich, H.P., Jackson, S.E., Günther, D. (1996): Laser ablationin ductively coupled plasma mass spectrometric transient signal data acquisition and analyte concentration calculation. Journal of Analytical Atomic Spectrometry, 11, 899-904.

Ludwig, K.R. (2001): Isoplot/Ex version 2.49, Geochronological toolkit for Microsoft excel. Berkeley Geochronology Center Special Publications 1a.

Macheva, L., Peytcheva, I., von Quadt, A., Zidarov, N., Tarassova, E. (2006): Petrological, geochemical and isotope features of Lozen metagranite, Belasitza Mountain–evidence for widespread distribution of Ordovician metagranitoids in the Serbo-Macedonian Massif, SW Bulgaria. In: National Conference ‘‘Geosciences 2006’’, proceedings, Sofia 2006, pp. 209-212.

Mandl, G.W., Ondrejickova, A. (1993): Radiolarien und Conodonten aus dem Meliatikum im Ostabschnitt der Nördlichen Kalkalpen (Österreich). Jahrbuch der Geologischen Bundesanstalt, 136, 841–871.

Marchev, P., von Quadt, A., Peytcheva, I., Ovtcharova, M. (2006): The age and origin of the Chuchuliga and Rozino granites, Eastern Rhodopes. In: National Conference “Geosciences 2006”, proceedings, Sofia 2006, pp. 213-216.

Marchev, P., Georgiev, S., Singer, B. (2015): Onset of Late Cretaceous magmatism in the Eastern Balkan, Bulgaria: results from 40Ar/39Ar dating of amphibole from volcanic rocks. In: National Conference “Geosciences 2015”, proceedings, Sofia 2015, pp. 69-70.

Markl, G., Bucher, K. (1997) Proterozoic eclogites from the Lofoten islands, northern Norway. Lithos, 42, 15-35.

Massonne, H.-J. (2016): Tertiary high-pressure metamorphism recorded in andalusite-bearig mica-schist, southern Pirin Mts., S Bulgaria. European Journal of Mineralogy, 28(6), 1187-1202.

McKenzie, D.P. (1977): The initiation of trenches: A finite amplitude instability. In: M. Talwani & W.C. Pittman: Island Arcs, Deep Sea Trenches, and Back-Arc Basins. Maurice Ewing Ser., Vol. I, pp. 57-61, AGU, Washington, D.C.

Meinhold, G., Kostopoulos, D.K. (2013): The Circum-Rhodope Belt, northern Greece: Age, provenance, and tectonic setting. Tectonophysics, 595, 55-68.

Melcher, F., Meisel, T. (2004): A metamorphosed Early Cambrian crust – mantle transition in the Eastern Alps, Austria. Journal of Petrology, 48, 1689–1723.

Meyer, W. (1968): Zur Altersstellung des Plutonismus im Südteil der Rila-Rhodope-Masse (Nordgriechenland). Geologica et Paleontologica, 2, 173-192.

Michard, A., Goffé, B., Liati, A., Mountrakis, D. (1994): Blueschist-facies assemblages in the peri-Rhodopian zone and hints for an Eohellenic HP/LT belt in northern Greece. Bulletin of the Geological Society of Greece, 30, 185-192.

Miller, C., Stosch, H.G., Hoernes, St. (1988): Geochemistry and origin of eclogites from the type locality Koralpe and Saualpe, Eastern Alps, Austria. Chemical Geology, 67, 103–118.

Miller, C. (1990): Petrology of the type locality eclogites from the Koralpe and Saualpe (Eastern Alps), Austria. Schweizerische Mineralogische und Petrologische Mitteilungen, 70, 287-300.

Miller, C., Thöni, M. (1995): Origin of eclogites from the Austroalpine Ötztal basement (Tirol, Austria): geochemistry and Sm-Nd vs. Rb-Sr isotope systematics. Chemical Geology, 122, 199-225.

Miller, C., Thöni, M. (1997): Eo-Alpine eclogitisation of Permian MORB-type gabbros in the Koralpe (Eastern Alps, Austria): new geochronological, geochemical and petrological data. Chemical Geology, 137, 283–310.

Miller, C., Thöni, M., Konzett, J., Kurz, W., Schuster, R. (2005a): Eclogites from the Koralpe and Saualpe type-localities, Eastern Alps, Austria. Mitteilungen der Österreichischen Mineralogischen Gesellschaft, 150, 227–263.

Miller, C., Mundil, R., Thöni, M., Konzett, J. (2005b): Refining the timing of eclogite metamorphism: a geochemical, petrological, Sm–Nd and U–Pb case study from the Pohorje Mountains, Slovenia (Eastern Alps). Contributions to Mineralogy and Petrology, 150, 70–84.

Miller, C., Zanetti, A., Thöni, M., Konzett, J. (2007): Eclogitisation of gabbroic rocks: redistribution of trace elements and Zr in rutile thermometry in an Eo-Alpine subduction zone (Eastern Alps). Chemical Geology, 239, 96–123.

Mitchell, A.H.G. (1996): Distribution and genesis of some epizonal Zn-Pb and Au provinces in the Carpathian—Balkan region. Transactions of the Institution of Mining and Metallurgy (Section B: Applied Earth Science), 105, 127-138.

Moritz, R., Jacquat, S., Chambefort, I., Fontignie, D., Petrunov, R., Georgieva, S., von Quadt, A. (2003): Controls on ore formation at the high-sulphidation Au–Cu Chelopech deposit, Bulgaria: evidence from infrared fluid inclusion microthermometry of enargite and isotope systematics of barite. In: Eliopoulos, D. et al. (eds): Mineral Exploration and Sustainable Development. Millpress, Rotterdam, pp. 1209-1212.

Moulas, E., Schenker, F.L., Burg, J.-P., Kostopoulos, D. (2017): Metamorphic conditions and structural evolution of the Kesebir-Kardamos dome: Rhodope metamorphic complex (Greece-Bulgaria). International Journal of Earth Sciences, 106, 2667-2685.

Mposkos, E.D., Kostopoulos, D.K. (2001): Diamond, former coesite and supersilicic garnet in metasedimentary rocks from the Greek Rhodope: A new ultrahigh-pressure metamorphic province established. Earth and Planetary Science Letters, 192, 497-506.

Mposkos, E., Baziotis, I., Proyer, A. (2012): Pressure-temperature evolution of eclogites from the Kechros complex in the Eastern Rhodope (NE Greece). International Journal of Earth Sciences, 101, 973-996.

Münker, C., Weyer, S., Scherer, E.E., Mezger, K. (2001): Separation of high field strength elements (Nb, Ta, Zr, Hf) and Lu from rock samples for MC-ICPMS measurements. Geochemistry, Geophysics, Geosystems, 2, 1064.

Nagel, T.J., Schmidt, S., Janák, M., Froitzheim, N., Jahn-Awe, S., Georgiev, N. (2011): The exposed base of a collapsing wedge: The Nestos Shear Zone (Rhodope Metamorphic Province, Greece). Tectonics, 30, TC4009.

Nagel, T.J., Herwartz, D., Rexroth, S., Münker, C., Froitzheim, N., Kurz, W. (2013): Lu-Hf dating, petrography, and tectonic implications of the youngest Alpine eclogites (Tauern Window, Austria). Lithos, 170-171, 179-190.

Naydenov, K., Peytcheva, I., von Quadt, A., Sarov, S., Kolcheva, K., Dimov, D. (2013): The Maritsa strike-slip shear zone between Kostenets and Krichim towns, South Bulgaria — Structural, petrographic and isotope geochronology study. Tectonophysics, 595-596, 69-89.

Neubauer, F., Frisch, W. (1993): The Austro-Alpine metamorphic basement east of the Tauern Window. In: von Raumer, J.F., Neubauer, F. (eds) Pre-Mesozoic Geology in the Alps. Berlin, Springer, pp. 515–536.

Neubauer. F., Hoinkes, G., Sassi, F.P., Handler, R., Höck, V., Koller, F., Frank, W. (1999a): Pre-Alpine metamorphism of the Eastern Alps. Schweizerische Mineralogische und Petrologische Mitteilungen, 79, 41-62.

Neubauer, F., Dallmeyer, R., Takasu, A. (1999b): Conditions of eclogite formation and age of retrogression within the Sieggraben unit, Eastern Alps: Implications for Alpine-Carpathian tectonics. Schweizerische Mineralogische und Petrologische Mitteilungen, 79, 297–307.

Neubauer, F., Genser, J., Handler, R. (2000a): The Eastern Alps: Result of a two-stage collision process. Mitteilungen der Österreichischen Geologischen Gesellschaft, v. 92, p. 117–134.

Neubauer, F., Höck, V. (2000b): Aspects of geology in Austria and adjoining areas: introduction. Mitteilungen der Österreichischen Geologischen Gesellschaft, 92, 7–14.

Neubauer, F. (2002): Contrasting Late Cretaceous with Neogene ore provinces in the Alpine-Balkan-Carpathian-Dinaride collision belt. In: Blundell, D.J., Neubauer, F., von Quadt, A. (ed): The major ore deposits in an evolving orogen. Geological Society London Special Publications, 204, 81-102.

Nikolaeva, K., Gerya, T.V., Marques, F.O. (2010): Subduction initiation at passive margins: numerical modelling. Journal of Geophysical Research, 115, B03406.

Nicolaysen, L.O. (1961): Graphic interpretation of discordant age measurements of metamorphic rocks. Annals of the New York Academy of Sciences, 91, 198-206.

Obata, M., Morten, L. (1987): Transformation of spinel lherzolite to garnet lherzolite in ultramafic lenses of the Austridic crystalline complex, northern Italy. Journal of Petrology, 28, 599–623.

Oberhänsli, R., Bousquet, R., Engi, M., Goffé, B., Gosso, G., Handy, M., Höck, V., Koller, F., Lardeaux, J.M., Polino, R., Rossi, P., Schuster, R., Schwartz, S., Spalla, M.I. (2004): Metamorphic structure of the Alps. Commision of the Geological Map World.

Oberti, R., Cannillo, E., Toscani, G. (2012): How to name amphiboles after the IMA2012 report: rules of thumb and a new PC program for monoclinic amphiboles. Periodico di Mineralogia, 81, 257-267.

Okay, A., Satır, M., Tüysüz, O., Akyüz, S., Chen, F. (2001): The tectonics of the Strandja Massif: late-Variscan and mid-Mesozoic deformation and metamorphism in the northern Aegean. International Journal of Earth Sciences, 90, 217-233.

Otamendi, J.E., de la Rosa, J.D., Patiño Douce, A.E., Castro, A. (2002): Rayleigh fractionation of heavy-rare earths and yttrium during metamorphic garnet growth. Geology, 30, 159-162.

Ovtcharova, M., von Quadt, A., Cherneva, Z., Sarov, S., Heinrich, C., Peytcheva, I. (2004): U-Pb dating of zircon and monazite from granitoids and migmatites in the core and eastern periphery of the Central Rhodopean Dome, Bulgaria. Geochimica et Cosmochimica Acta, 68, A664.

Page, F.Z., Essene, E.J., Mukasa, S.B. (2003): Prograde and retrograde history of eclogites from the Eastern Blue Ridge, North Carolina, USA. Journal of Metamorphic Geology, 21, 685-698.

Papanikolaou, D. (2009): Timing of tectonic emplacement of the ophiolites and terrane paleogeography in the Hellenides. Lithos, 108, 262-280.

Penniston-Dorland, S.C., Kohn, M.J., Manning, C.E. (2015): The global range of subduction zone thermal structures from exhumed blueschists and eclogites: Rocks are hotter than models. Earth and Planetary Science Letters, 428, 243-254.

Perraki, M., Proyer, A., Mposkos, E., Kaindl, R., Hoinkes, G. (2006): Raman micro-spectroscopy on diamond, graphite and other carbon polymorphs from the ultrahigh-pressure metamorphic Kimi Complex of the Rhodope Metamorphic Province, NE Greece. Earth and Planetary Science Letters, 241, 672-685.

Petrík, I., Janák, M., Froitzheim, N., Georgiev, N., Yoshida, K., Sasinková, V., Konečný, P., Milovská, S. (2016): Triassic to Early Jurassic (c. 200 Ma) UHP metamorphism in the Central Rhodopes: evidence from U-Pb-Th dating of monazite in diamond-bearing gneiss from Chepelare (Bulgaria). Journal of Metamorphic Geology, 34, 265-291.

Peytcheva, I., von Quadt. A. (1995): U–Pb zircon dating of metagranites from Byala Reka region in the east Rhodopes, Bulgaria. Geological Society of Greece Special Publications, 4, 637-642.

Peytcheva, I. (1997): The Alpine metamorphism in Eastern Rhodopes – Rb-Sr isotope data. Review of Bulgarian Geological Society, 58, 3, 157-165.

Peytcheva, I., Ovtcharova, M., Sarov, S., Kostitsin, J. (1998): Age and metamorphic evolution of metagranitoids from Kesebir reka region, eastern Rhodopes – Rb-Sr isotope data. XVI CBGA Congress Vienna Abstract, p. 471.

Peytcheva, I., von Quadt, A., Kouzmanov, K., Bogdanov, K. (2003): Elshitsa and Vlaykov Vruh epithermal and porphyry Cu (–Au) deposits of central Srednogorie, Bulgaria: source and timing of magmatism and mineralisation. In: Eliopoulos, D. et al. (eds): Mineral Exploration and Sustainable Development. Millpress, Rotterdam, pp. 371-374.

Peytcheva, I., von Quadt, A., Sarov, S., Voinova, E., Kolcheva, K. (2009): Ordovician protoliths of metamorphic rocks in Eastern Pirin-Western Rhodopes – Are they part of the Ograzhden Unit? In: National Conference ‘‘Geosciences 2009’’, proceedings, Sofia 2009, pp. 17-18.

Peytcheva, I., Macheva, L., von Quadt, A., Zidarov, N. (2015): Gondwana-derived units in Ograzhden and Belasitsa Mountains, Serbo-Macedonian Massif (SW Bulgaria): combined

geochemical, petrological and U-Pb zircon-xenotime age constraints. Geologica Balcanica, 44, 1-3, 51-84.

Peytcheva, I., von Quadt, A., Macheva, L., Kolceva, K., Sarov, S. (2018): Relics of Devonian oceanic lithosphere in Byala Reka Dome, Eastern Rhodopes: evidence from zircon U-Pb dating and Hf-isotope tracing. Proceedings of the Bulgarian Academy of Sciences, 71, 1657-1664.

Platt, J.P. (1993): Exhumation of high-pressure rocks: a review of concepts. Terra Nova, 5, 119-133.

Pleuger, J., Georgiev, N., Jahn-Awe, S., Froitzheim, N., Valkanov, N. (2011): Kinematics of Palaeogene low-angle extensional faults and basin formation along the eastern border of the Central Rhodopes (Bulgaria). Zeitschrift der Deutschen Gesellschaft für Geowissenschaften, 162, 171-192.

Polino, R., Dal Piaz, G. Gosso, G. (1990): Tectonic erosion at the Adria margin and accretionary processes for the Cretaceous orogeny of the Alps. Mémoires de la Societé Géologique de France, 156, 345–367.

Poupinet, G., Avouac, J., Jiang, M., Wei, S., Kissling, E., Herquel, G., Guilbert, J., Paul, A., Wittlinger, G., Su, H., Thomas, J. (2002): Intracontinental subduction and Palaeozoic inheritance of the lithosphere suggested by a teleseismic experiment across the Chinese Tien Shan. Terra Nova, 14, 18-24.

Ranero, C.R., Villasenor, A., Phipps Morgan, J., Weinrebe, W. (2005): Relationship between bend-faulting at trenches and intermediate-depth seismicity. Geochemistry Geophysics Geosystems, 6, Q12002.

Ravna, E.J.K., Terry, M.P. (2004): Geothermobarometry of UHP and HP eclogites and schists — an evaluation of equilibria among garnet-clinopyroxene-kyanite-phengite-coesite/quartz. Journal of Metamorphic Geology, 22, 579-592.

Ricou, L.-E., Burg, J.-P., Godfriaux, I., Ivanov, Z. (1998): Rhodope and Vardar: the metamorphic and the olistostromic paired belts related to the Cretaceous subduction under Europe. Geodinamica Acta, 11(6), 285-309.

Roda, M., Spalla, M.I., Marotta, A.M. (2012): Integration of natural data within a numerical model of ablative subduction: a possible interpretation for the Alpine dynamics of the Austroalpine crust. Journal of Metamorphic Geology, 30, 973-996.

Sandmann, S., Nagel, T.J., Herwartz, D., Fonseca, R.O.C., Kurzawski, R.M., Münker, C., Froitzheim, N. (2014): Lu-Hf garnet systematics of a polymetamorphic basement unit: new evidence for coherent exhumation of the Adula Nappe (Central Alps) from eclogite-facies conditions. Contributions to Mineralogy and Petrology, 168, 1075.

Sandmann, S., Herwartz, D., Kirst, F., Froitzheim, N., Nagel, T.J., Fonseca, R.O.C., Munker, C., Janák, M. (2016): Timing of eclogite-facies metamorphism of mafic and ultramafic rocks from the Pohorje Mountains (Eastern Alps, Slovenia) based on Lu-Hf garnet geochronometry. Lithos, 262, 576-585.

Sarov, S., Yordanov, B., Valkov, V., Georgiev, S., Kamburov, D., Raeva, E., Grozdev, V., Balkanska, E., Moskovska, L., Dobrev, G. (2007a): Geological Map of the Republic of Bulgaria 1:50 000, Map Sheet K-35-88-G (Chernichevo) and K-35-100-B (Kechros). Sofia, Ministry of Environment and Water.

Sarov, S., Yordanov, B., Valkov, V., Georgiev, S., Kamburov, D., Raeva, E., Grozdev, V., Balkanska, E., Moskovska, L., Dobrev, G., Voinova, E., Ovtcharova, M. (2007b) Geological Map of the Republic of Bulgaria 1:50 000, Map Sheet K-35-88-V (Krumovgrad) and K-35-100-A (Egrek). Sofia, Ministry of Environment and Water.

Sarov, S., Naydenov, K., Jelezarsky, T., Marinova, R., Georgieva, I., Ivanova, D., Popov, A., Markov, N. (2009): Geological Map of the Republic of Bulgaria 1:50 000, Map Sheet K-35-73-G (Devin). Sofia, Ministry of Environment and Water.

Sarov, S., Voinova, E., Georgieva, I., Nikolov, D., Markov, N. (2011): Geological Map of the Republic of Bulgaria 1:50 000. Map Sheet K-34-71-G (Rilski Manastir). Sofia, Ministry of Environment and Water.

Scherer, E.E., Cameron, K.L., Blichert-Toft, J. (2000): Lu-Hf garnet geochronology: Closure temperature relative to the Sm-Nd system and the effects of trace mineral inclusions. Geochimica et Cosmochimica Acta, 64, 3413-3432.

Schenker, F.L., Fellin, M.G., Burg, J.-P. (2015): Polyphase evolution of Pelagonia (northern Greece) revealed by geological and fission-track data. Solid Earth, 6, 285-302.

Scherer, E.E., Münker, C., Mezger, K. (2001): Calibration of the Lutetuim-Hafnium clock. Science, 293, 683-687.

Schmid S.M., Fügenschuh B., Kissling E., Schuster R. (2004): Tectonic map and overall architecture of the Alpine orogen. Eclogae Geologicae Helvetiae, 97, 93-117.

Schmidt, M.W., Poli, S. (1998): Experimentally based water budgets for dehydrating slabs and consequences for arc magma generation. Earth and Planetary Science Letters, 163, 361-379.

Schmidt, S., Nagel, T.J., Froitzheim, N. (2010): A new occurrence of microdiamond-bearing metamorphic rocks, SW Rhodopes, Greece. European Journal of Mineralogy, 22, 189-198.

Schulz, B. (1993): Mineral chemistry, geothermobarometry and pre-Alpine high-pressure metamorphism of eclogitic amphibolites and mica schists from the Schobergruppe, Austroalpine Basement, Eastern Alps. Mineralogical Magazine, 57, 189–202.

Schulz, B,, Bombach, K, (2003): Single zircon Pb-Pb geochronology of the Early-Paleozoic magmatic evolution in the Austroalpine basement to the south of the Tauern Window. Jahrbuch der geologischen Bundesanstalt, 143, 303–321.

Schulz, B., Steenken A., Siegesmund, S. (2008): Geodynamic evolution of an Alpine terrane—the Austroalpine basement to the south of the Tauern Window as a part of the Adriatic Plate (eastern Alps). Geological Society, London, Special Publications, 298, 5-44.

Schuster, R., Frank, W. (1999): Metamorphic evolution of the Austroalpine units east of the Tauern Window: indications for Jurassic strike slip tectonics. Gesellschaft der Geologie- und Bergbaustudenten in Österreich, 42, 37-58.

Schuster, R., Scharbert, S., Abart, R., Frank, W. (2001); Permo-Triassic extension and related HT/LP metamorphism in the Austroalpine—Southalpine realm. Mitteilungen der Gesellschaft der Geologie- und Bergbaustudenten in Österreich. 45, 111–141.

Schuster, R., Stüwe, K. (2008): Permian metamorphic event in the Alps. Geology, 36, 603–606.

Shu, Q., Brey, G.P., Gerdes, A., Hoefer, H. (2014): Mantle eclogites and garnet pyroxenites – the meaning of two-point isochrones, Sm-Nd and Lu-Hf closure temperatures and the cooling of the subcratonic mantle. Earth and Planetary Science Letters, 389, 143-154.

Skora, S., Mahlen, N., Baumgartner, L.P., Johnson, C., Pilet, S. (2005): Garnet zoning pattern, growth mechanisms and the development of Lu-depleted halos in eclogites. Geochimica et Cosmochimica Acta, 69(10), Supplement 403.

Skora, S., Baumgartner, L.P., Mahlen, N.J., Johnson, C.M., Pilet, S., Hellebrand, E. (2006): Diffusion-limited REE uptake by eclogite garnets and its consequences for Lu-Hf and Sm-Nd geochronology. Contributions to Mineralogy and Petrology, 152, 703-720.

Skora, S., Baumgartner, L.P., Mahlen, N.J., Lapen, T.J., Johnson, C.M., Bussy, F. (2008): Estimation of a maximum Lu diffusion rate in a natural eclogite garnet. Swiss Journal of Geosciences, 101, 637-650.

Smit, M.A., Scherer, E.E., John, T., Janssen, A. (2011): Creep of garnet in eclogite: Mechanisms and implications. Earth and Planetary Science Letters, 311, 411-419.

Smit, M., Scherer, E., Mezger, K. (2013): Lu–Hf and Sm–Nd garnet geochronology: chronometric closure and implications for dating petrological processes. Earth and Planetary Science Letters, 381, 222–233.

Sobel, E.R., Chen, J., Schoenbohm, L.M., Thiede, R., Stockli, D.F., Sudo, M., Strecker, M.R. (2013): Oceanic-sytle subduction controls late Cenozoic deformation of the Northern Pamir orogen. Earth and Planetary Science Letters, 363, 204-218.

Söderlund, U., Patchett, P.J., Vervoort, J.D., Isachsen, C.E. (2004): The 176Lu decay constant determined by Lu-Hf and U-Pb isotope systematics of Precambrian mafic intrusions. Earth and Planetary Science Letters, 219, 311-324.

Sölva, H., Thöni, M., Grasemann, B., Linner, M. (2001): Emplacement of eo-Alpine high-pressure rocks in the Austroalpine Ötztal Complex (Texel Group, Italy/Austria). Geodinamica Acta, 14, 345–360.

Sölva, H., Grasemann, B., Thöni, M., Thiede, R.C., Habler, G. (2005): The Schneeberg Normal Fault Zone: Normal faulting associated with Cretaceous SE-directed extrusion in the Eastern Alps (Italy/Austria). Tectonophysics, 401, 143–166.

Spear, F.S., Daniel, C.G. (1998): 3-dimensional imaging of garnet porphyroblast sizes and chemical zoning: nucleation and growth history in the garnet zone. Geological Materials Research, 1, 1–44.

Spear, F.S., Daniel, C.G. (2001): Diffusion control of garnet growth, Harpswell Neck, Maine USA. Journal of Metamorphic Geology, 19, 179–795.

Stampfli, C.M., Mosar, J. (1999): The making and becoming of Apulia. Mémoires Sécience Géologie, University of Padua, 51, 141-154.

Steltenpohl, M., Hames, W., Andresen, A., Markl, G. (2003): New Caledonian eclogite province in Norway and potential Laurentian (Taconic) and Baltic links. Geology, 31, 985-988.

Steltenpohl, M.G., Kassos, G., Andresen, A. (2006): Retrograded eclogite-facies pseudotachylytes as deep-crustal paleoseismic faults within continental basement of Lofoten, north Norway. Geosphere, 2, 61-72.

Steltenpohl, M.G., Kassos, G., Andresen, A., Rehnström, E.F., Hames, W.E. (2011): Eclogitization and exhumation of Caledonian continental basement in Lofoten, North Norway. Geosphere, 7, 202-218.

Stern, R.J. (2004): Subduction Initiation: Spontaneous and Induced. Earth and Planetary Sciience Letters, 226, 275-292.

Stern, R.J., Gerya, T. (2018): Subduction initiation in nature and models: A review. Tectonophysics, 746, 173-198.

Stüwe, K., Schuster, R. (2010): Initiation of subduction in the Alps: Continent or ocean? Geology, 38, 175-178.

Syracuse, E.M., van Keken, P.E., Abers, G.A. (2010): The global range of subduction zone thermal models. Physics of the Earth and Planetary Interiors, 183, 73-90.

Teiml, X., Hoinkes, G. (1996): Der P-T Pfad der Millstätter Serie und ein Vergleich mit dem südlichen Ötztal-Stubai-Kristallin. Mitteilungen der Österreichischen Mineralogischen Gesellschaft, 141, 228-229.

Tenczer, V., Stüwe, K. (2003): The metamorphic field gradient in the eclogite type locality Koralpe region, Eastern Alps. Journal of Metamorphic Geology, 21, 377–393.

Terry, M.P., Robinson, P., Ravna, E.J.K. (2000): Kyanite eclogite thermobarometry and evidence for thrusting of UHP over HP metamorphic rocks, Nordøyane, Western Gneiss Region, Norway. American Mineralogist, 85, 1637-1650.

Thöni, M. (1983): The thermal climax of the early Alpine metamorphism in the Austroalpine thrust sheet. Sciences Géologiques – Memoires, 36, 211–238.

Thöni, M., Jagoutz, E. (1992): Some new aspects of dating eclogites in orogenic belts: Sm–Nd, Rb-Sr, and Pb–Pb isotopic results from the Austroalpine Saualpe and Koralpe type locality (Carinthia/Styria, southeastern Austria). Geochimica et Cosmochimica Acta, 56, 347–368.

Thöni, M., Jagoutz, E. (1993): Isotopic constraints for eo-Alpine high-P metamorphism in the Austroalpine nappes of the Eastern Alps: bearing on Alpine orogenesis. Schweizerische Mineralogische und Petrographische Mitteilungen, 73, 177-189.

Thöni, M., Miller, C. (1996): Garnet Sm–Nd data from the Saualpe and the Koralpe (Eastern Alps, Austria): chronological and PT constraints on the thermal and tectonic history. Journal of Metamorphic Geology, 14, 453–466.

Thöni, M. (1999): A review of geochronolagical data from the Eastern Alps. Schweizerische Mineralogische und Petrologische Mitteilungen, 79, 209-230.

Thöni, M. (2006): Dating eclogite-facies metamorphism in the Eastern Alps - approaches, results, interpretations: a review. Mineralogy and Petrology, 88, 123-148.

Thöni, M., Miller, C., Blichert-Toft, J., Whitehouse, M.J., Konzett, J., Zanetti, A. (2008): Timing of high-pressure metamorphism and exhumation of the eclogite type-locality (Kupplerbrunn–Prickler Halt, Saualpe, south-eastern Austria): constrains from correlations of the Sm–Nd, Lu–Hf, U–Pb and Rb–Sr isotopic systems. Journal of Metamorphic Geology, 26, 561–581.

Thöni, M., Miller, C. (2010): Andalusite formation in a fast exhuming high-P wedge: Textural, microchemical, and Sm-Nd and Rb-Sr age constraints for a Creatceous P-T-t

path at Keinberg, Saualpe (Eastern Alps). Austrian Journal of Earth Sciences, 103, 118-131.

Thöny, W., Tropper, P., Schennach, F., Krenn, E., Finger, F., Kaindl, R., Bernhard, F., Hoinkes, G. (2008): The metamorphic evolution of migmatites from the Ötztal Complex (Tyrol, Austria) and constraints on the timing of the pre-Variscan high-T event in the Eastern Alps. Swiss Journal of Geosciences, 101, Suppl. 1, 111-126.

Tirone M, Ganguly J, Dohmen R, Langenhorst F, Hervig R, and Becker H-W (2005) Rare earth diffusion kinetics in garnet: Experimental studies and applications. Geochimica et Cosmochimica Acta 69: 2385–2398.

Tollmann, A. (1977): Geologie von Österreich. Band 1. Die Zentralalpen: Vienna, Deuticke, 766 p.

Tucker, R.D., Robinson, P., Solli, A., Gee, D.G., Thorsnes, T., Krogh, T.E., Nordgulen, O., Bickford, M.E. (2004): Thrusting and extension in the Scandian hinterland, Norway: New U-Pb ages and tectonostratigraphic evidence. American Journal of Science, 304, 477-532.

Tull, J.F. (1977): Geology and structure of Vestvågøy, Lofoten, north Norway. Norges Geologiske Undersøkelse, 42, 109 p.

Tumiati, S., Thöni, M., Nimis, P., Martin, S., Mair, V. (2003): Mantle–crust interactions during Variscan subduction in the Eastern Alps (Nonsberg–Ulten Zone); geochronology and new petrological constraints. Earth and Planetary Science Letters, 210, 509–526.

Turpaud, P., Reischmann, T. (2010): Characterization of igneous terranes by zircon dating: implications for UHP occurrences and suture identification in the Central Rhodope, northern Greece. International Journal of Earth Sciences, 99, 567-591.

Van Orman, J., Grove, T., Shimizu, N., Layne, G. (2002): Rare earth element diffusion in a natural pyrope single crystal at 2.8 GPa. Contributions to Mineralogy and Petrology, 142, 416–424.

Van Roermund, H.L.M., Drury, M.R. (1998): Ultra-high pressure (P > 6 GPa) garnet peridotites in Western Norway: exhumation of mantle rocks from > 185 km depth. Terra Nova, 10, 295–301.

von Quadt, A., Peytcheva, I., Cvetkovic, V. (2003): Geochronology, geochemistry and isotope tracing of the Cretaceous magmatism of east-Serbia and Panagyurishte District (Bulgaria) as part of the Apuseni–Timok–Srednogorie metallogenic belt in eastern Europe. In: Eliopoulos, D. et al. (eds): Mineral Exploration and Sustainable Development. Millpress, Rotterdam, pp. 407-410.

von Quadt, A., Peytcheva, I. (2005): The southern extension of the Srednogorie type Upper Cretaceous magmatism in Rila-Western Rhodopes: constraints from isotope geochronological and geochemical data. Bulgarian Geological Society 80th Anniversary, 113-116.

von Quadt, A., Moritz, R., Peytcheva, I., Heinrich, C.A. (2005): Geochronology and geodynamics of Late Cretaceous magmatism and Cu-Au mineralization in the Panagyurishte region of the Apuseni-Banat-Timok-Srednogorie belt, Bulgaria. Ore Geology Reviews, 27, 95-126.

von Quadt, A., Peytcheva, I., Sarov, S., Liati, A. (2010): Late Cretaceous subduction and magmatism in the Rhodopes: geochronological and isotope-geochemical evidence. In: National Conference “Geosciences 2010”, proceedings, Sofia 2010, pp. 13-14.

Vrabec, M., Janák, M., Froitzheim, N., De Hoog, J.C.M. (2012): Phase relations during peak metamorphism and decompression of the UHP kyanite eclogites, Pohorje Mountains (Eastern Alps, Slovenia). Lithos, 144, 40–55.

Wawrzenitz, N., Mposkos, E. (1997): First evidence for Lower Cretaceous HP/HT metamorphism in the Eastern Rhodope, North Aegean Region North-East Greece. European Journal of Mineralogy, 9, 659-664.

White, R.W., Powell, R., Holland, T.J.B. (2007): Progress relating to calculation of partial melting equilibria for metapelites. Journal of Metamorphic Geology, 25, 511-527.

Wiesinger, M., Neubauer, F., Handler, R. (2005): Exhumation of the Saualpe eclogite unit, Eastern Alps: constraints from 40Ar/39Ar ages and structural investigations. Mineralogy and Petrology, 88, 149-180.

Zanchetta, S., Langone, R., Mair, V., Poli, S. (2007): First report of sillimanite within the metapelites of the Schneeberg Complex. Mitteilungen der Österreichischen Mineralogischen Gesellschaft, 153, pp. 137.

Zanchetta, S., Poli, S., Rubatto, D., Zanchi, A., Bove, G.M. (2013): Evidence for deep subduction of Austroalpine crust (Texel Complex, NE Italy). Rendiconti Lincei: Scienze Fisiche e Naturali, 24, 163-176.

Zidarov, N., Nenova, P., Dimov, V. (1995): Coesite in kyanite eclogite of Ograzden Mts., SW Bulgaria. Comptes Rendus de l'Academie Bulgare des Sciences, 48, 11-12, 59-62.

Ziegler, P.A., Cloetingh, S., van Wees, J.-D. (1995): Dynamics of intra-plate compressional deformation: the Alpine foreland and other examples. Tectonophysics, 252, 7–59.

Appendix

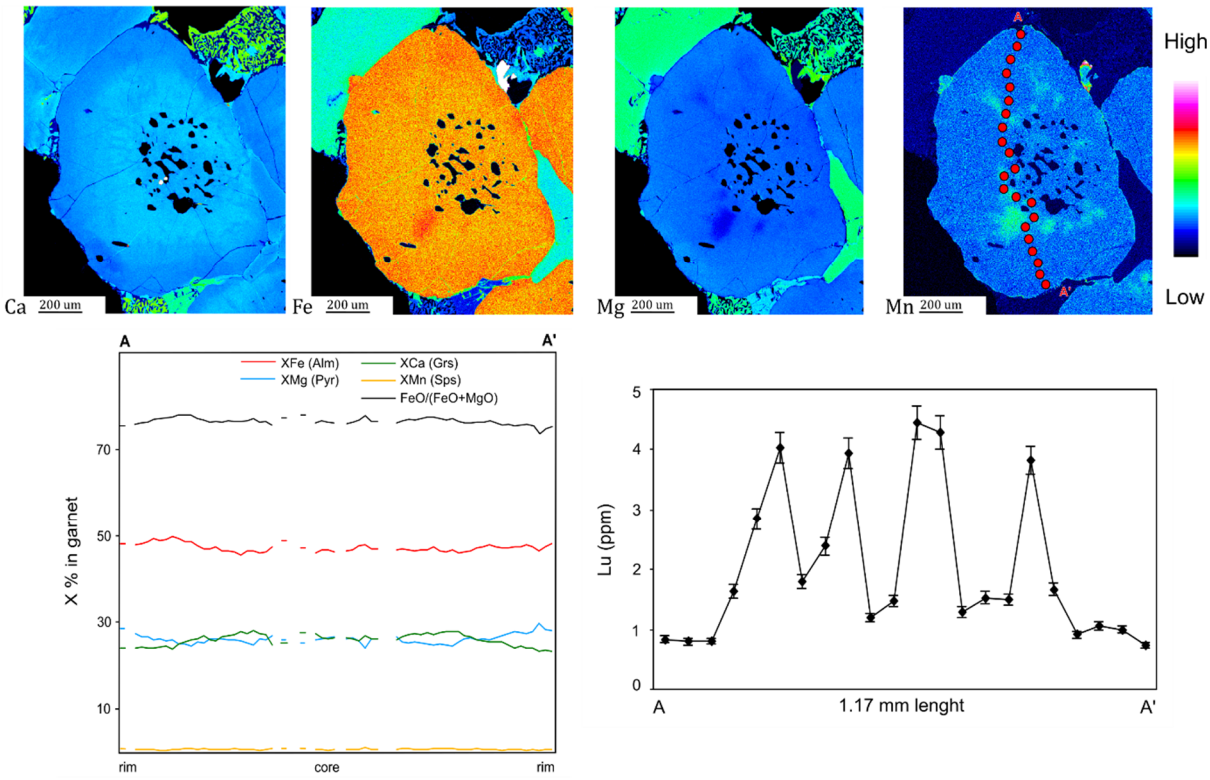

Fig. A-1. Major element distribution maps and compositional and Lu concentration profiles through garnet from sample Ho1.

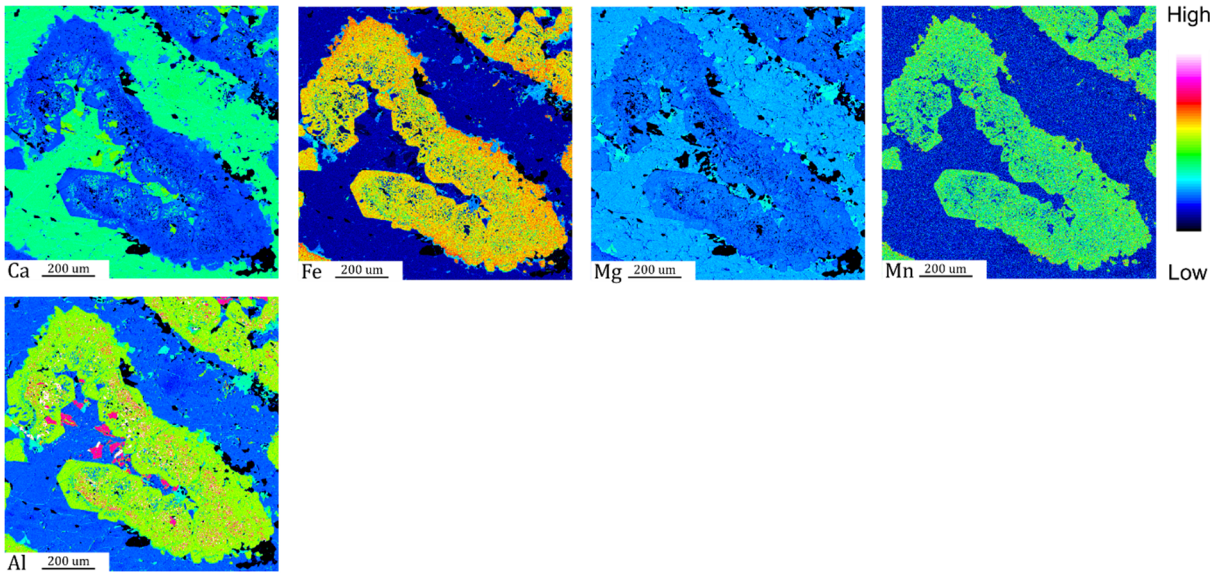

Fig. A-2. Major element distribution maps of garnet from sample Ho2.

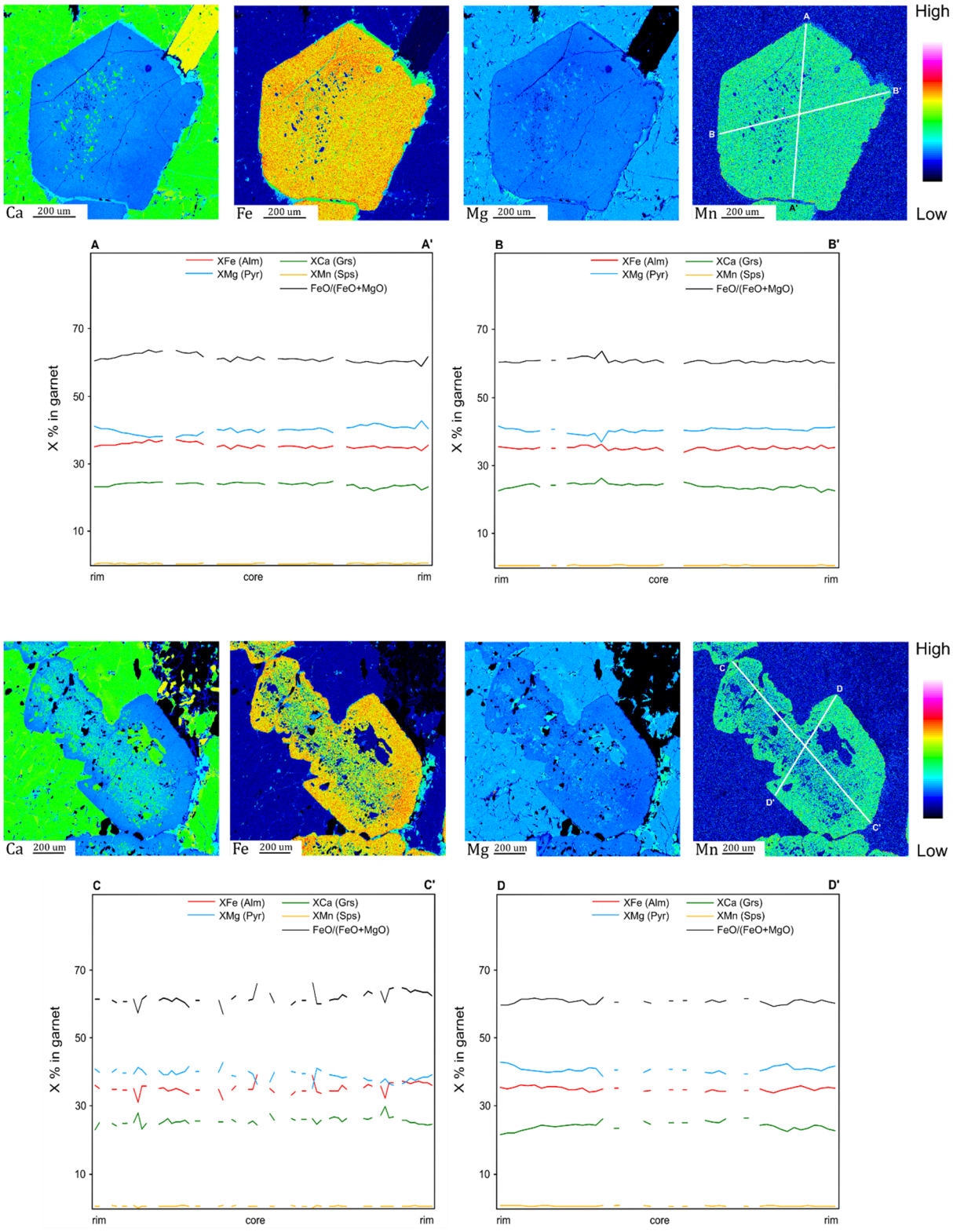

Fig. A-3. Major element distribution maps and compositional profiles through garnet from sample Ho2.

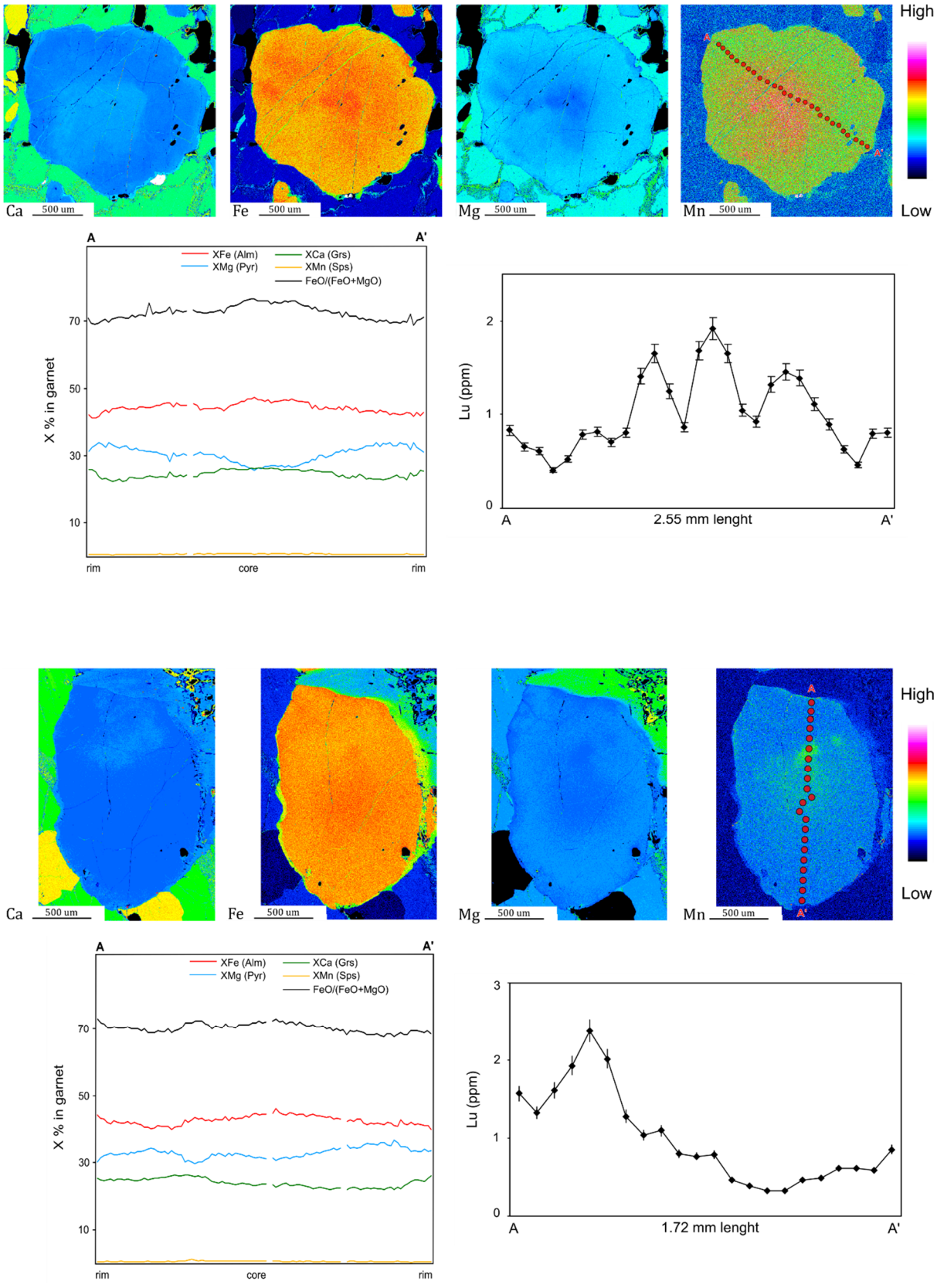

Fig. A-4. Major element distribution maps and compositional and Lu concentration profiles through garnets from sample Grü2.

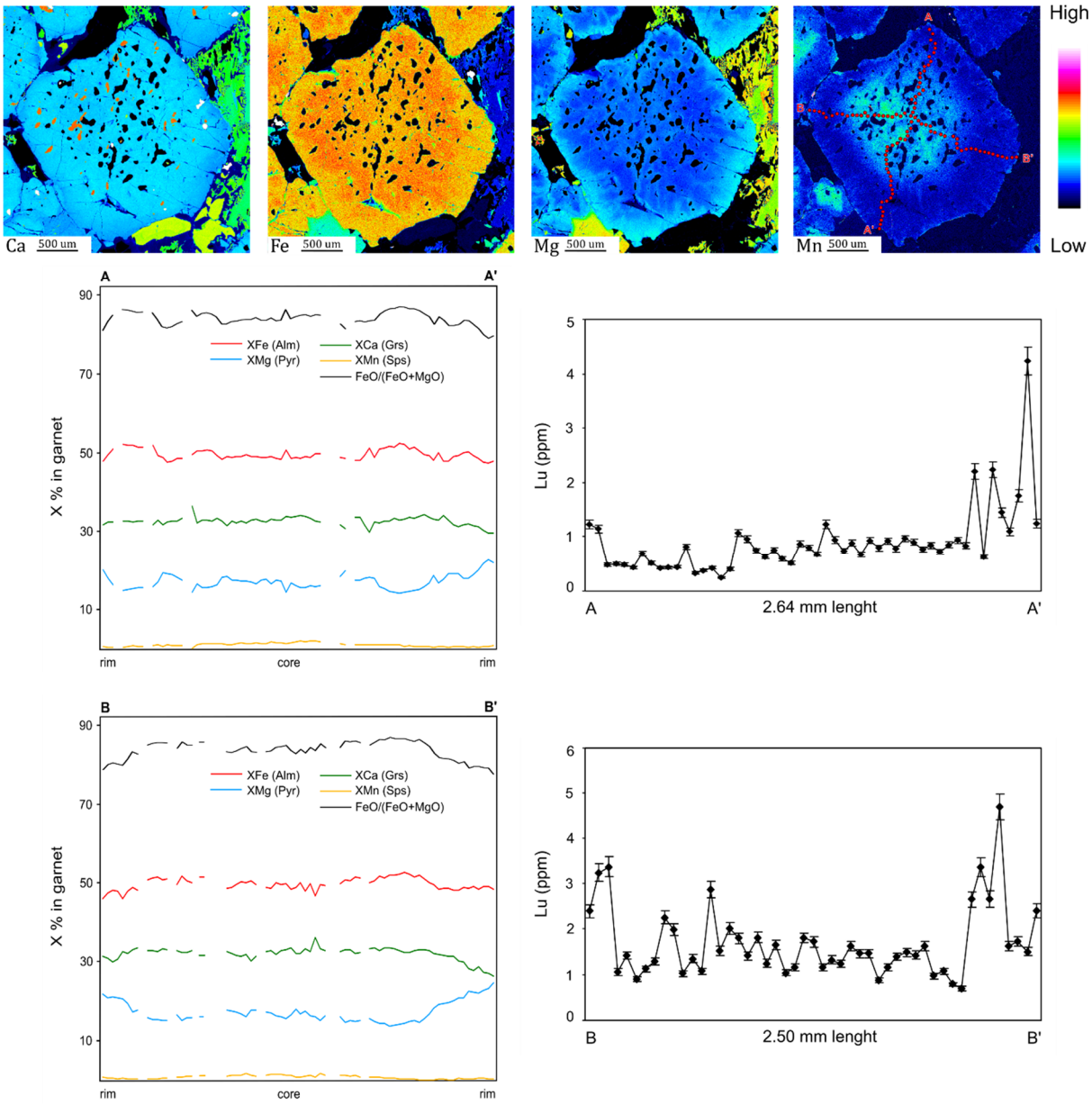

Fig. A-5. Major element distribution maps and compositional and Lu concentration profiles through garnet from sample Wol1.

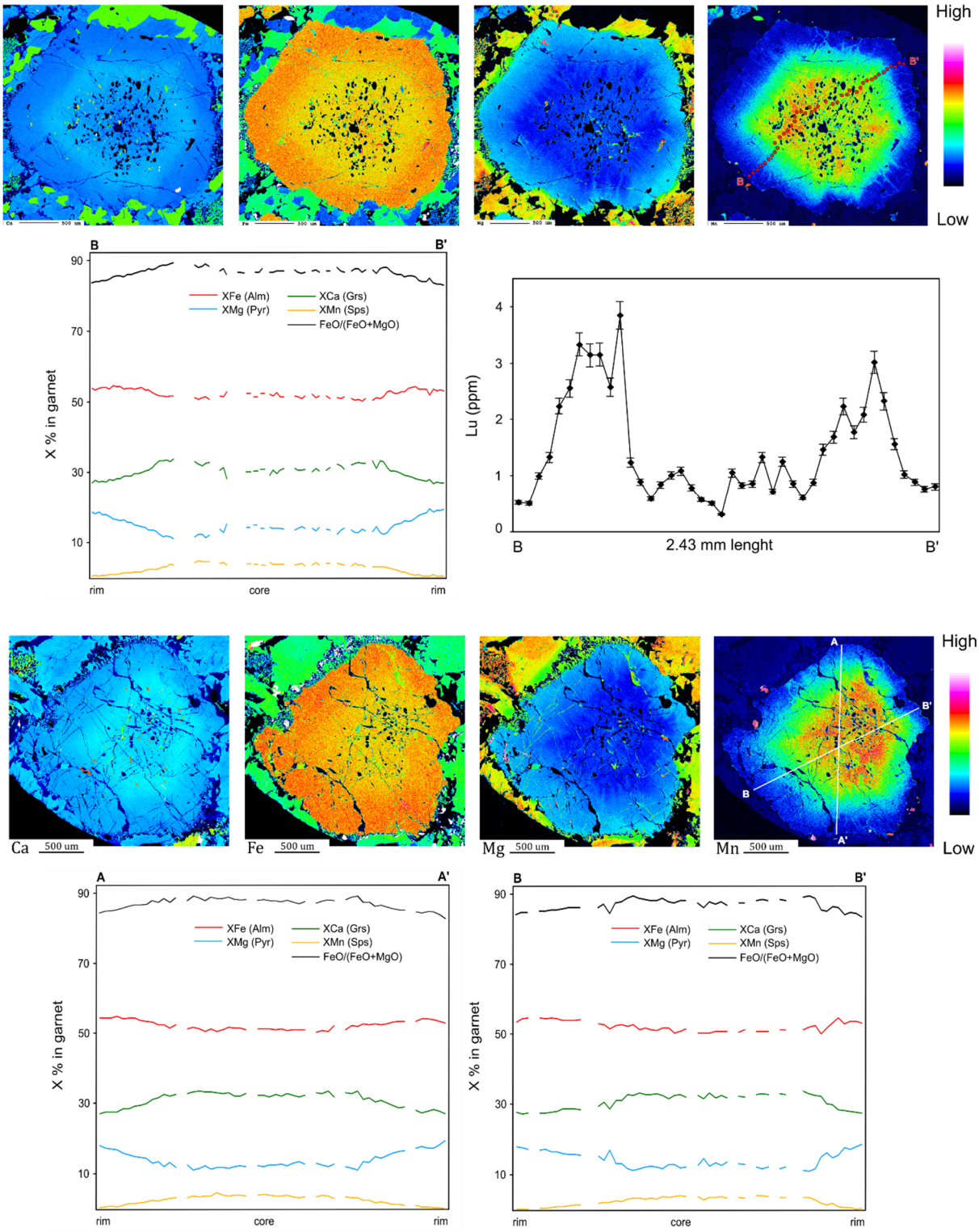

Fig. A-6. Major element distribution maps and compositional and Lu concentration profiles through garnets from sample Sig3.

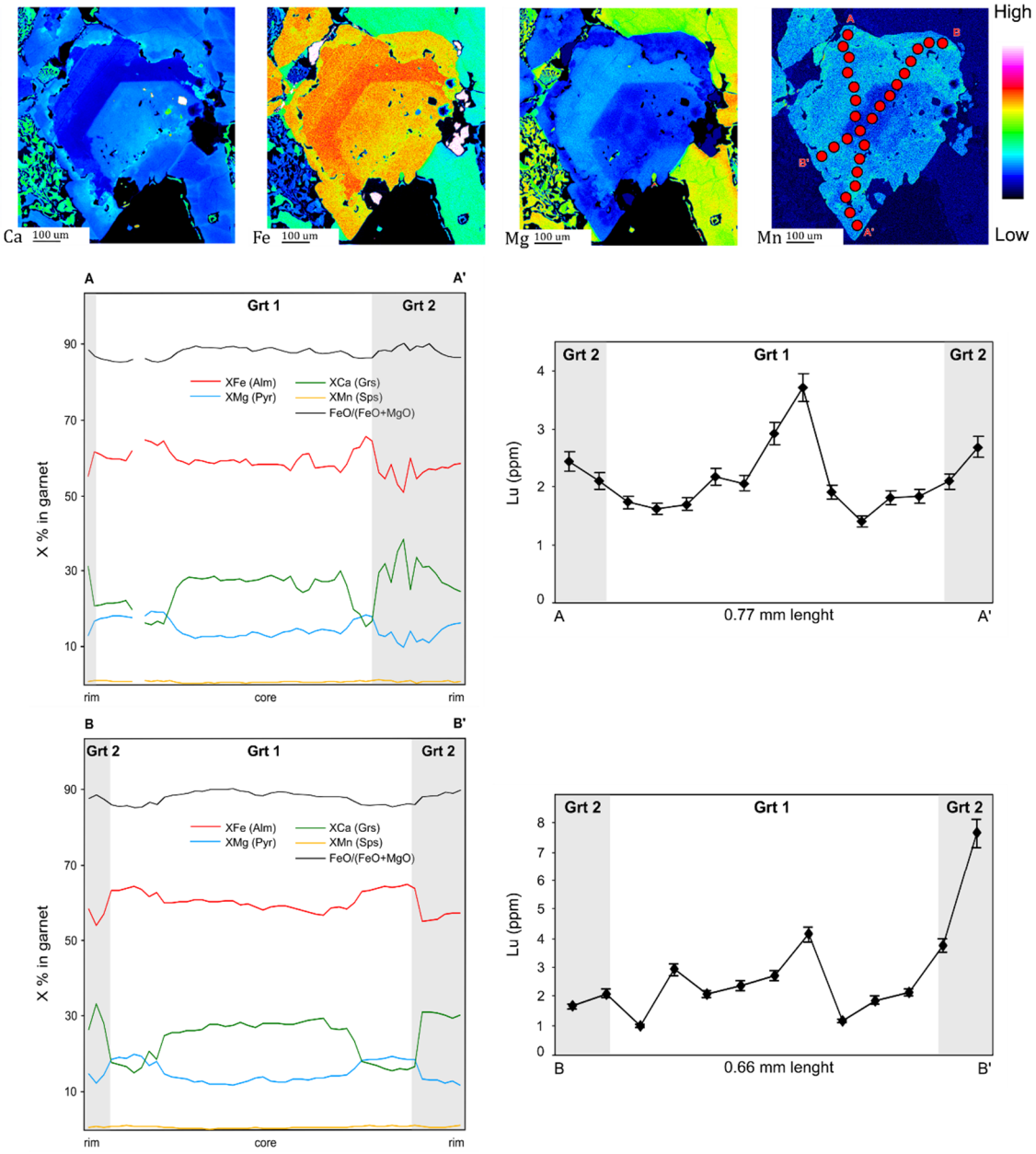

Fig. A-7. Major element distribution maps and compositional and Lu concentration profiles through garnet from sample Sal1.

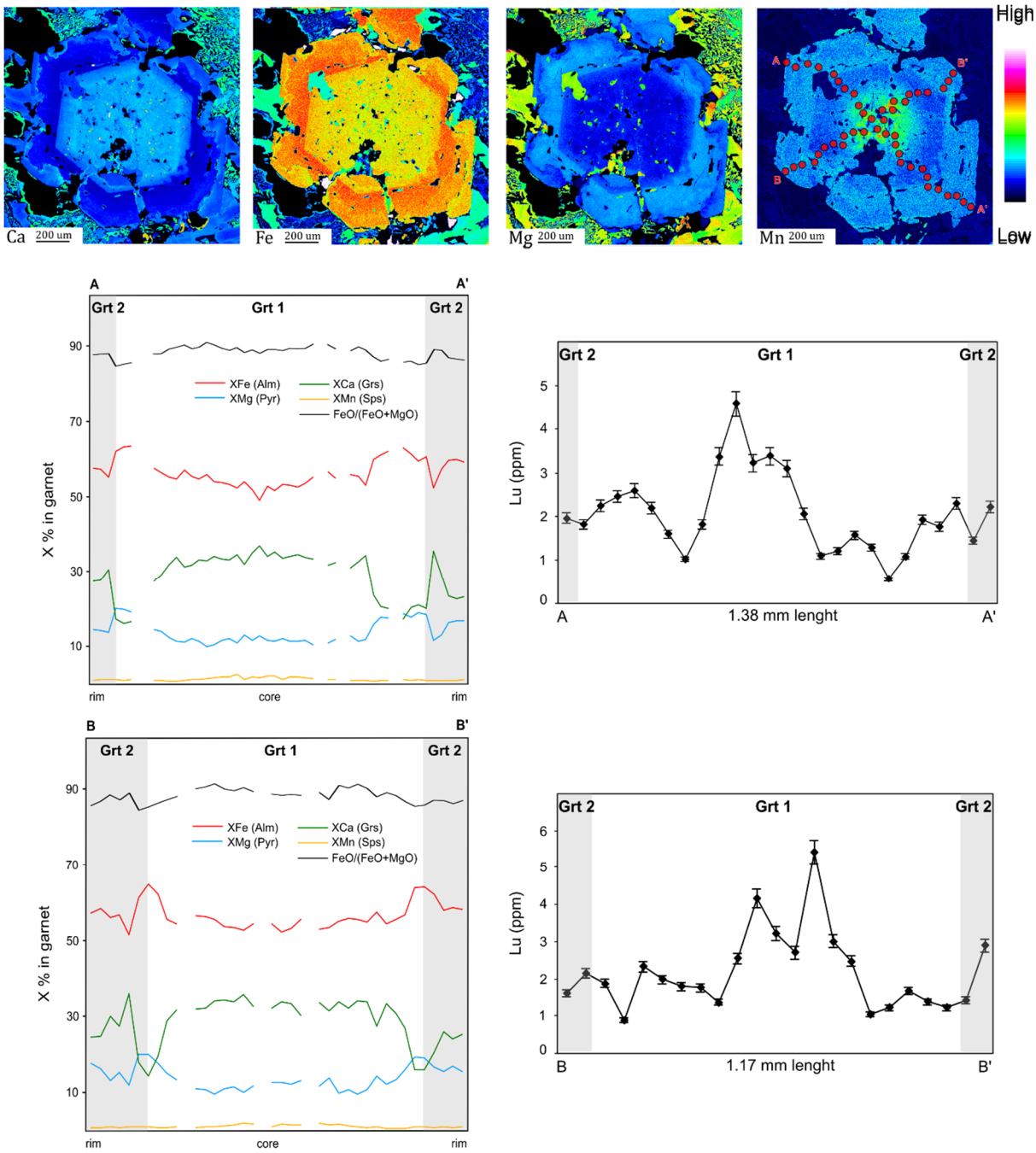

Fig. A-8. Major element distribution maps and compositional and Lu concentration profiles through garnet from sample Sal1.

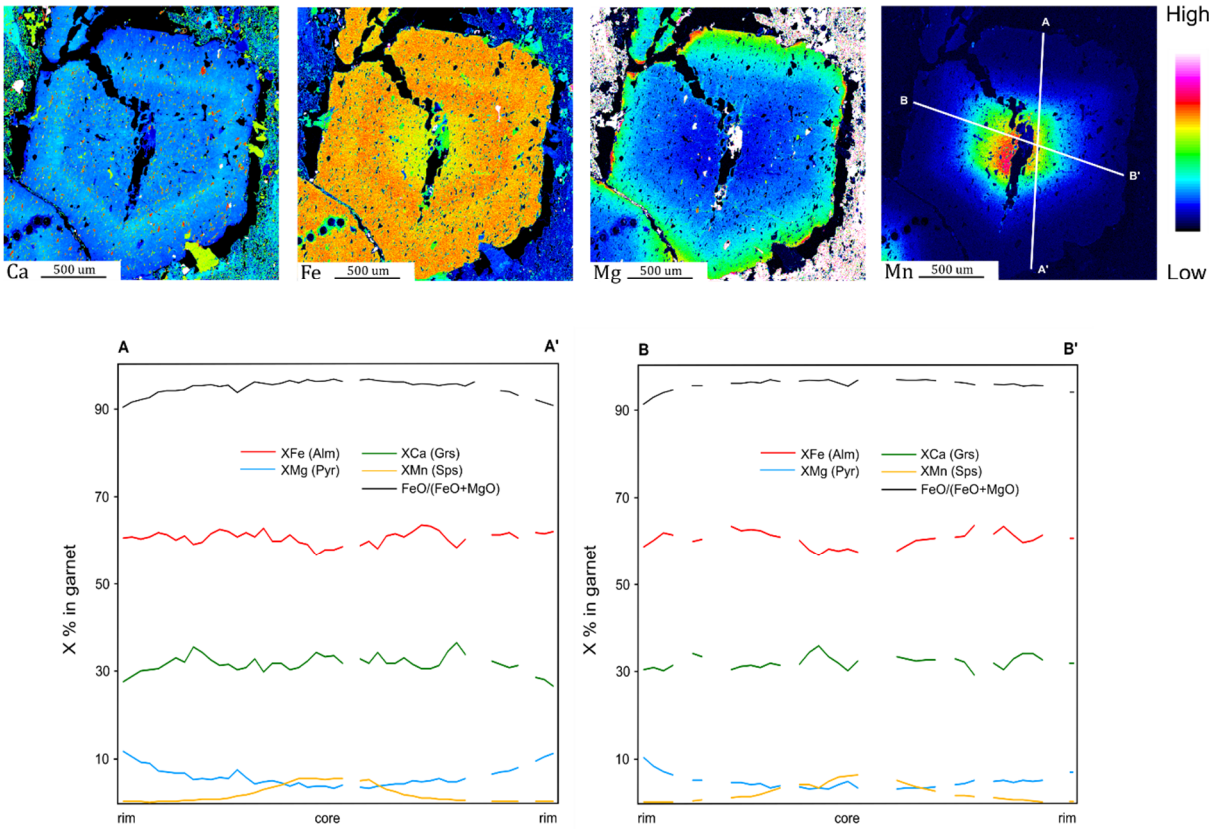

Fig. A-9. Major element distribution maps and compositional profiles through garnet from sample Kas2.

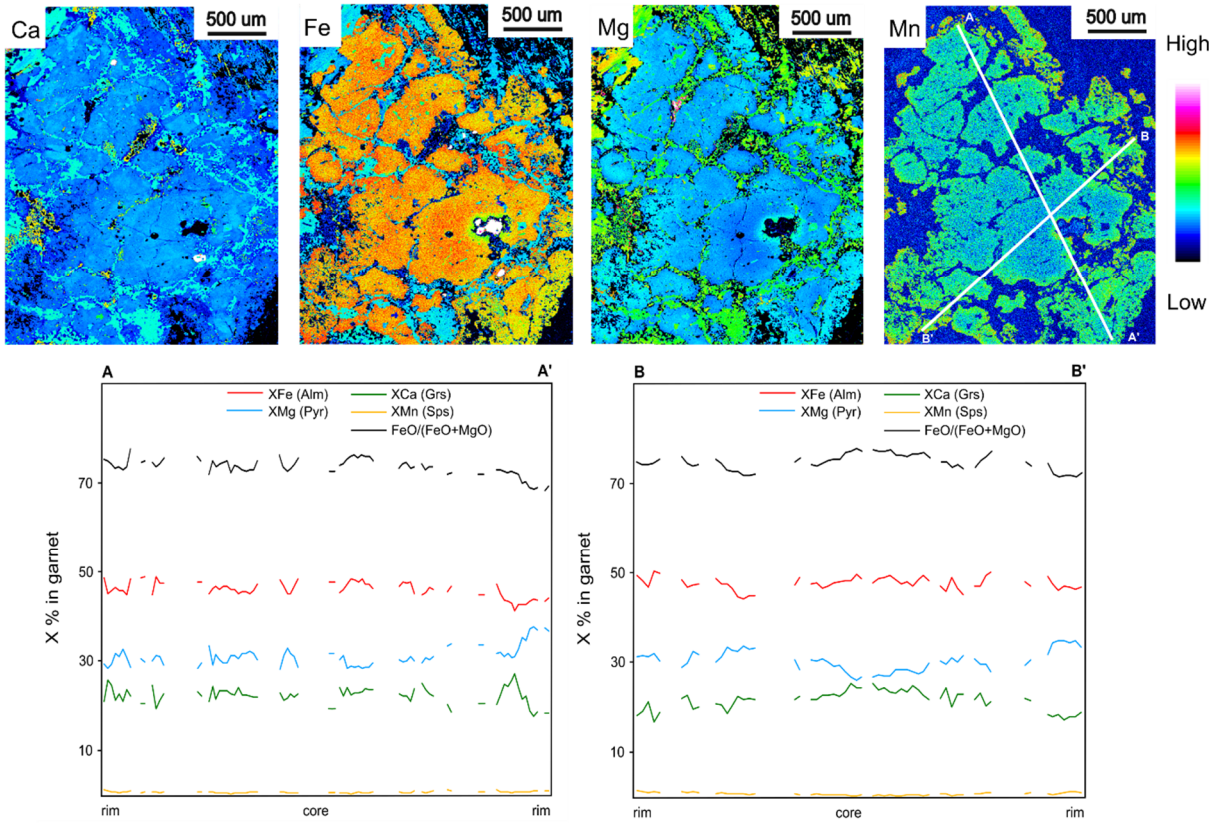

Fig. A-10. Major element distribution maps and compositional profiles through garnet from sample LOF 3/12.

Table A-1. Electron microprobe analyses from sample Ho1.

Sample	SiO_2	TiO_2	Al_2O_3	FeO	MnO	MgO	CaO	Na_2O	K_2O	Cr_2O_3	Sum
Ho1	54.59	0.17	9.81	5.55	0.06	8.87	14.78	5.96	0.00	0.00	99.79
	54.04	0.20	10.18	5.14	0.05	8.75	14.71	5.95	0.00	0.00	99.03
	52.62	0.21	9.74	6.27	0.12	8.83	15.64	5.34	0.00	0.05	98.82
	53.46	0.04	2.19	9.01	0.09	12.15	20.88	1.97	0.00	0.04	99.84
	55.06	0.09	10.56	5.21	0.04	8.92	14.38	6.08	0.01	0.00	100.34
	53.60	0.20	10.19	5.55	0.00	8.83	15.02	5.46	0.00	0.00	98.84
	54.57	0.21	10.24	5.79	0.01	8.82	15.21	5.84	0.00	0.02	100.71
	0.01	102.24	0.05	0.52	0.05	0.00	0.13	0.02	0.00	0.05	103.07
	0.02	102.39	0.04	0.34	0.04	0.00	0.04	0.00	0.01	0.14	103.01
	0.03	55.11	0.01	45.12	0.28	1.60	0.10	0.01	0.00	0.04	102.31
	43.58	0.73	13.17	13.19	0.06	12.67	10.42	3.47	0.41	0.01	97.71
	0.07	101.94	0.01	0.18	0.01	0.00	0.14	0.00	0.00	0.11	102.46
	38.49	0.17	28.27	5.85	0.00	0.19	23.73	0.02	0.00	0.00	96.72
	38.18	0.16	28.40	5.49	0.00	0.17	23.69	0.03	0.01	0.02	96.14
	38.30	0.20	28.62	5.59	0.01	0.21	23.37	0.02	0.00	0.00	96.32
	54.23	0.19	10.31	5.05	0.02	8.90	14.55	5.95	0.00	0.03	99.22
	54.19	0.21	10.18	5.04	0.05	9.03	14.62	5.97	0.00	0.06	99.34
	52.68	0.31	6.99	6.75	0.07	10.71	18.94	3.34	0.00	0.00	99.79
	65.21	0.00	22.57	0.20	0.02	0.02	2.93	10.36	0.04	0.00	101.34
	65.26	0.00	22.19	0.18	0.01	0.00	2.64	10.19	0.03	0.04	100.54
	64.22	0.00	22.98	0.21	0.00	0.00	3.21	10.02	0.02	0.00	100.66
	39.25	0.05	21.46	22.70	0.25	7.37	8.51	0.06	0.01	0.06	99.70
	39.38	0.05	21.41	22.55	0.35	7.30	8.66	0.00	0.02	0.10	99.81
	38.93	0.10	21.61	23.05	0.33	7.24	8.71	0.06	0.00	0.10	100.12
	39.32	0.07	21.86	22.65	0.36	7.13	8.91	0.06	0.01	0.08	100.44
	39.38	0.00	21.63	22.90	0.39	7.18	8.82	0.05	0.02	0.05	100.41
	38.96	0.00	21.94	23.14	0.33	7.18	8.96	0.04	0.01	0.15	100.70
	39.21	0.07	21.63	22.85	0.32	7.03	9.08	0.04	0.01	0.14	100.39
	38.87	0.04	21.67	22.32	0.44	6.92	9.36	0.08	0.00	0.07	99.76
	38.97	0.04	21.51	22.48	0.44	6.61	9.64	0.06	0.01	0.07	99.84
	38.98	0.10	21.80	22.92	0.45	6.45	9.80	0.04	0.01	0.05	100.60
	38.96	0.06	21.55	22.36	0.46	6.19	9.77	0.02	0.01	0.02	99.40
	39.15	0.03	21.73	22.58	0.46	6.24	10.05	0.00	0.01	0.02	100.25
	38.84	0.10	21.62	22.41	0.46	6.32	10.04	0.05	0.01	0.04	99.89
	39.03	0.11	21.73	22.28	0.42	6.44	9.99	0.05	0.01	0.01	100.06
	39.20	0.04	21.58	22.07	0.40	6.57	9.94	0.09	0.00	0.04	99.93
	39.53	0.01	21.97	22.27	0.48	6.63	10.22	0.04	0.01	0.03	101.20
	39.20	0.06	21.79	22.52	0.51	6.56	9.89	0.07	0.00	0.03	100.63
	39.07	0.06	21.43	21.97	0.46	6.41	10.05	0.07	0.01	0.03	99.55
	38.76	0.16	21.50	22.05	0.43	6.70	9.93	0.05	0.00	0.01	99.59
	39.84	0.07	19.83	22.35	0.39	6.94	9.67	0.04	0.01	0.01	99.16
	39.12	0.08	21.65	22.35	0.38	6.80	9.81	0.07	0.03	0.02	100.30
	39.58	0.06	21.77	22.18	0.42	6.76	9.63	0.16	0.03	0.01	100.60

Sample	SiO_2	TiO_2	Al_2O_3	FeO	MnO	MgO	CaO	Na_2O	K_2O	Cr_2O_3	Sum
Ho1	33.71	0.04	24.90	21.65	0.46	5.49	9.49	0.00	0.03	0.03	95.79
	34.54	0.05	2.57	21.74	0.35	6.81	5.91	0.01	0.03	0.05	72.04
	39.55	0.12	21.89	22.34	0.33	6.90	9.64	0.02	0.01	0.04	100.84
	2.51	94.41	1.30	2.16	0.08	0.33	1.03	0.00	0.00	0.11	101.92
	39.13	0.30	21.73	22.57	0.36	6.84	9.59	0.05	0.01	0.01	100.59
	39.21	0.14	21.75	22.42	0.34	7.03	9.53	0.03	0.00	0.04	100.48
	39.34	0.05	21.43	21.81	0.40	6.90	9.26	0.01	0.01	0.00	99.20
	39.16	0.07	21.70	22.04	0.37	7.00	9.68	0.05	0.01	0.07	100.13
	38.95	0.09	21.69	22.45	0.39	6.88	9.52	0.03	0.01	0.01	100.02
	39.13	0.13	21.43	22.91	0.39	6.86	9.34	0.01	0.00	0.02	100.22
	36.89	0.00	23.67	22.11	0.30	6.62	8.90	0.42	0.01	0.02	98.94
	39.45	0.14	21.28	22.18	0.33	6.89	9.57	0.03	0.00	0.14	100.01
	8.83	78.10	5.13	5.29	0.11	1.54	2.30	0.00	0.00	0.05	101.33
	39.51	0.11	21.44	22.39	0.36	7.10	9.24	0.02	0.00	0.02	100.19
	39.18	0.09	21.96	22.57	0.39	7.07	9.27	0.00	0.03	0.02	100.57
	97.32	0.02	0.03	0.45	0.01	0.00	0.01	0.00	0.01	0.00	97.85
	97.41	0.02	0.00	0.37	0.02	0.01	0.02	0.02	0.00	0.03	97.88
	97.59	0.00	0.01	0.48	0.01	0.01	0.03	0.02	0.01	0.02	98.17
	39.35	0.00	21.76	22.50	0.33	6.97	9.33	0.04	0.01	0.00	100.28
	39.30	0.11	22.11	22.62	0.36	6.93	9.46	0.00	0.02	0.03	100.95
	39.77	0.02	20.45	22.26	0.34	7.51	7.90	0.04	0.56	0.00	98.86
	39.69	0.10	21.95	22.66	0.35	7.14	9.09	0.03	0.01	0.02	101.04
	98.20	0.00	0.05	0.61	0.00	0.02	0.08	0.02	0.03	0.03	99.03
	39.33	0.06	21.58	22.62	0.37	6.88	9.65	0.05	0.01	0.07	100.60
	39.42	0.12	21.60	22.27	0.35	6.90	9.72	0.05	0.01	0.08	100.52
	97.10	0.02	0.12	0.70	0.00	0.02	0.08	0.03	0.02	0.00	98.09
	39.49	0.00	21.52	21.47	0.28	6.64	9.78	0.02	0.02	0.06	99.27
	39.06	0.08	21.68	22.47	0.37	6.95	9.69	0.03	0.00	0.12	100.43
	39.27	0.02	21.36	22.20	0.32	7.08	9.51	0.04	0.01	0.08	99.89
	39.28	0.09	21.60	22.42	0.38	6.89	9.18	0.01	0.00	0.00	99.84
	39.28	0.04	21.89	22.50	0.28	7.00	9.15	0.02	0.01	0.04	100.21
	39.18	0.09	21.24	22.14	0.33	6.89	9.70	0.05	0.00	0.08	99.70
	39.20	0.05	21.59	22.13	0.38	6.79	9.84	0.00	0.01	0.04	100.03
	39.40	0.12	21.55	22.22	0.37	6.72	9.89	0.02	0.01	0.01	100.29
	38.97	0.04	21.38	21.79	0.42	6.43	10.16	0.02	0.00	0.03	99.22
	39.30	0.08	21.63	22.42	0.43	6.36	10.18	0.00	0.02	0.00	100.41
	39.32	0.10	21.62	22.50	0.42	6.33	10.21	0.00	0.01	0.02	100.51
	39.08	0.03	21.66	21.93	0.34	6.56	10.18	0.02	0.03	0.01	99.84
	39.40	0.09	21.66	21.89	0.34	6.58	10.15	0.00	0.00	0.00	100.10
	39.35	0.00	21.56	22.21	0.37	6.78	9.69	0.00	0.01	0.00	99.97
	38.95	0.00	21.73	21.96	0.32	6.82	9.67	0.02	0.00	0.03	99.50
	38.83	0.02	21.62	22.16	0.32	6.98	9.37	0.00	0.02	0.10	99.42
	39.41	0.05	21.58	22.60	0.34	6.89	9.20	0.00	0.00	0.08	100.15
	39.32	0.00	21.68	22.41	0.31	7.14	9.40	0.02	0.03	0.05	100.36

Sample	SiO_2	TiO_2	Al_2O_3	FeO	MnO	MgO	CaO	Na_2O	K_2O	Cr_2O_3	Sum
Ho1	39.11	0.09	21.79	22.58	0.38	6.91	9.16	0.04	0.01	0.08	100.13
	38.87	0.00	21.55	22.57	0.37	7.01	9.05	0.04	0.01	0.16	99.63
	38.94	0.00	21.61	22.55	0.26	6.91	8.81	0.10	0.01	0.10	99.30
	39.54	0.06	22.09	23.16	0.31	7.08	8.41	0.01	0.00	0.06	100.72

Table A-2. Electron microprobe analyses from sample Ho2.

Sample	SiO_2	TiO_2	Al_2O_3	FeO	MnO	MgO	CaO	Na_2O	K_2O	Cr_2O_3	Sum
Ho2	54.63	0.23	8.19	2.45	0.02	12.22	17.61	3.98	0.00	0.05	99.38
	39.53	0.02	32.12	1.04	0.00	0.04	23.39	0.00	0.01	0.11	96.25
	39.29	0.07	32.22	1.04	0.02	0.05	23.44	0.00	0.01	0.07	96.21
	63.40	0.06	23.08	0.06	0.00	0.01	4.24	9.34	0.08	0.00	100.26
	39.39	0.16	32.30	1.21	0.01	0.09	23.34	0.03	0.01	0.03	96.58
	54.58	0.14	7.89	2.52	0.03	12.56	18.00	3.64	0.00	0.09	99.44
	54.29	0.21	7.87	2.24	0.02	12.55	18.55	3.48	0.00	0.04	99.26
	54.53	0.13	8.15	2.55	0.00	12.32	18.19	3.84	0.00	0.08	99.79
	36.98	0.03	61.59	0.28	0.00	0.03	0.11	0.01	0.00	0.04	99.07
	39.54	0.07	32.22	1.14	0.02	0.08	23.63	0.03	0.01	0.00	96.72
	61.73	0.04	23.75	0.11	0.00	0.00	5.09	8.92	0.01	0.00	99.65
	62.69	0.00	23.24	0.04	0.01	0.00	4.54	9.16	0.01	0.00	99.69
	54.75	0.10	8.02	2.52	0.03	12.17	17.80	3.91	0.00	0.07	99.37
	46.80	0.44	13.10	5.77	0.01	16.34	10.55	2.55	0.22	0.09	95.88
	46.64	0.42	14.04	5.91	0.03	15.91	10.55	2.82	0.18	0.08	96.58
	46.34	0.54	13.59	5.62	0.03	16.20	11.03	2.60	0.19	0.07	96.19
	54.48	0.20	8.59	2.61	0.04	3.52	18.70	12.07	0.02	0.00	100.23
	39.55	0.11	34.47	0.89	0.00	0.00	24.93	0.03	0.01	0.02	100.00
	37.29	0.00	64.40	0.30	0.00	0.00	0.04	0.01	0.01	0.08	102.14
	37.51	0.14	64.36	0.20	0.00	0.00	0.01	0.06	0.01	0.12	102.40
	40.88	0.00	23.37	16.90	0.23	11.07	8.75	0.00	0.00	0.05	101.25
	40.56	0.05	23.09	17.20	0.29	10.96	8.80	0.04	0.02	0.02	101.04
	40.53	0.00	23.30	17.36	0.28	11.07	8.85	0.03	0.02	0.09	101.53
	40.88	0.03	23.37	17.22	0.18	10.82	9.04	0.00	0.00	0.07	101.61
	40.76	0.03	23.45	17.22	0.28	10.53	9.06	0.06	0.00	0.04	101.43
	40.68	0.02	23.01	17.33	0.24	10.50	9.19	0.00	0.01	0.04	101.02
	40.85	0.03	23.03	17.47	0.22	10.35	9.12	0.02	0.00	0.00	101.09
	40.99	0.07	23.34	17.56	0.28	10.41	9.34	0.00	0.00	0.06	102.05
	39.72	0.12	21.98	17.33	0.23	9.90	8.89	0.02	0.00	0.05	98.25
	40.58	0.08	23.13	17.39	0.30	10.21	9.15	0.00	0.00	0.01	100.85
	40.46	0.06	23.21	17.62	0.21	10.18	9.17	0.00	0.00	0.03	100.95
	38.65	0.00	46.81	7.50	0.07	3.98	4.15	0.02	0.00	0.00	101.17
	40.72	0.04	23.37	17.94	0.26	10.30	9.19	0.00	0.01	0.02	101.85
	40.51	0.06	22.97	17.56	0.21	10.35	9.07	0.02	0.00	0.05	100.78
	41.08	0.03	23.46	17.67	0.18	10.49	9.28	0.01	0.01	0.05	102.25
	40.56	0.05	23.53	17.92	0.21	10.46	9.32	0.00	0.00	0.04	102.10
	41.83	0.10	23.16	17.50	0.29	10.86	9.15	0.17	0.00	0.06	103.12
	54.37	0.19	8.67	2.90	0.04	12.25	18.44	3.22	0.03	0.08	100.18
	41.00	0.02	23.13	16.89	0.19	10.81	9.11	0.01	0.00	0.07	101.22
	40.71	0.06	23.60	17.16	0.23	10.82	9.07	0.03	0.00	0.04	101.72
	40.97	0.10	23.50	16.61	0.27	10.99	9.22	0.02	0.01	0.03	101.72
	40.96	0.02	23.28	17.34	0.24	10.76	9.46	0.00	0.01	0.06	102.11
	40.83	0.00	23.27	17.03	0.24	10.85	9.25	0.02	0.00	0.07	101.56

Sample	SiO_2	TiO_2	Al_2O_3	FeO	MnO	MgO	CaO	Na_2O	K_2O	Cr_2O_3	Sum
Ho2	40.82	0.07	23.36	16.92	0.27	11.01	9.28	0.01	0.00	0.05	101.80
	40.86	0.13	26.49	16.71	0.32	10.39	8.97	0.00	0.00	0.04	103.91
	40.75	0.00	23.34	17.13	0.33	11.02	9.18	0.02	0.01	0.02	101.78
	49.19	0.14	12.97	6.63	0.09	11.62	16.19	2.52	0.01	0.10	99.44
	40.64	0.00	23.73	16.83	0.22	10.70	9.16	0.02	0.00	0.03	101.33
	40.92	0.05	23.69	17.10	0.21	10.93	9.16	0.00	0.00	0.00	102.06
	40.78	0.08	23.46	17.26	0.22	11.00	9.10	0.03	0.00	0.05	101.97
	40.71	0.09	23.34	16.76	0.22	10.73	9.06	0.02	0.00	0.00	100.93
	40.92	0.06	23.63	16.46	0.26	10.68	9.10	0.11	0.04	0.00	101.25
	40.81	0.00	23.45	17.32	0.28	11.09	9.11	0.05	0.01	0.04	102.14
	40.96	0.00	23.23	16.57	0.24	10.92	9.12	0.01	0.00	0.09	101.15
	40.89	0.05	23.29	16.78	0.20	10.87	9.17	0.00	0.01	0.07	101.33
	39.16	0.04	23.80	16.63	0.24	10.40	9.20	0.03	0.00	0.07	99.57
	37.97	0.07	23.33	16.77	0.26	9.52	8.83	0.00	0.00	0.01	96.76
	40.76	0.07	23.48	17.18	0.22	11.12	9.03	0.04	0.00	0.05	101.94
	40.90	0.00	23.54	16.76	0.28	11.11	9.07	0.01	0.00	0.07	101.75
	40.85	0.04	23.49	16.95	0.28	11.35	8.70	0.00	0.01	0.04	101.71
	40.88	0.03	23.44	16.87	0.19	11.10	8.64	0.00	0.00	0.04	101.18
	41.01	0.02	23.45	17.20	0.26	11.47	8.38	0.00	0.01	0.02	101.82
	40.77	0.00	23.24	16.80	0.31	11.39	8.63	0.02	0.01	0.07	101.24
	41.31	0.04	23.40	17.09	0.33	11.26	8.83	0.00	0.00	0.00	102.26
	40.92	0.06	23.50	16.94	0.26	11.09	9.04	0.00	0.00	0.03	101.84
	40.97	0.01	23.23	16.92	0.27	11.11	8.89	0.01	0.01	0.08	101.49
	40.92	0.02	23.27	16.74	0.30	11.05	8.93	0.00	0.00	0.06	101.29
	41.21	0.05	23.33	16.89	0.20	10.95	9.01	0.04	0.01	0.01	101.70
	43.06	0.04	21.46	17.05	0.33	11.92	8.70	0.01	0.01	0.06	102.62
	40.45	0.00	23.39	17.79	0.35	11.07	8.92	0.00	0.01	0.04	102.02

Table A-3. Electron microprobe analyses from sample Grü1.

Sample	SiO_2	TiO_2	Al_2O_3	FeO	MnO	MgO	CaO	Na_2O	K_2O	Cr_2O_3	Sum
Grü1	54.12	0.18	11.10	4.48	0.00	9.05	14.91	5.73	0.01	0.06	99.63
	53.49	0.16	11.02	4.70	0.01	8.81	15.48	5.49	0.01	0.02	99.19
	63.80	0.00	23.51	0.20	0.03	0.01	3.75	9.81	0.03	0.01	101.15
	52.25	0.22	7.84	5.55	0.01	11.34	19.71	3.05	0.00	0.03	100.00
	53.77	0.19	11.19	4.38	0.01	8.96	14.69	5.94	0.01	0.01	99.14
	39.25	0.14	23.34	22.14	0.31	8.03	9.04	0.03	0.00	0.07	102.35
	51.83	0.19	10.00	5.48	0.00	10.09	18.22	3.86	0.00	0.07	99.75
	62.32	0.00	22.18	0.49	0.00	0.83	5.35	9.21	0.02	0.01	100.42
	96.12	0.00	0.00	0.06	0.02	0.01	0.02	0.03	0.01	0.01	96.26
	95.91	0.04	0.00	0.17	0.02	0.00	0.02	0.02	0.00	0.04	96.23
	0.01	103.85	0.04	0.20	0.00	0.00	0.03	0.03	0.00	0.07	104.23
	39.23	0.00	23.15	22.92	0.45	6.95	9.60	0.02	0.00	0.02	102.34
	0.08	102.49	0.03	0.98	0.05	0.01	0.41	0.04	0.03	0.13	104.24
	0.04	56.95	0.04	43.52	0.19	1.79	0.17	0.02	0.00	0.03	102.73
	0.06	103.89	0.01	0.25	0.00	0.00	0.09	0.00	0.00	0.04	104.34
	95.38	0.00	0.00	0.19	0.00	0.00	0.03	0.00	0.00	0.02	95.62
	0.04	102.81	0.02	0.46	0.02	0.02	0.26	0.00	0.00	0.09	103.72
	38.97	0.01	23.31	22.15	0.24	7.29	9.75	0.02	0.02	0.01	101.76
	43.38	0.57	16.67	10.79	0.01	12.34	9.64	4.17	0.14	0.02	97.74
	94.62	0.01	0.00	0.20	0.00	0.00	0.05	0.00	0.00	0.00	94.88
	53.11	0.01	1.48	7.04	0.04	14.46	21.45	1.61	0.00	0.06	99.24
	39.00	0.00	22.18	21.58	0.29	7.80	9.36	0.00	0.00	0.03	100.23
	39.18	0.00	22.33	21.50	0.30	7.90	9.15	0.02	0.01	0.04	100.42
	38.94	0.08	21.82	21.65	0.29	8.25	8.83	0.07	0.00	0.09	100.01
	39.46	0.08	22.03	21.53	0.26	8.25	8.99	0.03	0.01	0.10	100.73
	38.96	0.03	22.25	21.32	0.26	8.15	8.97	0.01	0.01	0.07	100.02
	39.02	0.05	22.21	21.43	0.31	8.29	8.95	0.00	0.00	0.04	100.30
	39.00	0.04	21.88	21.69	0.25	8.36	8.75	0.03	0.02	0.03	100.05
	39.26	0.02	22.30	21.07	0.25	8.17	9.03	0.03	0.00	0.00	100.13
	39.42	0.04	22.08	21.90	0.35	8.48	8.96	0.07	0.00	0.06	101.34
	39.08	0.02	22.04	21.32	0.30	7.98	9.38	0.02	0.00	0.00	100.15
	39.05	0.08	22.02	21.34	0.26	7.75	9.63	0.06	0.02	0.06	100.26
	38.87	0.06	22.12	21.96	0.31	7.45	9.47	0.04	0.02	0.07	100.36
	38.67	0.04	21.63	23.00	0.36	6.56	9.49	0.08	0.00	0.00	99.83
	38.55	0.09	21.97	23.78	0.46	6.18	9.63	0.04	0.02	0.00	100.70
	38.54	0.05	21.80	23.73	0.44	6.06	9.58	0.01	0.00	0.03	100.22
	38.60	0.14	21.97	23.11	0.47	6.19	9.48	0.05	0.01	0.04	100.08
	38.76	0.07	21.89	23.42	0.58	6.51	9.28	0.00	0.00	0.05	100.55
	38.90	0.04	21.86	22.70	0.58	6.74	9.09	0.00	0.00	0.01	99.93
	38.51	0.11	21.64	22.89	0.58	6.99	9.10	0.02	0.00	0.00	99.85
	38.91	0.11	21.79	23.36	0.65	7.13	8.98	0.07	0.02	0.03	101.04
	38.55	0.09	21.74	23.07	0.59	7.23	8.70	0.12	0.01	0.05	100.14
	38.36	0.03	22.24	22.04	0.43	7.45	8.79	0.07	0.00	0.00	99.40

Sample	SiO_2	TiO_2	Al_2O_3	FeO	MnO	MgO	CaO	Na_2O	K_2O	Cr_2O_3	Sum
Grü1	39.09	0.13	21.91	22.46	0.42	7.72	9.01	0.03	0.00	0.05	100.81
	38.91	0.11	21.79	22.04	0.43	7.90	8.78	0.05	0.01	0.00	100.03
	39.01	0.60	21.83	21.89	0.32	7.79	9.22	0.06	0.00	0.01	100.72
	38.74	0.27	21.75	22.16	0.34	7.96	9.34	0.06	0.01	0.04	100.65
	38.82	0.25	21.98	21.93	0.33	7.95	8.79	0.00	0.00	0.01	100.06
	38.62	0.38	21.99	21.56	0.29	7.82	9.23	0.01	0.02	0.01	99.92
	38.36	0.31	21.76	22.27	0.28	7.48	9.34	0.05	0.00	0.04	99.89
	38.46	0.09	21.92	21.64	0.37	7.40	9.80	0.03	0.00	0.03	99.73
	38.47	0.08	21.81	21.94	0.34	7.37	9.58	0.02	0.00	0.02	99.62
	38.48	0.09	21.81	22.06	0.40	7.27	9.59	0.06	0.01	0.03	99.79
	38.50	0.07	21.95	21.55	0.32	7.40	9.60	0.06	0.03	0.00	99.48
	38.75	0.09	21.69	21.95	0.29	7.46	9.50	0.03	0.00	0.00	99.74
	38.75	0.05	21.95	21.52	0.33	7.62	9.58	0.07	0.03	0.03	99.92
	38.84	0.13	21.85	21.84	0.31	7.61	9.43	0.01	0.01	0.00	100.03
	28.32	0.14	25.04	20.72	0.29	4.91	9.23	0.09	0.00	0.01	88.76
	38.40	0.10	21.86	21.70	0.32	7.68	9.37	0.02	0.00	0.01	99.46
	38.73	0.11	21.88	21.80	0.33	7.89	9.24	0.03	0.00	0.07	100.09
	38.91	0.10	22.06	21.57	0.28	7.81	9.22	0.02	0.00	0.00	99.96
	38.81	0.19	22.24	21.81	0.26	8.04	9.04	0.05	0.00	0.01	100.44
	39.05	0.09	22.13	21.84	0.31	8.13	9.01	0.01	0.01	0.01	100.60
	38.98	0.09	21.76	21.89	0.26	8.14	9.01	0.02	0.01	0.00	100.15
	39.00	0.01	22.24	21.49	0.25	8.26	8.95	0.04	0.00	0.02	100.26
	40.94	0.07	19.35	21.25	0.26	9.10	8.29	0.02	0.01	0.01	99.29
	38.93	0.04	22.23	21.76	0.22	8.42	8.55	0.00	0.00	0.04	100.18
	11.72	0.11	25.16	19.22	0.21	1.74	8.16	0.14	0.04	0.00	66.51
	43.24	0.02	15.05	21.04	0.28	10.21	8.07	0.04	0.00	0.01	97.96
	38.97	0.06	22.09	21.89	0.30	8.59	8.47	0.04	0.01	0.00	100.43
	39.05	0.08	22.27	21.88	0.22	8.63	8.56	0.04	0.00	0.03	100.76

Table A-4. Electron microprobe analyses from sample Grü2.

Sample	SiO_2	TiO_2	Al_2O_3	FeO	MnO	MgO	CaO	Na_2O	K_2O	Cr_2O_3	Sum
Grü2	38.62	0.09	22.57	23.72	0.69	6.86	9.21	0.04	0.00	0.01	101.81
	38.63	0.07	22.17	23.42	0.63	7.12	9.31	0.06	0.00	0.00	101.41
	39.10	0.05	22.27	21.29	0.52	9.21	8.62	0.06	0.00	0.04	101.16
	53.25	0.18	10.06	4.29	0.00	9.65	16.06	5.10	0.00	0.03	98.62
	53.53	0.21	9.97	4.23	0.08	9.81	15.78	5.03	0.01	0.02	98.69
	54.04	0.14	10.01	4.22	0.00	9.72	15.93	4.81	0.01	0.00	98.87
	54.45	0.19	10.24	3.98	0.05	9.74	15.65	5.30	0.01	0.02	99.62
	39.65	0.04	31.09	1.95	0.00	0.05	24.15	0.05	0.01	0.05	97.04
	39.30	0.06	31.19	2.37	0.00	0.06	24.11	0.00	0.00	0.05	97.15
	46.16	0.86	13.96	8.68	0.11	13.92	10.00	3.48	0.13	0.04	97.33
	45.06	0.97	14.33	9.03	0.05	13.96	10.27	3.75	0.12	0.08	97.61
	45.10	0.49	15.29	9.21	0.00	13.11	10.00	3.61	0.11	0.12	97.03
	54.97	0.13	10.05	3.88	0.00	9.67	15.53	5.25	0.00	0.03	99.50
	54.85	0.17	9.79	3.95	0.04	9.67	15.65	5.37	0.01	0.01	99.50
	57.18	0.02	27.83	0.16	0.02	0.00	8.98	6.83	0.00	0.03	101.04
	63.38	0.00	23.04	0.07	0.00	0.01	3.59	9.98	0.00	0.02	100.10
	39.31	0.05	22.83	20.14	0.22	8.83	9.50	0.00	0.00	0.05	100.94
	39.13	0.00	23.05	19.18	0.25	8.65	9.54	0.03	0.02	0.07	99.91
	39.47	0.03	22.78	19.38	0.24	8.88	9.37	0.03	0.01	0.05	100.25
	39.36	0.07	22.54	19.28	0.24	9.05	9.12	0.03	0.00	0.00	99.69
	39.08	0.16	22.77	19.76	0.21	8.62	9.07	0.08	0.02	0.00	99.78
	39.76	0.01	22.82	20.13	0.22	9.08	8.79	0.00	0.01	0.02	100.83
	39.26	0.00	23.11	20.42	0.22	8.94	8.86	0.03	0.01	0.01	100.84
	39.31	0.01	22.84	20.17	0.20	9.15	8.72	0.05	0.02	0.05	100.51
	39.32	0.01	22.82	20.14	0.17	8.93	8.85	0.00	0.01	0.15	100.41
	39.35	0.01	22.97	19.81	0.26	8.87	8.83	0.03	0.02	0.03	100.16
	39.17	0.06	23.19	20.53	0.19	8.96	8.91	0.00	0.01	0.08	101.09
	39.28	0.00	23.17	20.78	0.19	8.84	8.67	0.00	0.00	0.06	100.99
	39.23	0.03	22.98	20.18	0.21	8.74	8.83	0.05	0.00	0.00	100.24
	39.06	0.02	22.80	20.37	0.21	8.77	8.65	0.03	0.01	0.05	99.96
	23.63	0.12	16.38	16.56	0.12	11.53	10.91	0.00	0.05	0.16	79.46
	13.11	0.03	5.73	21.45	0.09	15.46	5.89	0.35	0.08	0.03	62.22
	39.31	0.11	22.72	20.79	0.18	8.73	8.62	0.06	0.02	0.07	100.61
	39.50	0.09	22.63	21.04	0.19	8.53	8.56	0.10	0.02	0.05	100.71
	39.62	0.06	22.77	21.36	0.27	8.64	8.73	0.02	0.01	0.00	101.47
	39.65	0.05	22.59	21.70	0.21	8.60	8.50	0.13	0.04	0.10	101.56
	39.47	0.10	23.01	21.45	0.18	8.57	8.52	0.01	0.02	0.04	101.35
	39.07	0.17	22.64	20.75	0.23	8.43	8.70	0.05	0.01	0.07	100.12
	39.40	0.13	22.56	21.25	0.24	8.41	8.63	0.03	0.00	0.00	100.66
	39.44	0.09	22.41	21.81	0.15	8.26	8.66	0.07	0.00	0.02	100.89
	39.30	0.03	22.54	21.25	0.18	8.33	8.61	0.07	0.01	0.11	100.43
	39.42	0.08	22.76	21.60	0.33	8.23	8.65	0.00	0.00	0.03	101.09
	39.10	0.05	22.78	21.32	0.23	8.30	8.70	0.03	0.00	0.07	100.57

Sample	SiO_2	TiO_2	Al_2O_3	FeO	MnO	MgO	CaO	Na_2O	K_2O	Cr_2O_3	Sum
Grü2	39.57	0.06	22.95	22.08	0.23	8.26	8.58	0.09	0.01	0.05	101.89
	39.45	0.11	22.52	21.27	0.24	8.14	8.71	0.04	0.01	0.04	100.52
	39.50	0.05	22.63	21.52	0.31	8.27	8.68	0.05	0.00	0.00	101.00
	39.45	0.04	22.75	21.66	0.24	8.12	8.90	0.01	0.02	0.01	101.20
	39.39	0.04	22.62	20.86	0.32	8.07	8.88	0.01	0.01	0.05	100.24
	39.72	0.04	22.80	21.37	0.33	7.84	8.99	0.05	0.01	0.01	101.15
	38.58	0.00	22.46	21.36	0.25	8.12	8.90	0.06	0.02	0.07	99.83
	39.29	0.10	22.62	20.76	0.29	7.55	9.36	0.06	0.02	0.07	100.11
	39.50	0.03	22.56	21.98	0.29	7.58	9.54	0.06	0.02	0.00	101.57
	39.13	0.07	22.86	21.44	0.27	7.38	9.57	0.05	0.01	0.05	100.85
	39.34	0.14	22.48	21.56	0.28	7.19	9.44	0.06	0.02	0.01	100.52
	39.09	0.07	22.12	21.83	0.17	7.16	9.61	0.03	0.01	0.11	100.19
	39.18	0.06	22.51	21.78	0.34	6.91	9.60	0.03	0.00	0.09	100.52
	39.30	0.03	22.59	22.61	0.29	7.01	9.67	0.11	0.02	0.06	101.67
	39.25	0.08	22.43	22.30	0.33	6.77	9.67	0.04	0.01	0.14	101.03
	38.69	0.09	22.08	22.24	0.27	6.68	9.64	0.08	0.01	0.17	99.95
	38.59	0.11	22.34	22.29	0.31	6.83	9.57	0.07	0.00	0.02	100.13
	38.81	0.14	22.39	22.21	0.27	6.69	9.60	0.02	0.00	0.05	100.19
	39.02	0.09	22.51	21.98	0.29	7.04	9.43	0.04	0.02	0.12	100.54
	39.07	0.04	22.52	21.45	0.28	7.11	9.47	0.02	0.02	0.06	100.04
	39.31	0.08	22.61	22.03	0.32	7.12	9.48	0.05	0.01	0.07	101.06
	38.92	0.08	22.42	22.10	0.34	7.08	9.60	0.02	0.01	0.02	100.60
	39.15	0.00	22.56	21.99	0.32	7.13	9.56	0.03	0.02	0.01	100.76
	39.06	0.02	22.46	21.75	0.29	7.18	9.39	0.03	0.00	0.05	100.23
	39.26	0.05	22.72	22.21	0.35	7.01	9.52	0.02	0.02	0.08	101.25
	39.32	0.03	22.53	22.12	0.42	7.20	9.38	0.00	0.03	0.12	101.16
	39.11	0.09	22.54	21.50	0.30	7.25	9.46	0.04	0.00	0.05	100.34
	39.21	0.04	22.47	21.05	0.32	7.40	9.51	0.05	0.01	0.13	100.19
	39.17	0.01	22.43	21.47	0.32	7.34	9.48	0.05	0.02	0.04	100.33
	39.16	0.03	22.40	20.96	0.35	7.51	9.60	0.06	0.03	0.08	100.19
	39.20	0.00	22.55	21.12	0.36	7.45	9.43	0.01	0.01	0.11	100.22
	39.33	0.12	22.68	21.73	0.27	7.61	9.46	0.02	0.03	0.02	101.26
	39.44	0.04	22.39	21.40	0.38	7.75	9.52	0.07	0.00	0.09	101.09
	39.49	0.05	22.37	21.30	0.32	7.68	9.59	0.01	0.02	0.00	100.83
	39.21	0.14	22.48	21.72	0.38	7.62	9.39	0.01	0.03	0.03	101.01
	39.23	0.12	22.52	21.17	0.33	7.63	9.34	0.03	0.02	0.02	100.39
	39.17	0.08	22.67	22.06	0.32	7.58	9.41	0.04	0.04	0.04	101.42
	39.54	0.05	22.69	21.48	0.27	7.65	9.45	0.08	0.03	0.05	101.28
	39.50	0.13	22.48	21.71	0.35	7.73	9.46	0.00	0.01	0.00	101.37
	39.50	0.14	22.36	21.09	0.28	7.57	9.38	0.03	0.02	0.09	100.45
	39.61	0.00	22.57	21.23	0.18	7.59	9.46	0.04	0.00	0.11	100.79
	39.54	0.13	22.64	21.55	0.36	7.69	9.39	0.05	0.01	0.09	101.44
	39.36	0.07	22.40	21.05	0.33	7.88	9.39	0.04	0.00	0.01	100.54
	39.02	0.01	22.95	21.31	0.35	7.94	9.39	0.02	0.03	0.07	101.10

Sample	SiO_2	TiO_2	Al_2O_3	FeO	MnO	MgO	CaO	Na_2O	K_2O	Cr_2O_3	Sum
Grü2	39.28	0.06	22.93	21.09	0.26	8.03	9.15	0.03	0.02	0.06	100.91
	39.35	0.09	22.51	20.77	0.31	8.09	9.36	0.05	0.02	0.08	100.62
	39.37	0.12	22.65	21.21	0.33	8.20	9.28	0.03	0.00	0.00	101.17
	39.43	0.11	22.91	21.19	0.26	8.24	9.16	0.04	0.03	0.06	101.42
	39.34	0.08	22.60	21.27	0.22	8.40	9.16	0.05	0.00	0.00	101.11
	38.91	0.12	22.07	20.42	0.26	8.15	9.08	0.00	0.00	0.08	99.08
	39.43	0.16	22.55	20.95	0.27	8.38	8.94	0.04	0.00	0.03	100.76
	39.42	0.00	22.71	20.79	0.35	8.42	9.10	0.04	0.01	0.06	100.91
	39.59	0.12	22.76	20.81	0.25	8.38	8.75	0.02	0.01	0.01	100.70
	39.76	0.17	22.80	20.67	0.31	8.43	8.88	0.01	0.01	0.03	101.07
	39.37	0.11	22.83	21.45	0.26	8.63	8.81	0.06	0.02	0.00	101.53
	39.77	0.10	22.95	21.71	0.27	8.67	8.73	0.10	0.02	0.08	102.39
	39.76	0.08	22.95	21.42	0.20	8.88	8.68	0.10	0.01	0.08	102.15
	39.53	0.08	22.70	20.79	0.26	8.84	8.74	0.03	0.01	0.03	100.99
	39.17	0.11	22.97	20.94	0.24	8.85	8.49	0.04	0.00	0.04	100.86
	39.39	0.06	22.79	20.48	0.21	9.03	8.58	0.07	0.01	0.07	100.70
	39.44	0.11	23.03	20.29	0.22	9.08	8.67	0.04	0.01	0.04	100.93
	39.28	0.02	22.84	20.81	0.18	9.12	8.55	0.06	0.01	0.00	100.88
	39.38	0.09	22.84	20.80	0.19	9.03	8.34	0.01	0.02	0.07	100.79
	39.68	0.00	22.97	21.02	0.24	9.28	8.34	0.08	0.03	0.03	101.68
	39.69	0.05	23.02	20.54	0.23	9.09	8.57	0.01	0.03	0.00	101.21
	39.63	0.00	23.25	20.55	0.14	9.06	8.68	0.01	0.00	0.06	101.37
	39.59	0.10	22.86	20.46	0.16	9.19	8.75	0.02	0.02	0.04	101.18
	39.37	0.00	22.85	19.91	0.17	9.19	8.50	0.01	0.00	0.04	100.04
	39.72	0.06	22.92	20.59	0.25	9.32	8.69	0.05	0.00	0.06	101.66
	39.37	0.01	23.13	20.82	0.22	9.00	8.87	0.03	0.00	0.00	101.46
	39.53	0.12	22.84	20.90	0.18	8.86	8.90	0.08	0.02	0.03	101.45
	39.60	0.00	22.98	20.57	0.20	9.25	8.75	0.06	0.03	0.00	101.44
	39.39	0.10	23.04	19.94	0.20	9.05	9.14	0.03	0.02	0.00	100.91

Table A-5. Electron microprobe analyses from sample Wol1.

Sample	SiO_2	TiO_2	Al_2O_3	FeO	MnO	MgO	CaO	Na_2O	K_2O	Cr_2O_3	Sum
Wol1	55.65	0.13	10.31	3.76	0.00	9.75	15.77	5.34	0.00	0.08	100.79
	39.97	0.10	31.94	1.52	0.00	0.05	24.31	0.00	0.01	0.11	98.02
	0.02	98.74	0.02	0.19	0.01	0.00	0.04	0.06	0.00	0.06	99.14
	65.17	0.04	22.56	0.11	0.03	0.01	3.62	10.20	0.05	0.00	101.80
	53.70	0.23	8.57	4.38	0.00	11.12	19.27	3.05	0.00	0.06	100.38
	39.47	0.08	22.37	22.54	0.16	6.61	10.35	0.00	0.01	0.01	101.59
	65.69	0.00	21.63	0.06	0.03	0.00	2.86	10.37	0.04	0.01	100.70
	39.22	0.02	32.19	1.23	0.02	0.07	24.35	0.00	0.01	0.00	97.10
	66.58	0.00	21.69	0.02	0.00	0.01	2.92	10.13	0.02	0.00	101.36
	0.02	96.00	0.00	0.20	0.00	0.00	0.16	0.07	0.02	0.10	96.56
	66.05	0.00	21.99	0.02	0.02	0.00	3.08	9.89	0.03	0.00	101.08
	38.76	0.00	31.87	1.25	0.01	0.06	24.21	0.05	0.01	0.05	96.28
	0.03	97.20	0.05	0.14	0.02	0.00	0.11	0.04	0.01	0.06	97.65
	64.99	0.04	21.24	0.12	0.02	0.01	2.80	9.67	0.02	0.00	98.91
	38.31	0.06	32.03	1.25	0.01	0.07	24.12	0.06	0.00	0.00	95.91
	43.78	0.77	14.39	11.79	0.02	12.38	10.85	3.29	0.33	0.01	97.60
	38.73	0.13	21.98	24.97	0.20	4.24	11.70	0.03	0.00	0.05	102.04
	30.23	37.50	1.13	0.35	0.02	0.04	28.36	0.02	0.00	0.07	97.70
	38.63	0.10	21.66	21.47	0.28	5.26	11.81	0.02	0.02	0.02	99.25
	38.91	0.11	21.54	21.45	0.28	5.31	11.90	0.03	0.01	0.01	99.55
	38.67	0.07	21.51	21.35	0.39	5.23	11.61	0.01	0.01	0.07	98.90
	38.73	0.06	21.52	21.85	0.32	5.26	11.67	0.00	0.01	0.05	99.48
	38.58	0.03	21.54	22.04	0.35	5.30	11.71	0.05	0.00	0.08	99.68
	38.45	0.08	21.53	21.32	0.31	5.14	11.84	0.00	0.02	0.08	98.75
	38.59	0.15	21.74	21.93	0.33	5.07	11.70	0.01	0.00	0.10	99.62
	38.80	0.10	21.61	21.51	0.37	5.15	11.69	0.00	0.02	0.08	99.32
	38.60	0.03	21.55	21.89	0.32	5.30	11.44	0.10	0.00	0.08	99.30
	38.61	0.22	21.66	21.93	0.35	5.45	11.06	0.03	0.02	0.07	99.39
	38.52	0.04	21.72	21.61	0.34	5.40	11.42	0.03	0.01	0.11	99.19
	38.64	0.18	21.72	21.43	0.30	5.30	11.71	0.00	0.00	0.07	99.34
	38.36	0.17	21.69	21.57	0.39	5.28	11.62	0.03	0.02	0.07	99.20
	38.12	0.22	21.32	21.65	0.35	5.17	11.75	0.03	0.01	0.09	98.71
	96.87	0.11	0.04	0.58	0.03	0.02	0.08	0.02	0.01	0.00	97.74
	38.51	0.19	21.62	21.60	0.32	5.12	11.60	0.07	0.01	0.08	99.13
	38.84	0.20	21.50	21.96	0.35	5.13	11.57	0.02	0.00	0.09	99.66
	38.43	0.29	21.52	21.73	0.33	5.23	11.55	0.02	0.00	0.13	99.22
	38.60	0.22	21.63	22.00	0.33	5.23	11.70	0.06	0.01	0.11	99.90
	38.59	0.19	21.46	21.49	0.35	5.20	11.51	0.05	0.00	0.07	98.92
	38.57	0.13	21.42	21.39	0.37	5.15	11.74	0.00	0.02	0.04	98.81
	38.71	0.24	21.53	21.54	0.41	5.17	11.74	0.06	0.01	0.21	99.62
	38.82	0.16	21.62	21.82	0.41	5.23	11.78	0.06	0.03	0.06	99.98
	38.33	0.17	21.45	21.77	0.37	5.19	11.78	0.00	0.00	0.10	99.15
	38.71	0.05	21.52	21.94	0.36	5.32	11.40	0.02	0.01	0.14	99.46

Sample	SiO_2	TiO_2	Al_2O_3	FeO	MnO	MgO	CaO	Na_2O	K_2O	Cr_2O_3	Sum
Wol1	38.81	0.00	21.34	22.18	0.33	5.01	11.44	0.00	0.00	0.05	99.15
	38.58	0.16	21.70	22.29	0.36	5.13	11.71	0.03	0.02	0.15	100.12
	38.34	0.12	21.21	21.50	0.35	5.08	11.85	0.04	0.01	0.11	98.61
	38.32	0.11	21.57	21.25	0.38	5.12	11.96	0.02	0.01	0.15	98.87
	38.88	0.05	21.50	21.99	0.41	5.14	11.32	0.02	0.00	0.20	99.52
	38.69	0.01	21.49	21.36	0.41	5.25	11.51	0.02	0.01	0.17	98.91
	38.49	0.16	21.45	21.63	0.44	5.03	11.95	0.04	0.00	0.14	99.33
	38.52	0.23	21.35	21.70	0.38	5.09	12.00	0.08	0.00	0.16	99.51
	38.73	0.23	21.22	21.23	0.49	4.87	11.93	0.11	0.01	0.16	98.98
	38.45	0.28	21.51	21.59	0.44	4.88	12.06	0.04	0.00	0.07	99.32
	38.46	0.25	21.31	21.65	0.43	4.98	11.98	0.09	0.00	0.06	99.20
	38.86	0.19	21.19	21.39	0.58	4.62	12.27	0.07	0.02	0.12	99.29
	38.11	0.14	21.26	21.47	0.53	4.37	12.31	0.08	0.01	0.07	98.35
	38.20	0.27	21.51	21.63	0.60	4.46	12.06	0.00	0.00	0.05	98.78
	38.57	0.13	21.51	22.32	0.61	4.39	11.92	0.03	0.00	0.10	99.59
	38.76	0.11	21.41	22.45	0.56	4.45	12.00	0.04	0.01	0.17	99.97
	38.56	0.04	21.49	22.96	0.54	4.56	11.77	0.06	0.02	0.02	100.03
	38.62	0.17	21.34	22.07	0.49	4.36	11.89	0.05	0.00	0.08	99.08
	38.99	0.12	21.46	21.51	0.38	4.73	12.09	0.04	0.01	0.07	99.40
	38.37	0.09	17.60	21.97	0.81	3.13	10.65	0.02	0.02	0.25	92.91
	36.52	0.10	19.94	22.56	0.94	2.54	11.24	0.00	0.01	0.19	94.03
	37.89	0.04	22.81	22.54	0.45	4.52	11.98	0.02	0.03	0.16	100.46
	38.60	0.08	21.64	22.54	0.43	4.29	12.06	0.03	0.00	0.19	99.85
	38.42	0.13	21.56	21.94	0.51	4.16	12.23	0.03	0.00	0.06	99.03
	38.73	0.18	21.41	22.00	0.37	4.31	12.01	0.02	0.01	0.04	99.07
	38.83	0.12	21.22	22.36	0.35	4.51	12.23	0.02	0.00	0.08	99.72
	38.71	0.11	21.27	21.76	0.42	4.70	12.05	0.04	0.01	0.10	99.16
	38.85	0.17	21.29	21.84	0.40	4.71	12.29	0.02	0.00	0.10	99.66
	39.13	0.06	21.48	21.92	0.30	4.86	11.62	0.01	0.00	0.09	99.47
	54.06	0.18	10.19	4.57	0.04	9.12	15.65	5.07	0.01	0.10	98.98
	38.83	0.03	21.41	21.65	0.36	5.17	11.49	0.00	0.01	0.13	99.07
	39.66	0.14	20.65	21.56	0.34	4.89	11.75	0.05	0.01	0.10	99.16
	38.50	0.19	21.46	23.00	0.28	4.20	11.94	0.04	0.00	0.14	99.76
	38.76	0.08	21.36	22.80	0.32	4.24	12.04	0.05	0.01	0.09	99.73
	38.66	0.07	21.51	22.10	0.27	4.60	12.26	0.02	0.00	0.09	99.58
	38.61	0.11	21.32	21.57	0.29	5.11	12.02	0.03	0.01	0.08	99.15
	38.57	0.01	21.64	21.43	0.34	5.05	11.89	0.07	0.01	0.00	99.01
	38.81	0.05	21.75	21.78	0.31	5.22	11.78	0.00	0.02	0.06	99.79
	38.25	0.04	21.72	21.93	0.31	5.24	11.76	0.06	0.00	0.05	99.37
	38.71	0.07	21.68	22.06	0.22	5.21	11.83	0.02	0.04	0.04	99.86
	38.59	0.04	21.57	21.54	0.23	5.29	11.57	0.05	0.01	0.07	98.95
	38.76	0.08	21.82	21.88	0.24	5.40	11.41	0.03	0.00	0.07	99.69
	38.67	0.06	21.71	22.11	0.30	5.27	11.17	0.08	0.01	0.02	99.41
	38.86	0.00	21.49	22.14	0.41	5.27	11.12	0.00	0.00	0.07	99.36

Table A-6. Electron microprobe analyses from sample Sig3.

Sample	SiO_2	TiO_2	Al_2O_3	FeO	MnO	MgO	CaO	Na_2O	K_2O	Cr_2O_3	Sum
Sig3	42.50	0.91	13.12	14.04	0.03	11.55	11.24	2.39	0.45	0.01	96.24
	43.81	0.88	13.23	14.23	0.04	11.28	9.76	3.16	0.63	0.05	97.07
	38.46	0.19	27.95	7.14	0.01	0.16	23.48	0.00	0.00	0.03	97.43
	37.88	0.21	28.19	7.20	0.00	0.12	23.27	0.04	0.01	0.00	96.93
	64.77	0.06	22.54	0.23	0.00	0.01	3.14	9.26	0.08	0.00	100.08
	52.85	0.17	3.74	8.27	0.06	11.39	19.84	2.62	0.00	0.00	98.94
	52.51	0.24	4.13	8.55	0.04	10.97	19.68	2.57	0.00	0.05	98.76
	65.36	0.00	22.35	0.27	0.00	0.00	2.88	9.76	0.05	0.00	100.67
	65.13	0.02	22.64	0.25	0.00	0.00	3.01	9.62	0.08	0.00	100.76
	51.68	0.14	5.50	8.52	0.02	10.01	18.75	2.93	0.01	0.00	97.55
	66.15	0.00	22.44	0.11	0.01	0.03	2.83	9.76	0.08	0.00	101.41
	38.61	0.16	28.02	7.36	0.03	0.14	23.56	0.00	0.00	0.01	97.90
	66.86	0.04	22.64	0.25	0.00	0.02	2.83	9.62	0.12	0.01	102.39
	30.14	39.94	0.98	0.63	0.02	0.02	28.45	0.00	0.00	0.00	100.18
	37.38	0.06	21.75	13.77	0.06	0.02	22.95	0.00	0.01	0.00	96.00
	96.27	0.10	0.02	0.39	0.02	0.01	0.05	0.04	0.02	0.00	96.92
	0.46	98.48	0.06	0.75	0.00	0.00	0.80	0.02	0.01	0.04	100.61
	64.02	0.00	17.67	0.48	0.04	0.01	0.00	0.24	16.14	0.00	98.59
	62.84	0.04	18.34	0.65	0.05	0.00	0.06	0.43	16.17	0.00	98.59
	38.20	0.33	21.21	23.16	1.67	3.50	10.39	0.03	0.01	0.00	98.49
	0.06	99.20	0.03	0.89	0.01	0.01	0.34	0.04	0.00	0.04	100.62
	38.72	0.07	22.15	25.31	0.26	4.71	9.86	0.00	0.00	0.00	101.10
	38.57	0.11	22.09	25.21	0.32	4.52	9.97	0.04	0.00	0.00	100.82
	38.99	0.04	21.80	25.06	0.44	4.46	9.97	0.08	0.00	0.03	100.85
	38.81	0.08	21.94	25.31	0.34	4.38	9.92	0.05	0.01	0.01	100.86
	38.68	0.02	21.71	24.57	0.55	4.09	10.13	0.06	0.02	0.02	99.85
	38.46	0.02	21.84	25.13	0.72	4.02	10.29	0.04	0.01	0.03	100.55
	38.18	0.14	21.63	24.70	0.75	3.82	10.39	0.11	0.01	0.00	99.73
	38.45	0.16	21.78	24.32	0.88	3.76	10.48	0.04	0.00	0.08	99.95
	38.72	0.09	21.67	24.13	1.00	3.69	10.59	0.02	0.02	0.00	99.92
	38.32	0.12	21.29	23.80	1.17	3.28	10.87	0.02	0.02	0.02	98.90
	38.40	0.11	21.65	23.93	1.08	3.45	11.25	0.08	0.00	0.01	99.96
	38.13	0.08	21.75	23.59	1.28	3.07	11.46	0.09	0.01	0.03	99.49
	40.14	0.09	19.39	23.01	1.35	3.32	11.22	0.12	0.01	0.04	98.69
	38.47	0.10	21.94	23.66	1.46	3.03	11.49	0.00	0.02	0.02	100.20
	62.42	0.00	22.33	1.37	0.08	0.15	4.43	8.20	0.08	0.05	99.10
	38.60	0.05	21.80	22.96	1.42	3.16	11.50	0.09	0.01	0.04	99.63
	38.61	0.14	21.96	23.31	1.65	2.84	11.78	0.05	0.00	0.03	100.37
	38.42	0.11	21.68	22.86	1.61	2.91	11.71	0.00	0.01	0.01	99.32
	38.63	0.19	21.42	22.92	1.67	3.16	11.87	0.03	0.02	0.10	99.99
	38.43	0.17	21.69	23.08	1.70	2.90	11.73	0.07	0.01	0.00	99.78
	38.38	0.18	21.72	22.63	2.06	2.96	11.53	0.02	0.01	0.00	99.49
	38.16	0.08	21.85	22.57	1.80	2.94	11.38	0.00	0.00	0.00	98.78

Sample	SiO_2	TiO_2	Al_2O_3	FeO	MnO	MgO	CaO	Na_2O	K_2O	Cr_2O_3	Sum
Sig3	38.46	0.28	21.57	22.98	1.68	2.89	11.46	0.08	0.01	0.06	99.47
	38.33	0.06	21.50	22.90	1.78	3.06	11.18	0.06	0.01	0.00	98.86
	37.92	0.13	21.49	22.86	1.75	3.11	11.10	0.06	0.01	0.03	98.44
	38.45	0.26	21.37	22.54	1.69	3.03	11.33	0.04	0.01	0.08	98.80
	61.74	0.02	23.77	3.60	0.19	0.49	4.48	7.87	0.13	0.00	102.29
	38.72	0.21	21.73	23.01	1.81	3.14	11.36	0.11	0.01	0.03	100.12
	38.36	0.20	21.42	22.59	1.82	3.03	11.16	0.09	0.02	0.03	98.72
	39.21	0.23	22.04	23.23	1.85	3.20	11.31	0.04	0.08	0.04	101.23
	38.60	0.23	21.68	22.55	1.65	3.15	11.24	0.05	0.01	0.00	99.15
	38.62	0.31	21.68	22.70	1.67	3.22	11.16	0.04	0.01	0.04	99.44
	37.80	0.28	21.28	22.98	1.84	3.16	11.60	0.08	0.01	0.01	99.03
	38.36	0.27	21.36	22.74	1.61	3.28	11.31	0.03	0.00	0.02	98.98
	37.95	0.21	21.48	22.70	1.51	3.40	11.10	0.09	0.00	0.03	98.46
	38.75	0.16	21.85	23.22	1.64	3.31	11.56	0.08	0.01	0.00	100.60
	51.36	0.08	20.19	11.64	0.81	1.61	7.21	3.46	0.08	0.04	96.47
	38.32	0.18	21.76	22.31	1.55	3.29	11.48	0.10	0.00	0.05	99.04
	38.40	0.20	21.64	22.67	1.76	3.17	11.46	0.05	0.02	0.05	99.42
	38.35	0.25	21.64	22.70	1.65	3.09	11.75	0.03	0.01	0.00	99.47
	38.63	0.05	21.47	23.67	1.38	3.27	11.33	0.02	0.00	0.05	99.86
	37.77	3.35	20.01	20.97	1.46	2.76	13.55	0.03	0.00	0.05	99.94
	38.34	0.16	21.52	23.11	1.60	3.11	11.71	0.06	0.01	0.00	99.61
	38.47	0.13	21.79	23.26	1.43	2.91	11.42	0.00	0.01	0.02	99.44
	38.47	0.09	21.45	23.20	1.47	2.81	11.73	0.06	0.01	0.00	99.28
	38.45	0.02	21.98	23.79	1.21	3.44	11.05	0.03	0.01	0.00	99.97
	39.04	0.03	21.99	24.20	1.16	3.48	11.36	0.02	0.01	0.01	101.30
	38.50	0.03	21.75	24.09	0.86	3.85	10.85	0.03	0.01	0.00	99.95
	39.20	0.08	22.33	24.26	0.95	3.78	11.13	0.07	0.00	0.00	101.78
	39.09	0.06	22.12	24.30	0.88	3.94	10.89	0.02	0.01	0.02	101.33
	39.43	0.07	21.92	24.61	0.65	4.16	10.70	0.05	0.00	0.01	101.60
	39.31	0.03	22.22	24.83	0.60	4.31	10.49	0.07	0.01	0.03	101.90
	39.09	0.11	22.07	24.56	0.56	4.28	10.41	0.07	0.03	0.01	101.18
	37.31	0.07	21.28	25.96	0.47	5.43	8.85	0.02	0.05	0.01	99.45
	38.69	0.08	21.76	24.22	0.51	4.40	9.98	0.09	0.00	0.01	99.73
	38.96	0.03	22.16	24.73	0.29	4.60	9.74	0.06	0.00	0.00	100.57
	39.18	0.02	21.86	24.99	0.35	4.48	10.04	0.02	0.01	0.03	100.96
	38.53	0.17	21.97	24.62	0.23	4.46	10.07	0.11	0.00	0.05	100.21
	39.30	0.04	22.26	24.88	0.27	4.81	10.13	0.08	0.00	0.05	101.82
	39.05	0.04	22.27	24.44	0.13	5.09	9.81	0.00	0.01	0.04	100.88

Table A-7. Electron microprobe analyses from sample Sal1.

Sample	SiO_2	TiO_2	Al_2O_3	FeO	MnO	MgO	CaO	Na_2O	K_2O	Cr_2O_3	Sum
Sal1	30.50	40.18	0.76	0.61	0.00	0.01	27.33	0.04	0.02	0.02	99.47
	53.14	0.15	7.16	7.78	0.02	9.37	16.01	5.03	0.02	0.02	98.69
	69.90	0.04	20.23	0.18	0.02	0.00	0.61	11.34	0.02	0.02	102.37
	44.38	0.58	12.15	15.44	0.04	10.75	8.42	4.31	0.53	0.06	96.66
	45.17	0.75	13.00	11.88	0.00	12.33	7.97	4.74	0.54	0.08	96.44
	52.72	0.12	4.12	9.79	0.00	10.57	17.86	3.77	0.02	0.00	98.97
	44.58	0.65	13.32	15.03	0.03	10.47	7.57	4.60	0.53	0.00	96.78
	42.61	0.48	14.54	15.44	0.07	10.19	9.49	3.94	0.32	0.06	97.15
	38.31	0.02	21.35	27.77	0.47	4.01	7.97	0.04	0.01	0.00	99.95
	54.76	0.13	10.25	7.39	0.00	7.27	11.94	7.69	0.01	0.07	99.51
	52.94	0.57	6.11	9.02	0.05	9.39	16.28	5.06	0.02	0.02	99.45
	0.02	54.78	0.05	43.56	0.20	1.91	0.18	0.00	0.01	0.00	100.70
	0.04	101.56	0.02	0.70	0.06	0.02	0.19	0.02	0.00	0.06	102.66
	52.30	0.08	4.24	8.68	0.00	11.12	18.89	3.15	0.01	0.07	98.53
	54.28	0.12	9.53	7.45	0.04	7.68	13.25	6.95	0.02	0.05	99.34
	68.71	0.00	19.98	0.33	0.01	0.00	0.59	11.08	0.02	0.06	100.79
	38.11	0.22	26.82	7.36	0.05	0.09	21.90	0.02	0.00	0.03	94.60
	36.21	0.07	25.00	7.59	0.01	0.32	19.69	0.02	0.00	0.00	88.91
	37.35	0.09	25.90	7.22	0.02	0.20	21.07	0.00	0.00	0.02	91.86
	42.53	0.71	13.01	15.42	0.04	10.55	9.93	3.80	0.38	0.03	96.39
	67.78	0.05	21.19	0.32	0.01	0.01	1.57	11.36	0.03	0.00	102.32
	38.97	0.21	21.38	26.35	0.29	3.68	9.73	0.06	0.02	0.04	100.72
	38.96	0.74	21.20	26.01	0.42	3.57	9.82	0.03	0.00	0.05	100.80
	38.52	0.32	21.35	25.61	0.39	3.49	10.96	0.00	0.03	0.00	100.67
	38.81	0.03	21.57	28.50	0.41	5.16	6.10	0.00	0.01	0.03	100.61
	38.47	0.04	21.41	28.81	0.36	5.02	5.70	0.06	0.00	0.00	99.86
	38.73	0.04	21.18	28.82	0.44	4.87	5.82	0.00	0.04	0.00	99.93
	39.15	1.49	18.93	22.62	0.32	5.86	7.23	2.48	0.32	0.00	98.40
	43.46	1.32	13.89	13.96	0.02	10.30	7.99	4.58	0.55	0.05	96.12
	38.39	0.21	21.01	26.33	0.32	3.63	9.73	0.08	0.00	0.00	99.70
	38.16	0.07	21.22	26.03	0.31	3.55	10.34	0.02	0.00	0.02	99.72
	38.19	0.15	21.21	25.55	0.26	3.10	11.38	0.06	0.01	0.00	99.91
	39.19	0.10	21.44	25.07	0.21	2.87	12.06	0.04	0.01	0.00	100.98
	39.04	0.04	21.38	26.10	0.33	2.81	11.14	0.03	0.01	0.00	100.88
	39.03	0.16	21.60	25.40	0.41	3.06	11.29	0.00	0.00	0.06	101.00
	38.40	0.32	21.56	24.54	0.39	2.83	11.56	0.05	0.03	0.03	99.70
	38.69	0.10	21.42	25.65	0.56	2.53	11.73	0.02	0.00	0.02	100.72
	38.91	0.14	21.20	24.73	0.64	2.66	12.19	0.04	0.02	0.07	100.60
	38.90	0.21	21.19	24.58	0.70	2.91	11.88	0.00	0.00	0.00	100.37
	39.21	0.17	21.70	24.10	0.70	3.01	11.71	0.07	0.02	0.05	100.73
	38.53	0.18	21.49	23.61	1.05	2.74	12.18	0.08	0.01	0.05	99.91
	38.36	0.27	21.27	24.96	0.46	3.31	11.43	0.04	0.02	0.00	100.12
	38.02	0.30	21.42	23.59	0.79	2.92	12.42	0.05	0.01	0.00	99.51

Sample	SiO_2	TiO_2	Al_2O_3	FeO	MnO	MgO	CaO	Na_2O	K_2O	Cr_2O_3	Sum
Sal1	37.40	0.14	20.54	23.73	0.60	3.19	12.99	0.04	0.00	0.01	98.66
	38.92	0.18	21.25	24.11	0.81	2.94	12.12	0.05	0.02	0.03	100.41
	38.72	0.19	21.41	23.38	0.82	2.85	12.40	0.03	0.03	0.01	99.84
	39.41	0.06	22.07	24.22	0.43	3.05	11.90	0.04	0.01	0.01	101.20
	38.44	0.19	21.11	24.35	0.73	2.90	12.11	0.05	0.02	0.00	99.89
	38.71	0.07	21.28	24.25	0.72	2.91	12.34	0.02	0.01	0.00	100.30
	38.70	0.13	21.08	24.62	0.62	2.91	12.10	0.07	0.00	0.00	100.23
	38.96	0.12	21.48	24.67	0.55	2.58	11.65	0.05	0.04	0.04	100.15
	31.71	35.11	3.01	1.61	0.02	0.08	27.72	0.04	0.00	0.03	99.31
	39.23	0.05	21.19	25.76	0.42	2.73	11.28	0.07	0.03	0.00	100.75
	39.27	0.07	21.21	25.27	0.42	3.03	11.57	0.07	0.00	0.00	100.90
	55.42	0.20	10.02	7.16	0.07	7.33	12.70	7.28	0.01	0.04	100.23
	38.72	0.34	21.39	25.30	0.32	3.18	10.93	0.09	0.01	0.01	100.29
	38.49	0.28	21.50	25.52	0.27	2.91	11.68	0.02	0.02	0.00	100.70
	38.31	0.14	21.22	24.18	0.32	2.98	12.21	0.01	0.02	0.03	99.41
	38.65	0.06	21.66	27.62	0.25	4.05	8.50	0.04	0.02	0.00	100.84
	38.92	0.04	21.46	28.02	0.28	4.54	7.36	0.04	0.00	0.00	100.65
	38.47	0.44	21.63	28.07	0.27	4.38	7.06	0.04	0.00	0.04	100.39
	0.03	102.86	0.00	0.57	0.03	0.02	0.10	0.00	0.01	0.00	103.61
	39.07	0.21	21.87	28.63	0.44	4.74	6.10	0.05	0.01	0.00	101.11
	39.00	0.01	21.60	27.94	0.27	4.53	7.22	0.02	0.00	0.02	100.60
	38.68	0.05	21.53	27.72	0.40	4.87	7.52	0.07	0.02	0.00	100.85
	38.91	0.03	21.79	28.09	0.32	4.78	7.24	0.00	0.02	0.00	101.17
	38.84	0.08	21.60	24.09	0.33	2.94	12.70	0.00	0.00	0.00	100.58
	38.37	0.00	21.95	26.00	0.35	3.25	10.28	0.03	0.00	0.07	100.31
	38.63	0.02	21.62	27.59	0.29	4.16	8.41	0.00	0.02	0.00	100.73
	38.55	0.03	21.91	27.73	0.33	4.31	8.14	0.05	0.00	0.02	101.06
	39.05	0.08	22.16	27.15	0.38	4.31	8.24	0.05	0.01	0.00	101.42

Table A-8. Electron microprobe analyses from sample Kas2.

Sample	SiO_2	TiO_2	Al_2O_3	FeO	MnO	MgO	CaO	Na_2O	K_2O	Cr_2O_3	Sum
Kas2	49.64	0.13	8.33	13.61	0.00	13.38	8.70	3.05	0.14	0.02	97.00
	0.07	102.25	0.03	0.77	0.01	0.01	0.38	0.00	0.00	0.00	103.53
	94.35	0.02	0.00	0.45	0.01	0.01	0.03	0.00	0.00	0.01	94.88
	51.74	0.04	4.95	11.45	0.00	16.38	9.80	1.92	0.15	0.00	96.43
	48.39	0.22	8.66	17.12	0.02	10.84	8.30	3.35	0.09	0.02	97.01
	44.11	0.21	10.53	19.36	0.03	9.22	9.24	3.03	0.10	0.00	95.81
	42.60	0.35	12.22	19.23	0.06	8.86	9.56	3.05	0.15	0.04	96.11
	35.97	0.14	25.93	11.53	0.10	0.03	23.22	0.01	0.00	0.03	96.96
	53.61	0.01	8.33	8.13	0.00	8.61	14.93	6.28	0.01	0.03	99.94
	53.44	0.02	8.64	7.94	0.05	8.28	14.63	6.20	0.00	0.06	99.25
	36.76	0.15	25.85	11.96	0.08	0.04	23.32	0.00	0.00	0.03	98.19
	37.74	0.46	26.68	10.93	0.00	0.06	23.52	0.00	0.00	0.04	99.43
	37.56	0.16	21.90	28.78	0.07	3.00	9.89	0.01	0.00	0.00	101.38
	37.73	0.16	21.83	29.16	0.09	2.66	10.32	0.05	0.02	0.04	102.08
	37.72	0.18	21.70	28.34	0.09	2.38	10.76	0.02	0.00	0.01	101.20
	37.71	0.10	21.32	29.07	0.05	2.28	10.77	0.05	0.00	0.02	101.37
	37.80	0.13	21.24	29.41	0.10	1.87	10.90	0.02	0.02	0.00	101.49
	37.58	0.19	21.22	29.16	0.12	1.74	11.24	0.04	0.00	0.02	101.31
	37.91	0.15	21.30	28.42	0.15	1.73	11.76	0.05	0.02	0.06	101.55
	37.87	0.02	21.20	29.02	0.21	1.69	11.36	0.00	0.03	0.01	101.42
	37.38	0.18	21.27	28.23	0.19	1.33	12.55	0.04	0.02	0.01	101.18
	37.42	0.20	21.37	28.78	0.29	1.37	12.21	0.02	0.03	0.03	101.72
	37.11	0.14	21.22	29.38	0.30	1.32	11.46	0.01	0.00	0.01	100.95
	37.26	0.14	21.43	29.08	0.31	1.43	11.01	0.02	0.02	0.04	100.73
	37.23	0.23	21.11	29.48	0.45	1.36	11.13	0.00	0.01	0.04	101.04
	37.87	0.16	20.18	28.80	0.64	1.87	10.67	0.07	0.10	0.00	100.36
	37.53	0.22	21.42	28.70	0.76	1.46	10.87	0.08	0.00	0.03	101.08
	37.93	0.13	21.11	28.46	1.02	1.08	11.60	0.00	0.00	0.01	101.33
	38.13	0.11	20.99	28.95	1.30	1.20	10.52	0.06	0.01	0.03	101.31
	37.98	0.18	21.01	27.58	1.52	1.25	11.27	0.06	0.02	0.02	100.86
	38.19	0.15	21.13	27.13	1.73	1.13	11.30	0.00	0.02	0.01	100.78
	38.26	0.11	20.97	27.48	2.06	0.95	10.63	0.02	0.01	0.05	100.55
	38.04	0.16	20.89	26.78	2.39	1.10	10.77	0.05	0.00	0.04	100.21
	38.02	0.25	20.79	26.43	2.39	0.86	11.25	0.00	0.01	0.05	100.04
	37.58	0.14	20.81	25.01	2.39	0.93	11.81	0.02	0.03	0.00	98.71
	38.02	0.23	21.04	25.82	2.31	0.93	11.60	0.04	0.00	0.01	100.01
	37.83	0.23	21.02	25.79	2.44	0.81	11.64	0.02	0.00	0.00	99.78
	37.76	0.15	21.04	26.33	2.48	0.99	11.19	0.02	0.02	0.00	99.98
	38.10	0.09	24.17	11.21	0.18	0.00	23.30	0.00	0.02	0.09	97.16
	37.69	0.17	21.21	26.31	2.18	0.89	11.44	0.00	0.01	0.02	99.92
	37.51	0.23	21.21	26.88	2.34	0.84	11.12	0.02	0.00	0.00	100.15
	37.62	0.31	20.89	26.53	1.76	0.93	12.07	0.01	0.00	0.02	100.14
	37.54	0.16	21.10	27.67	1.36	1.03	11.13	0.00	0.00	0.11	100.09

Sample	SiO_2	TiO_2	Al_2O_3	FeO	MnO	MgO	CaO	Na_2O	K_2O	Cr_2O_3	Sum
	38.31	0.14	21.18	28.47	1.07	1.08	11.36	0.02	0.00	0.01	101.63
	37.93	0.18	21.12	28.37	0.78	1.10	11.75	0.01	0.00	0.01	101.25
	37.52	0.22	21.16	28.26	0.63	1.27	11.08	0.00	0.02	0.04	100.20
	38.19	0.21	21.41	29.28	0.50	1.24	10.90	0.03	0.00	0.00	101.76
	38.43	0.13	21.11	29.69	0.42	1.31	10.95	0.06	0.03	0.03	102.16
	38.14	0.16	21.20	29.31	0.38	1.39	11.19	0.03	0.02	0.00	101.82
	37.66	0.19	21.45	28.44	0.33	1.24	12.29	0.02	0.01	0.03	101.64
	38.30	0.13	21.01	27.59	0.22	1.19	13.00	0.01	0.00	0.04	101.49
	38.42	0.18	21.25	28.75	0.19	1.41	12.12	0.00	0.01	0.01	102.33
	30.34	37.17	2.13	2.43	0.04	0.09	27.23	0.02	0.01	0.00	99.45
	30.56	38.47	1.21	1.35	0.04	0.00	28.08	0.03	0.02	0.00	99.75
	38.33	0.15	21.35	29.00	0.10	1.64	11.56	0.05	0.00	0.09	102.25
	38.33	0.07	21.16	29.47	0.13	1.77	11.31	0.05	0.00	0.03	102.33
	38.63	0.17	21.46	29.50	0.10	1.86	11.12	0.03	0.00	0.02	102.88
	38.52	0.13	21.20	28.68	0.06	2.07	11.25	0.02	0.01	0.00	101.94
	30.46	38.50	1.24	1.43	0.06	0.02	27.64	0.02	0.01	0.10	99.46
	38.70	0.11	21.50	28.97	0.10	2.44	10.33	0.00	0.00	0.03	102.18
	38.36	0.08	21.45	29.07	0.08	2.69	10.06	0.04	0.01	0.00	101.85
	38.70	0.15	21.62	29.48	0.06	2.93	9.61	0.10	0.00	0.01	102.66

Table A-9. Electron microprobe analyses from sample LOF 3/12.

Sample	SiO_2	TiO_2	Al_2O_3	FeO	MnO	MgO	CaO	Na_2O	K_2O	Cr_2O_3	Sum
LOF 3/12	48.17	1.36	8.98	8.64	0.04	16.51	11.43	2.03	0.41	0.03	97.60
	54.04	0.17	7.93	4.82	0.07	11.49	17.31	4.19	0.00	0.01	100.02
	39.27	0.11	22.17	22.92	0.59	8.36	7.53	0.07	0.00	0.00	101.02
	39.43	0.30	21.60	22.59	0.50	8.04	8.02	0.13	0.02	0.00	100.62
	44.69	0.82	12.06	10.82	0.10	14.24	11.09	2.29	0.62	0.02	96.74
	63.13	0.00	22.72	0.32	0.00	0.00	4.16	8.98	0.16	0.00	99.47
	38.90	0.06	21.97	24.14	0.70	7.62	6.77	0.02	0.02	0.00	100.19
	38.89	0.25	21.95	24.22	0.69	7.70	6.95	0.01	0.01	0.00	100.66
	41.15	0.47	15.21	12.22	0.08	12.98	11.37	2.66	1.02	0.00	97.14
	61.44	0.04	23.82	0.17	0.03	0.03	5.56	8.36	0.12	0.00	99.55
	42.44	0.63	13.71	12.06	0.05	13.45	11.32	2.41	0.92	0.00	96.99
	63.21	0.00	23.45	0.32	0.01	0.00	4.52	8.86	0.17	0.00	100.53
	36.33	0.03	61.71	0.79	0.00	0.03	0.03	0.02	0.00	0.01	98.95
	39.70	0.09	21.67	24.61	0.65	8.33	6.66	0.00	0.01	0.02	101.75
	39.86	0.13	21.72	24.15	0.62	8.43	7.11	0.01	0.01	0.05	102.08
	39.55	0.21	21.74	23.76	0.43	8.32	7.84	0.04	0.00	0.02	101.91
	39.62	0.10	21.96	24.94	0.58	8.48	6.21	0.00	0.00	0.01	101.89
	39.92	0.11	21.78	24.89	0.49	8.10	7.01	0.03	0.00	0.00	102.32
	39.58	1.54	16.46	11.63	0.08	11.93	11.85	2.54	1.14	0.00	96.74
	41.68	1.47	15.88	11.24	0.03	13.07	11.64	2.58	1.03	0.01	98.63
	40.13	1.62	14.87	11.29	0.05	12.76	11.64	2.80	0.97	0.05	96.17
	39.85	0.16	21.64	24.34	0.51	7.71	8.09	0.03	0.00	0.00	102.33
	39.84	0.25	21.87	23.36	0.47	7.99	8.38	0.08	0.00	0.00	102.23
	39.85	0.16	21.86	24.42	0.53	8.67	7.28	0.01	0.00	0.00	102.78
	39.61	0.22	21.85	24.11	0.50	8.44	7.41	0.00	0.00	0.00	102.14
	30.72	1.36	15.45	11.78	0.03	9.95	9.96	2.34	0.83	0.00	82.41
	43.90	1.82	13.71	10.21	0.02	14.60	11.81	2.47	0.92	0.03	99.49
	39.42	0.12	22.02	24.34	0.39	7.98	7.67	0.03	0.00	0.00	101.97
	38.96	0.21	21.81	24.17	0.43	8.25	7.59	0.04	0.00	0.05	101.51
	40.01	0.09	21.49	24.15	0.38	8.90	6.93	0.05	0.00	0.04	102.05
	40.13	0.30	22.01	23.32	0.38	8.76	7.57	0.02	0.00	0.00	102.48
	39.67	0.18	21.85	23.31	0.34	8.70	8.32	0.08	0.01	0.02	102.48
	40.01	0.19	22.13	23.15	0.31	9.08	8.15	0.06	0.00	0.02	103.11
	39.54	0.29	22.25	22.49	0.28	8.78	8.19	0.02	0.00	0.00	101.85
	39.87	0.29	21.84	23.20	0.32	8.91	8.08	0.08	0.00	0.05	102.63
	39.21	0.18	22.12	24.12	0.35	7.75	8.19	0.00	0.00	0.03	101.94
	63.72	0.00	22.92	0.30	0.02	0.00	4.64	8.89	0.16	0.01	100.65
	53.84	0.09	2.03	5.97	0.01	14.81	22.33	1.29	0.02	0.00	100.40
	53.82	0.10	1.48	5.66	0.05	15.34	22.85	0.97	0.00	0.02	100.27
	36.74	1.56	13.99	8.82	0.04	11.66	11.90	3.02	0.68	0.00	88.40
	43.52	1.58	14.49	9.58	0.02	15.01	11.57	2.96	0.71	0.00	99.44
	39.26	0.16	21.81	24.12	0.33	8.08	8.02	0.05	0.00	0.01	101.85
	38.99	0.29	23.25	23.50	0.24	7.56	8.35	0.09	0.00	0.00	102.26

Sample	SiO_2	TiO_2	Al_2O_3	FeO	MnO	MgO	CaO	Na_2O	K_2O	Cr_2O_3	Sum
LOF 3/12	53.90	0.11	4.25	5.59	0.04	13.99	21.04	2.07	0.02	0.04	101.03
	39.89	0.28	21.73	23.53	0.25	8.13	8.01	0.03	0.00	0.01	101.85
	36.21	10.10	19.96	21.34	0.30	7.59	7.57	0.14	0.00	0.01	103.21
	39.88	0.24	21.65	24.07	0.17	8.24	8.41	0.05	0.00	0.00	102.71
	39.51	0.27	21.71	24.04	0.24	8.03	8.38	0.07	0.00	0.00	102.25
	39.66	0.35	21.94	23.79	0.27	7.76	8.52	0.07	0.01	0.00	102.36
	39.61	0.22	21.92	23.95	0.21	7.84	8.30	0.07	0.01	0.02	102.13
	39.55	0.26	21.63	24.62	0.25	7.41	8.69	0.06	0.00	0.00	102.47
	39.45	0.40	21.58	23.91	0.10	7.06	9.29	0.09	0.00	0.01	101.89
	39.59	0.43	21.95	24.31	0.16	6.94	8.99	0.12	0.00	0.04	102.53
	39.37	0.93	21.81	23.97	0.21	7.13	8.99	0.06	0.01	0.01	102.48
	0.05	102.37	0.00	0.48	0.01	0.00	0.25	0.03	0.00	0.02	103.21
	39.46	0.35	21.56	24.43	0.15	7.12	9.36	0.09	0.00	0.01	102.51
	39.76	0.37	21.53	24.25	0.23	7.22	8.86	0.08	0.00	0.00	102.29
	39.75	0.22	21.90	24.44	0.12	7.17	9.01	0.03	0.00	0.00	102.64
	39.35	0.34	21.90	24.79	0.22	7.19	8.66	0.08	0.00	0.04	102.58
	39.32	0.23	21.62	24.00	0.16	7.51	8.49	0.11	0.01	0.01	101.44
	39.13	0.33	21.80	24.10	0.08	7.54	8.84	0.04	0.02	0.00	101.87
	39.13	0.66	21.85	23.61	0.18	7.51	8.63	0.06	0.00	0.03	101.67
	38.30	0.33	21.14	23.68	0.22	7.24	8.91	0.09	0.00	0.00	99.90
	39.22	0.24	22.17	23.88	0.18	7.30	8.83	0.08	0.01	0.02	101.93
	39.59	0.20	21.67	24.46	0.16	7.41	8.32	0.05	0.01	0.00	101.86
	39.76	0.16	21.68	25.00	0.18	7.99	8.10	0.01	0.00	0.06	102.92
	41.34	0.84	17.13	11.51	0.03	11.83	10.25	3.27	1.50	0.00	97.71
	40.20	0.21	21.52	23.99	0.32	8.14	8.22	0.09	0.01	0.02	102.72
	39.58	0.37	21.84	23.59	0.33	7.91	9.02	0.09	0.03	0.03	102.78
	11.12	74.87	6.50	6.63	0.04	2.36	2.12	0.01	0.00	0.02	103.68
	39.64	0.27	21.72	23.18	0.24	8.01	8.47	0.08	0.00	0.04	101.65
	39.57	0.23	21.97	22.93	0.28	8.41	8.53	0.02	0.00	0.02	101.95
	18.25	6.54	23.05	19.84	0.29	3.04	7.76	0.13	0.01	0.00	78.91
	39.74	1.06	21.80	22.88	0.31	8.24	8.08	0.06	0.00	0.00	102.16
	39.64	0.20	21.63	23.67	0.32	7.84	8.53	0.01	0.00	0.00	101.82
	39.41	0.07	21.81	25.06	0.39	7.86	7.51	0.02	0.00	0.03	102.16
	39.25	0.19	21.55	25.08	0.39	7.37	7.79	0.07	0.01	0.00	101.69
	43.06	1.61	13.15	11.36	0.00	13.73	11.66	2.56	0.99	0.05	98.14
	44.51	1.26	11.91	10.78	0.00	14.88	11.72	2.15	0.83	0.04	98.07
	43.70	1.38	13.09	11.94	0.01	14.15	11.65	2.40	0.87	0.00	99.19
	47.94	0.95	11.45	10.92	0.06	16.35	11.61	2.09	0.68	0.00	102.03
	62.42	0.07	23.79	0.58	0.00	0.02	5.40	8.34	0.16	0.00	100.77
	39.49	0.49	21.70	23.22	0.38	7.77	8.10	0.01	0.00	0.07	101.22
	39.16	0.60	21.83	22.88	0.49	8.07	7.91	0.06	0.02	0.00	101.02
	41.87	0.02	22.64	25.56	0.45	7.62	6.10	1.01	0.01	0.00	105.27
	15.13	0.02	18.96	19.25	0.40	1.57	4.84	1.18	0.05	0.04	61.42
	39.92	0.02	21.82	24.72	0.33	8.50	6.85	0.01	0.00	0.01	102.18

Sample	SiO_2	TiO_2	Al_2O_3	FeO	MnO	MgO	CaO	Na_2O	K_2O	Cr_2O_3	Sum
LOF 3/12	40.09	0.03	22.19	24.08	0.25	9.25	6.66	0.08	0.01	0.00	102.64
	40.21	0.13	22.29	23.76	0.39	9.44	6.90	0.04	0.00	0.00	103.17
	39.99	0.01	22.20	24.03	0.44	9.40	6.45	0.01	0.00	0.00	102.51
	39.97	0.17	22.14	23.54	0.57	9.21	6.66	0.05	0.00	0.00	102.30
	39.80	0.13	22.32	23.55	0.61	9.34	6.69	0.03	0.00	0.00	102.46
	39.53	0.08	22.08	23.37	0.50	8.90	6.97	0.06	0.01	0.00	101.51

Acknowledgements

First and foremost, I would like to thank Prof. Dr. Niko Froitzheim for giving me the opportunity to do a PhD thesis at the Steinmann Institute in Bonn. I highly appreciate all the support and confidence he had given me through the years ever since I came to Bonn. I am very grateful for the interesting field trips, the fruitful discussions and the helpful advices.

I am furthermore highly grateful to Prof. Dr. Thorsten Nagel for teaching me metamorphic petrology and helping me with many scientific questions troubling my mind and, in particular, the thermodynamic modelling. For always been able to find a good idea and advice I remain thankful.

My best thanks go to Dr. Neven Georgiev for his fundamental help and guidance that brought me all the way to and through my PhD.

Special acknowledgments are given to Dr. Sascha Sandmann who introduced me to Lu-Hf dating and garnet geochronology in general. I thank Dr. Raúl Fonseca for his support at the LA-ICP-MS and helpful advices on the data reduction.

I appreciate all advices and the help with obtaining and interpreting the geochronological data from Prof. Dr. Carsten Münker and Dr. Peter Sprung.

I would like to thank all former and present members of the structural geology workgroup, especially Jacek, Ruth and Freddi for their great support, Matze for the help preparing the samples, also Kathrin, Gerrit, Davood, Michael and Linus. I also want to thank all the people from the Schloss as well as the isotope geochemistry workgroup from the University of Cologne for creating a great working atmosphere: Renate, Henrik, Alessandro, Felipe, Maria, Max, Julia, Christiane, Ashlea, Lisa, Markus, Bo, Frank etc.

I thank Dr. Marian Janák for the collaboration and the short course in thermodynamic modelling.

Finally yet importantly, my heartfelt thanks go to my family for their endless support, patience and encouragement. Most of all I thank my beloved sister for always being my best friend and giving me the great gift of being an aunty. I love you!

Mladen Ivanov, my dearest love, I thank you for your support in good and darkest times. You have always been there for me and I appreciate that deeply!